Oxygen dynamics in shallow coastal water sediments of the Southwestern Baltic Sea

Dissertation

to obtain the degree of

Doctor of Natural Sciences (Dr. rer. nat.)

from the Faculty of Mathematics and Natural Sciences

at the University of Rostock, Germany

Submitted by

Werna Werna

born in Makale, the Republic of Indonesia

Hanseatic and University City of Rostock, June 2024

https://doi.org/10.18453/rosdok_id00005063

Date of Submission: 14.06.2024

Date of Defense: 25.10.2024

Reviewers:

PD Dr. Stefan Forster
Department of Marine Biology
Institute of Bioscience
Faculty of Mathematics and Natural Sciences
University of Rostock

Dr. Frank Wenzhöfer
MPI for Marine Microbiology
Bremen, Germany

This research has been conducted in the working group of Marine Biology, Faculty of Mathematics and Natural Sciences, University of Rostock, within the framework of the Research Training Group Baltic TRANSCOAST funded by the DFG (Deutsche Forschungsgemeinschaft) under the grant number GRK 2000

“When we trust that we are the ocean, we are not afraid of the waves”

-Sayadaw U. Pandita

Table of Contents

List of Figures

List of Tables

List of abbreviations

ANOVA	analysis of variance
Br^-	Bromide
C	Carbon
chl	Chlorophyll
d	day
DNRA	dissimilatory nitrate reduction to ammonium
DIC	dissolve inorganic carbon
DIN	dissolved inorganic nitrogen
DIP	dissolves inorganic phosphate
DOC	dissolved organic carbon
DOM	dissolve organic matter
DOU	diffusive oxygen exchange
Dp	differential pressure
DW	dry weight
GP	gross production
GP_{LDS}	gross production calculated with light-dark shift
h	hour
H. diversicolor	*Hediste diversicolor* (O.F. Muller, 1776)
i.d.	in diameter
ind.	Individuals
k	permeability
(L_{dif})	light diffusive
(L_{adv})	light advective
(D_{adv})	dark advective
LOI	loss in ignition
MPB	Microphytobenthos
n	number of individuals
n.a	not available
N	nitrogen
$Na_2S_2O_4$	sodium dithionite
N_2	dinitrogen
NH_4^+	ammonium
NO_2^-	nitrite
NO_3^-	nitrate
NP	net production
O_2	oxygen
OM	organic matter
OCR	Oxygen consumption rates
M. arenaria	*Mya arenaria* (Linnaeus, 1758)
M. neglecta	*Marenzelleria neglecta* (Sikorski & Bick, 2004)
P	phosphorous
p	significant level
P/I	photosynthesis-irradiance
PO_4^{3-}	phosphate
POC	particulate organic carbon
POM	particulate organic matter
R_{Dark}	dark respiration
R_{vol}	volumetric rate
rpm	rounds per minute
RC	reduced compounds
ROI	region of interest
Rdark	respiration in the dark
Rlight	respiration in the light

SD	standard deviation
SiO_2	silicate
SO_4^{2-}	sulfate
S^{2-}	sulfide
SWI	substrate water interface
TOU	total oxygen uptake
TP	total production

List of formula symbols

A	(m^2)	surface area of cores
dp	(Pa)	differential pressure
β	(%)	water content
δ		delta
Ds	(cm^2 s^{-1})	diffusion coefficient of solutes
h	(cm-m)	height of water inside the cores
$J_{(x)}$	(mmol m^{-2} d^{-1})	diffusive oxygen flux across the SWI
Φ		porosity
ρ	(gr cm^{-3})	bulk density
ρ_s	(gr cm^{-3})	particle density
T	(°C)	temperature

Explanation

Data for Experiment 1: Bioirrigation of *Hediste diversicolor* in different coastal substrates of the Southwestern Baltic Sea (MCF Exp 1) and Experiment 3: 2D O_2 dynamics in sediment (marine) and soil (terrestrial) colonized by *Hediste diversicolor* (MCF Exp 3) were collected by N.K. in a context of a master thesis project (Kimpel, 2020). In the context of this doctoral dissertation, all data presentation, analysis, and interpretation were newly generated and written by W.W.

Summary

Though measurements of the availability and turnover of oxygen (O_2) are essential when evaluating the biological status of benthic communities and biogeochemical processes in shallow coastal environments, the investigation of benthic O_2 dynamics in shallow coastal water of the Southwestern Baltic Sea is still limited. Home to different coastal environmental settings, the biotic and abiotic factors regulating benthic O_2 in the Southwestern Baltic Sea vary spatiotemporally. Beyond the daily and seasonal cycle to increasing climactic extremes, benthic O_2 dynamics in shallow coastal water may undergo sudden and extreme disturbance, which could be exacerbated by anthropogenic stressors such as excessive nutrient loading and coastal protection and restoration measures (e.g., coastal realignment).

This dissertation explored benthic O_2 dynamics in different coastal settings of the Southwestern Baltic Sea: graded shoreline with sandy sediment and Bodden shoreline with terrestrial and degraded peat soil. This was achieved through a series of laboratory experiments. Firstly, using sandy permeable sediment, we investigated the role of light, pore water advection, and different nutrient treatments (without reduced compounds "C" and with reduced compounds "RC") in governing benthic O_2 distribution and metabolism associated with microphytobenthos (MPB) primary production. These investigations were conducted through benthic chamber incubations, employing three different techniques: O_2 microelectrode, O_2 planar optode, and O_2 sensor spot. Secondly, we explored benthic O_2 spatiotemporal dynamics in marine sediment, terrestrial soil, and burrow lining of *Hediste diversicolor* in the context of bioirrigation performance of the polychaete. Finally, we conducted a mesocosm experiment to examine the influence of key bioturbators (*Hediste diversicolor, Mya arenaria, Marenzelleria neglecta*) on O_2 uptake, solute, and nutrient fluxes in a rewetted coastal peatland. We then compared our experimental results with field observations to assess the potential success of key bioturbators in the early colonization of the restored coastal peatland.

Our microelectrode measurements at an illumination range of 0-100 µmol photon m^{-2} s^{-1} revealed that the influence of light on O_2 penetration depth in the sediment was generally stronger than that of advective pore water flow. O_2 penetration depth was deeper in organic matter-poor sandy sediment than in the rich ones. Light fueled benthic O_2 production and consumption. O_2 concentrations in the porewater varied a lot due to pore water washout and the availability of reduced dissolved compounds. The average O_2 consumption rate in the sediment in the dark (R_{Dark}) ranged from 2 ± 0.4 - 3 ± 1 mmol m^{-2} d^{-1} and 4 ± 2 - 6 ± 2 mmol m^{-2} d^{-1} in C and RC chambers, respectively. The corresponding average net production (NP)

varied between 7 ± 2 - 29 ± 28 mmol m^{-2} d^{-1} in C chambers and 10 ± 3 - 22 ± 6 mmol m^{-2} d^{-1} in RC chambers. The obtained gross production (GP) by summing R_{Dark} and NP was much lower than the estimated gross production by light-dark shift technique (GP_{LDS}), the latter exceeding by a factor of 1 - 5 in C chambers and by a factor of 3 – 5 in RC chambers. Light-enhanced O_2 consumption and possibly rapid carbon cycling in the sediment's photic zone were indicated by the respiration value obtained in the light (R_{Light}), which was much higher than R_{Dark} (2 - 18 fold). R_{Light} also increased with increasing light intensities. Parallel to the microelectrode measurement of R_{Dark}, the average total O_2 uptake (TOU) from RC chambers (43 ± 6 mmol m^{-2} d^{-1}) was about twice as high as values in C chambers.

Regardless of the nutrient treatments, the MPB communities were low-light adapted, with compensation irradiance (Ic) ranging from 0.6 – 16 µmol photon m^{-2} s^{-1} and saturation irradiance (Ik) ranging from 9 – 81 µmol photon m^{-2} s^{-1}. Photosynthetic capacity (Pm) was low, ranging from 8 – 85 mmol m^{-2} d^{-1}. The dominance of light in governing benthic O_2 dynamic was further confirmed by the higher O_2 consumption rate (OCR) after exposure to light (4 – 64 µmol O_2 l^{-1} min^{-1}) than exposure to combine light and advection (8 – 23 µmol O_2 l^{-1} min^{-1}), and exposure to advection in the dark (0.4 – 7 µmol O_2 l^{-1} min^{-1}).

Our planar optode measurement of vertical and horizontal O_2 distribution and the respective O_2 fluxes under different light and flow conditions matched well with microprofile measurements. However, the values were slightly lower than those obtained with microelectrodes. The time-dependent 2D O_2 distribution and fluxes revealed significant variations at the millimeter scale, primarily due to the uneven distribution of MPB and difference in nutrient treatments.

Within the scope of the Bodden coastal setting, our 2D imaging of O_2 distribution at the sediment-water interface (SWI) and in the substrates around the burrow of *H. diversicolor* showed significant heterogeneity, varying spatially and temporally. This variability was associated with the ventilation activity of the animals, the distance of the burrow from the SWI, and the size of the burrow. *H. diversicolor* irrigated more frequently in sediment than in soil. The O_2 concentration and average O_2 fluxes at the SWI were higher than the O_2 fluxes across the burrow wall. *H. diversicolor* stimulated diffusive O_2 fluxes more in soil than sediment, likely due to higher porosity and a higher content of reduced compounds in the soil.

The influence of *H. diversicolor in* stimulating TOU (111%) was only observed in soil with background TOU of 12.8 ± 1.27 mmol m^{-2} d^{-1}. One-third of this stimulation was due to fauna respiration, while 67% was associated with microbial respiration. Although the impact on

microbial respiration was less pronounced than in sediment, *H. diversicolor* could perform bioirrigation in the inundated soil. Changes in the distribution of pore water nutrients with depth due to fauna ventilation were only noticeable in sediment.

All tested key bioturbators in the colonization experiment with peat soil survived relatively well (26 – 96 %). However, they ventilated less, and the polychaetes exhibited avoidance behavior. The physical properties of peat soil challenged the animals' burrowing capacities and the bioturbators seemed to have low tolerance towards the highly concentrated pore water nutrients. TOU and nutrient release were slightly stimulated by the presence of the fauna, with higher fluxes in the experiment colonized by *H. diversicolor* and *M. neglecta*. The stimulation of TOU was most likely due to the reoxidation of reduced compounds, which masked any small signals of faunal respiration. This conclusion is further supported by the increase in TOU and nutrient fluxes throughout the incubation in the azoic control experiments.

The observed obstacle to burrowing activity in laboratory experiments (peat soil structure) was also evident in the field. Although the occasional field sampling in the flooded coastal peatland showed that the early colonizer benthic macrofauna community in the newly restored area was similar to the community at the adjacent coastal water, the rapid colonization of *H. diversicolor* only occurred in areas with mud-sand content, and *M. arenaria* was observed mainly at the surface of peat soil, unable to burrow.

Our study in the sandy coastal setting emphasizes the importance of light and pore water advection in regulating the benthic O_2 dynamics in permeable sandy sediment, as well as the important contribution of the MPB community to primary production in the sandy sediment of the Southwestern Baltic Sea. Our findings call for further field studies to assess the fate of O_2 produced by the MPB community. In the Bodden coastal setting, our findings demonstrate the importance of fauna-substrate interaction (both physical and chemical) in mediating the O_2 and nutrient dynamics of restored coastal peatlands. Our results also emphasize the need to integrate this complexity into current and future coastal peatland restoration design. A careful assessment of benthic fauna resilience towards substrate's physical properties and potential nutrients released due to flooding with seawater is necessary if benthic macrofauna recolonization is a concern.

Zusammenfassung

Obwohl Messungen der Verfügbarkeit und des Umsatzes von Sauerstoff (O_2) für die Bewertung des biologischen Zustands benthischer Gemeinschaften und biogeochemischer Prozesse in flachen Küstenumgebungen von wesentlicher Bedeutung sind, sind die Untersuchungen der benthischen O_2-Dynamik im flachen Küstensedimenten der südwestlichen Ostsee immer noch begrenzt. Die biotischen und abiotischen Faktoren, die den benthischen O_2-Gehalt in der südwestlichen Ostsee regulieren, variieren aufgrund der unterschiedlichen Umweltbedingungen in den Küstengebieten räumlich und zeitlich. Über den täglichen und saisonalen Zyklus hinaus bis hin zu zunehmenden klimatischen Extremen kann die benthische O_2-Dynamik im flachen Küstenwasser plötzlichen und extremen Störungen ausgesetzt sein, die durch anthropogene Stressfaktoren wie übermäßige Nährstoffbelastung und Küstenschutz- und -wiederherstellungsmaßnahmen (z. B. Küstenumgestaltung) noch verstärkt werden könnten.

In dieser Dissertation wurde die benthische O_2-Dynamik in verschiedenen Küstengebieten der südwestlichen Ostsee untersucht: Außenküste mit sandigem Sediment und Boddenküste mit terrestrischem degradiertem Torfboden. In einer Reihe von Laborexperimenten untersuchten wir zunächst an sandigen permeablem Sediment die Rolle von Licht, Porenwasseradvektion und verschiedenen Nährstoffbehandlungen (ohne reduzierte Verbindungen „C“ und mit reduzierten Verbindungen „RC“) bei der Steuerung der benthischen O_2-Verteilung und des Umsatzes in Verbindung mit der Primärproduktion des Mikrophytobenthos (MPB). Diese Untersuchungen wurden in benthischen Kammern unter Verwendung von drei verschiedenen Techniken durchgeführt: O_2-Mikroelektrode, O_2-Planar-Optode und O_2-Sensorspot. Zweitens untersuchten wir die räumlich-zeitliche Dynamik von O_2 im Sediment, in terrestrichem Boden und in der Gangwandung von *Hediste diversicolor* im Zusammenhang mit der Bioirrigation des Polychaeten. Schließlich führten wir ein Mesokosmen-Experiment durch, um den Einfluss der wichtigsten Bioturbatoren (*Hediste diversicolor*, *Mya arenaria*, *Marenzelleria neglecta*) auf den O_2-Verbrauch, die Flüsse gelöster Substanzen und Nährstoffe in einem wieder vernässten Küstenmoor zu untersuchen. Anschließend verglichen wir unsere experimentellen Ergebnisse mit Feldbeobachtungen, um den potenziellen Erfolg der wichtigsten Bioturbatoren bei der frühen Besiedlung des wieder vernässten Küstenmoores zu bewerten.

Unsere Mikroelektrodenmessungen zeigten in einem Beleuchtungsbereich von 0-100 µmol Photon m^{-2} s^{-1}, dass der Einfluss des Lichts auf die O_2-Eindringtiefe in das Sediment im Allgemeinen stärker war als der des advektiven Porenwasserflusses. Die O_2-Eindringtiefe

war in sandigen Sedimenten, die arm an organischer Substanz waren, tiefer als in den reichhaltigeren. Licht förderte die benthische O_2-Produktion und den O_2-Verbrauch. Die O_2-Konzentrationen im Porenwasser schwankten aufgrund der Auswaschung des Porenwassers und der Verfügbarkeit von reduzierten gelösten Verbindungen stark. Der durchschnittliche O_2-Verbrauch im Sediment im Dunkeln (R_{Dark}) lag zwischen 2 ± 0,4 - 3 ± 1 mmol m^{-2} d^{-1} und 4 ± 2 - 6 ± 2 mmol m^{-2} d^{-1} in den C- und RC-Kammern. Die entsprechende durchschnittliche Nettoproduktion (NP) variierte zwischen 7 ± 2 und 29 ± 28 mmol m^{-2} d^{-1} in C-Kammern und 10 ± 3 und 22 ± 6 mmol m^{-2} d^{-1} in RC-Kammern. Die durch Addition von R_{Dark} und NP ermittelte Bruttoproduktion (GP) war wesentlich geringer als die nach der Ligh-Dark-Shift-Methode (GP_{LDS}) geschätzte Bruttoproduktion, wobei letztere in C-Kammern um den Faktor 1 - 5 und in RC-Kammern um den Faktor 3 - 5 höher lag. Der durch Licht verstärkte O_2-Verbrauch und ein möglicherweise schnelles Kohlenstoff-Recycling in der photischen Zone des Sediments wurden durch die Respiration im Licht (R_{Light}) verdeutlicht, die viel höher war als R_{Dark} (2 - 18-fach). R_{Light} stieg auch mit zunehmender Lichtintensität an. Parallel zur Mikroelektrodenmessung von R_{Dark} war die durchschnittliche Gesamt-O_2-Aufnahme (TOU) aus RC-Kammern (43 ± 6 mmol m^{-2} d^{-1}) etwa doppelt so hoch wie die Werte in C-Kammern.

Unabhängig von den Nährstoffbehandlungen waren die MPB-Gemeinschaften an schwaches Licht angepasst, wobei die Kompensationspunk (Ic) zwischen 0,6 und 16 µmol Photon m^{-2} s^{-1} und die Lichtsättigung (Ik) zwischen 9 und 81 µmol Photon m^{-2} s^{-1} lag. Die photosynthetische Kapazität (Pm) war gering und lag zwischen 8 und 85 mmol m^2 d^{-1}. Die Dominanz des Lichts bei der Steuerung der benthischen O_2-Dynamik wurde ferner durch die höhere O_2-Verbrauchsrate (OCR) nach Lichtexposition (4 - 64 µmol O_2 l^{-1} min^{-1}) als nach kombinierter Licht- und Advektionsexposition (8 - 23 µmol O_2 l^{-1} min^{-1}) und nach Advektionsexposition im Dunkeln (0,4 - 7 µmol O_2 l^{-1} min^{-1}) bestätigt.

Unsere planare Optodenmessung der vertikalen und horizontalen O_2-Verteilung und der entsprechenden O_2-Flüsse unter verschiedenen Licht- und Strömungsbedingungen stimmte gut mit den Mikroprofilmessungen überein. Allerdings waren die Werte etwas niedriger als die mit Mikroelektroden gemessenen. Die zeitabhängige 2D- O_2-Verteilung und die O_2-Flüsse zeigten erhebliche Schwankungen im Millimeterbereich, die in erster Linie auf die ungleichmäßige Verteilung von MPB und die unterschiedlichen Nährstoffbehandlungen zurückzuführen sind.

Bei den Untersuchungen der Boddenküste zeigte unsere 2D-Bildgebung der O_2-Verteilung an der Sediment-Wasser-Grenzfläche (SWI) und in den Substraten rund um den Bau von *H.*

diversicolor erhebliche Heterogenität, die räumlich und zeitlich variierte. Diese Variabilität stand im Zusammenhang mit der Belüftungsaktivität der Tiere, dem Abstand des Gangabschnittes zur SWI und der Größe des Ganges. *H. diversicolor* pumpte überstehendes Wasser im Sediment häufiger als in terrestrischem Boden. Die O_2-Konzentration und die durchschnittlichen O_2-Flüsse an der SWI waren höher als die O_2-Flüsse durch die Gangwand. *H. diversicolor* stimulierte die diffusiven O_2-Flüsse im Boden stärker als im Sediment, was wahrscheinlich auf die höhere Porosität und den höheren Gehalt an reduzierten Verbindungen im Boden zurückzuführen ist.

Der Einfluss von *H. diversicolor* auf die Stimulierung des TOU (111 %) wurde nur in Böden mit einem Hintergrund-TOU von 12,8 ± 1,27 mmol m^{-2} d^{-1} beobachtet. Ein Drittel dieser Anregung war auf die Atmung der Fauna zurückzuführen, während 67 % mit der mikrobiellen Atmung in Verbindung gebracht wurden. Obwohl die Auswirkungen weniger ausgeprägt waren als im Sediment, konnte *H. diversicolor* auch im überschwemmten Boden Bioirrigation betreiben. Veränderungen in der Verteilung der Porenwassernährstoffe mit der Tiefe, die auf Bioirrigationdurch die Fauna zurückzuführen sind, wurden nur im Sediment festgestellt.

Alle getesteten Schlüsselbioturbatoren im Besiedlungsversuch mit Torfboden überlebten relativ gut (26 - 96 %). Sie zeigten jedoch eine etwas schwächere Bioirrigationsaktivität und die Polychaeten zeigten ein Vermeidungsverhalten. Die physikalischen Eigenschaften des Torfbodens stellten eine Herausforderung für die Wühltätigkeit der Tiere dar und die Bioturbatoren schienen eine geringe Toleranz gegenüber den hochkonzentrierten Nährstoffen im Porenwasser zu haben. TOU und die Nährstofffreisetzung wurden durch die Fauna leicht stimuliert, wobei die Flüsse in dem von *H. diversicolor* und *M. neglecta* besiedelten Experiment höher waren. Die Stimulierung des TOU war höchstwahrscheinlich auf die Reoxidation reduzierter Verbindungen zurückzuführen, die geringere Reaktionen der tierischen Atmung überdeckte. Diese Schlussfolgerung wird auch durch den Anstieg des TOU und der Nährstoffflüsse während der gesamten Inkubation in den azoischen Kontrollversuchen bestätigt.

Die in den Laborexperimenten beobachtete Wühltätigkeit gegen Widerstände (Torfbodenstruktur) war auch im Freiland zu beobachten. Obwohl die gelegentlichen Feldbeprobungen im überfluteten Küstenmoor zeigten, dass die Gemeinschaft der frühen Besiedlung der benthischen Makrofauna in dem neu wiederhergestellten Gebiet der Gemeinschaft im angrenzenden Küstengewässer ähnlich war, erfolgte die rasche Besiedlung

von *H. diversicolor* nur in Bereichen mit Schlamm- oder Sand-Gehalt und war *M. arenaria* wurde hauptsächlich an der Oberfläche des Torfbodens beobachtet unfähig zu graben.

Unsere Studie in der sandigen Küstenumgebung unterstreicht die Bedeutung von Licht und Porenwasseradvektion bei der Regulierung der benthischen O_2-Dynamik in permeablem sandigen Sedimenten, sowie den wichtigen Beitrag der MPB-Gemeinschaft zur Primärproduktion in den sandigen Sedimenten der südwestlichen Ostsee. Unsere Ergebnisse unterstreichen, dass weitere Feldstudien erforderlich sind, um den Verbleib des von der MPB-Gemeinschaft produzierten O_2 zu verstehen. In der Küstenlandschaft der Boddengewässer zeigen unsere Ergebnisse die Bedeutung der Interaktion zwischen Fauna und Substrat (sowohl physikalisch als auch chemisch) bei der Steuerung der O_2- und Nährstoffdynamik von wiederhergestellten Küstenmooren. Unsere Ergebnisse unterstreichen auch die Notwendigkeit, diese Komplexität in die aktuelle und künftige Planung der Wiederherstellung von Küstenmooren mit einzubeziehen. Eine sorgfältige Bewertung der Widerstandsfähigkeit der benthischen Fauna gegenüber den physikalischen Eigenschaften des Substrats und den potenziellen Nährstoffen, die durch die Überflutung mit Meerwasser freigesetzt werden, ist notwendig, wenn die Wiederbesiedlung mit benthischer Makrofauna angestrebt wird.

1 INTRODUCTION

Marine coastal zones are among the most ecologically and socio-economically vital on the planet (Harley et al., 2006). They encompass less than 20 % of the earth's surface (Crossland et al., 2005), where the land is significantly influenced by the sea, and vice versa. Being located in the transitional zone between land and sea, the main function of coastal zones lies on their transport, buffer, and filter capacity (Schiewer 2008). This renders this region to be sensitive, towards bidirectional environmental changes. Coastal areas are susceptible to natural disturbance such as rising temperature, accelerated sea-level rise (SLR), sinking coast, and variation in storm activity. On the other side, anthropogenic perturbation consists of mainly land use such as habitation, agri-aqua culture, transport, tourism, water treatment and development of on-offshore structures. Continues change in coastal zone may lead to changes and degradation of the physical, chemical, biological, and biogeochemical properties of this system and ultimately will change the morphology and delivery of ecosystem service provided. Due to the high population densities and extensive infrastructure and property development in coastal areas, disasters will have major consequences. Continual monitoring and management of coastal environments is therefore critical to preserve these services.

One fundamental measure in shallow coastal water ecosystems, state and function, is oxygen (O_2) availability. O_2 is prerequisite for life, essential to almost all eukaryotes as the terminal acceptor in energy production (respiration), and a main molecule in regulating biogeochemical processes. O_2 is produced as a byproduct of photosynthesis by cyanobacteria, eukaryotic algae, and plants. The produced O_2 is introduced into surface water and consumed in the water column and in the sediment. Throughout the direct involvement of O_2 in these processes, O_2 is transported and exchange between atmosphere, lithosphere, hydrosphere, and biosphere. Thus, O_2 represents an excellent indicator for biological activity and is an absolute key measure when evaluating the cycling of essential elements such as carbon, nitrogen, phosphorus, sulfur, and metals, locally as well as globally (Canfield et al., 2005; Glud, 2008).

O_2 concentration and distribution in shallow coastal water reflects the balance between O_2 supply (reaeration at the water surface and O_2 production via photosynthesis), O_2 removal (respiration and reoxidation of reduced compounds) and O_2 transport across atmosphere–water and benthic–water boundaries. Each of these processes has the potential to be significant in shallow ecosystems due to high fluxes and low water volumes. In the lower water column (water-seafloor interface), oxygenation through oxic bottom water ventilation may be inhibited, while the rates of benthic production and consumption can be high and relatively more important than in water column. Beside high metabolic rate, the variation in O_2 concentration is further influence by the spatial and temporal variation of hydrodynamic forces and their interaction with organisms and the seafloor. Hydrodynamic forces and organism activity can induce small-scale spatial variability in the seafloor and generate small scale heterogeneity with intensive microbial processes and steep concentration of redox species.

Production. In shallow coastal water, microphytobenthos (MPB) might exhibit high rates of photosynthesis and contribute significantly to total primary production of the ecosystem (Middleburg et al. 2000); Cahoon et al. 1999; Underwood and Kromkam, 1999; MacIntyre et al. 1996) as well as the production of benthic O_2. The microphytobenthic

community can make up to 30 – 50 % of the total coastal primary production (Santema & Huettel 2018; Cahoon, 1999;). In addition to regulating carbon transfer among trophic levels, MPB facilitate nutrient cycling at the substrate-water interface (SWI) and stabilize sediment through excretion of extrapolymeric substance (EPS). A microphytobenthic community may consist of cyanobacteria, dinoflagellates, chlorophytes, euglenids, and diatoms, of which benthic diatoms has been reported as the dominant group (Cahoon, 1999). According to their lifestyle (life-strategy), benthic diatoms has been divided into epipelon and epipsammon. The epipelon consist of motile diatoms that can move freely between sediment particles, while the epipsammon comprise of smaller, non-motile diatoms that are attached to sediment particle (mostly sand). A motile diatom cell is able to actively search for optimal microenvironment (light, temperature, flow condition) and exhibit vertical migratory rhythm. Non motile diatom photoregulate solely through physiological mechanism. Through these mechanisms benthic diatoms are likely to cope and thrive in the complex and dynamics environment of shallow coast with steep physical and chemical micro gradient.

Light, temperature, dissolve inorganic carbon (DIC), nutrients, and to a lesser extent salinity has been identified as the most limiting factor in regulating benthic primary production of MPB in coastal water (Larkum et al. 2003; Kromkamp et al., 1995). Light attenuation in the water, turbidity of the water column, and decrease in water clarity due to pelagic primary producer affect the availability of light for the benthic community at the seafloor, nevertheless studies have shown that the amount of light reaching the sea bottom may still sustain significant benthic primary production. In particular, MPB can sustain growth at irradiance well below average value of 5 -10 µmol photons m^{-2} s^{-1}, while minimum irradiance where community metabolism has been detected was 46 µmol photons m^{-2} s^{-1} (Gattuso et al., 2006). In addition, temperature regulates physiochemical factors such as solute diffusion, solubility, water viscosity, and the thickness of the diffusive boundary layer (DBL), all involved in solute transport at the SWI and in the sediment.

Light, temperature, dissolve inorganic carbon (DIC), nutrients, and to a lesser extent salinity has been identified as the most limiting factor in regulating benthic primary production of MPB in coastal water (Larkum et al. 2003; Kromkamp et al., 1995). Light attenuation in the water, turbidity of the water column, and decrease in water clarity due to pelagic primary producer affect the availability of light for the benthic community at the seafloor, nevertheless studies have shown that the amount of light reaching the sea bottom may still sustain significant benthic primary production. In particular, MPB can sustain growth at irradiance well below average value of 5 -10 µmol photons m^{-2} s^{-1}, while minimum irradiance where community metabolism has been detected was 46 µmol photons m^{-2} s^{-1} (Gattuso et al., 2006). In addition, temperature regulates physiochemical factors such as solute diffusion, solubility, water viscosity, and the thickness of the diffusive boundary layer (DBL), all involved in solute transport at the SWI and in the sediment.

Consumption. In shallow coastal water, O_2 is used for heterotrophic respiration, degradation of organic matter (OM), and re oxidation of reduced compounds from degradation. Due to the shallow depth and high productivity (pelagic and benthic primary production) in coastal waters and seabeds, the bacterial mediated degradation of deposited

OM originating from water column and seafloor, together with heterotrophic respiration, easily exhaust the available O_2 at the SWI. Limited transport via diffusion, particularly in muddy sediment, further constrain the capacity to resupply O_2 from the overlying water. As a consequence, O_2 penetration depths in marine substrates are very limited, ranging from < 1 mm in active muddy sediment to a few cm in permeable sandy sediment (Glud, 2008). O_2 limitation initiates a cascade of alternative electron acceptor use by anaerobic organisms (mainly microbes) in degradation of OM sequentially, though several respiration pathways often overlapped. A vertical redox zonation of oxidant depletion in coastal sediments often exhibit the order O_2 > nitrate (NO_3^-) > manganese oxide (MnO_2) > ferric oxides ($Fe(OH)_3$ > sulfate (SO_4^{2-}) (Thamdrup and Canfield 2000). Degradation of OM produces various reduced compounds such as ammonium (NH_4^+), iron (II) (Fe^{2+}), manganese (II) (Mn^{2+}), hydrogen sulphide (HS^-) and methane (CH_4), which are generally re-oxidized within sediments through chemical and microbial mediated process involving O_2 and other electron acceptor according to the redox sequence (Canfield et al., 2005). Several studies have reported that reoxidation process can contribute to 75 % of the O_2 consumption in coastal sediments (Glud, 2008; Soetaert et al., 1996; Jørgensen, 1982). Thus, although O_2 consumption cannot directly be equated with aerobic respiration, O_2 consumption provides a reliable estimate of total respiration, i.e. total benthic carbon mineralization rate.

The rate of benthic O_2 uptake largely depends on water depth, pelagic net primary production, light, temperature, nutrient availability, carbon input (OM quality), bioturbating fauna, and physical factors (hydrodynamics). Water depth controls the input of OM to the seabed, while the quantity of the produced OM relay on the light and nutrient dependent-net production in the photic zone of the water column and seafloor. Temperature control on O_2 consumption originates from the temperature dependency of chemical, biological, and physical process in general and is well captured in the seasonal variation in O_2 consumption. The variation is a combined effect of accelerated respiration rate of the benthic organisms at higher temperature and accelerated influx of fresh OM to feed their respiration during spring and summer. It is generally accepted that benthic O_2 uptake is directly related to the input of labile organic matter to the sediment. Seasonal fluctuations in fresh detritus influx are most prominent in coastal regions experiencing spring phytoplankton blooms (Jørgensen, 1996; Graf et al., 1983a; 1982). Rapid temporal change in O_2 concentration as a response of the diurnal cycle of light create a dynamic chemical microenvironment through up and down movement of the oxic/anoxic interface. This process may have serious implications for the zonation of aerobic and anaerobic microbial processes in the upper sediment layers.

Animals living at or in the sediments not only depend on the resources and conditions above and within the sediments, but also modify the texture and geochemistry of their environment (Meysman et al., 2006). Animals can alter sediment porosity, permeability, particle size, cohesion, organic content and, perhaps more importantly, spatial heterogeneity of these properties, and thus generate niches for smaller organisms (microbes, micro-, meioand macrobenthos). The contribution of meiofauna to total sediment respiration is rather small (less than a few percent), but macrofauna typically contributes 10–30% of total respiration (Herman et al. 1999). The contribution of fauna to total respiration can be partitioned into direct contributions due to faunal respiration and indirect contributions due

to faunal stimulated bacterial activities (Glud et al. 2003; Aller and Aller 1998;). Apart from their own respiration, benthic fauna affect benthic O_2 uptake through bioturbation, i.e. "all transport processes carried out by animals that directly or indirectly affect sediment matrices. These processes include both particle reworking and burrow ventilation" (bioirrigation) (Kristensen et al. 2012). The occurrence of fauna increase the extent of the sediment-water interface and of the diffusive O_2 flux through their burrow structures. Through bioirrigation, i.e. fauna-induced exchange of solutes between overlying and interstitial waters, fauna increases the influx of electron acceptors - most notably O_2 - into the sediment, leading to enhanced microbial mediated aerobic mineralization of OM and re-oxidation of reduced products of anaerobic pathways. At the same time it increases the efflux of mineralization products such as dissolved inorganic carbon or ammonium from the sediment, which promotes primary production at the SWI or in the overlying water. Furthermore, fauna introduce reactive substrates in the form of mucus secretions in their burrow lining. The lining generate hot spots of intensive microbial processes in the burrow wall, which is responsible for a rapid loss of O_2. For instance, bioirrigation may stimulate nitrification by supply of O_2, but may also stimulate effluxes of NH_4^+ and NO_3^- with the result that the net effect on nitrogen cycling (nitrification, denitrification and anammox) depends in a complex way on bio-irrigation (Aller, 2001). The extent to which these effects are realized depends on the functional groups of animals present, their abundance, taxonomic peculiarities and the size of individuals (Kristensen, 2000).

Transport. The transport of solutes from the water column to static sediment and the interstitial water inside the sediment is affected by the condition at the SWI. Solute transport across the SWI transitions from free-surface turbulent flows, where solute mixing is ensured by eddy transport and advection, to laminar pore water flow in the sediment bed, where solute transport is mainly mediated by diffusion. The region where this occurs is termed the benthic boundary layer (BBL). The BBL is formed due to the frictional interaction between water and the sediment surface. The BBL generally comprises the logarithmic, viscous, and diffusive boundary layers (DBL). Vertical mixing is rapid due to turbulence in the logarithmic layer, while eddy diffusivity becomes smaller than kinematic viscosity in transporting momentum through the water in the viscous layer. Towards the direction of the sediment surface, molecular diffusivity eventually becomes more critical than eddy diffusivity at DBL. Within most of the DBL, solute concentration gradients are linear; this region has no net advection or chemical reaction. The DBL is a relatively thin (0.2 - 1 mm) (Gundersen & Jørgensen, 1990; Jørgensen & Revsbech, 1985) layer and is affected by the flow in the overlying water, the roughness of the sediment surface, and the occurrence of microtopography, i.e., small scale surface topography from patches of microalgae, fecal and detritus deposit, and tracts of moving fauna. The thickness of DBL regulates the transport of solutes, including O2, across SWI, which has implications for aerobic microbial activity. Overall, the BBL is highly dynamic and, together with near-bed flows, plays an essential role in regulating solute and particle fluxes to and from the water column, thus the strength of benthic-pelagic coupling.

O_2 and dissolved substances in general can be transported across the SWI via diffusion and/or via advection. Diffusion is defined as the movement of a substance from an

area of high concentration to an area of low concentration driven by molecular random movement, while advection is the transfer of mass with flow. Interfacial and in-bed transport processes depend largely on the composition of the seabed and the activities of the benthic fauna (Ziebis et al., 1996; Forster and Graf, 1995; Aller, 1983). While diffusion is the major transport mechanism for solutes in muddy, cohesive sediments (Berner, 1980), advective transport processes gain significance in sandy beds where permeability exceeds 10^{-12} m^2 (Glud et al., 1996; Huettel et al., 1996; Huettel and Gust, 1992). Advection occurs as a consequence of small-scale pressure gradient generated by water flow over sediment topography features (e.g. ripple and mounds). Pressure gradients as small as 1 Pa cm^{-1}, generated when bottom flows are deflected by small sea bed topography, can force water several centimeters into permeable sediments and draw pore fluid from more than 10 cm depth to the surface. Velocities of these pore flows may reach 1–3 cm h^{-1}. The main causes for pressure gradients that drive pore water flow are bottom currents, waves, and pumping activity of benthic animals. Other factors that can lead to porewater flow include undulating pressures at the seafloor due to the passage of surface gravity waves (“wave pumping”), groundwater seepage, fluid venting, gas bubble emergence, and temperature or salinity gradients (see Huettel & Webster, (2001) and references therein).

Advective transport can result in transport rates with orders and magnitudes higher than diffusion, thus enhancing transport of solutes such as O_2, other dissolved compounds, and even small particulate organic matter (POM) (Precht et al. 2004; Precht and Huettel 2003; Huettel et al. 1996) eventually influencing diagenesis process in the sediment. Advection can increase O_2 penetration depth in the sediment (Forster et al., 1996; Ziebis et al., 1996) and has been shown to enhance the O_2 consumption rate (OCR) and organic matter degradation (Reimers et al., 2004; Huettel and Rusch, 2000). Advective pore water flows are particularly strong close to the sediment-water interface (Shum, 1992) where they effectively wash out solutes from pore space and sustain upwelling pore waters from below. Thus, pore water flows control biogeochemical zonation in permeable sediment (Huettel et al., 1998) and affect gradients across the sediment-water interface. They complicate the measurement of fluxes compared to cohesive sediment, derived either from concentration gradients in the sediment or concentration changes with time in the overlying water.

Transport in soil, particularly peat soil. The main mechanism of solute transport (including O_2) described above are also found in soil. O_2 transport in soil is additionally divided into vertical and horizontal movement in the gaseous phase due to the respective O_2 concentration gradients within a given soil profile above the water table in the air-filled pores. Beside these two dominant flow direction, another movement mechanism found in soil is the preferential flow (Liu & Lennartz, 2015; Baird & Gaffney, 2000). It is a movement of free (gravitational) water and any solutes through distinct pathways that are usually macropores formed by worms, burrowing insects and animals, plant roots, undecomposed plant materials, cracks and fissures, or cultivation practices that alter subsoil structure. Preferential flow affects solute movement by allowing water to bypass large areas of porous soil, regarded as macropores.

Recent studies indicate the dominant occurrence of preferential flow in highly degraded peat soil (Liu et al., 2017). Peat soils typically have high porosities and are usually water-

saturated. When the water table drops, a fraction of the pore space volume, previously filled with water, drains, and air-filled porosity, increases. As diffusion is 10^4 times faster in air than in water, air-filled porosity is thought to control significantly transport rates of gases, i.e., O_2 and CO_2, in the peat profile. Thus, solute concentrations in peat pore water reflect the balance between transport and turnover rates of these gases, which are affected by changes in air-filled porosity as the water table fluctuates (Deppe et al., 2010; Knorr & Blodau, 2009). In addition, soil physical properties such as water content, organic content, and pore water chemistry have been reported to play an essential role in water flow and the transport of solutes in peat soil.

1.1 Ecological and biogeochemical consequence of O_2 availability

Climate change and variability have a significant impact on O_2 availability in coastal environments at local, regional, and global scales. Rising temperatures decrease O_2 solubility, contribute to water column stratification, and alter wind patterns, affecting O_2 transport and mixing. Changes in hydrology can influence the delivery of nutrients and organic matter from land to coastal systems, impacting O_2 consumption. Hydrological changes can also lead to salinity modifications and increased stratification due to elevated evapotranspiration in arid areas or freshwater lenses from excessive rainfall or land runoff. Higher temperatures and salinity changes can also affect organisms' metabolic and respiratory rates, leading to increased biological O_2 demand and energy demand for the ionic regulation of marine organisms. These physical changes can alter food availability and distribution patterns for many species, ultimately affecting species composition and interactions.

The primary anthropogenic perturbation influencing the O_2 balance in coastal waters is increased nutrient loading and atmospheric CO_2. Human activity in the coastal zone has driven excessive nutrient input into the coastal water, leading to eutrophication and a vicious cycle of hypoxia. Eutrophication stimulates primary production and may lead to large algal blooms that can sink (as particulate and dissolved OM) to the seabed. When bottom waters cannot mix with surface waters due to stratification, the consumed O_2 cannot be replaced, and hypoxia (defined as an O_2 concentration of less than 62 μmol/kg) or anoxia develops. Stream discharges of nitrogen and phosphorus nutrients are mainly driven by land-use activities (mainly associated with agricultural activities) and wastewater discharges from urban areas. The increased atmospheric CO_2 may directly affect productivity (thus production and consumption of O_2) and acidification, i.e., lowering the pH. Acidification affects organisms through CO_3^{2-} dissolution and ionic regulation, altering biochemical reactions in coastal environments.

The decrease in O_2 concentration (deoxygenation) in coastal water disrupts the biogeochemical cycle of major bioactive elements such as carbon, nitrogen, phosphorus, sulfur, and trace metals. With a lack of O_2, aerobic degradation of OM is limited while the anaerobic pathway thrives. This shift, especially in coastal regions, can lead to the release of NH_4^+, PO_4^{3-}, toxic H_2S, and CH_4 from the seafloor. The reaction of O_2 with these compounds (reoxidation) can contribute to further O_2 loss (Testa & Kemp, 2012). Moreover, low O_2 facilitates multiple biogeochemical feedback. For instance, more efficient recycling

of NH_4^+ and PO_4^{3-}, iron, and manganese from sediment may fuel further algal blooms, thus further reducing O_2 availability. The strength of this feedback ("legacy of hypoxia"), which is particularly relevant in coastal systems, depends on how much OM accumulates at the seabed and the residence time of the overlying water.

O_2 strongly controls the distribution of benthic fauna (Gogina et al., 2016; Laine, 2003; Carman & Cederwall, 2001). There is accumulating evidence and growing concern that low O_2 (i.e., hypoxic) conditions are proliferating in marine coastal environments worldwide (Diaz & Rosenberg, 2008; Gray et al., 2002; Diaz, 2001). Hypoxia can directly and indirectly affect organisms' functioning and survival. Low O_2 leads to migration, reduced respiration rate, and energetically expensive processes such as reproduction, digestion, movement, and mortality of marine animals. Hypoxia affects the behavior, physiology, and ecology of soft-bottom invertebrate communities in ways that translate ultimately to reduced bioirrigation and bioturbation and loss of structural spatial heterogeneity. The changes in sediment benthic communities, in turn, correspond to reduced rates of solute pumping and particle mixing and a shallowing of irrigation and particle-mixing activities within the sediment column (Nilsson & Rosenberg, 2000; Rhoads & Boyer, 1982; Aller, 1980).

1.2 The German Baltic Coast

With the lack of tidal force, the fluctuation of water level in the whole Baltic Sea is mainly driven by meteorological forcing, including wind and precipitation, with its temporal and spatial variability. According to their salinity, the German Baltic coastal waters (inner and outer coastal water bodies) were classified from oligo (salinity: < 5) to mesohaline (salinity: 5 to <18).This coastal marine ecosystem is affected by salinity fluctuation, steady mixing, variation in light level, tight benthic and pelagic coupling, and washout effect (pollution, eutrophication, and hypoxia) from both sea and land load. Short-term thermal stratification may occur during calm periods. On the other hand, small islands and low-lying coastal land are subject to extensive flooding, wind-wave-driven erosion, and sedimentation. In addition to these natural factors, anthropogenic and climatic changes are the main factors shaping the ecological status and biogeochemical function of the coastal zone.

The German Baltic coast is characterized by the mainland and Bodden coast (Lampe, 1996). The development of these coastal types was mainly driven by their geological and geomorphological features, formed predominantly during the Weichselian glaciation period. The mainland coast, also known as the graded shoreline, is very recent and developed only after the last glaciation, ~10,000 years BP. The lithology consists of mainly unconsolidated sediment, predominated by eroded moraine material (glacial and pre-glacial deposits) (Winterhalter et al., 1981). Under westerly wind-induced west-east marine currents, erosion, transport, and sediment accumulation formed the present smooth coastline with beaches and sand dunes. The Bodden coast emerges from the grading processes of Pleistocene island cores, which generate peninsulas and a shallow coastal lagoon system called Bodden and Haff, with outer and inner coastlines. Behind the outer coast, coastal paludification fens often developed, which are episodically flooded with sea water. While coastal flooding fens developed at most of the inner coast shores, the inner coasts are almost entirely lined with coastal wetlands of varying widths. Erosion and accumulation of sandy moraine material predominate the outer coastline, while sedimentation of photogenic material (peat deposit)

fills up the inner coast. These different coastal types existed within a relatively small area and developed into different coastal ecosystems, structures, functions, and processes resulting from the interplay between physical, chemical, and biological factors. Under current and future anthropogenic impact and climate change scenarios, these systems are thought to experience different trajectories. Thus, a system-specific approach is required to understand, monitor, manage, and protect these ecosystems.

In particular, sea level rise driven by climate change is expected to impact ~70% of the global coastlines during the 21st century, including the Baltic Sea (Von Storch et al., 2015; Meier, 2006). The increase in amplitude and frequency of storm surges will lead to more incidences of broken coastal defenses and floods, and strategies to cope with this problem are required. Besides the classical strategy of improving coastal defenses, other ways of adapting to climate change are under consideration. An increasingly popular strategy is "managed coastal realignment," where low-lying coastal areas are permanently flooded with seawater by intentionally breaching existing dikes and building new dikes further inland. The newly flooded area will generate buffer zones for storm surges and protect the more valuable agricultural areas and settlements inland.

Some low-lying coastal areas comprise coastal soil and drained peat soil that will be permanently flooded , forming newly flooded habitats (Turner et al., 2007) . On the one hand, flooding with seawater will cause a shift towards anoxic conditions below a few millimeters in contrast to terrestrial soil, which is more oxygenated in most cases. Anoxic conditions will limit soil OM degradation to mainly anaerobic processes such as fermentation and stimulate respiration with alternative electron acceptors, such as sulfate reduction or denitrification (Sjøgaard et al., 2017; Vasander et al., 2003). On the other hand, the newly inundated area will provide new habitat to early colonizers originating from the marine environment. Pioneering benthic macrofauna such as polychaetes and bivalves are the foundation for food webs and ecological functioning (bioturbation activities) in coastal marine ecosystems. Thus, they will likely modulate overall ecological developments in newly flooded coastal soils. Previous studies imply various levels of benthic macrofauna colonization and succession in constructed marine wetlands depending on larval dispersion strategy, species eco-physiology, and local environmental conditions (Valdermarsen et al., 2018; Garbutt et al., 2006; Bolam et al., 2004; Moseman et al., 2004; Levin et al., 1996). The most critical environmental factors controlling the colonization and succession of benthic fauna are distance to water exchange (i.e., water circulation) and characteristics of the substratum (Garbutt et al., 2006; Levin et al., 1996).

1.3 Objectives

1.3.1 Research Gaps

To date, there are significant knowledge gaps related to the identification and quantification of O_2 sinks and sources in the coastal environment of the Southwestern Baltic Sea. The few measurements conducted within the sandy coastal focus only on MPB species composition and the influence of light on MPB primary production and photosynthetic

performance of MPB (Karsten et al., 2021; Kuriyama et al., 2021; Rieder, 2006), without accounting for potential advective pore-water flow. The work of Schade (2019), within the permeable sediment of the Southwestern Baltic Sea, explored the influence of advection transport on O_2 transport and metabolism in a day cycle. However, the role of MPB was not fully addressed. The coupled effects of light and advective pore-water flow on benthic O_2 fluxes have never been mutually examined. The O_2 measurement conducted by the previous study mentioned above mainly employed a singular technique (microelectrode probed in the sediment or chamber enclosure probed in the water column), which could not provide detailed insight into O_2 distribution and the relative contributions of O_2 fluxes across the SWI.

Benthic infauna activity strongly influences O_2 and nutrient dynamics and acts as ecosystem engineers by changing the physical structure and physicochemical conditions of the SWI. In turn, their behaviors are affected by their environment. Although benthic infauna living in a dynamic coastal environment are known to be resilient, benthic infauna are better suited to specific environmental conditions. While studies on the influence of macrofauna on O_2 dynamic and nutrient fluxes have been mostly reported from their familiar substratum (e.g., benthic coastal marine organisms in coastal muddy-sandy sediment), the role of macrofauna in performing their basic function and influencing O_2 dynamic and nutrient fluxes in foreign substratum, such as flooded mineral and peat soil of a Bodden coast, has not. Furthermore, while both bioturbation studies in soil and sediment address particle reworking in a similar fashion, the magnitude of bioirrigation is rarely investigated in soil studies.

1.3.2 Aims

This thesis aims to investigate benthic O_2 dynamics in two different settings of the shallow coast of the Southwestern Baltic Sea through laboratory experiments.
In the sandy coastal setting (Figure 1.1, station WRD), we investigated the combined role of light, flow and nutrients in governing distribution and metabolism of O_2 produced by MPB. Additionally, we briefly explored the assumption that the MPB community's areal respiration during the light and dark periods is equal. We discuss how MPB affects net ecosystem metabolism, auto- and heterotrophy of the benthic system.

In a substrates typical for the Bodden coast (Figure 1.1, Station PD) we investigate the effect of common bioturbators on benthic O_2 dynamics, solutes, and nutrient fluxes. We compare the bioirrigation performance of *H. diversicolor* in marine sediment and terrestrial soil and assessed the capacity of key bioturbators (*H. diversicolor, M. arenaria,* and *M. neglecta*) to survive and perform bioirrigation in an inundated coastal peat soil. We explore the importance of benthic O_2 introduced through bioirrigation in the rewetted substrates (sediment, soil, and peat soil) and benthic O_2 dynamics around ventilated burrows of *H. diversicolor*. Finally, we compare our laboratory results with field observations to assess the potential success of bioturbators in the early colonization of the restored coastal peatland.

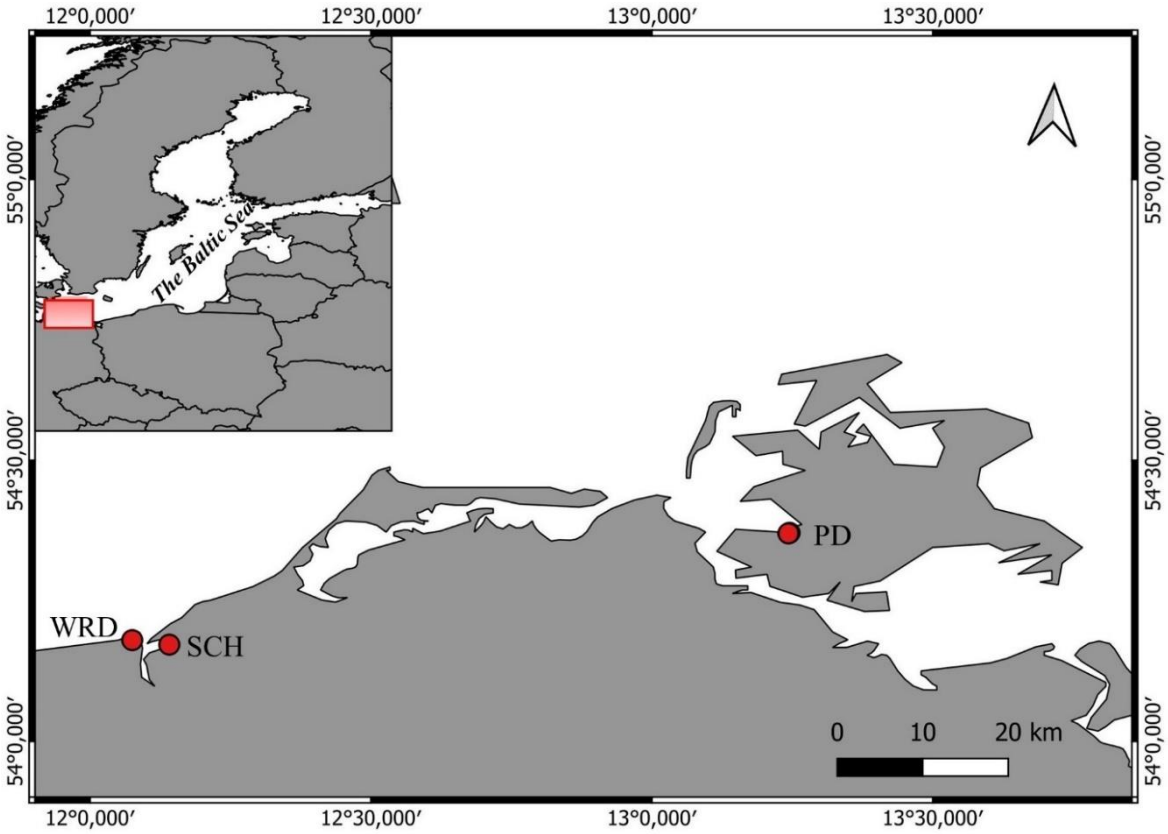

Figure 1. 1 Study sites at the Southwestern Baltic Sea. Sampled station at each site are indicated by the red dots.

2 MATERIALS AND METHODS

2.1 O_2 sensors

O_2 sensors are key tools in understanding O_2 dynamics related to microbial-driven-biogeochemical processes in aquatic environments. Particularly at the SWI, where various physical, biological, and chemical processes occur at the micro-macro scale and at various time scales, the need to measure O_2 concentration has led to the findings and development of O_2 sensors. Different types of O_2 sensors have been widely used to measure O_2 concentration with different spatial and temporal resolutions. Based on their measurement principle, O_2 sensors can be divided into electrochemical and optical sensors (optode). Electrochemical sensors convert chemical reactions involving O_2 into electrical signals, while optical sensors measure light signals due to the interaction between O_2 and immobilized indicator dyes. Furthermore, based on measurement coverage (dimension), the two types of sensors can be divided into needle-type and planar-type sensors. Needle-type sensors have a small sensor tip and measure O_2 at a single point (one dimension), while planar sensors measure O_2 in two dimensions.

This study used the two main O_2 sensors: electrochemical (O_2 microelectrode) and optical (O_2 planar optode and O_2 sensor spot). The following section briefly describes the used sensors and their working principle. The details of the measurement procedures and the parameters derived from O_2-sensor measurement are described in each experimental chapter.

2.1.1 O_2 microelectrode

The O_2 microelectrode used in this study is a miniature Clark-type O_2 sensor (Revsbech and Jørgensen, 1985; Revsbech, 1989) with a guard cathode (OX-25, Unisense). The sensor has a minute tip size (2-3 μm), fast response time (< 0.3 s), low stirring sensitivity (<1 %), detection limit of 0.1 μmol l^{-1}, and stability that could last for months. These characteristics facilitate accurate and fast O_2 measurement with excellent spatial resolution.

The O_2 microelectrode consists of a gold-coated cathode, an Ag/AgCl reference anode immersed in electrolyte solution within a glass casing, and a guard cathode. A permeable silicon membrane, which is ion-impermeable but gas-permeable, is attached to the glass casing, shielding the electrodes from the outside environment. The basic construction of the O_2 microelectrode is shown in Figure 2.1 after a publication by Revsbech (1989).

The O_2 microelectrode measurement system includes an O_2 microelectrode, temperature sensor, and pico-amperemeter (pA) (Fx 1, Unisense) with a USB connection to a PC. The system is integrated with software to calibrate the O_2 microelectrode, control the measurement, store the obtained data, and analyze the obtained data.

The O_2 microelectrode measures O_2 partial pressures. The working principle of O_2 microelectrodes is based on the diffusion of O_2 through the silicon membrane to the cathode, where O_2 is reduced by polarizing the cathode against the anode. The electrochemical reaction generated current, which is directly proportional to the partial pressures of O_2. The resulting current is read by a pico-amperemeter that converts the current to a signal. The guard cathode removes O_2 in the electrolyte, thus preventing O_2 from diffusing towards the sensor tip, minimizing zero-current, and shortening the pre-polarization time. The zero O_2 current was typically around 0 pA.

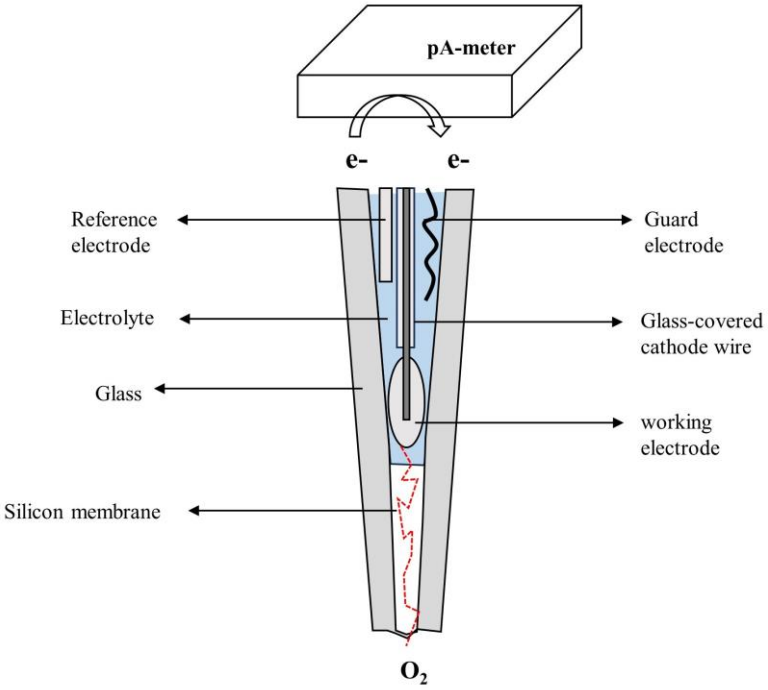

Figure 2. 1 Schematic of Clarke-type O_2 microsensor. Figure modified from Revsbech (1989) and Unisense (2020).

The invention and improvement of microelectrodes have tremendously facilitated direct measurement and understanding of O_2 dynamics on a micro-scale level. Nonetheless, microelectrodes still possess several limitations. Microelectrodes are notably sensitive to signal instability and fragile (prone to breakage) in chemically and physically extreme environments such as acidic, sulfidic, and solid-hard sediment surfaces.

2.1.2 O_2 Planar Optode

A planar optode is a two-dimension (2D) O_2 optical sensor that measures the change in photoluminescence as a function of O_2 (as the analyte) concentration with high spatial (in µm scale) and temporal resolution (Glud et al., 1996; Klimant et al., 1997; Holst et al., 1998; Precht et al., 2004; Polerecky et al., 2005). A general planar optode setup consists of a light sensitive indicator (fluorophore) immobilized in an analyte-permeable matrix coated onto a support material, light source to excite the indicator, and a camera-based imaging system to capture the fluorescent light emitted by the indicator.

O_2 planar optode measurements rely on the ability of O_2 to act as a dynamic quencher of the fluorescence intensity and fluorescence lifetime of an immobilized O_2 luminescent indicator (Klimant et al., 1995). While typically the excited luminophore returns to its ground state through photon emission, in the presence of the O_2, the de-excitation occurs via energy transfer to O_2 molecules (non-luminescent, less fluorescent return light). This process is known as “dynamic collisional quenching” (Figure 2.2). Consequently, the higher the O_2 concentration, the stronger the fluorescence quenching and the weaker the fluorescence emission.

In this study, O_2 concentration in a two-dimensional plane was measured using the planar optode system of VisiSense TD (PreSens – Precision Sensing GmbH, Regensburg,

Germany). The system is integrated with hardware for images acquisition (DU01-camera detector unit with integrated light sources), O_2 sensor foil (SF-RPSu4) for imaging sample surface or through transparent plastic or glass vessels, and software for image recording and image evaluation (VisiSens ScientifiCal and VisiSens AnalytiCal 1). Basic components and connections of VisiSens TD system is shown in Figure 2.3.

The camera detector unit with a resolution of 1292 x 964 pixels provides blue-LED light and detects the emitted light from the foil with a color RGB CMOS chip. Further, it contains a microscope lens with manual focus and optical filters for light diffusion, excitation, and emission. The camera field of view is up to 30 cm x 25 cm with a maximum spatial image resolution of ~2 µm pixel^{-1}. A standard USB connector powers the camera and LED light source. The camera can be used freehand or mounted to a stand.

The foils consist of three layers. (1) An optical isolation layer to prevent color or fluorescent interference from the sample. This layer is 20–50 µm thick, O_2-permeable but not reactive, and in direct contact with the sample. (2) An O_2-sensitive layer contains the fluorescent dyes. This layer is 6-8 µm thick and responds to O_2.

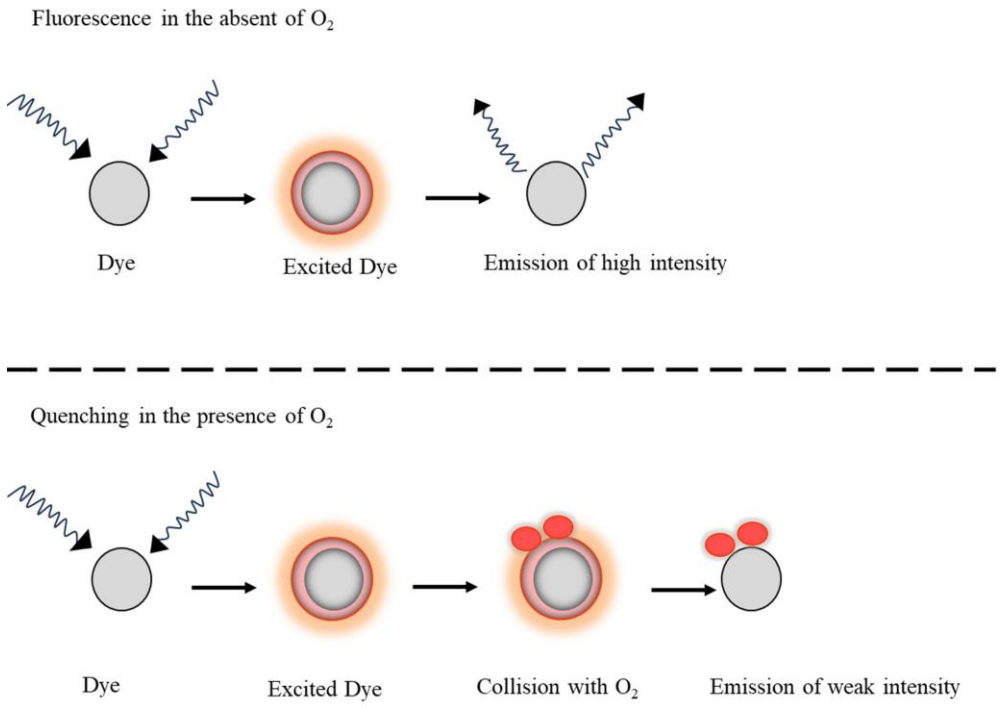

Figure 2. 2 Optodes working principle based on collisional quenching. (A) In the absence of O_2, the excited fluorophore returns to its ground state by emitting high-intensity fluorescence. (B) In the presence of O_2, the fluorescence is quenched by O_2, thus emitting a weaker fluorescence intensity.

(3) A transparent polyester support layer to which the O_2-sensitive layer is attached. This layer is glued to the inside wall of a transparent vessel, e.g., an aquarium. The sensitive layer is in contact with the sample, and the fluorescence is measured from the backside through the transparent vessel's wall. The O_2 sensitive layer consisted of a red luminescent layer, which is dynamically quenched in the presence of O_2, and a green luminescent reference dye that emits a constant green light signal (not affected by O_2). The platinum (II) complex of meso-tetrakis(pentafluorophenyl) porphyrinato complex (PtTFPP) emitting red

dye when excited, serves as the probe for O_2; the fluorophore N-(5-carboxypentyl)- 4-piperidino-1,8-naphthalimide, emitting green light, serves as reference dye. The response time of the foils is ~30 s.

Images were captured in the dark (without ambient light) and digitally recorded as PNG files through a USB connection on a laptop PC. The detector unit's sampling rate and light exposure were set in advance, while the optode foils were calibrated prior and after measurement. In image evaluation mode, before image calibration, the recorded images could be cleaned from interference signals, such as dark areas that do not belong to the sensor foil response and blacks out areas with too bright signals. Images were then smoothed with neighboring data points.

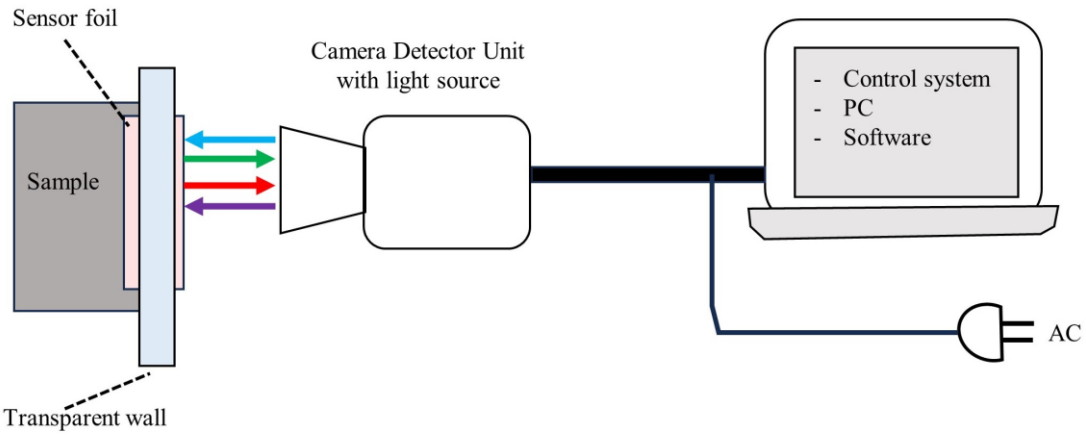

Figure 2. 3 Diagram of the main components of the VisiSense TD system (modified from VisiSens ScientifiCal Manual, 2018)

The VisiSense TD planar optode imaging system is based on color ratiometric imaging, which is part of luminescence intensity-based imaging. The O_2 concentration is calculated from the ratio (ratiometric calibration) by applying a calibration function (see below) derived from measuring the sensor response at known O_2 concentration. The captured color image is split into red, green, and blue (RGB) channels, and the intensity ratio of different color channels is then used to determine the O_2 concentration for every recorded pixel. The used optode shows a nonlinear decrease in the signal with increasing O_2 concentrations. Linearity conversion of the measured luminescence images to O_2 concentration was obtained by applying the Stern-Vollmer equation to the measured luminescence images (Tschiersch et al., 2011). These steps are incorporated in consecutive operations within the image processing software. Further details about optical O_2 imaging, sensor materials, measuring, and calibration procedures are given in the literature (Wang et al.,2010; Meier et al., 2011; Tschiersch et al., 2011; Tschiersch et al., 2012).

2.1.3 O_2 sensor spot

The O_2 sensor spot used in this study is a 1D (single point) fiber-optical O_2 sensor and relies on the same luminescence measuring principle as in planar optodes (above). The sensor spots are of 5-8 mm diameter (Pyroscience GmbH, FireStingO_2 User Manual). One side of the spot has a rough sensing surface coated with a particular dye (Redflash

technology) in direct contact with the measured object; the opposite side has a smooth PET foil as carrier material glued to the inner container walls of the measured object). With these features, the sensor spot enables O_2 measurement in a closed container with contactless read-out through a transparent surface, simplifying O_2 measurement (without sampling) and preventing potential contamination of the measured system.

The measuring system used in this study is commercially available, called Firesting O_2 (compact PC-based fiber optic O_2 meter), provided by PyroScience. The measuring configuration comprises sensor spots, fiber optics, and an O_2 meter operated via USB. Additionally, a temperature sensor can be incorporated for automatic temperature compensation of the O_2 measurement. The system is embedded with logging software (Pyro O_2 Logger, PyroScience), which facilitates calibration and O_2 measurement (in logging mode).

The Redflash indicators are excitable with red light (610-630 nm) and show O_2-dependent luminescence in the near-infrared (NIR 760-790 nm). The excitation light is supplied to the sensor patch via optical fiber fixed at the outer side of a transparent vessel. The O_2 meter (Firesting O_2 meter) measures the phase shift of the sinusoidally modulated red emission in the NIR. The phase shift is then converted into O_2 units based on the Stern-Vollmer Theory (Tschiersch et al., 2011).

2.2 O_2 dynamics in sandy permeable sediment inhabited by diatom dominated-MPB community- Laboratory Benthic chamber incubation

2.2.1 Field sampling

Sediment and seawater were sampled in April 2019 at 54° 0.018 N, 12° 0.075 E (Station WRD in Figure 1.1). During this day, the water temperature and salinity were 16.7 °C and 10, respectively. Sediment was shoveled and sieved through 1 mm mesh on site to remove shells and other detrital debris before they were transported to the laboratory. The collected sediment (submerged with seawater from the site in containers) and seawater were stored in a dark climate room of 15 ± 1 °C before use.

2.2.2 Experimental setup of laboratory benthic chambers

In September 2019, diatoms typical for the Baltic Sea (*Navicula perminuta, Nitzchia pusilla, Hyalodiscus scoticus*) were grown in plastic trays filled with 1.5 cm sediment submersed in 1-2 cm of seawater from the sampling site. These inoculates were kept in a climate room at 15 °C and under controlled light, mimicking the average in situ light condition (ca. 40 µmol photon m^{-2} s^{-1}) based on previous findings (Schade, 2019). The light was supplied by fiber-optic halogen light sources (fluorescent tube, Osram Lumilux Deluxe T8, daylight white) and LED (Kern & Sohn, daylight). This combination provided a photosynthetically active radiation (PAR) range of 400-700 nm. The specific inoculation irradiance was obtained by adjusting the distance between the light source and the sediment surface. During inoculation and later during the O_2 measurement, light intensity was measured by a planar underwater quantum irradiance sensor (LI-192, Li-Cor). The daily light regime during inoculation was set to 12 h darkness and 12 h illumination. Inorganic nutrients consisting of F/2-medium (20 ml l^{-1} seawater) and meta-silica (600 µl l^{-1} seawater)

were added biweekly to boost the growth of the diatoms and, eventually, the diatom-dominated-MPB mat.

In October 2019, benthic chambers (*n = 9*) were prepared before incubation with the developed MPB mat. The benthic chamber used in the laboratory experiment was made of a clear acrylic cylindrical chamber (32 cm height and 19 cm inner diameter) with a lid and sealed bottom. A flat transparent rotating disk (15 cm diameter) was attached to the lid to stir the water inside the chamber. The stirring of the disk was powered by a motor connected to the lid. The disc's rotation speed was set to produce a radial pressure field (Huettel & Gust, 1992), which generates advective pore water flow inside the incubated sediment if permeable (Huettel & Gust, 1992). Chamber calibration (stirring rotation speed vs. radial pressure gradient) was previously measured by Schade (2019), whose results were used to select the stirring rate in this study (see below). Chambers were equipped with a 1.5 cm x 8 cm (width x length) planar optode sensor foil (PreSens, GmbH) glued to the inside wall of the chambers such that 3 cm of the optode was above and 5 cm was below the level of the SWI.

Of the prepared chambers, three chambers were filled with only sediment (hereafter refers as C chambers) and seawater (salinity: 15), and six chambers with the addition of a bottom layer of finely chopped green macroalgae (*Ulvaceae*) mixed with 1 cm thick of agar (hereafter refers as RC chambers). This base layer acted as a source of reduced compounds diffusing upward into the otherwise organic-poor sand. The total volume of the sediment was adjusted to the chambers' stirring geometry (40 rpm ~ pressure gradient of 3.6 Pa) (Schade, 2019). The chambers were kept in the dark climate room at 15 ± 1 °C with continuous aeration by an air stream over the water surface (height of ~ 5 cm) for two weeks before adding the developed MPB mat. During this period, chambers were wrapped with a black sleeve to shield and protect the sensor foils from photo-aging.

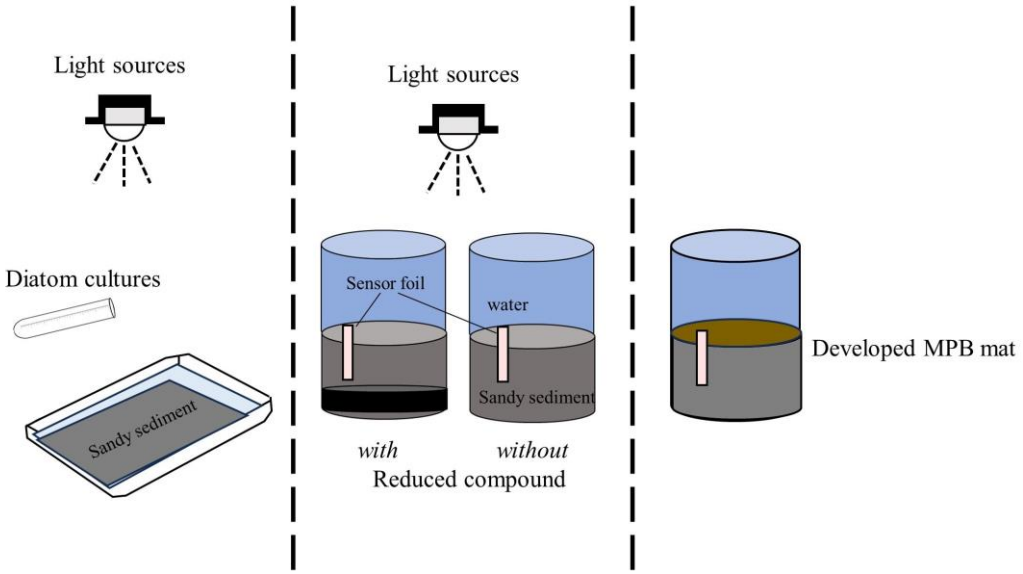

Figure 2. 4 Illustration of benthic chamber preparations: growing of MPB in the trays, benthic chamber preparation, and transfer of developed MPB into benthic chambers.

After six weeks, the MPB that had developed in the trays was transferred into the prepared benthic chambers, and the sediment surface was leveled. Chambers were kept in

the same climate room and under the same illumination setting as the trays during diatom inoculation and were continuously flushed with air. The same inorganic nutrient used in the trays was added biweekly during this incubation. Water salinity, temperature, dissolved O_2, and pH were monitored weekly with a multiparameter electrode (HQ Hach Lange). The development of the MPB mat in the benthic chambers was left from October 2019 – May 2020. Hereafter, a steady state was assumed. A schematic drawing of the experimental setup is illustrated in Figure 2.4.

2.2.3 O_2 Measurements

All O_2 measurements were conducted in the 15 ± 1 °C climate room, where benthic chambers were incubated after the MPB mat had been established in the benthic chambers (Figure 2.5). Microelectrodes were used to measure O_2 distribution, potential photosynthesis, and O_2 consumption rate. In parallel, planar optodes were used to assess two-dimensional O_2 distribution, fluxes, and consumption rate. Finally, total O_2 uptake (TOU) was measured using O_2 sensor spots.

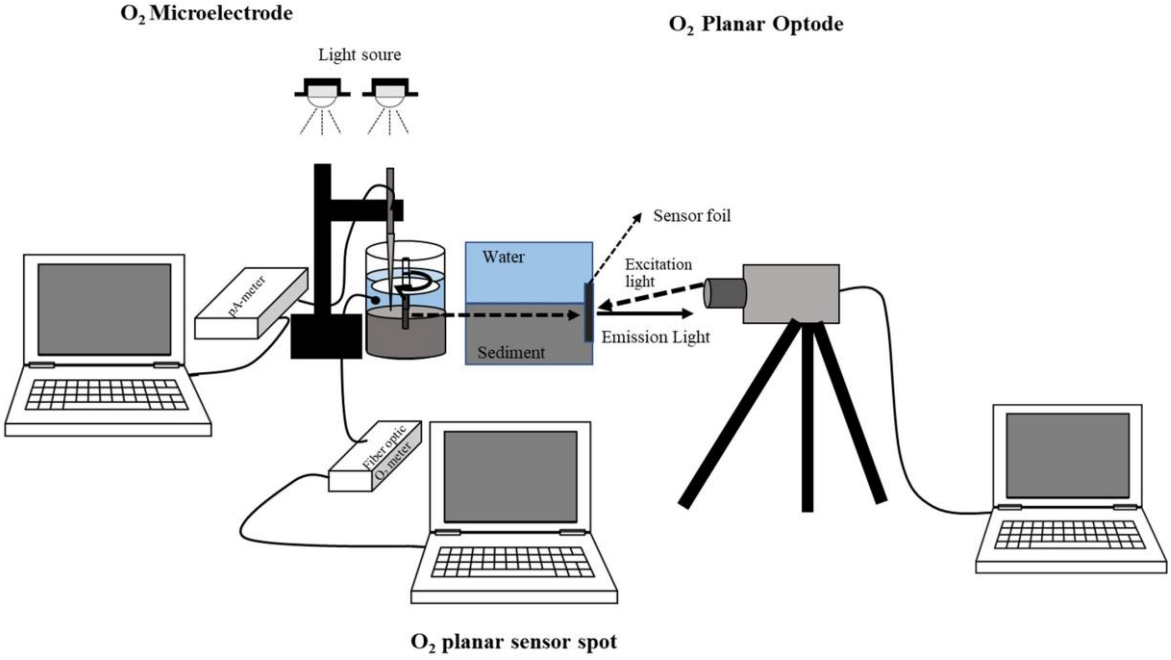

Figure 2. 5 Schematic of the laboratory benthic chamber setup showing an O_2 measurement with microelectrode (left), sensor spots (middle), and planar optode (right).

O_2 microelectrode measurements

O_2 microprofilling. Depth profiles of dissolved O_2 were measured starting at the water column into the sediment with O_2 microelectrode. The microelectrodes were mounted on a manual micromanipulator to control the vertical and horizontal position of the sensor. The Sensor Trace software (Unisense) provided control over data acquisition. Before the measurement, the sensor was routinely left to polarize and calibrated with 2-point linear calibration (100% saturation point in bubbled fresh water and 0% saturation point in sodium dithionite ($Na_2S_2O_4$) solution or the anoxic part of the sediment. For some measurements, e.g., a broken electrode, a calibration in retrospect was performed with previously recorded signals of 100% and 0% points.

O_2 profiles were recorded with a vertical resolution of 100 or 200 µm and with a waiting time of 3 s between point readings. Dark profiling was conducted in the morning after an overnight dark incubation (~10 – 12 h), followed by light profiling with stepwise increases in light intensity (0, 40, 70, 100 µmol m^{-2} s^{-1}). Different light intensities were obtained by manually shading the light path with a black screen mesh. Irrespective of whether experiments were run, the system was kept at the same light regime of 12 h darkness and 12 h illumination. A minimum of three microprofiles were recorded per chamber for each light level, located ~2 cm in front of the planar optode foil and within approximately 0.5-1 cm horizontal distance from each other to include the spatial variability of the mat. After every increase in light intensity level, 15 to 30 min of recuperation time was given. During microprofilling, the water column was carefully aerated with bubble stone to ensure complete mixing of the overlying water. The position of the SWI was determined from individual O_2 profiles by selecting the steepest O_2 concentration gradient with depth. The O_2 penetration depth was determined from the depth where the O_2 microelectrode signal reached zero current.

O_2 fluxes. Diffusive O_2 flux, J(x), was calculated from steady-state O_2 microprofiles by applying Fick's 1st law of one-dimensional diffusion (Revsbech et al., 1986):

$$J(x) = -\Phi\, Ds\,(x)\,\frac{dC(x)}{d(x)} \qquad (1)$$

where C(x) is O_2 concentration at depth x, ϕ is porosity, and Ds is the O_2 diffusion coefficient in the sediment. Ds is related to salinity and temperature-dependent free solution diffusion coefficient, D_0 (Boudreau, 1997) through the equation $Ds = D_0\,\phi$. Ds was corrected for sediment tortuosity following Archie's Law ($\theta = \phi^{1-m}$, with m = 2 for sand; Boudreau, 1997. Flux measurements are illustrated in Figure 2.6. *Dark respiration* (R_{Dark}) of the sediment was estimated as the flux of O_2 into the sediment ($J_{(x)\ down}$) calculated with Eq.1. *Net production* (NP) was calculated (also with Eq.1) as the sum of diffusive O_2 fluxes from the photic zone: upward towards the overlying water sediment ($J_{(x)up}$) and down into the sediment ($J_{(x)down}$) (Glud et al., 1992; Glud, 2006), from microprofiles obtained in the light. *Gross production* (GP) was calculated as the sum of R and NP at a given light intensity, assuming light respiration equals dark respiration (Revsbech et al., 1981; Glud et al., 1992; Glud, 2006).

Depth distribution of gross production at a given light intensity was additionally determined with the microelectrode light-dark shift technique (GP_{LDS}). GP_{LDS} was estimated as the initial decrease of O_2 upon a brief period of darkness. The theory of this method (Revsbech & Jørgensen,1983; Glud et al., 1992) is based on the transition following a steady state O_2 distribution in the light (eq. 2 and 3) into the shaded situation (eq. 3) without production (Pz) and a substitution of (4) into (2) yielding (5):

After Light: $$\frac{dC(z)}{dt} = Ds\,\frac{d^2C(z)}{dz^2} + P(z) - R(z) \qquad (2)$$

At steady state: $$\frac{dC(z)}{dt} = 0 \;\Leftrightarrow P(z) = R(z) - Ds\,\frac{d^2C(z)}{dz^2} \qquad (3)$$

In the dark: $$\frac{dC(z)}{dt} = -\left[R(z) - Ds\,\frac{d^2C(z)}{dz^2}\right] \qquad (4)$$

Thus: $$P(z) = -\frac{dC(z)}{dt} \quad (5)$$

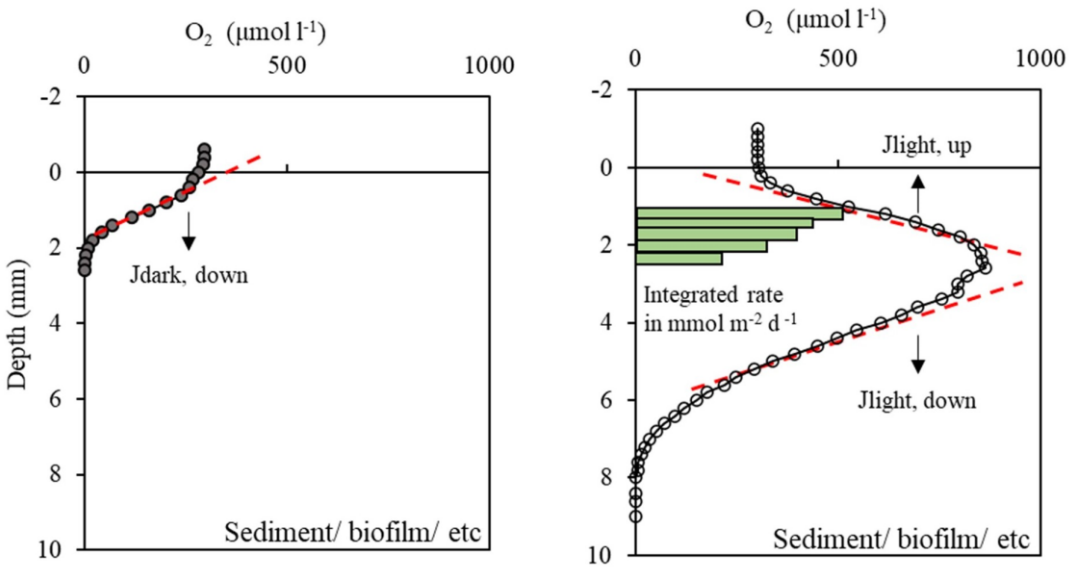

Figure 2. 6 Basic principle of O_2 fluxes calculation from two microprofiles measurements: in dark (left), in light of 100 µE m^{-2} s^{-1}(right). The green bars in the light profile indicate the gross photosynthetic rates measured by the light-dark-shift technique at depth. The illustration was modified from Glud (2006), and the graph was derived from own data.

Following O_2 light profiling, the O_2 concentration was continuously logged (with the logging mode of the Sensor Trace software) at respective depths, and shading with a black screen was manually applied. Depending on the photosynthetic rate, 2 to 10 seconds of darkness were necessary to record a decline in O_2 concentration. For the highest light intensity (100 µmol m^{-2} s^{-1}), photosynthetic activity was measured in 100 µm depth increments throughout the photic zone. At lower light intensity, the measurements were performed in a minimum of three discrete depths (upper part, peak, lower part of photic zone), selected according to the previous light profile. Three measurements were taken at each depth, and their mean value was used.

PI-curve. A photosynthesis irradiance (PI) curve was constructed from irradiance against calculated net production to describe the relationship between photosynthesis and irradiance (Figure 2.7, after Lally & Parson, 2004).
The curve was fitted by a simplified function of Plat et al. (1980) by Roberts et al. (2002):

$$P = Pm\,(1 - exp(-\alpha Id/Pm)) + R \quad (6)$$

where P is the photosynthetic rate, Pm is the maximal production rate at light saturation, α is the initial slope of the light curve before saturation, Id is the irradiance, and R is the respiration rate. Light acclimation intensity (Ik) was calculated as Ik = Pm/α, while the compensation irradiance (Ic) was calculated by solving the P/I equation for Id when P = 0. Gross photosynthesis is indicated by Pg, and net photosynthesis by Pn (see Figure 2.7, Pn=Pg - R). All P/I curve fitting was conducted with the Excel add-in Solver (MS Office 2019, Microsoft Cooperation).

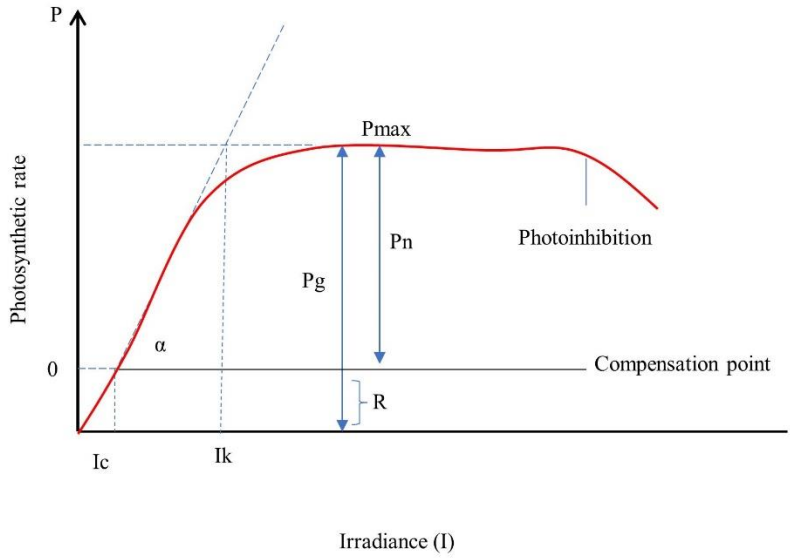

Figure 2. 7 Illustration of a PI-curve derived from the response of photosynthesis to change in irradiance (after Lally & Parson, 2004).

Respiration in the photic zone in light (R_{Light}) was calculated as the difference between the integrated rate of gross photosynthesis and net production.

Volume-specific O_2 production and consumption rates (R_{vol}) and integrated areal O_2 production and consumption were calculated from O_2 microprofiles (with the profiling mode of the Sensor Trace software). The program uses the shape of a measured concentration profile based on the method published by Berg et al. (1998). The volume-specific consumption and production were determined using Fick's 2nd law of diffusion:

$$Rvol = Ds \ \frac{d^2C}{dx^2} \qquad (7)$$

where R is the net volumetric rate (nmol cm^{-3} s^{-1}) of production (positive values) or consumption (negative values).

2.2.4 Impact of pore water advection

The following procedure was designed to explore the influence of advection on O_2 spatial distribution, fluxes, and consumption rate in the dark and in the light compared to diffusive settings.

O_2 distributions. Steady-state O_2 depth profiles were measured in the dark after incubating the chamber in darkness overnight. Subsequently, the sediment was exposed to advection by stirring the chamber (stirring of the water, one-way disk rotation of 40 rpm = ~ 3.6 Pa), which lasted for ~2 h. After stirring was stopped, O_2 microprofiles were measured immediately. The highest light intensity of 100 µmol m^{-2} s^{-1} was chosen for measurement in light. After overnight dark incubation, the following morning, chambers were illuminated for ~2 h before measuring steady-state O_2 depth in the light. A similar advection procedure (~2 h exposure to advection) was followed with continuous illumination. Subsequently, the stirring was stopped before the following O_2 depth profiling was started. The time lag between the end of stirring and the start of the profiling was ~ 15 min. The obtained profiles after exposure to advection were considered to inherit most of the properties of O_2

distribution under ongoing advection. The speed rotation of the disc was chosen based on the previous investigation by Schade (2019), reporting boundary layer flow velocity (under wave) of <0.14 m s^{-1} as the most frequent velocity in the shallow coast water of the sampling location. Between measurements in the dark and light, chambers were allowed to equilibrate in darkness (minimum overnight).

O_2 fluxes were calculated from the obtained O_2 profiles as described in section benthic O_2 fluxes.

O_2 consumption rate. Potential O_2 consumption rates (OCR) were determined as the initial slope of the observed decrease of O_2 concentration with time by regression analysis as described previously (Glud et al., 1992; Precht et al., 2004; Polerecky et al., 2005). O_2 concentration was recorded with microelectrode positioned at discrete depth of the sediment (close to the sediment surface, oxic layer, and oxic-anoxic boundary) after benthic chambers were exposed to different light and transport regimes: to only light of 100 µmol m^{-2} s^{-1} and diffusion (Ldif), to light of 100 µmol m^{-2} s^{-1} and stirring at 40 rpm (Ladv), and to only stirring at 40 rpm in the dark (Dadv). Each exposure lasted for ~ 2 h, followed by recording for at least 30 min.

2.2.5 O_2 planar optode measurements

Calibrations of O_2 sensor foils. Before and after experiments, a two-point calibration was performed as prescribed for the VisiSense optode system by recording images corresponding to 0 % and 100% air saturation. Image recording for 100 % calibration point was taken after exposing the sensor foil to aerated seawater, while the image for 0% point was taken after exposing the sensor foil to O_2 -free water (by dissolving $Na_2S_2O_4$ in the seawater) or from the deep anoxic part of the sediment captured in the image. Calibration was done at the same temperature and salinity as the respective experiment.

2D O_2 distributions and fluxes. 2D O_2 distributions were measured using the planar optode system of VisiSens TD (PreSens GmbH) with sensor foil previously fixed to the inside wall of every chamber. O_2 images were recorded following different light and transport regimes: from dark diffusive to light diffusive, light diffusive to light advective, and dark diffusive to dark advective. In contrast to microelectrode measurement, where profiling was conducted at the start and endpoint of each regime, optode measurements were conducted continuously with a temporal resolution of one image per 5 min over a ~2 h period per regime. During image acquisition, the pathway between the optode foil and the camera detector unit was shielded from light using black cloth. The camera detector unit was fixed at a constant distance of 5 cm from the foil for all measurements.

The acquired images covered an area of 6.8 x 9 cm with a spatial resolution of 14 to 15 pixels per millimeter (i.e., 0.07 mm $pixel^{-1}$). The light illuminating the chamber was set on a timer, which turned off the light for a 3 s period synchronized with the image acquisition time.

O_2 spatial distributions were further evaluated from depth concentration profiles of O_2. O_2 profiles were extracted from the calibrated O_2 image using the Image Profiler RC 0.5.1 (a software extension for VisiSense ScientifiCal software) by selecting a vertical region of interest (ROI) across the sediment. The software automatically generated O_2 concentration (% air saturation) from the chosen ROI, which was then converted to O_2

concentration in µmol l^{-1} using the solubility of O_2 in the water at respective temperature and salinity. From the obtained O_2 profile, the 1-dimensional diffusive O_2 fluxes were calculated following the manual procedure used for microelectrode.

2D O_2 consumption rate. 2D images of pore water O_2 concentration were immediately recorded after exposure to different light and transport regimes (see above) were stopped. O_2 images were continuously recorded in 5-minute intervals and typically during 30 min to ~ 3 h in chambers with a low consumption rate. Three ROIs were selected from every image: above the sediment surface, oxic layer in the sediment, and oxic-anoxic boundary in the sediment to monitor O_2 concentration over time. The area was manually selected from the optode image, which shows the most prominent area affected in the recorded time series. Averages of O_2 concentration were extracted from the designated ROI per recorded images using the Image Profiler RC 0.5.1 or the Z-axis profile and ROI statistics (a feature included in the VisiSens Scientifical image processing software). The 2D local OCR was calculated by fitting the change in the average O_2 concentration over time in pixels of each chosen ROI (Precht et al., 2004; Polerecky et al., 2005). OCR was expressed per volume of pore water.

2.2.6 O_2 sensor spot measurement

Total O_2 Uptake (TOU). The TOU of the sediment in each benthic chamber was measured in the darkness before the termination of the respective chamber. Chambers were equipped with an O_2 sensor spot fixed with silicon glue inside the chamber wall, filled with modified seawater (salinity 15), and carefully sealed (excluding air bubbles) with the chamber lid. The sensor spot system was set to measure O_2 concentration every 5 min over a ~15 h period, monitoring depletion of dissolved O_2 in the water column and calibrated before and after the measurement with a two-point calibration. The 100% O_2 saturation point was measured in O_2-saturated fresh water, while the 0% saturation point was achieved by adding $Na_2S_2O_4$. O_2 concentration was measured only under a diffusive setting (one-way rotation of 10 rpm = 0.2 Pa).

The TOU was quantified, assuming a linear change in O_2 concentration over time. The areal rate of TOU (mmol O_2 $m^{-2}d^{-1}$) was calculated from the change in O_2 concentration over time (ΔC [µmol l^{-1} d^{-1}]), taking into account the volume of the overlying water (V_{H_2O} [l]) and the area of the enclosed sediment (A_{Sed} [m^2]).

2.2.7 Liquid phase analysis

At the end of O_2 measurements in the laboratory benthic chamber experiment, overlying water and pore water were sampled for nutrient analysis before the termination of every chamber. Overlying water was sampled with a 30-ml syringe and filtered through a glass microfiber filter (0.45 µm GF/F, Whatmann), while pore water was directly extracted from the sediment with rhizon samplers (Rhyzophere). Here, rhizon samplers were vertically inserted into the sediment and sampled at depth intervals of 0-3 and 3-6 cm. Water samples were frozen immediately and stored until further analysis.

Overlying water and pore water samples were analyzed colorimetrically following the method of Grasshoff et al. (1999) on a continuous flow analyzer (QuAAtro, Seal). Methods were adjusted according to Seal's protocol and modified for small sample volumes of 1 ml

for all nutrient analyses. Furthermore, phenol was replaced by sodium salicylate. Detection limits differed between overlying water and pore water samples. Limits for overlying water analysis were: PO_4^{3-}: 0.1; NO_3^-: 0.2; NO_2^-: 0.05; NH_4^+: 0.5 and SiO_2: 1 µmol l^{-1}, while limits for pore water analysis were: PO_4^{3-}: 0.25; NO_3^- 0.5; NO_2^-: −: 0.1; NH_4^+: 1.5 and SiO_2: 2 µmol l^{-1}.

2.2.8 Solid phase analysis

Three replicates of sediment were sampled with core liners (3.6 cm i.d.) during sediment collection and after benthic chamber incubation for sediment physical property analysis. The top 2 cm layer from the core liner was sub-sampled with a 5 ml cut-off plastic syringe and homogenized to analyze bulk density, water content, porosity, total organic matter, and chlorophyll *a* (Chl. *a*) concentration.

Sediment bulk density was calculated as the weight of a known volume:

$$\rho = \frac{\text{sediment mass}}{\text{sediment volume}} \quad (8)$$

Sediment water content (β) was calculated as weight loss upon drying at 60 °C for 12-24 h as follows:

$$\beta = \frac{(\text{wet weight} - \text{dry weight})}{\text{wet weight}} \; X \; 100 \; (\%) \quad (9)$$

Porosity (ϕ) was determined from the sediment density and the weight loss after oven drying:

$$\phi = \beta \; \text{x} \frac{\rho}{100} \quad (10)$$

Sediment organic content was determined as percentage mass loss on ignition (LOI) from dried sediment samples combusted for 10 h at 500 °C as follows:

$$\text{LOI} = \frac{(\text{dry weight} - \text{ash weight})}{\text{dry weight}} \; X \; 100 \; (\%) \quad (11)$$

Chl. *a* content as a proxy for MPB biomass was measured fluorometrically (TD 700, Turner Design), employing deep-freezing (24 h) and 90 % ethanol for extraction at a volume ratio of 9:1. 1 cm3 of the sub-sampled sediment was mixed, homogenized, and placed in a test tube containing 9 ml ethanol. The test tubes were shaken vigorously and refrigerated in darkness during overnight extraction. After extraction, the test tubes were centrifuged (4000 rpm, 5 min), and the supernatant was then measured in the fluorimeter. Measurement was done before and after acidification (removal of phaeopigments) with the addition of 125 µl 1 N HCL. Chl. *a* content in the sediment is reported here as µg Chl *a* per ml sediment.

The C: N molar ratio of the sediment was calculated from C and N mass determination with a C: N elemental analyzer (NC2500, CE Instruments.). Approximately 100 g of dry sediment was mortared, wrapped in silver foil, and subsequently measured in the C: N analyzer.

Grain size analysis was performed by wet-sieving (>1000, 100-500, 500-250, 250-125, <63 µm) and oven dried at 60 °C for 12 - 24 h. 100 g sediment was weighed and rinsed through stacked sieves. The weight of grains <63 µm was estimated by subtracting the cumulated weight (all size fractions) from the initial dry weight of the sediment used in the analyses. The percentage in weight for every size fraction, the median diameter, and the sorting degree were calculated according to Folk and Ward (1957). The sediment was classified manually according to Wentworth's (1922) and with Gradistat, a particle size analysis software (Blott & Pye, 2002).

Permeability measurements were performed in an intact sediment core (3.6 cm i.d, 15 cm length) taken upon the termination of the benthic chamber incubation. Permeability was measured for the top 5 cm of the sediment with the falling head method (Head, 1982). A minimum of three replicate sediment cores were taken from every chamber, and measurement was performed repeatedly (3 times) for every sediment core.

2.3 O_2 dynamics associated with bioirrigation

2.3.1 Study site and pilot study

This study was conducted in association with the nature restoration project of the coastal floodplain at Polder Drammendorf, southwest of the island of Rügen, northeastern of the German Baltic Sea coast. The low-lying area (Station PD in Figure 1.1) has been dyked and drained from the brackish water of the Kubitzer Bodden (salinity 8- 9) for more than 100 years for land reclamation, mainly used for agriculture. Restoration of the area was done by breaching a selected section (~20 m wide) of the established dyke in November 2019. The adjacent water of Kubitzer Boden immediately flooded the area behind the dyke, and approximately 0.5 km^2 of the restored area (from 0.8 km^2 total restored area) was permanently flooded (average water depth of ~ 0.5 m). The water exchange between Kubitzer Boden and the newly flooded area is highly dynamic and directly influenced by the water level of the Baltic Sea. Eventually, it regulates the newly rewetted area's water coverage, temperature, and salinity.

The rewetted area is a former coastal peatland that has experienced long-term and intensive draining, leading to soil degradation and peat oxidation. The northern part of the area was primarily composed of mineral soil, while the southern part consisted of organic soil. Previous investigation suggests that the topsoil of the central part consists of up to 50–70 cm of highly degraded peat (Brisch, 2015), classified as H7 according to the von Post humification scale (Wang et al., 2021). Underneath the degraded topsoil is a well-preserved peat layer with a thickness of ~100 cm. The highly degraded topsoil layer was kept intact.

For this study, the study site has been occasionally visited and observed since June 2019 (Table A.4). Several soil cores were taken with acrylic core liner (3.6 cm i.d) to a depth of 20 – 25 cm for analysis of bulk density (wet and dry), water content, organic content via loss on ignition, particle density, porosity, carbon (C) content, and nitrogen (N) content (Table A.5). In the laboratory, every core was sliced in 1 or 2 cm intervals down to 6 cm depth, and vegetation that occupied the soil surface was carefully removed. The slicing is done by carefully pushing the soil core inside the liner up to the chosen thickness. Sampling for macrofauna at the seaside was also conducted several times before and after the

inundation (Table A.6). The method used to analyze soil characteristics and macrofauna sampling is described in the soil analysis and macrofauna colonization section. Sampling points of soil collection for laboratory experiments were chosen based on soil characteristics from our pilot study (Station 14, Table A.6), the predicted water level with future access to the site (Drammendorf site plan, UmweltPlan GmbH Stralsund, Germany), and comparison with other pilot studies within the project of Baltic-Transcoast.

2.3.2 Experiment 1: Bioirrigation of *Hediste diversicolor* in different coastal substrates of the Southwestern Baltic Sea (MCF Exp 1)

Collection of substrates and *Hediste diversicolor*

For the first experiment, loose soil was collected from the excavated topsoil prior to the rewetting in Polder Drammendorf in May 2020. Around the same time, marine sediment, hereafter referred to as sediment, was collected from Schnatermann (Station SCH in Figure 1.1.), a shallow brackish water bay located at the Warnow River near Rostock, Germany. Sediment was taken from a water depth of approximately 0.5 m. Both soil and sediment were sieved through 1 mm mesh and homogenized.

The polychaete *H. diversicolor* and seawater were collected from the same site as the sediment. The worm size was ~ 2 cm long, described as typical adult size, and weighed between 0.053 and 0.360 g ($\bar{x}$: 0.156 g). On this collection day, the water temperature was 20.4 °C, the salinity was 8.9, and the pH was 8.4. The animals were transferred to the institute and were kept in aquariums filled with approximately 3 cm of their original sediment for approximately two weeks under control conditions (Temperature: 15 °C, salinity: 9) for acclimation.

Before soil and sediment core preparation, the water column pH of the soil core inundated with seawater was observed over a week. This observation was conducted to ensure that *H. diversicolor* would withstand the incubation with the soil.

Experimental design

Eight 60 cm long acrylic core liners (10 cm i.d.) were filled with 12 cm homogenized sediment from Schnatermann (n = 8) and topsoil from Drammendorf (n = 8), respectively. The cores were each inundated with 1-2 cm height seawater (salinity: 9), sealed with plastic wrap, and pre-incubated for 4 weeks in the dark to gain a near-steady condition after the homogenization. The dissolved O_2 and pH of the water column were monitored with a multiparameter electrode once every week.

After the sediment had been allowed to settle within the cores for 4 weeks, a magnetic stirrer was attached to the inner wall of the sediment cores – approx 16 cm above the substrate surface. The cores were randomly divided and grouped (4 replicates each) into four treatments: azoic control of sediment (MC), sediment colonized with *H. diversicolor* (MHD), azoic control of Drammendorf soil (DC), and Drammendorf soil colonized with *H. diversicolor* (DHD).

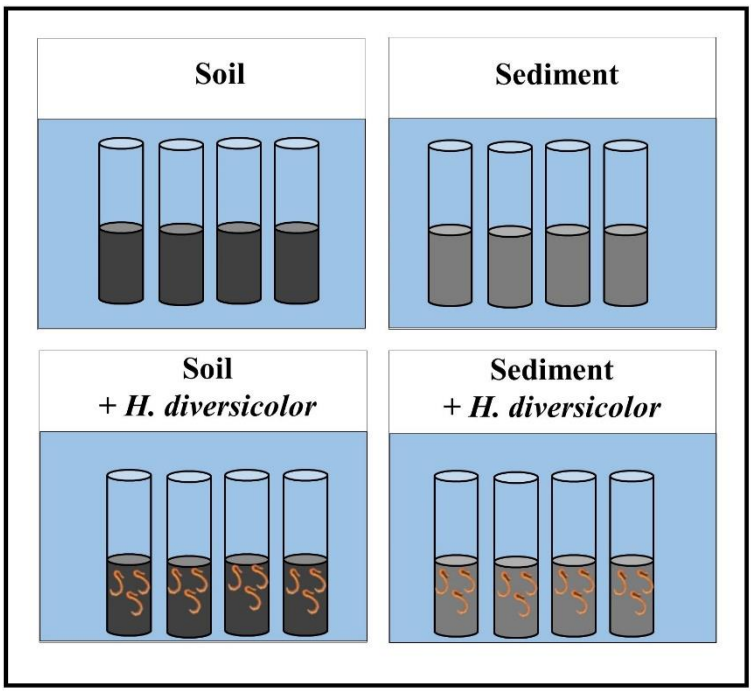

Figure 2. 8 Scheme of the experimental setup showing the different treatments and addition densities.

The grouped cores were then placed into four separate tanks (volume 60 l) filled with seawater (salinity: 9) and placed in a cooling basin of 15°C. Each treatment tank was equipped with a 12V motor of magnetic stirrer, placed in the middle of every tank to control the magnetic stirrer inside every core, thus ensuring a complete mixing of overlying water and sufficient O_2 supply into the sediment core. The water inside each tank was continuously aerated with air stones but with power adjustment to avoid resuspension of the substrate.

Three intact and healthy *H. diversicolor* were added to the treatment MHD and DHD. The total fresh weight of polychaetes per core (MHD: 0.5 ± 0.1 g, DHD: 1.0 ± 0.1 g) was determined before introducing the animals to the randomly chosen sediment and soil cores. This number equates to biomass of 64 g m^{-2} and 127 g m^{-2} for MHD and DHD, respectively, per individual of *H. diversicolor.*

The O_2 uptake (TOU)

The TOU of the substrate (all treatments and their respective replicate cores) was measured one week after adding *H. diversicolor.* The TOU of the soil and sediment was measured with an O_2 sensor spot system as used in the experiment with benthic chambers and calculated accordingly. However, the O_2 sensor spot was attached under every core's lid. During the measurement, the core was sealed with the lid, and the magnetic stirrer was utilized to ensure the mixing of the water column. O_2 concentration in the water column was recorded for 16 hours in 2 min intervals.

Bioirrigation activity

The bioirrigation activity of *H. diversicolor* was determined by Bromide (Br^-) tracer incubations (Martin & Banta, 1992; Forster et al., 1999). The water reservoir in every tank was enriched with sodium bromide (NaBr) to a final concentration of ~10 mM three days before the experiment was concluded. At the end of the incubation, every core was sliced one at a time, spanning the incubation time from 72 h to 77 h. Irrigation was quantified from the excess Br^-inventory in faunated sediment (see chapter calculation of Br^--inventories). The maximum bioirrigation depth (i.e., maximum burrow depth) was determined as the deepest layer where the concentration of Br^- was significantly elevated above the background.

Sectioning and pore water extraction

After 3 days, Br^- incubation was terminated, and the cores were subjected to slicing. Overlaying water inside each core was sampled (30 ml) before the water core was carefully drained. Sediment cores were sliced into 0.5 cm intervals to a depth of 1 cm, followed by a 1 cm interval to a depth of 5 cm and a 2 cm interval to 11 cm. The residence depth of polychaeta was noted during the sectioning. Subsamples of sediment and soil from every layer were taken to determine their characteristics (see section Laboratory Benthic Chamber Solid Phase Analysis for sediment and in the following section of soil analysis).

Porewater from every core was extracted from the subsample of each slice of the sediment core by centrifuging (2 min at 2000 rpm, The Heraeus® Megafuge® 1.0) in centrifuge tubes equipped with GF/F filters as described by Saager et al. (1990). The obtained pore water was stored frozen (-20 °C) until analysis with liquid ion chromatography and spectrophotometer (see section overlying water and porewater analysis).

Overlying and porewater analysis

Samples of overlying water and porewater were subject to bromide and nutrient analysis. Analysis of anions (Br^- and SO_4^{2-}) was carried out with the ion chromatograph "940 Professional IC Vario" and the autosampler "863 Compact Autosampler". The method is based on the stoichiometric chemical reaction between ions in stationary and mobile phases (Günther & Yilmaz, 2016). A carbonate eluent was used as the mobile phase or eluent. A "Metrosep A Supp 5" column was used as the stationary or solid phase. During flow, chemical-physical interactions between the solid and mobile phases and the running speed of the eluent through the column determine the retention of ions in the solid phase. Based on the previously measured standard, the respective ion concentration can be calculated from the measured arrival time at the detector (retention time). A "Multi-Element-Solution" from Roth® with a bromide concentration of 25 mg per liter was used as the standard. This solution was diluted at 1:2, 1:10, and 1:50 proportions for a four-point calibration.

Ammonium (NH_4^+) and phosphate (PO_4^{3-}) were analyzed spectrophotometrically immediately after sampling. A manual photometric determination of NH_4^+ was done following the method of Grasshoff et al. (1999). The analysis was based on the reaction of NH_4^+ with hypochlorite and the resulting monochloramine, which colors the sample phenol blue (Hansen & Koroleff, 1999). 1 ml samples were taken from the water samples and mixed thoroughly with 50 µl sodium citrate buffer. Then, 50 µl of phenolic reagent was added to the mixture and mixed thoroughly, followed by 50 µl of DTT solution. The sample was then placed in the dark for at least five hours before the extinction and measured at a wavelength of 630 nm on the "Spectronic® Genesys 5" photometer. Finally, the NH_4^+ concentration of the water sample was calculated employing a 0 – 10 µM NH_4^+ calibration curve prepared with NH_4^+-free deionized water. PO_4^{3-} determination was based on the reaction of phosphate with hexamolybdic acid in an acidic medium (pH < 1) to form a yellow molybdophosphoric acid. Adding ascorbate forms a blue heteropolyacid (Hansen & Koroleff, 1999). For the measurement, 50 µl ascorbic acid and 50 µl mixed reagent were added to each 1 ml pore water sample. The mixing reagent contained 200 ml 4.5 M H_2SO_4, 45 ml ammonium molybdate, and 5 ml potassium antimonyl tartrate. After samples were thoroughly mixed and a reaction time of at least 15 minutes was given, the extinction was measured at a

wavelength of 882 nm. The photometer used was also the "Spectronic® Genesys 5". Exactly as with the NH_4^+ measurement, the absorbance of the soil pore water samples before adding reagents was measured and subtracted from the actual absorbance value. With the help of a calibration line formed by six measured values, the measured absorbance could be converted into PO_4^{3-} concentrations.

Since the pore water samples of the soil cores already showed a (yellow) color before adding reagents, the extinction was additionally measured before adding the reagents. This value was then subtracted from the actual absorbance value of the sample, which prevented the NH_4^+ values from being measured due to the inherent color of the samples. The pore water samples of the marine sediment cores did not show any detectable coloration. For this reason, only absorbance after adding the reagents was measured.

Calculation of Bromide Inventories

The excess Br^- transport into the substrates is assumed a consequence of porewater transport driven by *H. diversicolor* irrigation. The excess Br^- inventory ($\sum\_Br^-$) is the total concentration of Br^- under an area of 1 m^2, calculated from the sum of the Br-concentrations in all layers of sliced substrates. The excess Br^- inventory (mmol Br^- m^{-2}) in the substrates was calculated from the thickness of the sliced layers and the respective volume (V_{sed}), the porosity (φ), and the Br^- concentration (C_{exBr-}) in the respective layer (after correction to background pore water Br^- concentration). C_{exBr-} represents the increased Br^- concentration in the water due to incubation.

$$\sum_{Br-} = V_{sed}\, x\, \varphi\, x\, C_{exBr-} \qquad (12)$$

By combining Br^- inventory per core over incubation time and Br^- concentration in the overlying water (corrected for Br^- background), area-specific bioirrigation volume (L m^{-2} d^{-1}) was calculated. Weight-specific bioirrigation (mL $g^{-1}d^{-1}$) per core was estimated from area-specific bioirrigation volume divided by the total recovered biomass per core (gr m^{-2}).

Soil analysis

For calculating the water content and the porosity, a soil core was randomly selected, from which sub-sample were sliced at 0.5 intervals (0-1 cm depth), 1 cm intervals (1-5 cm depth), and 2 cm intervals (5-11 cm depth). Every slice was weighed, and the soil wet bulk density (ρ_{bw}) was determined by dividing the mass of the soil slice by the total volume of the liner it occupied. Soil slices were then oven-dried at 60 °C for 12-24 h, and the dry bulk density (ρ_{bd}) was calculated by relating the soil dry mass to the volume of the liner. The water content of the soil (β), the C: N molar ratio, and the LOI were determined following the same procedure used for the sediment.

The LOI was then used to calculate the particle density (ρs) of the soil samples with standard values for organic (1.4 g cm^{-3}) and mineral (2.65 g cm^{-3}) components as follows:

$$\rho s = \frac{(1.4\ x\ LOI + 2.65\ X(100 - LOI))}{100} \qquad (13)$$

The total porosity was then calculated from dry bulk and particle densities according to:

$$\Phi = 1 - \frac{\rho b}{\rho s} \quad (14)$$

2.3.3 Experiment 2: Potential bioirrigation capacity of key bioturbator in coastal peatland restoration (MCF Exp 2)

Sampling of peat soil

Peat soil was collected a week before the flooding of the Drammendorf area with a 60 cm long acrylic core liner (10 cm i.d.) down to 20 cm depth and sealed with rubber stoppers on both ends. The sampling point was chosen after preliminary studies earlier that year (June- August 2019) on the soil characteristics (porosity, bulk density, and organic matter content) with consideration to the predicted water-covered area based on the site topography and predicted water level (UmweltPlan GmbH, Stralsund). Twenty-six soil cores were taken, transported to the institute, and kept outside the building throughout the winter (November 2019 – March 2020) with logged temperature and light sensor (Hobo logger).

Preparation of peat soil cores

In March 2020, small-scale inundation was performed in which 5 cm seawater (salinity: 10), equivalent to 0.392 l, was added on top of the soil cores. Temperature and light sensors were kept logged while the temperature, salinity, dissolved O_2 (DO), and pH of the overlying water were regularly checked with a multiparameter electrode. Regular measurements showed a general decline in pH, ranging from 8-9 of the added water and 3-5 after three days. Likewise, DO decreased from 95-100% to 60-70 % air saturation.

In August 2020, soil cores were divided into 4 groups (6 replicates each, in total 24 cores), flooded with seawater (salinity: 10) in 60-l water tanks, and kept in a regulated cooling water bath for a constant temperature of 15 °C. The water inside every tank was continuously aerated with air stones, and magnetic stirring was attached and utilized inside the core liner (~10- 15 cm above the soil surface) to ensure an even water circulation. The overlying water was renewed weekly during the experiment with fresh seawater to avoid excessive nutrient concentrations and maintain a pH level of 8-9. The inundated soil cores were left to acclimatize for 28 days in darkness.

Macrofauna collection

Three benthic macrofauna were chosen as the model for the bioirrigation experiment, namely *Hediste diversicolor*, *Mya arenaria*, and *Marenzellaria neglecta*. *H. diversicolor* and *M. arenaria* were collected from Schnatermann in September 2020 with sediment cores and sieved over a 500 µm - 1 mm mesh. The water temperature was 20.3°C, salinity was 11, and pH was 8.9. *M. neglecta* was collected from the coastal area of Bergen, Rügen Island, Germany, on several occasions. The first collection was in mid-September 2020 (15 September), followed by the second in early October 2020 (8 October 2020).

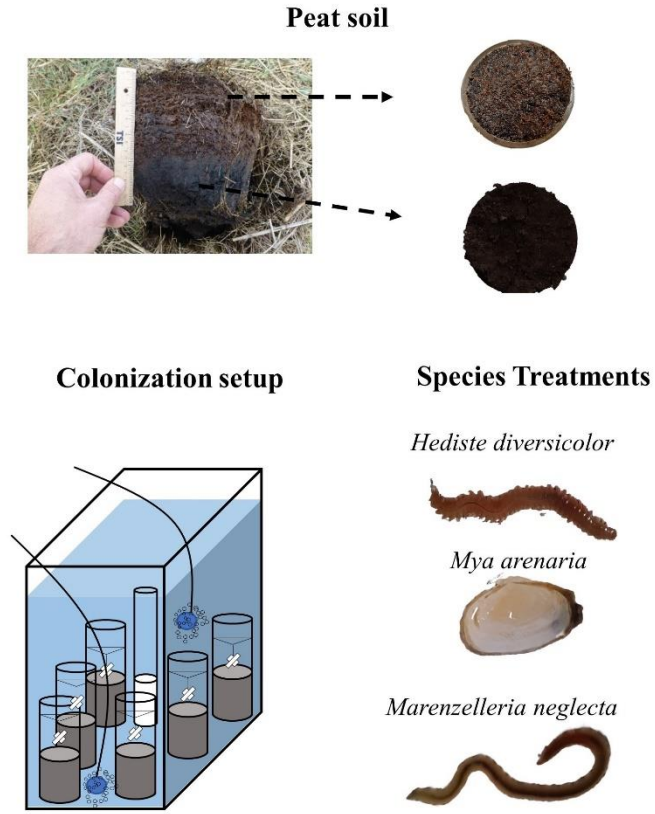

Figure 2. 9 Experimental design showing the peat soil characteristics, species treatment, and illustration of the cores in the water tank.

The water parameters in the first collection were: temperature: 12.8 °C, salinity: 7.5, and pH: 9.3. In the second collection, the temperature was 12.8 °C, salinity was 7.5, and pH was 9.3. All collected animals were kept in a climate room (15 °C) and submerged in their original sediment and artificial seawater (salinity: 10) to acclimatize for approximately 3 weeks before the start of the experiment. Animals were weighed just before they were added to the soil cores. In total, 4 individuals of *H. diversicolor* and *M. arenaria* were added, while 9 were added for the *M. neglecta* (1st round 5 October 2020, 2nd round 9 October 2020).

This number equates to biomass of 36 g m^{-2}, 35 g m^{-2}, and 18 g m^{-2} for *H. diversicolor*, *M. arenaria*, and *M. neglecta*, respectively. The corresponding abundances were ~510 individuals m^{-2} for *H. diversicolor* and *M. Arenaria*, and ~1147 individuals m^{-2} for *M. neglecta*.

TOU and nutrient fluxes

The baseline O_2 uptake of the peat soil (baseline-TOU), dissolved inorganic N (DIN = $NH_4^+ + NO_3^- + NO_2^-$), and dissolved inorganic P (DIP= PO_4^{3-}) were measured 2 weeks before the addition of macrofauna and once a week after fauna addition over the following 4 weeks of the experiment.

Initially (start point), water samples for DIN and DIP nutrients analysis were taken from the overlying water inside each core using a 60-ml syringe equipped with a 45 µm GFF Filter. The cores were then sealed, and the TOU measurement was commenced. TOU measurement was conducted according to the procedure described in MCF Exp 1. O_2 concentration in the water column was recorded over 12-16 hours long incubation, logged every 5 min after sealing of the core. Final water samples (endpoint) were taken upon the termination of the incubation as described for the initial samples.

Of the overlying water sampled, 15 ml was transferred into a 15 ml- centrifuge tube for DIN, DIP, and Silica (SiO_2) nutrient analysis. Samples were stored frozen (-20 °C) until analysis with a continuous flow analyzer as described in benthic chamber incubation (see liquid phase analysis). Area-specific (core surface area in m^2) DIN, DIP, and Silica fluxes (mmol m^{-2} d^{-1}) were calculated from concentration changes over time (start-end points) in overlying water during flux incubations accounting for the water volume.

Bioirrigation activity

The bioirrigation activity of the animals was determined by Bromide (Br^-) tracer incubations as described in MCF Exp 1. Likewise, the Br^- inventory, area-specific bioirrigation volume, and weight-specific bioirrigation were calculated according to MCF Exp 1.

Sectioning, pore water sampling, and nutrient measurements

The experiment was concluded 6 weeks after animal addition. Overlaying water inside each core was sampled with a 60-ml syringe and filtered through a 45 µm GFF Filter into a 15 ml centrifuge tube before the core was carefully drained. Sediment cores were sliced into 0.5 cm intervals to a depth of 1 cm, followed by a 1 cm interval to a depth of 5 cm and a 2 cm interval to 11 cm. The residence depth of the animals was noted during the sectioning. Sub-samples from every layer were taken to determine soil characteristics (see section soil analysis). Pore water extraction through centrifuging followed a similar procedure in Experiment 1. The obtained pore water was stored frozen (-20 °C) until analysis with liquid ion chromatography and spectrophotometer (see section overlying water and porewater analysis).

Of the pore water retrieved, 2 ml were collected and stored dark and cold (5°C) for major anions analysis (Br^- and SO_4^{2-}) with liquid ion chromatography (Metrohm 930 Compact IC Flex; Herisau, Switzerland). Before the analysis, pore water was refiltered (to protect the measurement device) through a 0.2 µm membrane filter (Thermo Scientific Polysulfone filter). Pore water NH_4^+ and PO_4^{3-} were measured using an AA3 Continuous Flow Analyzer (Seal Analytical, Norderstedt, Germany). DOC/DIC/TDN samples were analyzed using an Analytik Jena Multi N/C 2100s analyzer (Jena, Germany). Samples for DOC were burned at 7500C, while DIC samples were injected in phosphoric acid following manufacturer protocols. Blank samples from filtered distilled water were also analyzed.

Determination of peat soil characteristics

A sub-sample of peat soil was taken following the depth interval of the core slice for pore water extraction. Determination of wet bulk density, dry bulk density, water content, loss on ignition, porosity, and C: N molar ratio was conducted following the soil analysis method described in MCF Exp 1.

Micro-computer tomography

A micro-computer tomography scan (Phoenix X-ray nanotome®180, Baker Hughes) was conducted to visualize the structure of Drammendorf peat soil and estimate its porosity. Soil cores were taken in August 2020 with a 60 cm acrylic core liner (10 cm i.d.) at the same sampling point where soil cores were collected for laboratory experiments. Subsample of the soil cores was taken with a 20 cm acrylic core line (3.6 cm i.d.) to a thickness of 6 cm from the surface. The soil core scans were visualized 3-dimensionally via volume-rendering with Amira-Avizo 2020.2 (Thermo Fisher Scientific). Less x-ray opaque material is darker in the single slices and more transparent in the volume-rendering. Following this, the soil core pictures were segmented (segmentation editor) into the acrylic core liner, air, and soil core, all main components of the soil core. The pictures were then inverted to obtain a negative picture. Combining the volume rendering setting and the inversion setting

separated the content (soil core) from the acrylic core liner and the air trapped in between. The segmentation setting automatically differentiates and connects pixels with the same value (Opaque and air channel). Finally, the program calculated the volume (cm^3) of each component. The proportion of the air component over the whole soil core was equivalent to the porosity of the soil core.

2.3.4 Experiment 3: 2D O2 dynamics in sediment (marine) and soil (terrestrial) colonized by *Hediste diversicolor* (MCF Exp 3)

Experimental setup

The two-dimensional (2D) O_2 distributions within the artificial burrow and the burrow of *H. diversicolor* in different substrates (sediment and soil) were investigated with O_2 planar optode VisiSense TD system (PreSens GmbH, Regensburg, Germany) in laboratory experiments. The same substrates in Experiment 1 were used. Specimens of *H. diversicolor* (~ 2 to 5 cm long, wet weight between 0.05 g - 0.4 g) were also collected from the same site as in Experiment 1 (Schnatermann, Rostock, Germany). The substrates and animals were brought to the laboratory and kept in a climate room of 15 °C. The animals were kept in plastic trays containing Schnatermann sediment and seawater, aerated until use. The physical properties of the sediment and soil are listed in Table 3.3.

Prior to the experiment, 2 O_2 sensor foils (8 x 15 cm, width x height) were glued with silicon adhesive inside a transparent aquaria at the narrow side (20 x 20 cm, width x height) of the aquaria (25 cm long). The foil was attached carefully to avoid air bubble entrapment and left to equilibrate overnight. A thin plastic plate was placed into each aquarium ~ 1.5 cm from the optode foil to constrain the space for sediment and for the worm to burrow.

2D O_2 distributions within artificial burrow. Artificial burrows (one for each substrate) were constructed using a silicone tube with an outer diameter of 5 mm and a wall thickness of 1 mm. The tube was connected to a pump that continuously pumped O_2-rich water through the tube. The tube was positioned in the aquarium to penetrate deep enough into the sediment (approx. 10 cm) and was as close as possible to the sensor foil. Simultaneously, substrates were filled into respective aquaria to cover the artificial burrow completely (~ 450 cm^3) and followed by seawater of 4 cm height(~ 120 cm^3, salinity: 10, temperature 20 °C). The foil covered ~ 2 cm of the water column. The systems were left to settle for 3 days with continuous aeration of the overlying water with air and continuous flushing of the artificial burrow at room temperature of 20 °C. Initially, O_2 images of the established system and artificial burrow were taken. Subsequently, the flushing was switched off, and O_2 concentration was recorded continuously. The images were taken every 5 min for 1 to 5 h. Image acquisition was performed in the dark while the water temperature and aeration were kept constant during all measurements. The system (camera detector unit and foil) was set at a fixed distance for all experiments.

2D O_2 distributions within the burrow of *Hediste diversicolor*. A similar setup, but without an artificial burrow, was assembled for the O_2 imaging within the burrow of *H. diversicolor.* Likewise, after filling the aquaria with substrate, the system was allowed to settle for 3 days. A worm was then introduced to the aquarium in the space between the plastic plate and the sensor foil and was allowed to construct a burrow behind the foil. New

worms were added when the animal did not construct a burrow behind the foil. Image recording was started once an appropriate burrow had been established sufficiently close to the foil. Similar regimes (recording interval and duration)of image acquisition as in artificial burrow were applied.

Image processing and O_2 Flux calculation

Integrated software, VisiSens ScientifiCal 1, was used for image processing. Calibration images were taken from foil exposed to air-saturated distilled water (100 % air saturation) and $Na_2S_2O_4$ solution or anoxic part of the sediment (0 % air saturation). The calibration images were used to measure the red/green ratio of pixels of the selected region of interest (ROI) in each calibration image. A two-point calibration curve was derived from these two ratios. The calibration values were corrected for the backscattering signal or directly applied to the red/green ratio in each pixel of the subsequent recorded PNG images to create images of O_2 distribution (in % air saturation).

Further data evaluation of the O_2 images was performed with the VisiSens Image Profiler 0.5.1 plugin, a software extension for VisiSense TD and VisiSens ScientifiCal 1. Previously recorded images and their calibration values were loaded, and spatial calibration (conversion from pixel to mm) was performed by drawing a line of known length in the recorded image. ROIs were selected with a vertical direction at the SWI and perpendicularly to the burrow wall. Average O_2 concentration along this distance of chosen ROIs was derived by applying the calibration curve at each pixel of the recorded images. Once all images were processed, the software automatically generated a data file (.csv) per ROI containing distance (pixel and mm) and O_2 concentration (in % air saturation) per image.

The image covered an area of 9 x 6.75 cm. Taking the spatial resolution of the imaging system into account (1292 x 964 pixels), the spatial resolution of the O_2 images was 70 x 70 µm $pixel^{-1}$ (1mm =14 pixels, 1 pixel = 70 µm). The ROI used to derive the O_2 profile and calculate OCR accounted for an area of 1 x 0.5 cm (140 x 70 pixels). Air saturation values were converted to O_2 concentration (µmol l^{-1}) using the solubility of O_2 in water at salinity 10 and at a temperature of 20 °C. A time series of vertical or horizontal O_2 concentration profiles from each ROI was created by plotting O_2 concentration (µmol l^{-1}) against distance (mm).

From each O_2 profile, the position of the substrate-water interface was determined from the change in the slope of the O_2 concentration gradient. The burrow diameter and O_2 penetration depth were inferred directly from the O_2 profile. Diffusive fluxes of O_2 (J(x)) at the substrate water interface and fluxes of O_2 perpendicular to the burrow wall were calculated with Fick's first law of diffusion following the calculation of diffusive O_2 flux with microelectrode approach.

2.3.5 Macrofauna early colonization

Benthic macrofauna was sampled at the seaside station before and after the opening of the polder in Drammendorf and at the inundated area after the flooding. The relatively low sampling frequency (Table A.6) was due to the difficulty accessing the flooded area. The cattle intervened in the pathway to the designated stations, and the water level was higher than predicted, hampering the deployment of the core liner.

Three macrofauna samples were taken during each successful sampling using a 60 cm core liner (10 cm i.d.) down to 20 cm. The samples were shoveled and sieved through 1 mm mesh on site. The retained materials were transferred into plastic jars and preserved with 4% formalin. Samples were sorted in the laboratory, where all recovered macrofauna were stored until identification. The macrofauna was identified to the lowest possible taxonomic level and counted.

2.3.6 Statistical Analysis

The results are generally reported as mean ± 1 standard deviation (SD) of *n* replicate measurements. SigmaPlot (version 13) and R Core Team (2020) were used for statistical analysis. Normality and homogeneity of variance were checked prior to further statistical analysis.

Nonparametric statistics were used in the interpretation of the results when either normality or homogeneity were fulfilled. The Mann-Whitney Rank Sum test (*U*-test) was used to compare the distribution of values of two independent groups of measurements. The Kruskall-Wallis ANOVA on Ranks (*H*-test) was used to compare the distribution of values of three or more independent groups. Pairwise comparison (Tukey test) was performed when the *p*-value from ANOVA on Ranks was significant. Friedman repeated measures ANOVA on ranks was used to compare the effect of experimental treatments on a single group of individuals (sample of repeated measurements).

Unpaired t-tests were used to compare differences in the means between two groups of normally distributed data. One-way or Two-way ANOVA was performed to test differences in means between three or more groups. One-way or Two-way repeated measures ANOVA was used to compare the means of a sample with repeated measurements. Pairwise comparisons (Tukey Test) were implemented when ANOVA detected significant differences to identify which groups differed.

3 RESULTS

3.1 O_2 dynamics in sandy permeable sediment inhabited by diatom dominated-MPB community- Laboratory Benthic chamber incubation

3.1.1 Sediment properties

Based on their mean grain size, the used sediment was classified as medium sand (Wentworth, 1922) and was organic-poor (Table 3.1). On average, sediment with and without RC had similar porosity and permeability, however sediment in RC chambers had higher water content (t-test, $p < 0.001$) and was richer in Chl. *a* (t-test, $p < 0.05$). The C: N ratio was about twice as high in C chambers than in RC chambers. Chl. *a* content in the uppermost cm of the sediment was about three times higher in RC chambers than in C chambers.

Table 3. 1 Summary of the water parameters and sediment characteristics (measured post-incubation) used in laboratory benthic chamber experiments. Chlorophyll *a,* LOI, and C: N ratio values refer to the top 2 cm of the sediment, while permeability refers to the top 5 cm.

Parameter	C chambers	RC chambers
Temperature (°C)	15	15
Salinity	15	15
Bulk density (gr cm^{-3})	1.7 ± 0.1	1.9 ± 0.1
Sediment type	Medium Sand	Medium Sand
Grain size (median in μm)	283 ± 2.2	287 ± 2.3
Porosity	0.3 ± 0.01	0.4 ± 0.02
Water content (%)	17	19
Permeability k (x 10^{-12} m^2)	22	25
LOI (% DW)	0.5 ± 0.01	0.4 ± 0.2
C: N (mol mol^{-1})	66.7 ± 12	38 ± 19
Chl *a* (μg ml^{-1sed})	2.94 ± 0.7	7.64 ± 1.8

3.1.2 O_2 Microelectrode measurements

O_2 distribution. Evidence of small-scale variations between the O_2 depth profile replicates was noticeable in almost all the chambers (Figure 3.1 and Figure 3.2). The shapes of the O_2 profiles were highly variable, changing from a typical diffusive profile shape commonly observed in cohesive sediment to irregular profiles with deeper O_2 penetration depth. Under diffusive settings, both dark and light profiles showed a distinct shallow oxic layer, which deepened after dark flow in C chambers, while it shallowed in RC chambers (Figure 3.2 and Table 3.2). The maximum O_2 concentration in the sediment increased with increasing light intensity, from 249 μmol l^{-1} to 890 μmol l^{-1} in C chambers and 259 to 1100 μmol l^{-1} in RC chambers. Under illumination, the thickness of the euphotic zone was around 1 to 2 mm in both chamber types. O_2 penetration depth in C chambers was more profound (in the dark and light) than in RC chambers (Table A.1 and Table A.2). With increasing light intensity, O_2 penetration depth increased by 4.3 mm on average in C chambers, while it only increased by 3 mm in RC chambers.

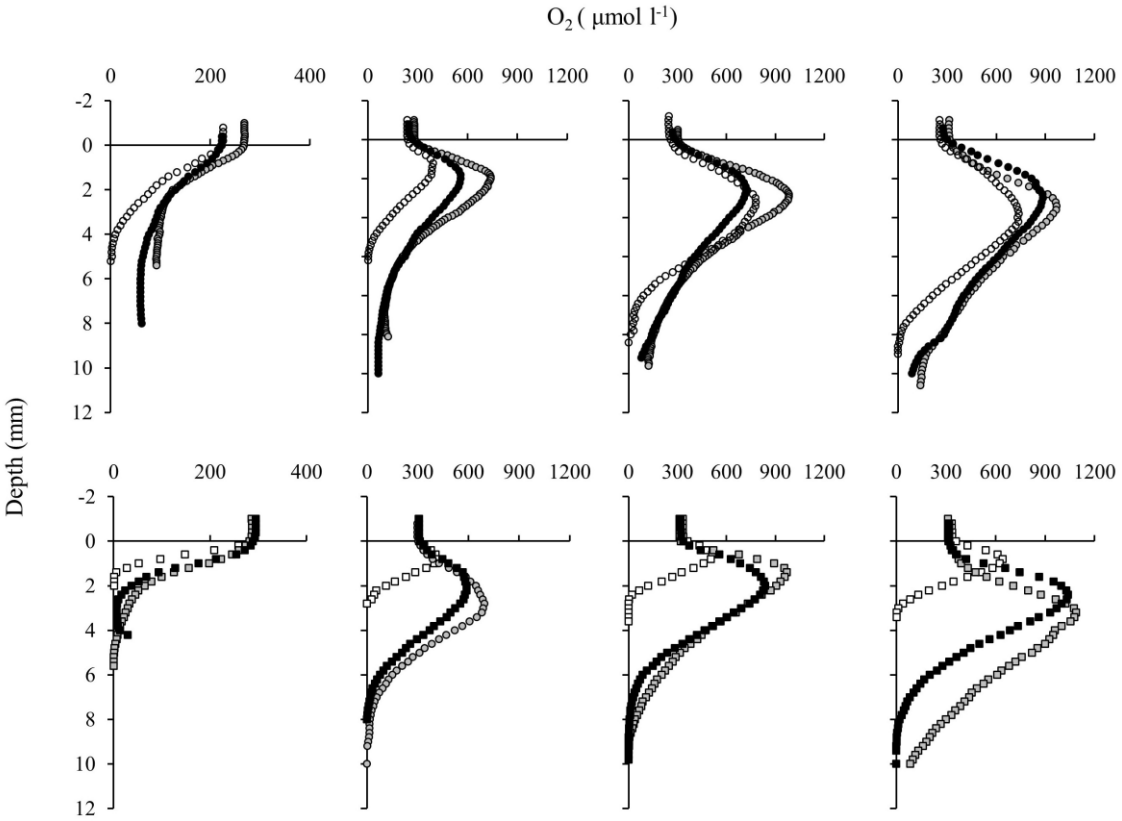

Figure 3. 1 Example of steady state O_2 profiles from chambers without (C Chambers, upper panel, n = 3) and with reduced compounds (RC chambers, lower panel, n = 3) in the dark and at different light intensities (left to right: 0 ((dark)), 40, 70, 100 µmol photon m^{-2} s^{-1}).

In general, the influence of light on O_2 distribution was stronger than advection (Table 3.2 and Table 3.3). Except for C chambers, a reduction of O_2 peak concentration (4 - 25 %) was observed upon advection. In all chambers and under all light regimes, advection reduced the vertical extent of the euphotic zone by 2 mm. Advection increased O_2 penetration depth, particularly in C chambers under dark conditions. In all light conditions, C chambers exhibited deeper penetration depth than RC chambers.

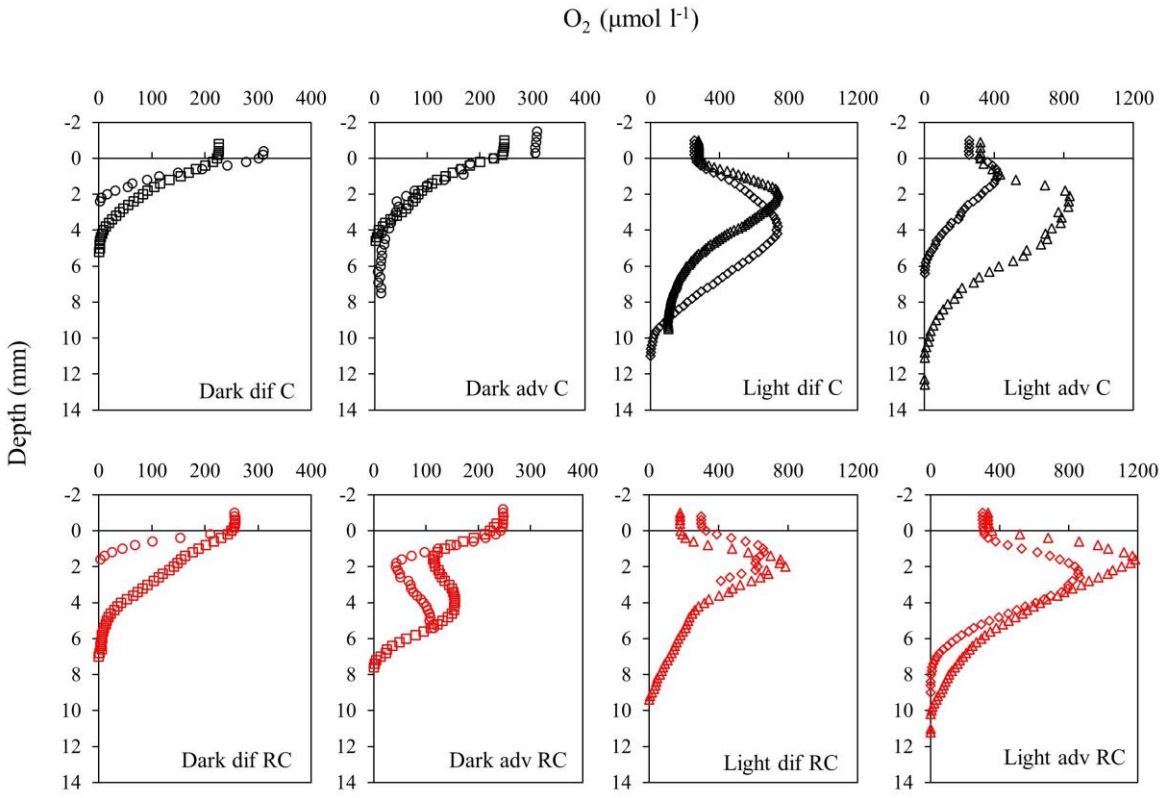

Figure 3. 2 Example of O_2 depth profiles at different light and transport regimes. Profiles were obtained from chambers without (C Chambers, upper panel, $n = 2$) and with reduced compounds (RC chambers, lower panel, $n = 2$). Light intensity was set at 100 µmol photon m^{-2} s^{-1}, while advection was induced by stirring of the disc of the benthic chambers at 40 rpm.

Benthic O_2 Fluxes. The fluxes estimated from concentration gradients were not significantly different from those calculated with Sensor Trace modeling software (Table A.1 and A.2). The average R_{Dark} was twice as high in RC chambers compared to C chambers. Advection increased R_{Dark} with slightly higher fluxes in RC chambers. In the presence of light, NP increased with increasing light intensity, with higher fluxes found in RC chambers (Two-way ANOVA, $p < 0.001$). A significant difference was detected between fluxes measured at the lowest and highest light intensity (Two-way ANOVA, $p < 0.001$). The effect of advection on NP varied across chamber types and calculation approaches. Overall, NP values were higher with only light than NP after exposure to combined light and advection. There were no statistical differences between GP under diffusive and advective settings (*H*-test, $p = 0.679$).

Calculated from O_2 profiles, GP rates increased with light in all chambers (Table A.1 and Table A.2), where higher fluxes were obtained in RC chambers (Two-way ANOVA, $p < 0.001$). GP rates of C vs RC chambers significantly differed at the highest light intensity (Two-way ANOVA, $p < 0.001$). Advection decreased GP rates in C chambers; advection slightly increased GP rates in RC chambers.

GP_{LDS} reached maximum values ranging from 4.5 – 31.15 mmol m^{-2} d^{-1} and were obtained from 0.0 mm down to 1.6 mm depth (Figure 3.3). From depth-integrated GP_{LDS} (5 depths), chambers with reduced compounds showed a saturation value of 66.7 mmol m^{-2} d^{-1} at 70 to 100 µmol m^{-2} s^{-1}, while the rates were still under saturation even at the highest

light intensity in chambers without reduced compounds. GP_{LDS} rates in both chamber types under different light intensities were statistically insignificant (C chambers: Two-way repeated measures ANOVA, p = 0.83; RC Chambers: Friedman repeated measured ANOVA on Ranks, $p = 0.65$).

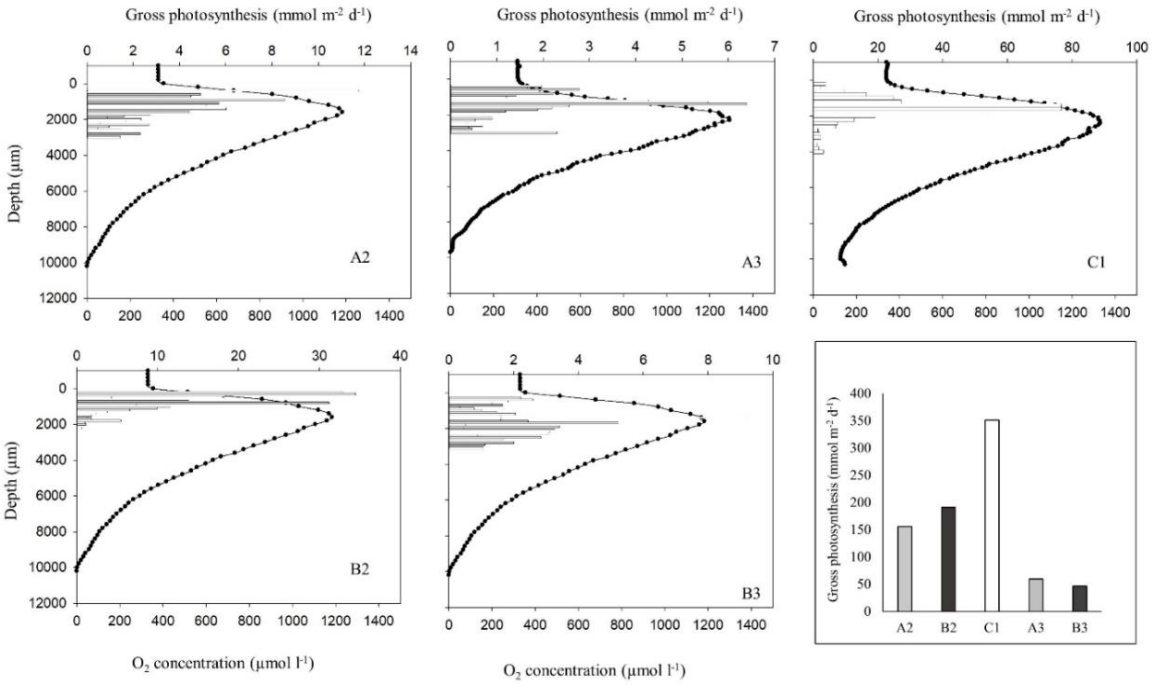

Figure 3. 3 Steady-state depth profiles of O_2 concentration (lines) and depth distribution of gross photosynthesis (GP_{LDS}) measured at an irradiance of 100 µmol m^{-2} s^{-1} (bar). The corresponding integrated depth distribution of the gross production is plotted in the lower right panel.

PI-curve modeling yielded an average saturation value (Ik) of 19 µmol m^{-2} s^{-1} in C chambers, while it reached saturation at 60 µmol m^{-2} s^{-1} in RC chambers (Figure 3.4). Pm ranged from 8-12 mmol m^{-2} d^{-1} in C chambers to 16-85 mmol m^{-2} d^{-1} in RC chambers. Details of the derived PI-curve variables are listed in Table A.3.

R_{Light} increased with increasing light intensity (Table A.2). At 40 µmol m^{-2} s^{-1}, R_{Light} in RC chambers was markedly higher (up to 15-fold) than in C chambers. The extreme value of R_{Light} (95 ± 65 µmol m^{-2} s^{-1}) in RC chambers at 100 µmol m^{-2} s^{-1} exceeded respiration in the dark about 13 times.

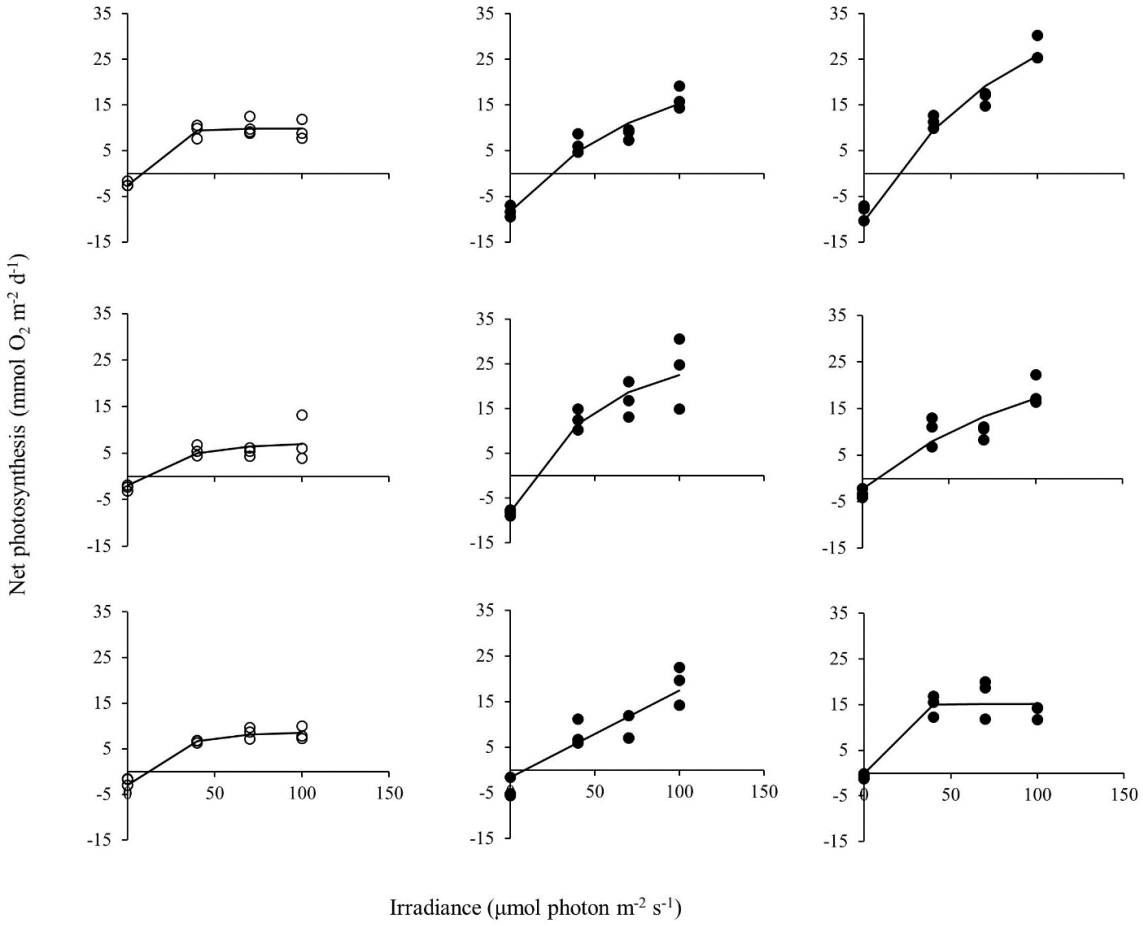

Figure 3. 4 Net photosynthesis rates (derived with O_2 microelectrode approach) plotted against light intensities of MPB diatom dominated sandy sediment: C Chambers (white circles), RC Chambers (black circles).

O_2 consumption rate (OCR). The measured OCR values are presented in Table 3.2. As can be seen, in both chambers, the highest OCR was obtained after exposure to light, followed by light and advection, and finally with only advection. When comparing OCR values between chamber types under the same light and transport regimes, a pronounced difference only occurred in RC chambers between the contrasting combined light and transport regime (Dadv vs Ldif: *H*-test, $p = 0.018$).

Table 3. 2 Summary of O_2 consumption rates (OCR in µmol O_2 l^{-1} min^{-1}) measured in the oxic layer of the sediment with microelectrode (ME) from chambers without reduced compounds (C) and with reduced compounds (RC) after different light and transport regimes; Ldif: light diffusive, Ladv: light advective, Dadv: dark advective.

	ME - C				ME - RC			
	mean		min	max	mean		min	max
L_{dif}	-25.46 ± 33.8	($n = 3$)	-3.93	-64.41	-20.36 ± 6.3	($n = 4$)	-15.05	-29.53
L_{adv}	-14.13 ± 7.1	($n = 4$)	-7.57	-22.62	-16.43 ± 5.2	($n = 9$)	-9.60	-22.80
D_{adv}	- 2.90 ± 1.7	($n = 4$)	-0.35	- 4.19	- 2.73 ± 2.1	($n = 7$)	-0.38	- 7.07

3.1.3 O_2 Planar optode measurements

O_2 spatiotemporal dynamic

After the long-term incubation, steady state O_2 distribution was considered to be reached in all incubated chambers. In general, O_2 distribution showed local maxima and minima; higher concentration in the overlying water and at the sediment surface and O_2-depleted to fully anoxic condition with depth. Vertical and horizontal variability of O_2 distributions were evident from optode images and extracted O_2 profiles as illustrated in Figure 3.5 and Figure 3.6.

Prior to any exposure and thus measurement, C chambers exhibited higher O_2 concentration than RC chambers (Figure 3.6, upper panel, 1st O_2 image from respective chamber). Local O_2-rich zones were observed in both chambers but most pronounced in C chambers. On the other hand, spots of permanent O_2 reduced zones occurred at the upper part of the sensor foil, which was in direct contact with the overlying water. Although the sediment surface was flattened, planar optode O_2 images still depicted uneven sediment surfaces.

The average O_2 penetration depth into the sediment in the dark under diffusive conditions was ~7 mm in C chambers and ~5 mm in RC chambers. Variations of O_2 penetration depth in each chamber and among chambers were observed and particularly associated with uneven sediment surface and bubble entrapment (Figure 3.7).

After the onset of light (~1 h), the O_2 maximum concentration in the immediate subsurface zone of the sediment increased rapidly, ranging from 1254 μmol l^{-1} to 1573 μmol l^{-1} in C chambers and from 482 μmol l^{-1} to 1706 μmol l^{-1} in RC chambers. These values were both associated with the occurrence of local O_2-rich zones. By excluding chambers with O_2-rich zones, which was only possible for RC chambers, the average maximum O_2 concentration of RC chambers was 538 ± 60 μmol l^{-1}. O_2 was observed down to 12 mm in C chambers, while it only reached 6 mm depth in RC chambers.

In the light with stirring-induced pore water advection (~2 h), the average O_2 concentration maximum decreased by ~4 % in both chambers. However, individual chambers in both treatments showed a variation in the impact of advection on O_2 concentration maximum (Figure 3.6). At the end of the stirring, O_2 penetrated deeper into the sediment, ~ 7 mm deeper in C chambers and 2 mm deeper in RC chambers.

Figure 3.6 (lower panel) depicts an example of the effect of exposing sediment to only advection. The figure generally demonstrated the transport of O_2-rich water deep into the sediment, where higher O_2 concentrations were observed in C chambers. After stirring the benthic chamber, the O_2 penetration depth increased to ~14.3 mm in C chambers and ~6 mm in RC chambers.

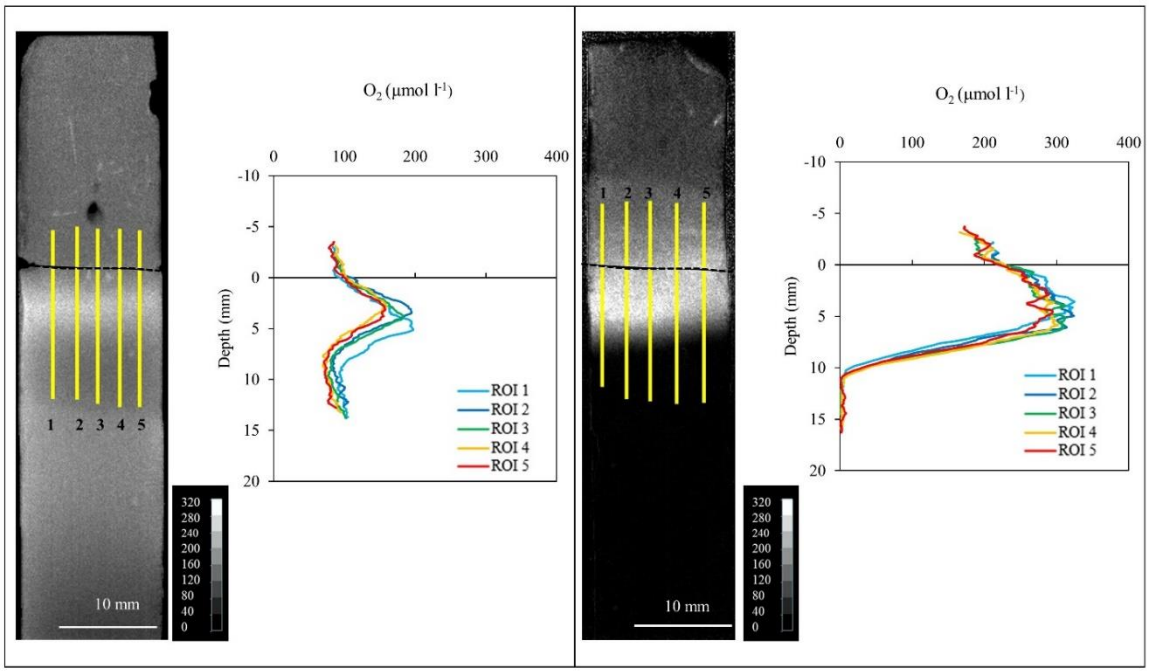

Figure 3. 5 Example of optode images of the spatial distribution of O_2 and extracted profiles after 60 min illumination (40 µmol photon m^{-2} s^{-1}) (left: C chamber, right: RC chamber). Profiles were extracted from each image along the vertical lines numbered 1 to 5. The horizontal black dashed lines indicate the sediment surface.

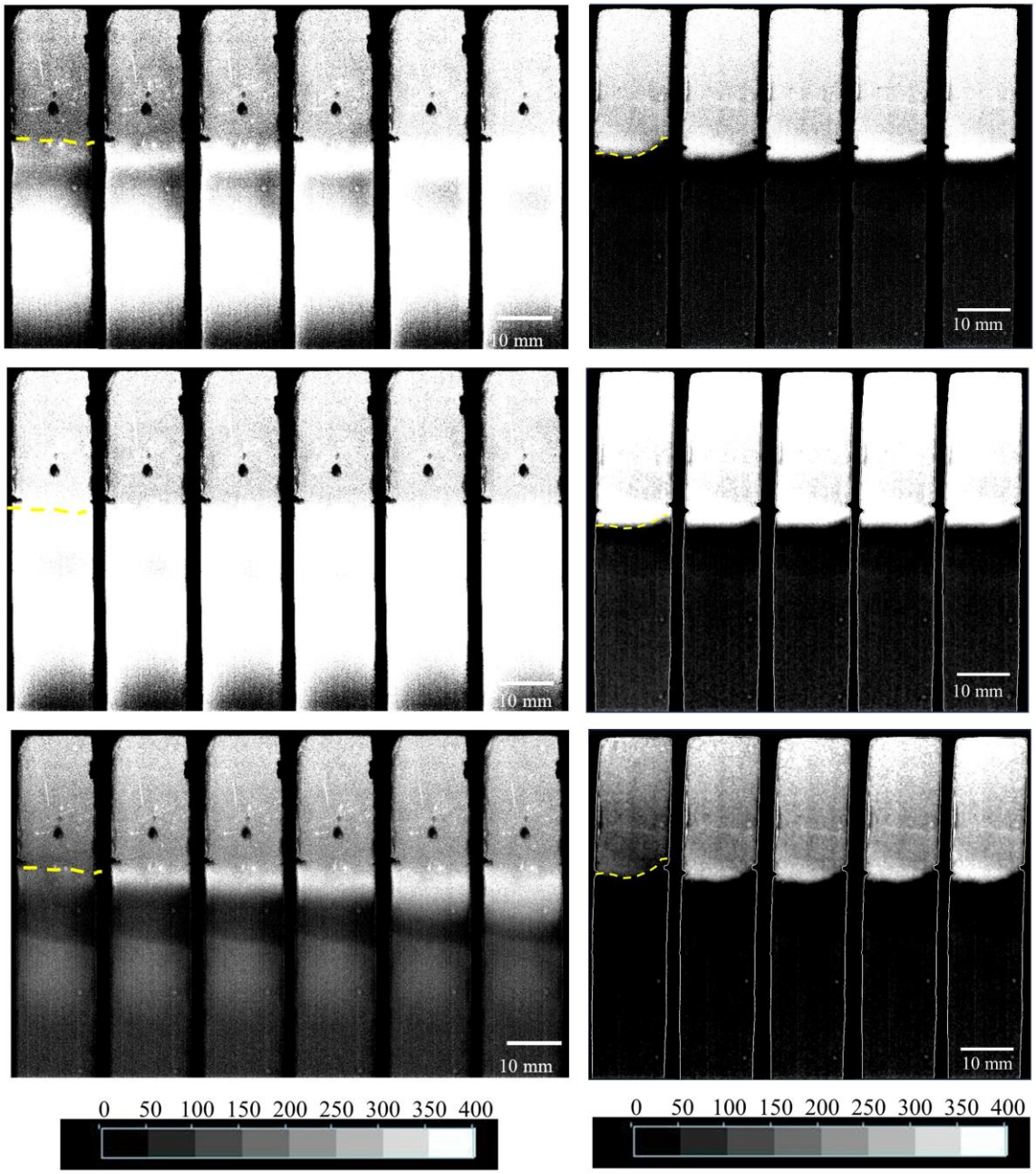

Figure 3. 6 Example of 2D O_2 images from C chambers (left panel at 0, 10, 20, 30, 60, 90 min) and RC chamber (right panel at 0, 10, 20, 30, 60 min) during dark to light diffusive (1st row), light diffusive to light advective (2nd row), and dark diffusive to dark advective (3rd row). The yellow dashed lines indicate the sediment surface. The color bar at the bottom indicates the gradation of O_2 concentration (μmol l^{-1}).

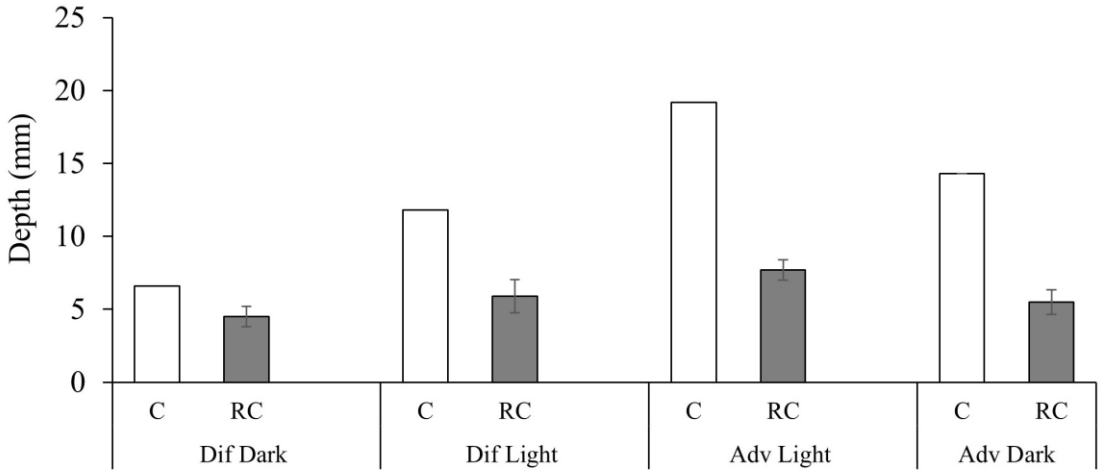

Figure 3. 7 Summary of O_2 penetration depth (derived from O_2 profiles extracted from planar optode images) at different light and transport regimes in C (white bars) and RC chambers (grey bars). Symbols represent the mean value, while the error bars represent the standard deviation (C: n = 1, RC: n = 5).

Benthic O_2 Fluxes. Benthic diffusive fluxes increased from -2.3 mmol O_2 m^{-2} d^{-1} (C chamber) and -3 ± 3 O_2 m^{-2} d^{-1} (RC chambers) in darkness to 18 O_2 m^{-2} d^{-1} and 11 O_2 m^{-2} d^{-1} at maximum light intensity (Figure 3.8, the first two bars from the right side). In the light, the occurrence of advection reduced the average net production by ~20% in the C chamber and ~4% in the RC chambers (Figure 3.8, the two bars in the middle). Consequently, the gross production decreased within a comparable percentage of ~18 % in the C chamber and ~3 % in the RC chambers. In the dark, the influence of advection was reversed, where benthic diffusive fluxes increased by ~ 31 % in both chambers.

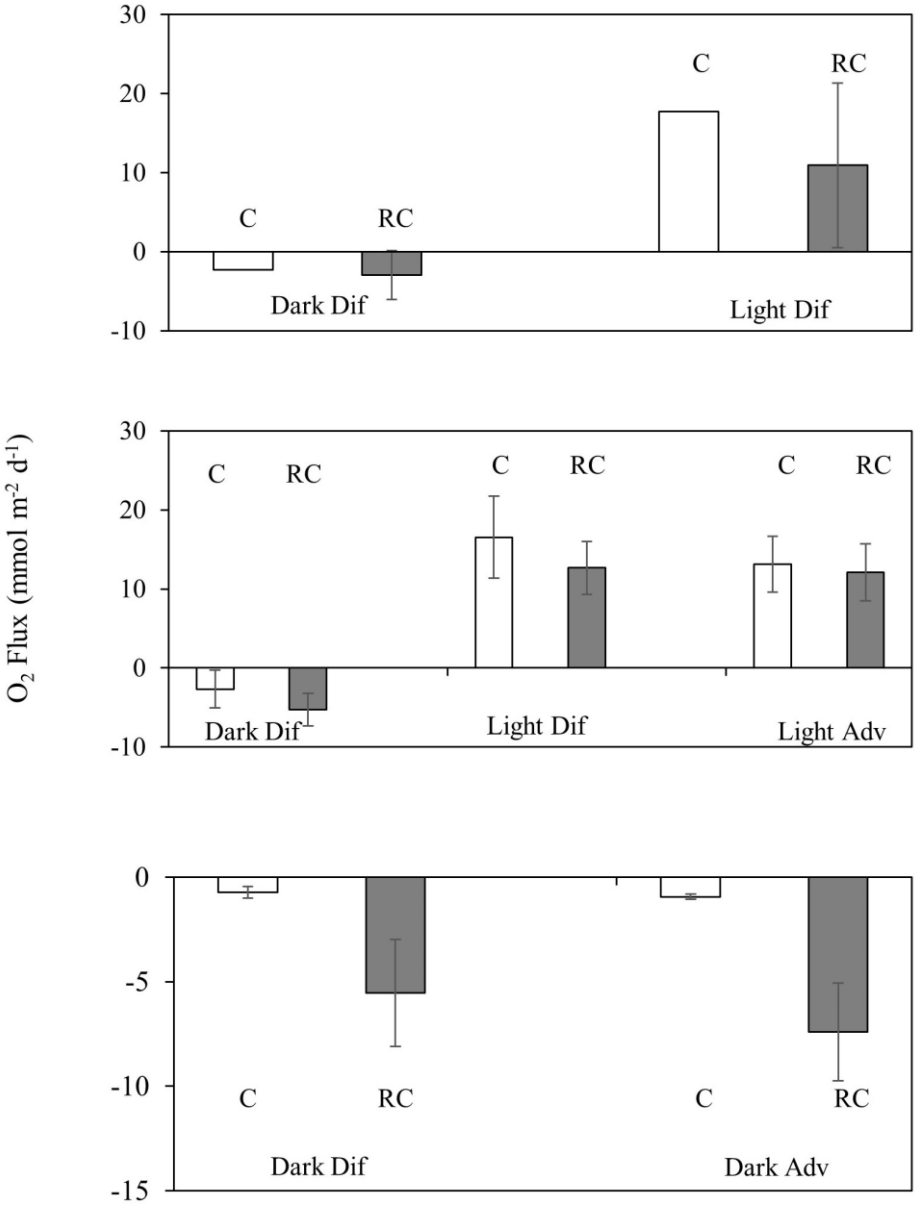

Figure 3. 8 O_2 fluxes (derived from O_2 profiles extracted from planar optode images) at different light and transport regimes in C (white bars) and RC (grey bars) chambers. Negative and positive values denote influx and efflux via the sediment surface. Symbols represent the mean value, while the error bars represent the standard deviation (C: $n = 2$, RC: $n = 6$).

O_2 consumption rates. Light enhanced OCR significantly with the highest value in C chambers. On the contrary, advection induced small OCR in the dark and a drop of OCR in the light. This observation was notably from planar optode in C chambers (transport vs light regimes: *H*-test, $p = 0.018$).

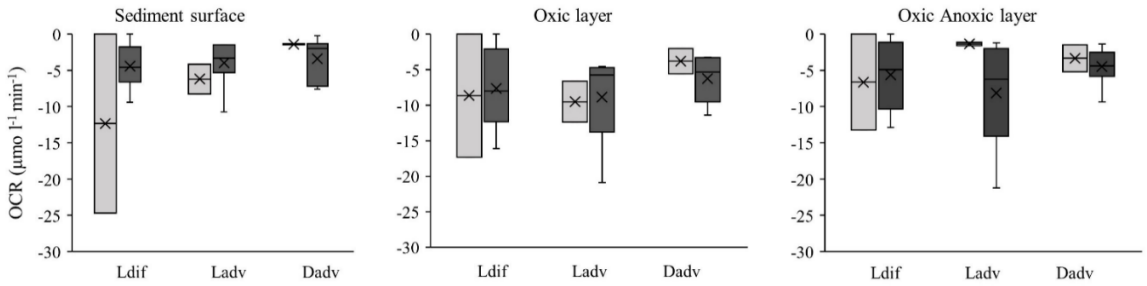

Figure 3. 9 Summary of O_2 consumption rate (OCR) after exposure to different light and transport regimes at various zones of the sediment measured with planar optode (PO) in laboratory experiments with different nutrient treatments (grey without RC and black with RC). X: mean, horizontal line: median.

OCR values showed high variability within chamber type and between replicate chambers. The dominance of light-intensifying OCR with and without advection was generally observed from the measurement of OCR in different zones of the planar optode sensor foil (Figure 3.9), with higher rates obtained from C chambers. On the contrary, after stirring had stopped in the dark, OCRs obtained from the different zones were slightly higher in RC chambers. The highest OCR was found close to the sediment surface and oxic zone, particularly from C chambers, albeit with pronounced variability. In the oxic sediment zone, the highest OCR values consistently occurred after light, followed by measurement after advection and light, and finally with only advection. The situation in the light was different in oxic-anoxic layer, where advection increased OCR more than light.

3.1.4 Total O_2 Uptake (TOU)

TOU yielded the highest value in RC chambers with an average of -43 ± 6 mmol m^{-2} d^{-1}. TOU from RC chambers was about twice as high as C chambers values (Figure 3.10). The difference between TOU from C and RC chambers was statistically significant (t-test, $p < 0.05$), while the deviations in TOU between individual chambers per treatment were relatively low.

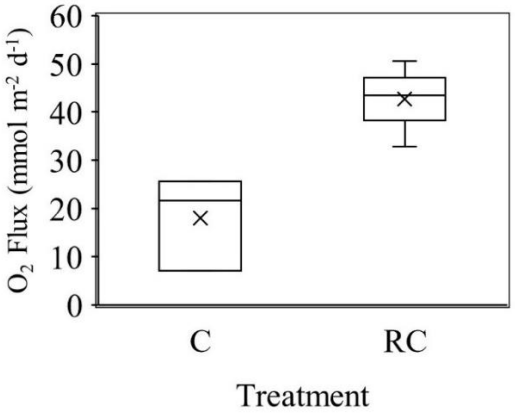

Figure 3. 10 Total O_2 uptake of laboratory benthic chamber experiment measured with planar O_2 sensor spot. Horizontal lines depict means, the boxes delineate the 25th and 75th percentiles, and the whiskers the 10th and 90th percentiles.

3.1.5 Pore water Nutrients

The distribution of pore water constituents (SiO_2, PO_4^{3-}, NH_4^+) from sediment cores is provided in Figure 3.11. Almost all the chambers showed a typical pattern of solute peak

concentration at the sediment depth of 2 to 5 cm and indicated nutrient fluxes up towards the water column. Pore water nutrient profiles demonstrate high variability between treatments. Nitrate and nitrite were below the detection limit (data not shown). A higher SiO_2 and PO_4^{3-} were found in the RC chambers, while C chambers exhibited a higher NH_4^+ concentration.

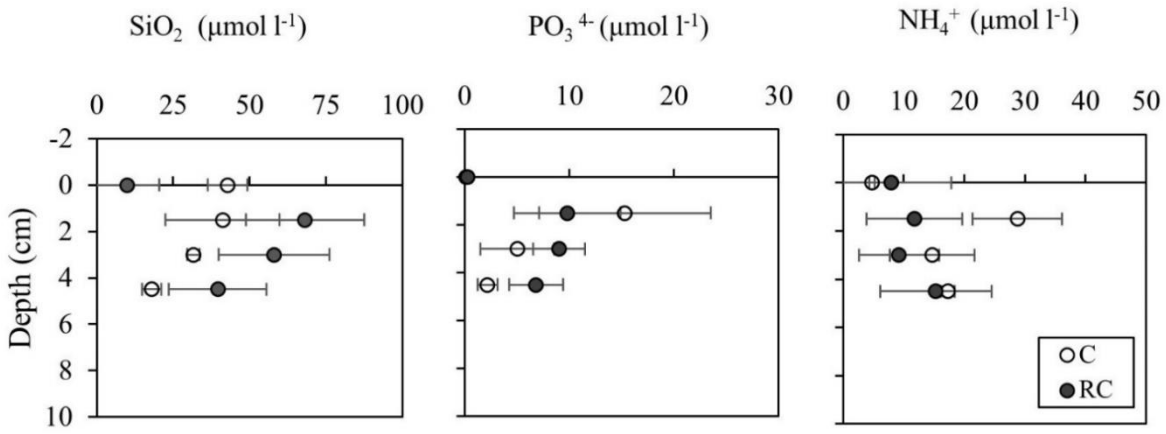

Figure 3. 11 Profiles of solutes from pore water extracted in the laboratory benthic chamber incubation. Symbols represent the mean value, while the error bars represent the standard deviation.

3.2 O_2 dynamics associated with bioirrigation

3.2.1 Experiment 1: Bioirrigation of *Hediste diversicolor* in different coastal substrates of the Southwestern Baltic Sea (MCF Exp 1)

Substrate characteristics

The bulk density, water content, and porosity of the sediment in the upper 1 cm were slightly higher than those of the deeper layers (Table 3.3). The same pattern with depth was observed in the water content and porosity of the soil. On the contrary, the bulk density of the soil slightly increased with depth. The mean LOI and carbon content of the soil were markedly higher than those of the sediment, 25 and 24 times higher, respectively.

Table 3. 3 Substrate physical characteristics and Ph of overlying water and pore water.

Substrate type-Sampling period	Depth (cm)	Bulk density wet	Water Content β (%)	Porosity (ϕ)	LOI (%)	Particle density	C-content (%)	Ph
Marine sediment-Pre Exp	0-1	1.98	19.50	0.39	0.73 ± 0.03	2.64 ± 0.01	0.37	8.36 ± 0.2
	1-2	1.86	18.46	0.35				
	2-3	1.88	18.15	0.34				
Marine sediment-Post Exp	0-1	1.87	19.64	0.37				8.86
	1-2	1.81	17.39	0.31				
	2-3	1.83	18.57	0.34				8.41
Terrestrial soil-Pre Exp	0-1	1.39	51.19	0.71	17.94 ± 0.4	2.4 ± 0.01	8.97	7.06 ± 0.2
	1-2	1.70	32.92	0.56				
	2-3	2.08	32.48	0.68				
Terrestrial soil-Post Exp	0-1	1.23	62.59	0.77				8.67
	1-2	1.38	44.72	0.62				
	2-3	1.56	44.04	0.69				7.33

Total O_2 Uptake (TOU)

The average TOU was highest in the control cores of marine sediment (36 mmol m^{-2} d^{-}) and lowest in the control cores of mixed soil (11 mmol m^{-2} d^{-}). The influence of *H. diversicolor* on TOU varied between the two substrates (Figure 3.12). The polychaeta increased the TOU in the soil (13 to 27 mmol m^{-2} d^{-}), while it decreased the TOU in the sediment (from 33 to 22 mmol m^{-2} d^{-}). The difference in TOU between control and inhabited cores of both substrates was statistically significant (*H*-test, p= 0.01).

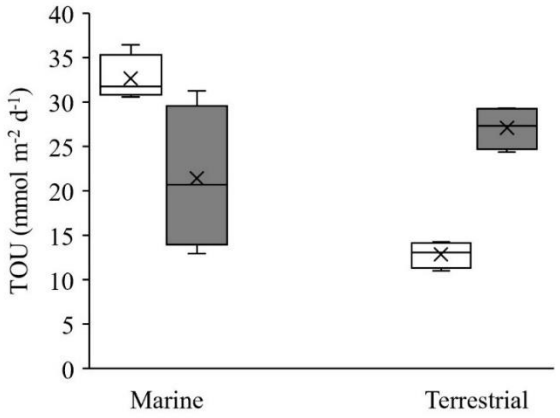

Figure 3. 12 Total O_2 uptake in sediment (Marine) and soil (Terrestrial) without (white boxes: MC, DC) and with (grey boxes: MHD, DHD) added *Hediste diversicolor.* X: mean, horizontal line: median, n = 4 .

Hediste diversicolor recovery and bioirrigation

All Added *H. diversicolor* were recovered from all cores. Br^- pore water profile indicated similar depth distribution within replicates of control cores, resembling diffusion-controlled profiles, with a steep decrease of Br^- between sediment depths of 0.3 to 4 cm: (9 mM to 4 mM) in sediment, (8 mM to 1 mM) in soil (Figure 3.13: left panel). Br^- background concentration was 0.5 mM in sediment and 0.46 mM in soil at 8 cm depth. Based on Br^- profiles, maximum bioirrigation depth varied from 8-10 cm in sediment and 4-5 cm in soil. Br^- inventory was slightly higher in colonized sediment than in colonized soil (Table 3.4); however, the differences were statistically insignificant (Two-way ANOVA, substrates p = 0.467, treatments p = 0.200). The difference in area-specific bioirrigation between substrate and treatment was insignificant (Two-way ANOVA, substrates p = 0.367, treatments p = 0.216).

Table 3. 4 Number and biomass (wet weight) of *H. diversicolor* added to marine sediment (Marine-Hd) and terrestrial mixed soil (Terrestrial-Hd).

	Marine-Hd	Terrestrial-Hd
Added Individual per core	3	3
Individual Biomass (mg ind $^{-1}$)	167	333
Individual per area(ind m^2)	382	382
Total Biomass (g m^{-2})	64	127
Recovery (%)	100	100
Br inventory -control cores (mmol Br− m^{-2})	116 ± 21	106 ± 14
Br inventory –colonized cores (mmol Br− m^{-2})	136 ± 32	124 ± 22
Area specific bioirrigation (L m^{-2} d^{-1})	5.15	4.82
Weight specific bioirrigation (mL g^{-1} d^{-1})	80.83	37.83

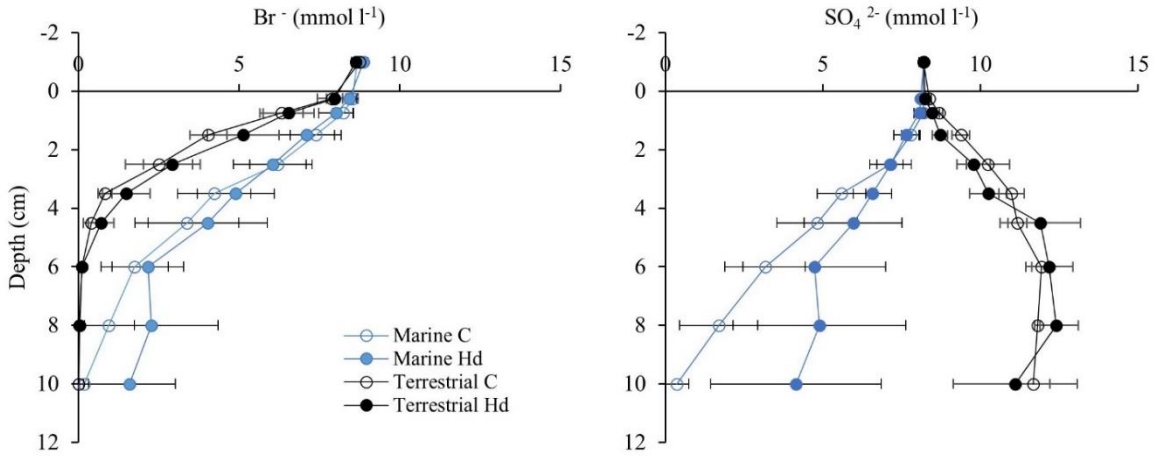

Figure 3. 13 Depth profile of pore water SO_4^{2-} and Br^- in marine sediment (Marine) and Terrestrial soil (Terrestrial), without (C) or with *H.diversicolor* (Hd). Symbols represent the mean value, while the error bars represent the standard deviation (n = 4).

Hediste diversicolor impact on pore water solutes

The SO_4^{2-} pore water profiles of the sediment indicated a release of SO_4^{2-} in the upper 1 cm layer followed by a continuous decrease with depth. In the presence of *H. diversicolor*, there was a slight decrease in SO_4^{2-} concentration at 6 to 8 cm depth. In soil, the pore water profile of SO_4^{2-} was characterized by a release of SO_4^{2-} in the upper 3.5 cm, a peak concentration at a sediment depth of 4 to 8 cm, and subsequently a slight decrease in concentration with depth. The pore water SO_4^{2-} was considerably higher in soil than in sediment (Figure 3.13: right panel). Except for the upper 3 cm of the soil, there was a clear impact of *H. diversicolor* on the vertical distribution of SO_4^{2-} in both substrates, where SO_4^{2-} concentration was higher in cores with animals. This impact was most pronounced in the sediment.

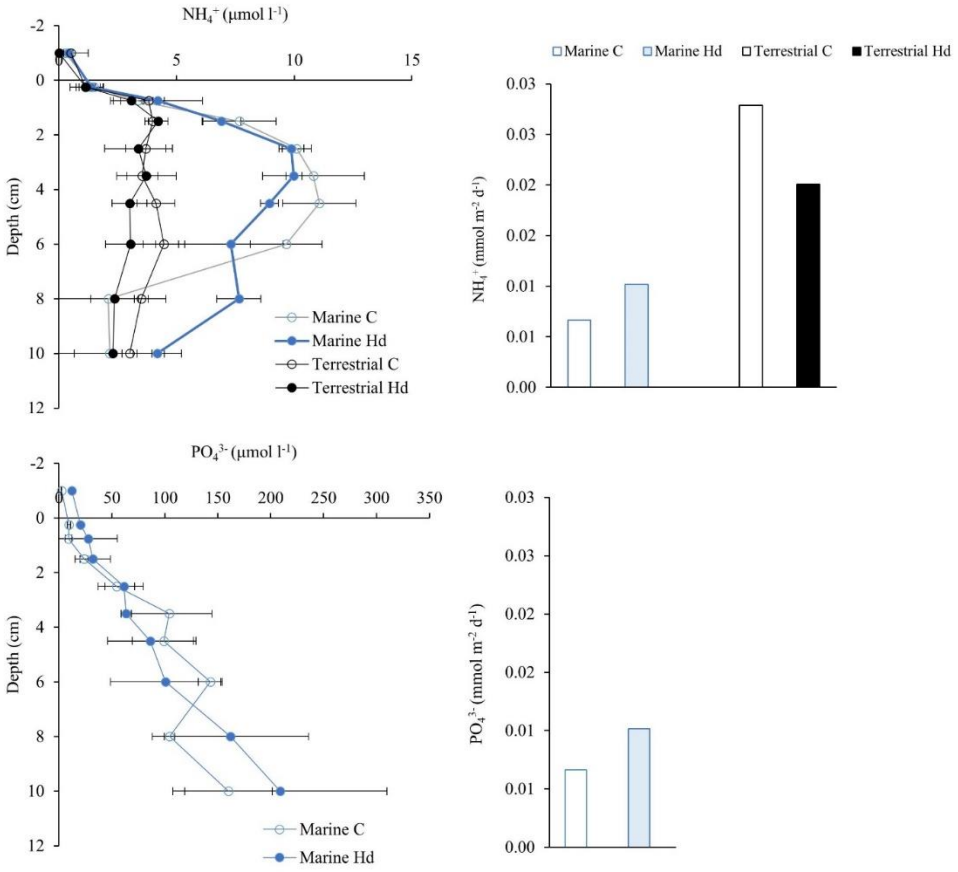

Figure 3. 14 Depth profile of NH_4^+ and PO_4^{3-} (left panel) and its respective fluxes in marine sediment (Marine) and Terrestrial soil (Terrestrial), without (C) or with *H. diversicolor* (Hd). Symbols represent the mean value, while the error bars represent the standard deviation (n = 4).

In general, the vertical distribution of pore water NH_4^+ was marked by an increase in concentration in the first upper layers, followed by a peak of concentration between 2 to 4.5 cm depth, and eventually a decrease with depth. The pore water NH_4^+ concentration in both substrates was higher in control cores than in cores with *H. diversicolor*, markedly evident at sediment depth of 3 cm downwards (Figure 3.14, upper panel). The pore water NH_4^+ concentration was significantly higher in sediment than in soil. The calculated NH_4^+ fluxes between substrates and overlying water showed slightly higher fluxes in soil. *H. diversicolor*

enhanced the release of NH_4^+ in sediment while it reduced the efflux in soil. Differences in NH_4^+ fluxes between all treatments were not significant.

The pore water PO_4^{3-} concentration of soil was significantly low (under the instrument's detection limit). In sediment, the pore water profiles were characterized by a gradual increase in concentration with depth, indicating a release of PO_4^{3-} into pore water (Figure 3.14, lower panel). The concentration in cores with *H. diversicolor was* higher than in control cores in the upper 2.5 cm, slightly lower at 2.5 to 6 cm depth, and slightly higher at 8 cm downwards. PO_4^{3-} fluxes were slightly higher in cores inhabited by *H. diversicolor* than in control cores. There were no detectable differences in PO_4^{3-} fluxes between treatments.

3.2.2 Experiment 2: Potential bioirrigation capacity of key bioturbator in coastal peatland restoration (MCF Exp 2)

Peat soil characteristics

Bulk density wet was higher than bulk density dry (Figure 3.15). The vertical pattern of the two bulk densities was similar, where an increased value was measured from the surface to 3 cm depth, followed by a gradual decline down to 8 cm depth and a gradual increase downwards. Particle density was higher in the first top layers to 4 cm depth and slightly decreased with depth.

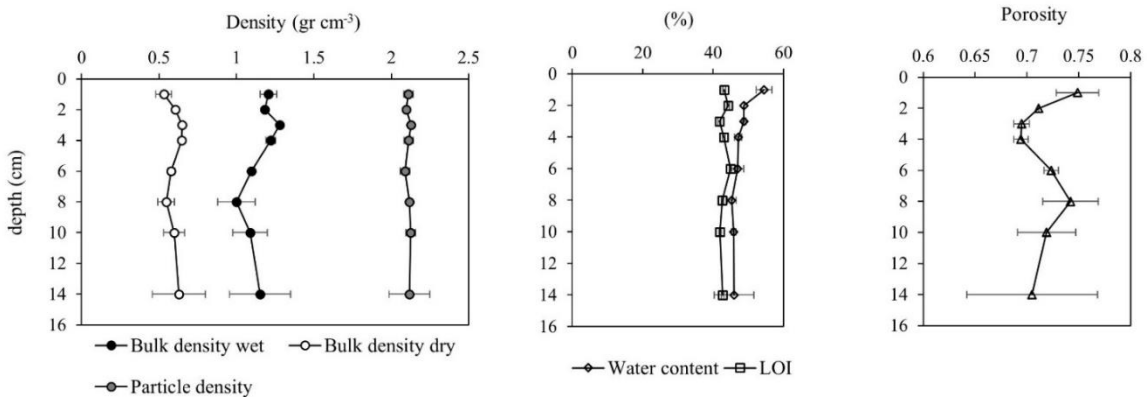

Figure 3. 15 Depth profiles of peat soil physical characteristics. Symbols represent the mean value, while the error bars represent the standard deviation (n = 2).

The porosity of the peat soil exhibited a dynamic trend with depth. The highest porosity was obtained at the surface. The values slightly declined with depth down to 4 cm before it rose again to reach the surface value at 8 cm depth. Below 8 cm, the porosity values gradually declined with depth. The MCT scan of the peat soil cores revealed the basic components of the peat soil (air, mineral, and organic materials) and the complex networks of roots and air channels throughout the cores. Through the MCT approach, the porosity of the peat soil ranged between 0.6 – 0.8. The vertical profile of water content and LOI was reversed at the top 4 cm layers. While water content peaked at 3 cm depth, LOI was the lowest. Furthermore, water content slightly decreased with depth, while LOI peaked at 6 cm before it decreased gradually with depth.

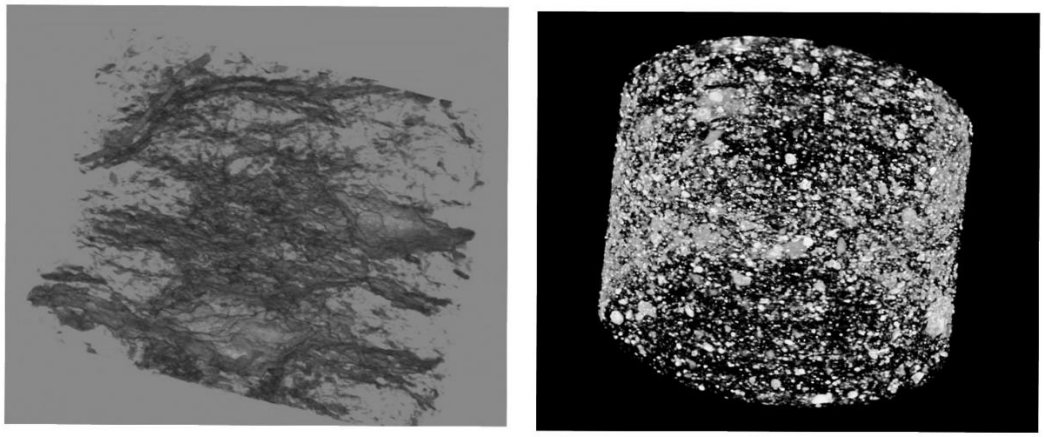

Figure 3. 16 Peat soil components obtained from MCT scan. Networks of fiber and air between the channel are shown in the left panel; 3D projection of mineral components is shown in the right panel.

Animal impact on soil biogeochemistry

At the start of the experiment, the TOU of cores later assigned as control cores showed high variation (19 ± 7.5 mmol m^{-2} d^{-1}), while the TOU of cores assigned for different fauna treatments had similar values (15 ± 4 mmol m^{-2} d^{-1}) (Figure 3.17). Throughout the week of incubation, the TOU of two of the control cores remained high, higher than that of the colonized cores, which were, therefore, excluded from further analysis.

In week 1, TOU increased in both control cores (13 %) and cores with animals (38 % in *H. diversicolor*, 36 % in *M. arenaria*, and 44 % in *M. neglecta*). TOU fluctuated throughout week 2 to week 4, with higher flux fluctuation in cores inhabited by *H. diversicolor* varied between 2 – 4 mmol m^{-2} d^{-1}). Significant difference in TOU between treatments was only detected in week 2 (One-Way ANOVA, $p = 0.002$). Average TOU from the time of animal addition indicated a slightly higher uptake of O_2 in cores with *M. neglecta* (21 ± 1.3 mmol m^{-2} d^{-1}), followed by cores with *H. diversicolor* (20 ± 1.5 mmol m^{-2} d^{-1}), and the lowest uptake in cores with *M. arenaria* (19 ± 1.1 mmol m^{-2} d^{-1}).

Baselines of NH_4^+ (7 ± 0.1 µmol l^{-1}), NO_3^- (34 ± 7.4 µmol l^{-1}), NO_2^- (5 ± 1.4 µmol l^{-1}), PO_4^{3-} (0.33 ± 0.02 µmol l^{-1}), and SiO_2 (12.1 ± 1 µmol l^{-1}) concentration in the overlying water were comparable in all treatments and their replicates with slightly higher concentration in *M. neglecta* cores. While nutrient concentrations in the added water remained stable throughout the experiment, nutrient concentrations varied among treatments during incubations (Figure 3.18). NH_4^+ concentration decreased from baseline to week 1 and remained stable until week 3. All cores showed increased NH_4^+ concentration throughout every incubation from baseline to week 3, before dropping in week 4.

NO_3^- concentrations in the water column of all cores were higher at the beginning of the experiment. NO_3^- concentration was elevated in most control cores during incubation, except on week 3. Cores inhabited by *H. diversicolor* and *M. arenaria* demonstrated a similar pattern of increased concentration in week 1 and 4 and decreased concentration in weeks 2 and 3. A decrease in NO_3^- concentrations during incubations occurred in *M. neglecta* cores, except in week 4. NO_3^- concentrations were increased during baseline incubation, with the highest value in control cores (5 µmol l^{-1}). In the following weeks until the end of incubation, NO_3^- concentrations were significantly low in all cores.

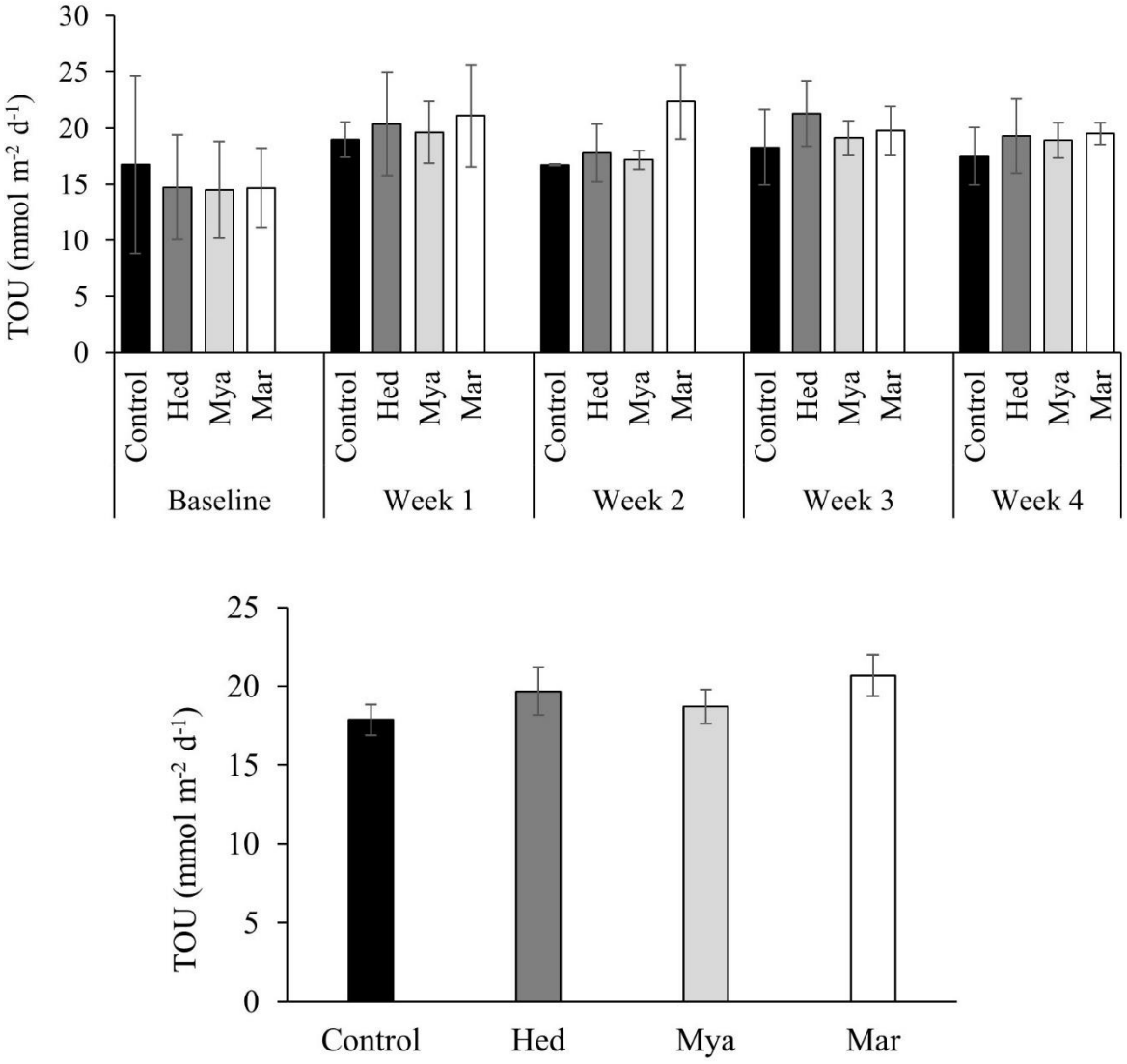

Figure 3. 17 Total O_2 uptake (TOU) in flooded peat soil without (Control) and with added animals (Hed: *H. diversicolor,* Mya: *M. arenaria,* and Mar: *M. neglecta*). Values were calculated from concentration gradients in the water column. The upper panel shows temporal patterns, and the lower panel shows averages from the time of animal addition. Error bars represent the standard deviation (n = 6).

Compared to control cores, PO_4^{3-} concentrations in the overlying water of colonialized cores decreased during baseline incubation. Throughout the following weeks, PO_4^{3-} concentration in control cores fluctuated, while all cores with animals experienced a decrease in PO_4^{3-} concentration.

SiO_2 concentration in the overlying water of control and *M. arenaria* cores fluctuated in a similar pattern, as did cores with *H. diversicolor* and *M. neglecta.* An increase in SiO_2 concentration occurred in almost all former incubations, while an increase in concentration only occurred in baseline and week 4 of the latter.

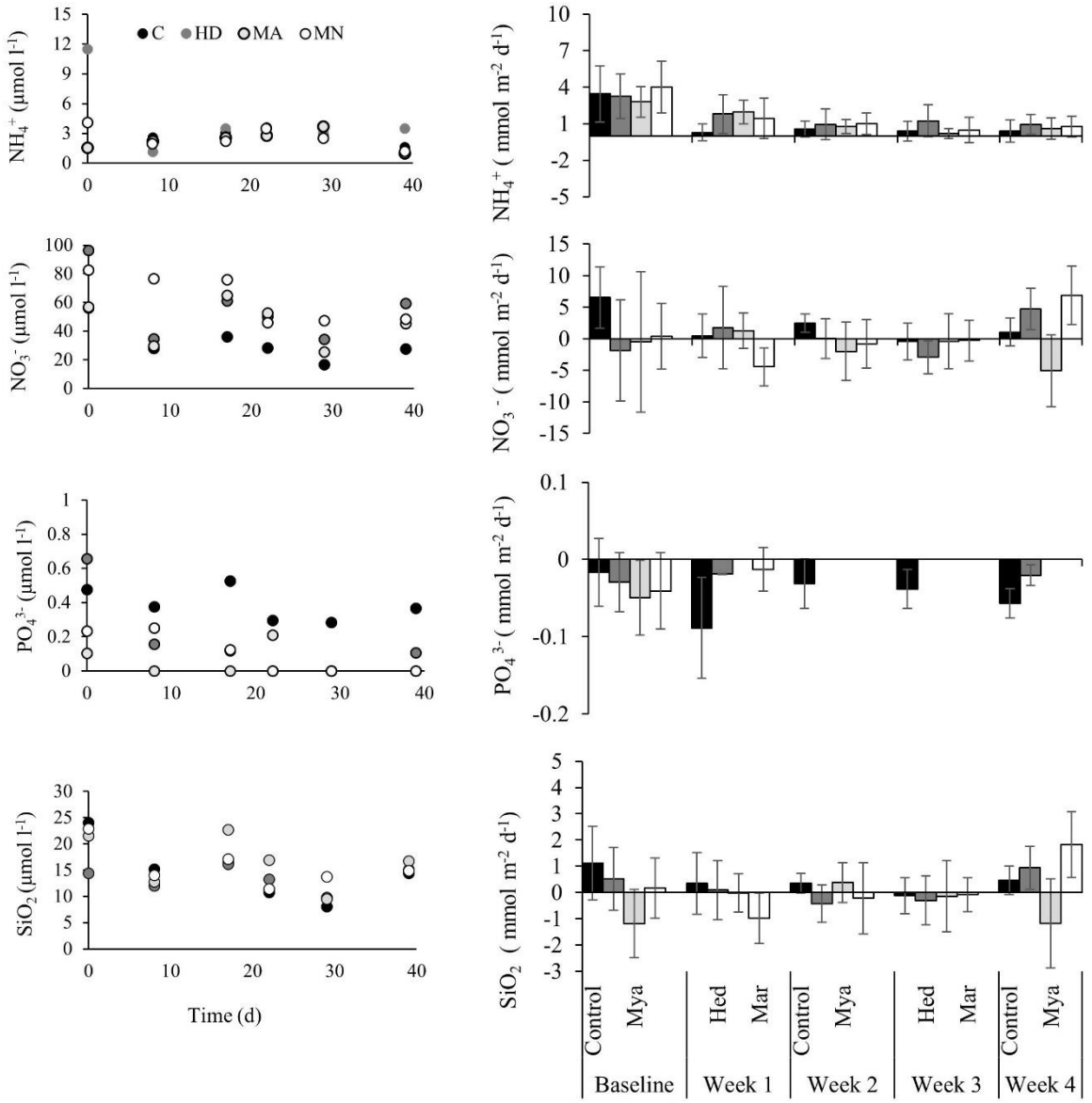

Figure 3. 18 Temporal pattern of nutrient concentrations in the overlying water (left panel) and fluxes calculated from concentration gradients in the water column (right panel) of peat soil without (C, Control) and with added animals (HD, Hed: *H. diversicolor,* MA, Mya: *M. arenaria,* and MN, Mar: *M. neglecta*). Error bars represent the standard deviation (n = 6).

Baseline NH_4^+ fluxes were comparable in all cores (3.4 ± 0.5 mmol m^{-2} d^{-1}) and directed out of the soil throughout all incubations. After a week of incubation, NH_4^+ fluxes in control cores dropped 11.6 times and remained low until the termination of the experiment. The release of NH_4^+ in all faunated cores was higher than in control cores and decreased with time. Compared to the other colonizer cores, cores with *H. diversicolor* released higher ammonium fluxes, except in week 1, when slightly higher fluxes were measured in cores with *M. arenaria.* The stimulation of tested fauna on NH_4^+ fluxes did not differ significantly. However, significant differences in weekly NH_4^+ fluxes were detected in all treatments (*H*-test, controls:p = 0.005, HD: p = 0.046, MA p = 0.001, MN p = 0.005).

At the start of the incubation, NO_3^- fluxes and direction varied among treatments, where high variability was found in *M. arenaria* cores. Nitrate flux directions in colonized

cores varied over time within the range of -4.76 to 6.6 mmol m^{-2} d^{-1}, where the polychaeta cores exhibited high fluxes. While control and *H. diversicolor* cores predominantly released NO_3^- into the water column, NO_3^- fluxes were mainly directed into the soil in *M. arenaria* and *M. neglecta* cores. A significant difference in NO_3^- fluxes was only observed in week 4 (*H*-test, $p = 0.003$).

Baseline PO_4^{3-} fluxes were low (-0.03 ± 0.02 mmol m^{-2} d^{-1}) in all treatment cores and all directed into the soil. Control cores experienced a significant PO_4^{3-} uptake in week 1, which decreased throughout weeks 2 and 3 before slightly increasing in week 4. Among faunated cores, only cores with *H. diversicolor* in week 1 and week 4 showed a small amount (-0.02 ± 0.01 mmol m^{-2} d^{-1}) of PO_4^{3-} uptake; however, the impact of fauna on PO_4^{3-} fluxes was only significant in cores with *M. arenaria* (*H*-test, $p = 0.004$).

SiO_2 fluxes were low with high variation in its direction. SiO_2 fluxes in control cores were the highest initially, decreased from week 1 to week 3, and slightly increased in week 4. Cores with added animals experienced fluctuation in amount (low: -1.3 to 2 mmol m^{-2} d^{-1}) and direction of SiO_2 flux. SiO_2 flux directions on the last week of incubation mirrored the baseline flux directions, where only cores with *M. arenaria* were directed into the soil.

Animal recovery and bioirrigation

Animal recovery varied among species (Table 3.5), with the highest recovery for *M. arenaria,* followed by *H. diversicolor* and *M. neglecta.* The survival rate of *M. arenaria* was significantly higher than *M. neglecta* (*H*-test, $p = 0.002$). A high proportion of *H. diversicolor* (42 %) and ~10 % of *M. neglecta* were retrieved from the bottom of the incubation tank and considered to have escaped the soil core during the incubation. Considering the escaper proportion, overall, *H. diversicolor* survival was considerably higher.

The burrowing depth of the animals was shallow and within the same ranges (Table 3.8). *M. neglecta* and *H. diversicolor* performed slightly deeper penetration than *M. arenaria.* Most recovered *M. arenaria* were found at the surface of the soil core. Br^- tracer incubation in control and colonized cores indicated a background Br^- concentration of 0.24 ± 0.03 mmol l^{-1} measured from 5 cm depth (Figure 3.19, upper panel). Based on Br^- depth profiles, the maximum bioirrigation depth varied from 2.5 to 3.5 cm. Br^- profiles were similar among control cores and cores with animals, resembling diffusion-controlled profiles. The Br^-concentration gradient was the steepest from 0.5 – 2.5 cm depth, with variations of Br^-concentration ranging from 1 to 8 mmol l^{-1}. Calculated Br^- inventories were comparable among treatments (*H*-test, $p = 0.647$) and approximately 36.83 ± 16 % higher than Br^- inventory in control cores. The area-specific bioirrigation was comparable between *M. arenaria* and *M. neglecta*, while *H. diversicolor* showed the lowest value. These differences, however, were statistically insignificant (*H*-test, $p = 0.960$). The weight-specific bioirrigation was significantly high in cores with *M. neglecta* (*H*-test, $p = 0.002$).

Table 3. 5 Number and biomass of the animals: *H. diversicolor (*Hed*), M. arenaria,* (Mya), and *M. neglecta* (Mar) used in flooded peat soil (colonization experiment) with their respective recovery, maximum depth of burrows, area- and weight- specific bioirrigation rates determined by the end of experiment.

	Hed	Mya	Mar
Added Individuals(per core)	4	4	9
Individual biomass (mg ind $^{-1}$)	286.3 ± 13	275.7± 20	141.2 ± 13
Total biomass (g m^{-2})	145.9 ± 0.1	140.5 ± 0.4	146.9 ± 0.01
Recovery (%)	37.5 ± 20.9	95.8 ± 10.2	25. 9 ± 8.2
Escaper (%)	41.6	0	10.2
Max. burrow depth	1.6 ± 0.6	1.2 ± 0.4	2 ± 0.6
Br Inventory (mmol Br m^{-2})	106 ± 27	131 ± 49	111 ± 74
Area specific bioirrigation (L m^{-2} d^{-1})	3.53 ± 1.3	4.50 ± 2.2	4.73 ± 4.4
Weight specific bioirrigation (mL Br g^{-1} d^{-1})	94.12 ± 35.7	43.87 ± 22	198.1 ± 77.7

Pore water nutrient profiles

The SO_4^{2-} pore water profile generally shared a similar trend between core treatments (Figure 3.19: lower panel). SO_4^{2-} was removed in the first 3.5 cm depth of the soil, relatively stable at 3.5 to 9 cm depth, and accumulated downwards. Pore water SO_4^{2-} concentration in control cores was considerably lower than in colonized cores. In the upper reactive layer,

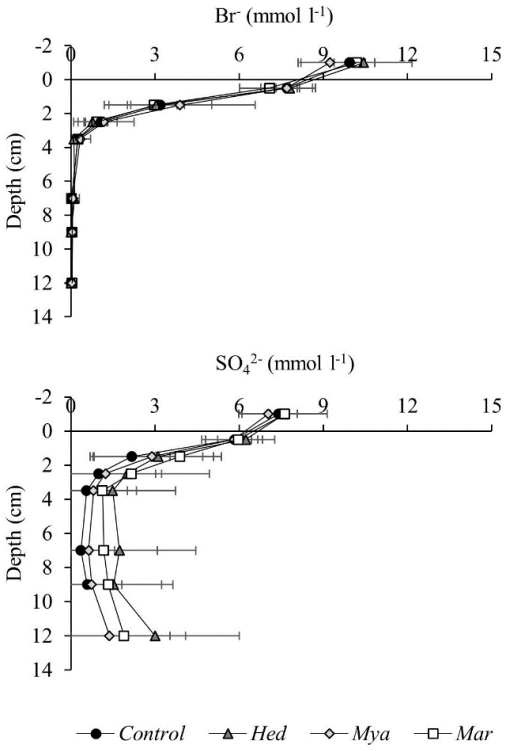

Figure 3. 19 Depth profiles of Br^- and SO_4^{2-} in peat soil without (Control) and with added animals (Hed: *H. diversicolor,* Mya: *M. arenaria,* and Mar: *M. neglecta*). Symbols represent the mean value, while the error bars represent the standard deviation (n = 6).

SO_4^{2-} concentration in control cores varied between 1 and 6 mmol l^{-1}, while within the presence of the animals, SO_4^{2-} concentrations ranged from 2 to 6 mmol l^{-1}. Among

colonized cores, cores with *M. arenaria* displayed the lowest concentration. In contrast, SO_4^{2-} concentration in *H. diversicolor* and *M. neglecta* cores showed higher concentration alternately in the upper and lower reactive layers.

Vertical distribution of NH_4^+ (Figure 3.20) followed a uniform shape and was generally less than 2.5 mmol l^{-1} in all treatments, with higher concentration found in cores with *M. arenaria*. NH_4^+ was released into pore water down to 3.5 cm in control and *M. arenaria* cores, while it was roughly 1 cm deeper in *H. diversicolor* and *M. neglecta* cores. Further down, NH_4^+ removal occurred, but only in colonized cores. It was detected at around 4.5 cm depth in cores with polychaeta and at 9 cm depth in *M. arenaria*.

NO_3^- downcore profiles exhibited a similar pattern among treatments, where a substantial decrease in concentration occurred from overlying water to 0.5 cm depth, followed by a slight increase at 2.5 cm depth, before it remained constant with depth (except for *M. neglecta* cores). Although similar in shape, pore water NO_3^- concentrations were slightly higher in control and *M. arenaria* cores. In the lower part of the profiles, at around 4.5 cm depth, NO_3^- removal and lowest concentration were measured in *M. neglecta* cores.

Pore water concentration of PO_4^{3-} in control cores was characterized by a weak subsurface maximum at 15 cm depth and a subsequent increase in concentration with depth. On the other hand, a well-defined peak (*M. areanaria* at 3 cm depth, *H. diversicolor* at 4 cm depth, *M. neglacta* at 4.5 cm depth) was found in animal-inhabited cores before it decreased with depth (down to 9 cm depth in *H. diversicolor* and *M. neglecta*, down to 7 cm depth in *M. arenaria*). An increase in concentration with depth was found in the lower part of the *M. arenaria* cores, mimicking the lower part of the profile of the control cores. Likewise, PO_4^{3-} concentration was higher in control and *M. Arenaria* cores compared to *H. diversicolor* and *M. neglecta* cores.

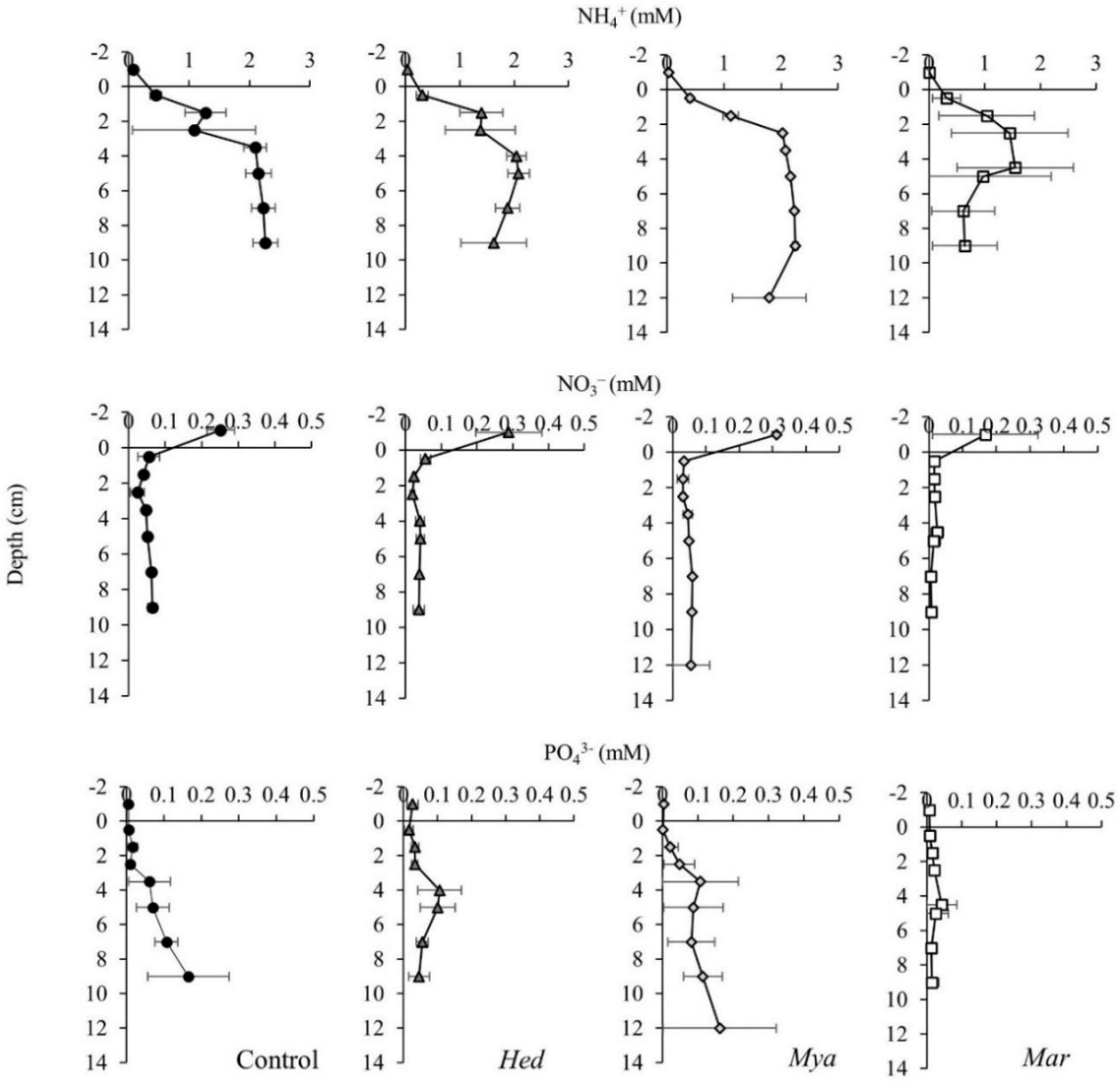

Figure 3. 20 Nutrient pore water profiles of inundated peat soil cores extracted at the end of the experiment without (Control) and with added animals (Hed: *H. diversicolor,* Mya: *M. arenaria,* and Mar: *M. neglecta*). Symbols represent the mean; error bars represent the standard deviation (n = 6).

Pore water profile of dissolved carbon, dissolved nitrogen, and C:N ratio

The total dissolved carbon (TDC) proportion was dominated by dissolved organic carbon (DOC) (Figure 3.21). As a result, DOC pore water profiles mimicked the TDC profiles shape in each treatment. Overall, TDC and DOC concentrations in the control cores were lower than in the colonized cores. TDC and DOC concentrations of control cores in the upper 2.5 cm of the soil were similar to those in the overlying water. Below 2.5 cm, both solute concentrations increased before remaining constant at 7 cm depth. TDC and DOC profiles in colonized cores were characterized by increased concentration in the upper layer and peak concentrations at 3.5 cm: *H. diversicolor*, 5 cm: *M. neglecta*, and 7 cm: *M. areanaria* before significantly decreasing. In particular, increased concentration occurred at greater depth in *H. diversicolor* and *M. neglecta* cores.

The concentration of DIC in control cores was generally lower than in faunated cores. A decrease in concentration from overlying water occurred, down to 0.5 cm depth in control cores, and with the presence of animals, roughly to 3 cm depth. Subsequently, a slight increase in concentration was measured in control and *M. arenaria* cores at 1.5 and 3 cm depth, respectively, in contrast to lower concentration in *H. diversicolor* and *M. neglecta* cores (both at 3 cm depth).

Between 4 and 9 cm depth, DIC concentration in control and *M. arenaria* cores remained stable, while a slight decrease occurred in *H. diversicolor* and *M.neglecta* cores. The shape of total dissolved nitrogen profiles was in agreement with TDC and DOC profiles. Likewise, the TDN concentration of control cores was lower than that of colonized cores. Conversely, the C: N ratio increased from overlying water to 2.5 cm depth in cores colonized by *M. arenaria* and *M. neglecta.* Of all faunated cores, a high C: N ratio plateau persisted to deeper layers (down to 5 cm depth) in cores with *M. neglecta*. While the C: N ratio remained constant in control cores, the C: N ratio decreased with depth in faunated cores.

The C: N ratio depth distribution was the lowest in control cores (7.8) and the highest in *M. arenaria* cores (12.2). Control cores and *H. diversicolor*-inhabited cores shared a similar shape on the C: N ratio vertical distribution in the upper layer of the soil. C: N value decreased from overlying water to 0.5 cm depth before increased and peaked at 2.5 cm.

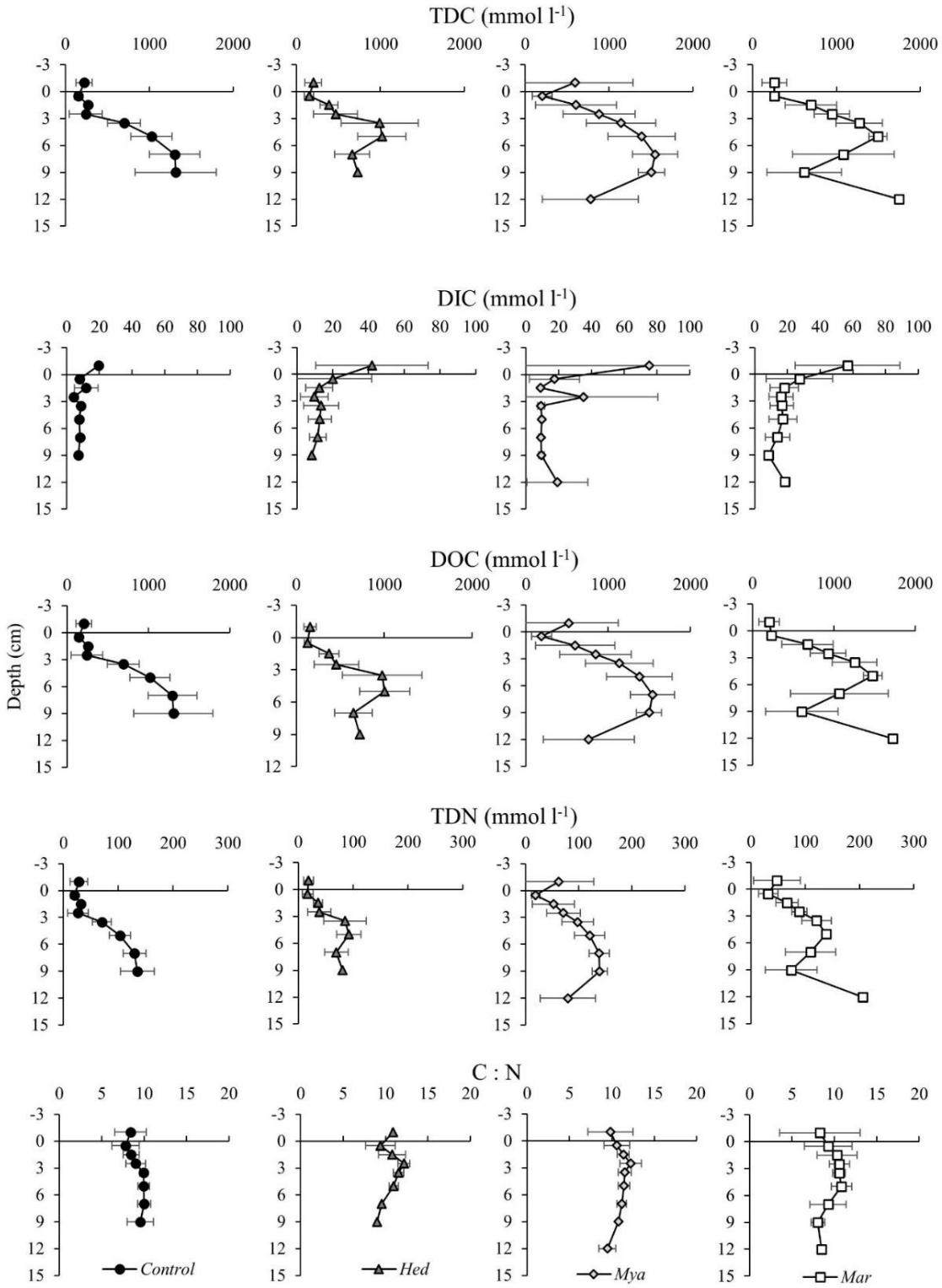

Figure 3. 21 Depth profile of TDC, DIC, DOC, TDN concentrations, and the respective C: N ratio from pore water of inundated peat soil extracted at the end of the experiment. Symbols represent the mean; error bars represent the standard deviation (n = 6).

3.2.3 Experiment 3: 2D O_2 dynamics in sediment (marine) and soil (terrestrial) colonized by *Hediste diversicolor* (MCF Exp 3)

2D O_2 distributions

For all measurements, O_2 concentration was higher at the SWI (Figure 3.25) than along the burrow (Figure 3.22, 3.23, 3.24) and decreased with depth. At the SWI, slightly higher O_2 concentrations were found in aquaria with artificial burrows (217 µM in sediment, 206 µM in soil) than in colonized aquaria (210 µM in sediment, 195 µM in soil). Examples of O_2 concentration time series recorded with the planar O_2 optode in sediment and soil containing artificial burrows and burrows of *H. diversicolor* are presented in Figure 3.22, 3.23, and 3.24. Extracted from the selected ROI across the burrows, the maximum O_2 concentration in the artificial burrow reached 165 µM in sediment, while it only peaked at 145 µM in soil. Two hours after switching off the pump, the concentration fell to 131 µM and 110 µM in sediment and soil, respectively. A completely anoxic condition in the artificial burrows and burrows of *H. diversicolor* had not been reached even after more than three hours of recording.

All added *H. diversicolor* burrowed immediately in both substrates. O_2 diffusion and burrow ventilation drove the O_2 dynamics in the colonized aquaria. O_2 concentration and distribution around the burrow of *H. diversicolor* in both substrates highly varied spatially and temporally. Within the 5-min temporal resolution, the average minimum and maximum O_2 concentration in the middle of the burrow of *H. diversicolor* varied between 65 ± 22 µM and 113 ± 18 µM in sediment and between 113 ± 18 µM and 170 ± 4 µM in soil.

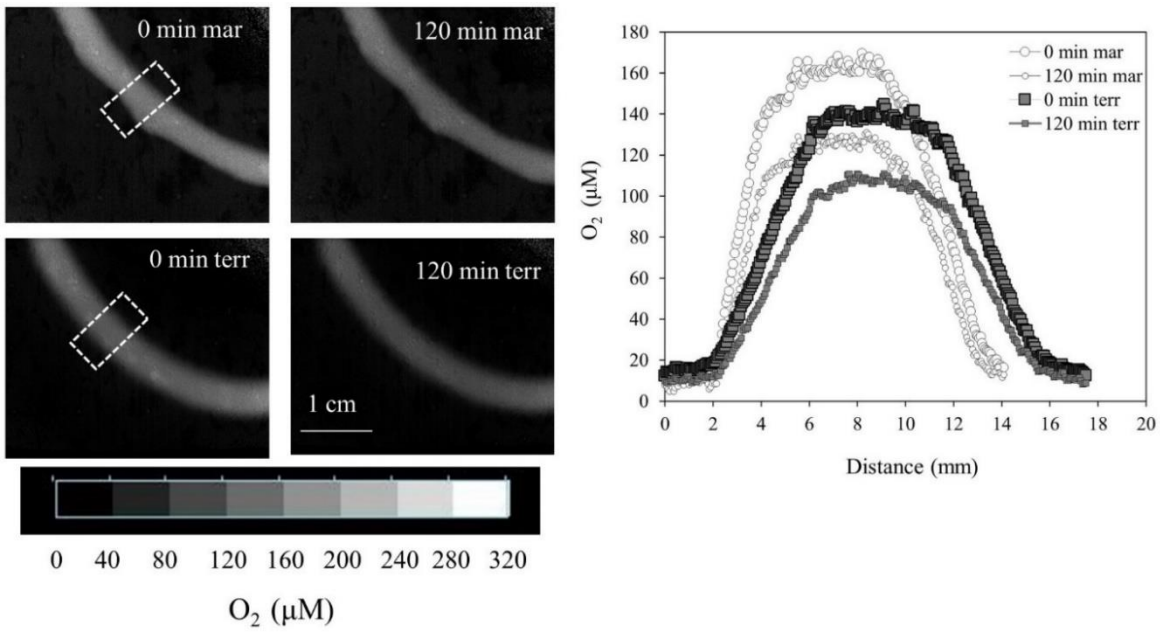

Figure 3. 22 Selected O_2 images showing spatial and temporal O_2 distribution in artificial burrows (left; upper panel: sediment (mar), lower panel: soil (terr)) before and 2 h after turning off the pump. O_2 concentration profiles perpendicular to burrow axes (right). The profiles were extracted perpendicularly to the burrow as indicated by the white rectangular) in the O_2 images.

As interpreted from the oscillation of O_2 concentration in the selected ROIs, the burrows were ventilated periodically in a sequence of pumping and resting periods. Oxygenation occurred more frequently in sediment than in soil. Pumping and resting events lasted 5 to 10 minutes in sediment, while the duration was longer in soil (30 min pumping event, 25 min resting event).

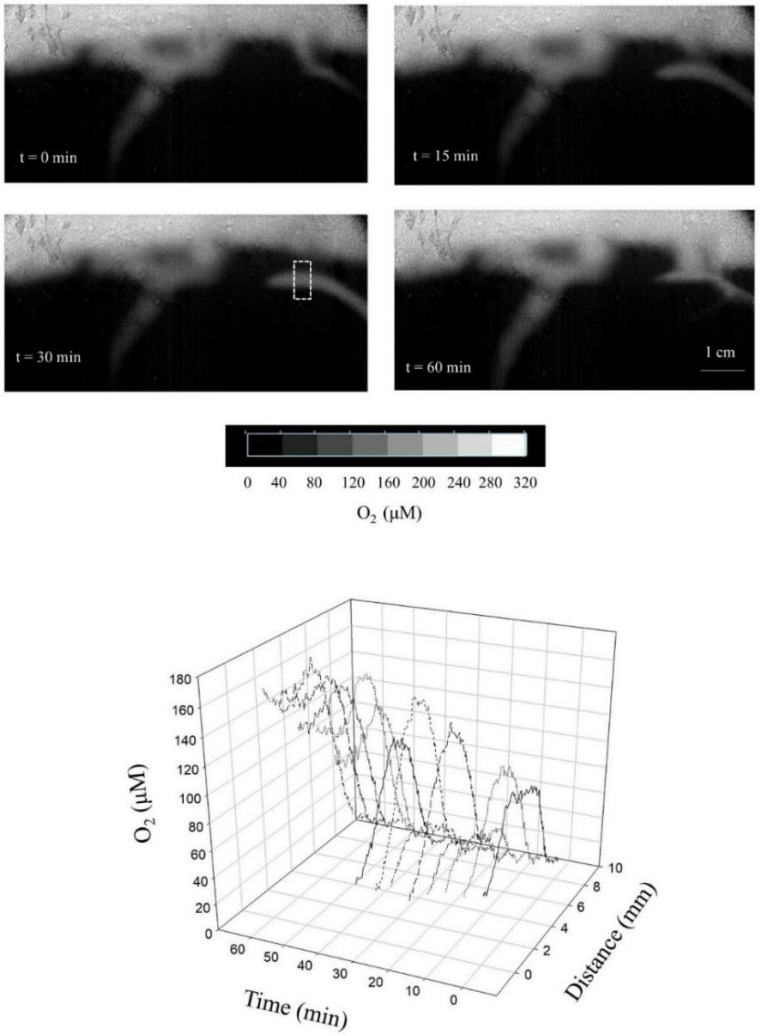

Figure 3. 23 Selected O_2 images showing spatial and temporal O_2 distribution in the burrow of *H. diversicolor* in sediment (upper panel) and horizontal O_2 concentration profiles (lower panel). The O_2 profiles in the lower panel were extracted at 5-min intervals perpendicular to the burrow axis, as indicated by the white rectangle in one O_2 image. Note that the lower panel contains more data points (5 min interval over 1 h period than the upper panel (15 min interval over 1 h period).

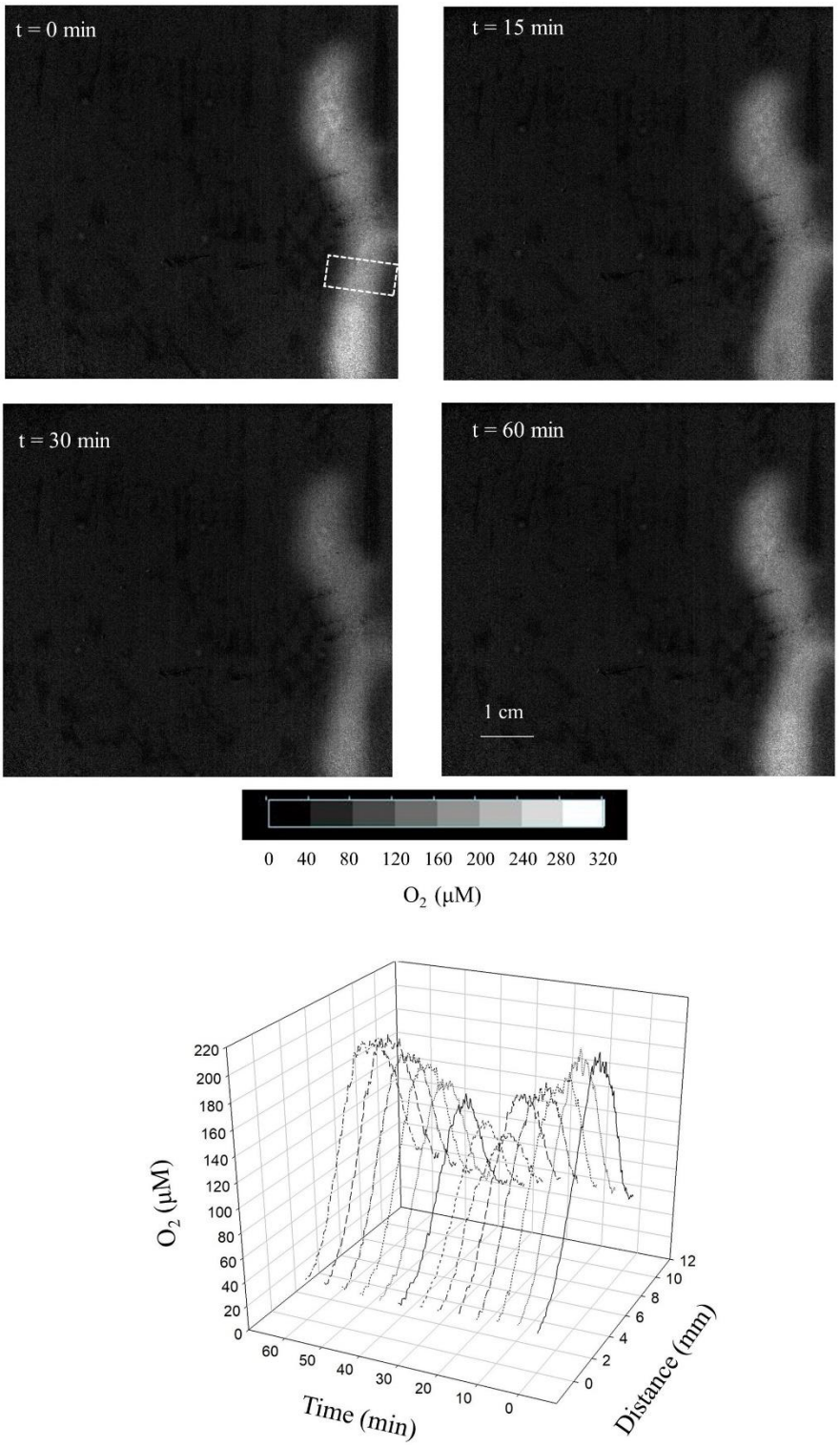

Figure 3. 24 Selected O_2 images showing spatial and temporal O_2 distribution in the burrow of *H. diversicolor* in soil (upper panel) and horizontal O2 concentration profiles (lower panel). The O_2 profiles in the lower panel were extracted at 5-min intervals perpendicular to the burrow axis, as indicated by the white rectangle in one O_2 image. Note that the lower panel contains more data points (5 min interval over 1 h period than the upper panel (15 min interval over 1 h period).

The vertical O_2 microprofiles (Figure 5, ROIs transect across SWI) extracted from O_2 images of aquaria with artificial burrows showed O_2 penetration depth of 4 - 6 mm and

6 - 8 mm in sediment and soil, respectively. The O_2 penetration depth in colonized sediment was slightly higher (8 – 6 mm), while in terrestrial soil, the value remained the same as in azoic aquaria.

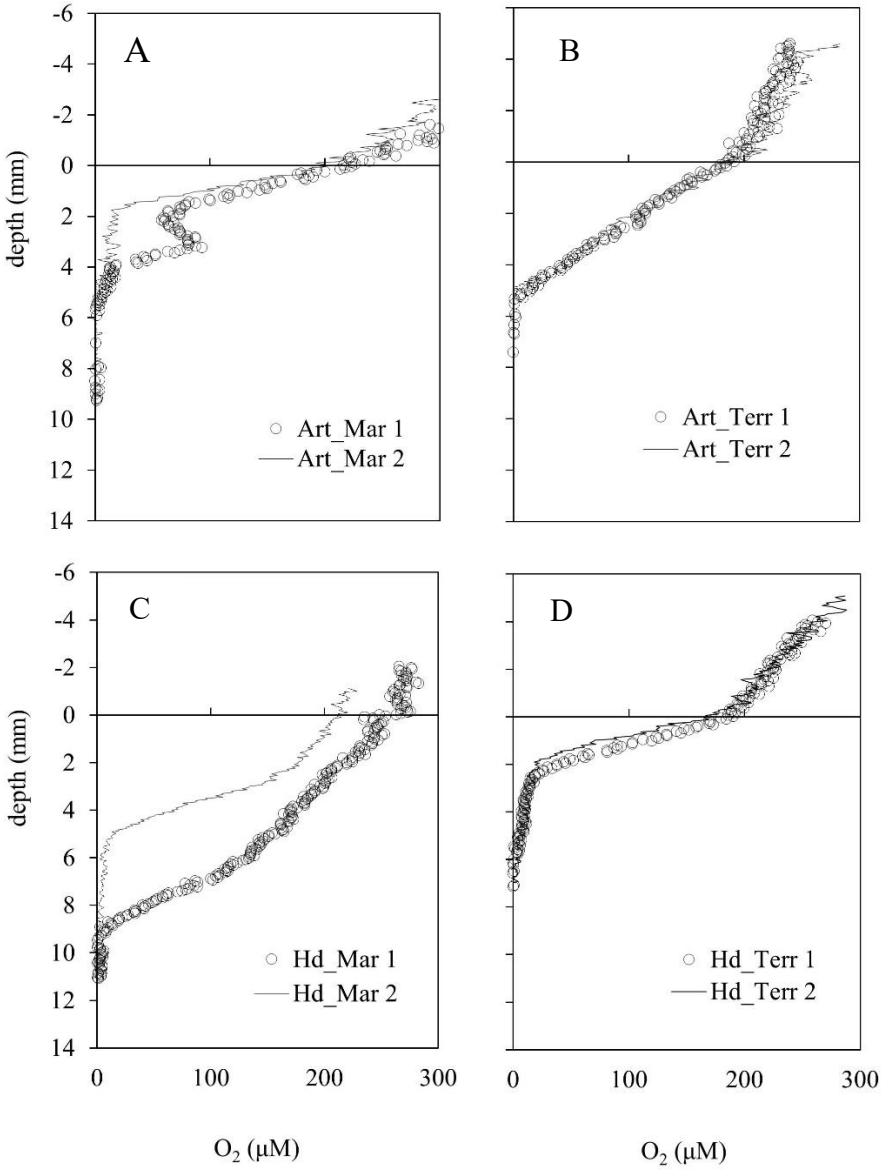

Figure 3. 25 Example of typical O_2 microprofile across the SWI extracted from O_2 images (n = 2 ROIs) of respective treatments; sediment with artificial burrow; Art_Mar (A), soil with artificial burrow, Art_Terr (B), sediment with *H. diversicolor*, Hd_Mar (C) and soil with *H. diversicolor,* Hd_Terr (D).

O_2 diffused from the burrow into the surrounding sediment and was consumed rapidly. Two hours after stopping the pump, the O_2 penetration depth in the artificial burrow had decreased from 4.6 mm to 3.8 mm in sediment and from 5 mm to 4 mm in terrestrial soil. O_2 penetration from the burrow wall of *H. diversicolor* into the substrate oscillated over time according to burrow ventilation and, most of the time, appeared to be asymmetric between wall sides. Interpreted from the transect across the burrows, the burrow diameter of *H. diversicolor* was approximately 2 ± 0.64 mm in marine sediment and 1.46 ± 0.2 mm in terrestrial soil. Between resting and pumping events, O_2 penetration from the burrow wall into the substrate was deeper in soil (3.7 - 5.5 mm) than in sediment (2 – 3.6 mm).

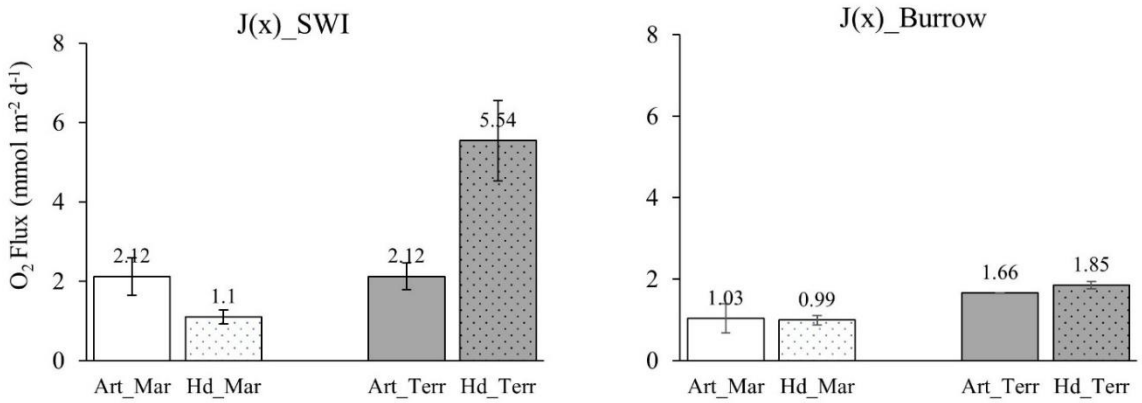

Figure 3. 26 Bar plots summarizing O_2 fluxes at the substrate-water interface (left pane) and the burrow wall of *H. diversicolor* (right panel). Error bars represent standard deviation (n = 3 at SWI, n = 2 at burrows). Color and Symbol represent substrate and burrow type: Mar: sediment, Terr: soil, Art: Artificial, Hd: *H. diversicolor*). Data were extracted from O_2 images over a 30-90 min period.

O_2 Flux

O_2 fluxes at SWI were similar in azoic aquaria, regardless of the substrate. On the other hand, fluxes were higher in colonized aquaria of terrestrial soil than in marine sediment (*H*-test; p = <0.001) (Figure 3.26). Although O_2 fluxes into the sediment across the burrow wall were lower than those at the surface interface, there was no significant difference in O_2 fluxes between treatments (*H*-test; p = <0.067). The flux of O_2 across the burrow of *H. diversicolor* varied with time and followed the pattern of burrow ventilation (Figure 3.27a, 3.27b). In sediment, over time, the change in O_2 penetration depth around the burrow slightly matched the pattern of O_2 concentration and O_2 flux (Figure 3.27). On the other hand, O_2 penetration depth in soil remained stable over time.

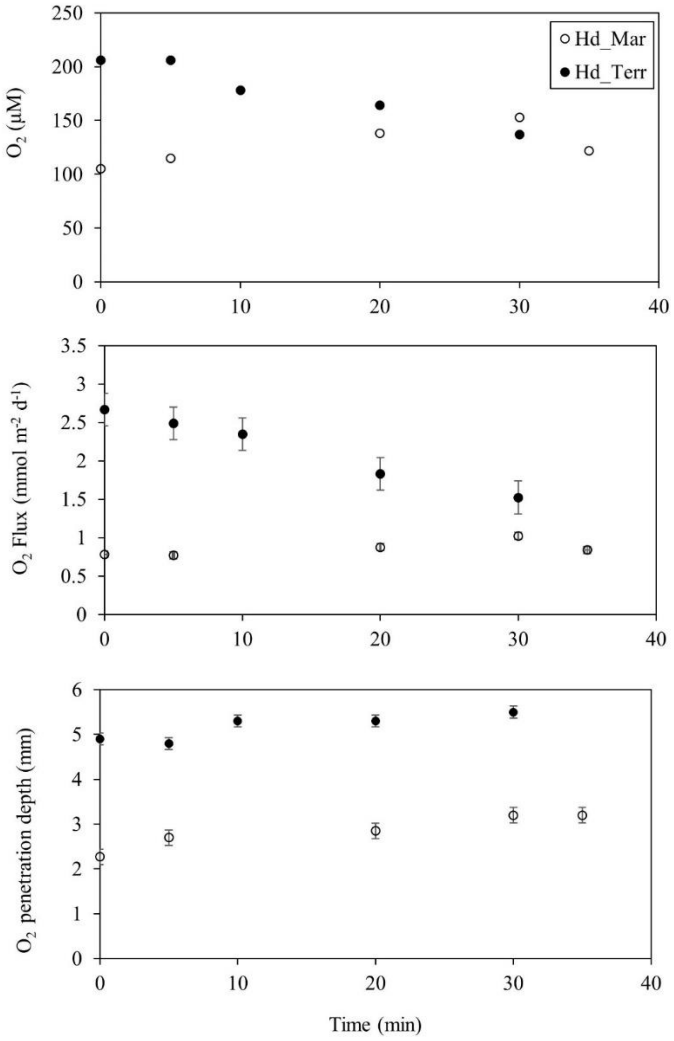

Figure 3. 27 Selected examples of O_2 spatiotemporal dynamics around the burrow of *H. diversicolor* in sediment (Hd_Mar) and soil (Hd_Terr) extracted from O_2 images over a 30-min period.

OCR and Oxygenation rates

OCR in the middle of the artificial burrow was slightly higher in sediment (0.3 µM min^{-1}) than in soil (0.2 µM min^{-1}). OCR in the middle of the artificial burrow was higher than in the burrow walls: 8 times higher in sediment and 6 times higher in soil. However, the difference was statistically insignificant (*H*-test; p= <0.133).

The average OCR in the middle of the burrow of *H. diversicolor* was 7.3 ± 3.8 µM min^{-1} in sediment and 3.7 ± 2.6 µM min^{-1} in soil. Likewise, OCR was higher in the middle of the burrow than in the burrow's walls, 10 times higher in sediment and 4 - 5 times higher in soil. A significant difference in OCR was detected between the middle and peripheral areas of the burrow (One–way ANOVA; p = 0.003). Tukey's HSD post hoc test showed the OCR obtained in the middle of the burrow of sediment to be significantly higher (p = 0.004).

Oxygenation rates, rates of increasing O_2-concentration, in the middle of the burrow of *H. diversicolor* were 9 ± 5 µM min^{-1} in sediment and 1.6 ± 1 µM min^{-1} in soil. The rates were damped with distance from the burrow wall (4 - 10 times lower in sediment, 1 - 3 times lower in soil).

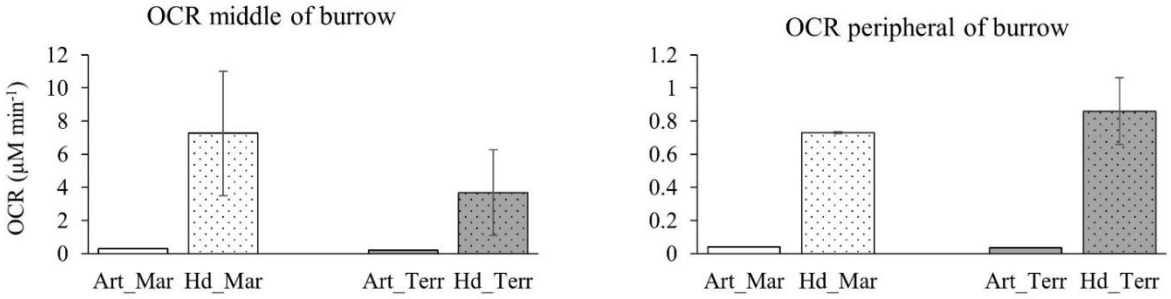

Figure 3. 28 Bar plots summarizing the O_2 consumption rate in the middle of the burrow (left panel) and in the areas around the burrow (right panel). Color and Symbol represent substrate and burrow type: Mar: sediment, Terr: soil, Art: Artificial, Hd: *H. diversicolor*). Data were extracted from O_2 images over a 30-90 min period. Error bars represent standard deviation (n = 3 - 5 burrow of *H. diversicolor*).

3.2.4 Initial colonization of benthic macrofauna in Drammendorf

Before inundation, the most abundant species at the seaside of the flooded coastal peatland of Drammendorf was *T. fluviatilis* in the spring and *P. jenkinsi* in the autumn. The second dominant taxa shift between *Hydrobia* (in spring) and *H. diversicolor* (in autumn). A considerable amount of oligochaete and several crustacean species from genus *Sphaeroma*, *Gammarus*, *Cyathura*, and *Idotea* were evident. Bivalve were represent by *Mya arenaria,* and *Cerastoderma sp.* Selected key species are presented in Figure. 3.29.

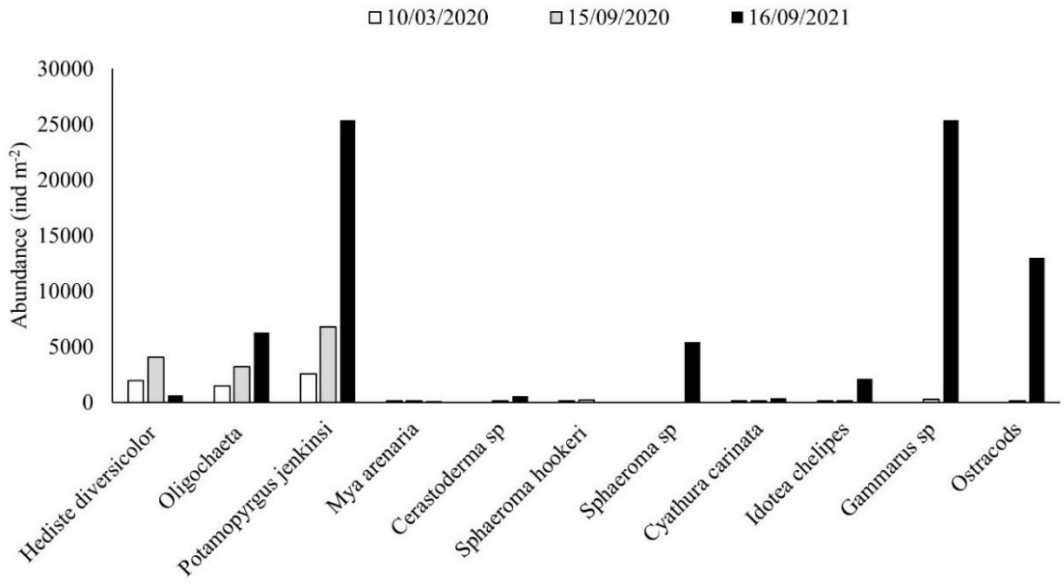

Figure 3. 29 Dominant taxa at the seaside of Polder Drammendorf after coastal flooding.

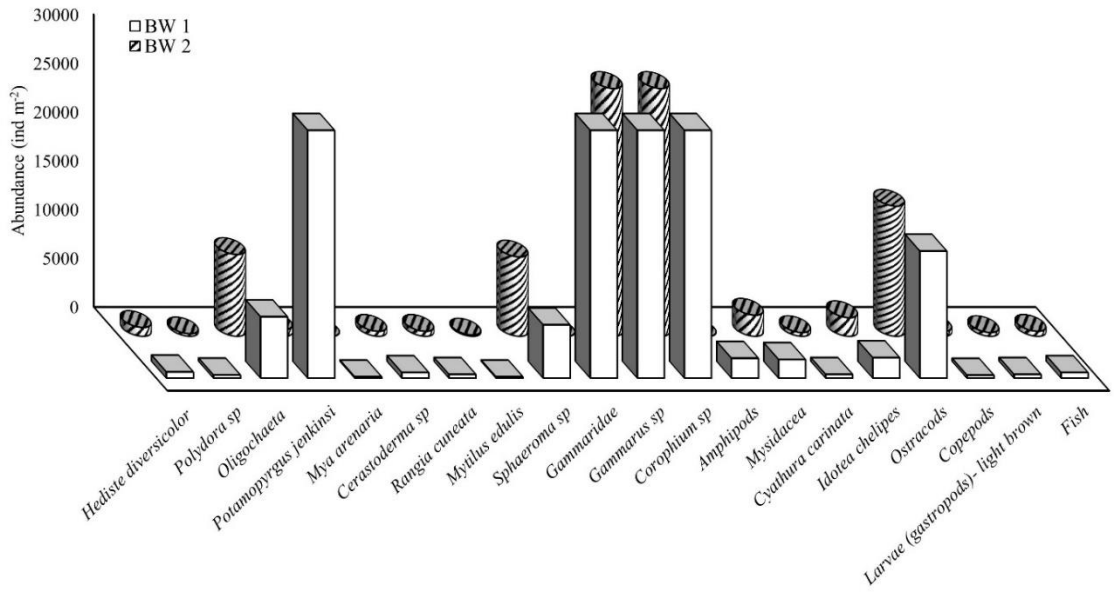

Figure 3. 30 Macrofauna species found inside the newly restored coastal peatland.

In September 2021 (~22 months after the flooding), *P. jenkinsi* and the crustaceans, with additions of several other species, appeared to be the dominant species in the inundated areas (Figure 3.30). In addition, new species were found from some key classes of macrofauna: bivalve (*R. cuneata* and *M. edulis*), crustaceans (*Amphipods, Corophiumand Mysidaceae*), and polychaetes (*Polydora sp*). Of the dominant species at the seaside, *T. fluviatilis* was markedly absent in the flooded area. In general, the total abundance of the dominant species increased with time: 2 times higher in the first year of colonization (spring to autumn 2020) and 4 times higher in the second year of colonization (autumn 2020 to autumn 2021).

4 DISCUSSION

The goal of this study is to improve our understanding of the role of benthic O_2 in coastal ecosystem of the southwestern Baltic Sea. This study outlines system-specific benthic O_2 dynamics to provide insights into the different role of O_2 in two major ecological systems of the shallow aquatic (coastal) environments of the southwestern Baltic Sea: sandy open low coast and lagoon "Bodden" type. Following a short discussion on the different methods used to measure O_2, this chapter focus on benthic O_2 distribution and metabolism associated with respective system.

4.1 Evaluation of the Methods

To date, there is no single ideal technique to measured benthic O_2 and its dynamics. Different techniques possess their advantages and disadvantages. From the deployment, to assumption, to data analysis and interpretation, every measurement is prone to biases. Therefore, some methodological issues which could have bias the results need to be addressed.

In this study, the diffusive O_2 fluxes obtained from microelectrode profiling were calculated from an O_2 concentration gradient just below the SWI, not within the DBL. The invasive nature of O_2 microsensors have been observed to change the structure of the DBL. Glud et al. (1994) suggest that the introduction of microelectrode from the water column accelerate the flow around the electrode shaft, which compress the DBL by ~25 – 45 % below the sensor tip. Compression of the DBL thus can affects the O_2 concentration gradient within the sediment or biofilm, which lead to a higher O_2 exchange (overestimation of diffusive O_2 fluxes).

Although microelectrodes has been shown as a powerful tool for measuring O_2 microprofiles and to follow changes of O_2 concentration, in this study, the duration between the end of one exposure regime (different light and transport regimes) to the start of O_2 profiling could only be taken at best after 10 - 15 min. This duration was used to install the microelectrode and set the acquisition procedure. With this time lag, consequently, the measurement did not fully catch the actual change in O_2 pore water concentration and distribution. Thus, the recorded O_2 profile captured changes corresponding to a given perturbation at different specific time steps. Diffusion of O_2 from overlying water may renew the O_2 pool close to SWI and create a new concentration gradient across the SWI. For instance, similar time lag of diffusion related artifacts have been estimated to contribute to underestimation of OCR values by 10 % (Polerecky et al., 2005).

The selection of the maximum O_2 concentration gradient just below the SWI for O_2 flux calculation is subject to observation bias. This could lead to an over- or underestimation of the calculated fluxes and could account to the variability of the O_2 fluxes. However, the high variability of O_2 profiles (shape and penetration depth) under steady state dark and light condition in this study evidently reflects the heterogeneity of the sediment. Hence, the bias proportion introduced by the calculation is limited. Moreover, the placement of the SWI in manual and modelling calculation of O_2 fluxes was based on the change in slope of the O_2

gradient at the sediment surface. With slight misplacement above or below the true interface, Rabouille et al. (2003) estimated a 10-20 % overestimation of O_2 fluxes.
The diffusive transport coefficient of O_2 in the sediment (Ds) used to calculate O_2 fluxes in this study could be another source of bias. Ds was related to tortuosity (manual gradient calculation) and to the empirical relation between diffusive transport coefficient of O_2 in the water (D_0) and porosity of the sediment (modelling). Both approach required independent determination of porosity profile in high resolution, which was not available in this study. The used porosity values were derived from conventional drying technique at a resolution of 1 cm, which was substantially exceeded the spatial resolution of O_2 concentration profile (100 µm). Using Ds derived from porosity has been found to overestimate the fluid-filled pore space, e.g., high intracellular water content in sediment and high water-saturated exopolymers in microbial mat (Revsbech (1989). Nevertheless, O_2 fluxes calculated with the manual and modelling approach were comparable, which excludes a major artefact of the interface localization through the gradient method and confirms the calculations of O_2 fluxes.

In a comparison of calculations from microprofiles with eddy covariance fluxes (EC), Berg et al. (2013) suggested that diffusive O_2 flux at the sediment surface of a permeable sediment may account for as little as 5% of the turbulent flux as determined several cm in the water above the sediment, indicating that vertical O_2 transport was almost exclusively advective. Using in situ chambers, Janssen et al. (2005) showed that advection may increase benthic O_2 uptake 2.5-fold. Advective pore water flows occur locally and depend on the physical structure of the surface sediment, topography and permeability (Huettel and Webster 2000; Ziebis et al., 1996; Huettel and Gust 1992). However, where this happens within the large sediment surface area observed during an EC measurement "foot-prints" cannot be resolved by EC. Nevertheless, current literature considers EC fluxes closest to "true" fluxes (Attard et al., 2019; Rodil et al., 2019). There is little knowledge currently on the relation of fluxes measured from large areas above the sediment (EC) and how this signal is composed by specific diffusive or advective fluxes occurring locally at the sediment interface with in this foot-print. Comparison of EC and other methods is not the issue in this study. Fluxes calculated here as diffusive transport, however, need to always be interpreted knowing that they may represent a lower limit and that advection would significantly enhance flux values.

Planar optode measurements have complemented the traditional microelectrode approach by providing non-invasive 2D insight of benthic O_2 dynamics with high spatial and higher temporal resolution. However, interpretation of derived O_2 images should be done with care and consideration of limitations of the sensor. Due to its working principle, the sensor act as an impermeable flat wall, which will alter the three dimensional O_2 distribution possessed by most of the studied objects, e.g. in this study sediment with MPB mat and animal's burrow (Glud, 2008; Glud et al., 1996). The wall behind the sensor foil will limit the distribution of O_2 causing a buildup of O_2. The altered diffusion geometry of the respective system will generate a distorted O_2 images, which lead to overestimation of the O_2 concentration, gradient, and fluxes in the system. Moreover, unlike with a microelectrode, where measurement can be conducted at any point in the sediment, measurement with a

planar optode is restricted to the areas in the sediment where the sensor is visible from outside.

In case of a cylindrical burrow, the placement of planar optode near a burrow would generate a "missing sediment effect" (Polerecky et al., 2006), which leads to a lower O_2 consumption rate. With O_2 transport around the burrow being diffusion-limited, a higher amount of O_2 would persist longer, leading to overestimation of O_2 penetration depth and volume of oxic sediment and underestimation of O_2 fluxes around the burrow (due to distorted concentration gradient). Conversely, the planar optode foil is not always in a direct contact with the burrows. It depends heavily on the animals being examined to construct their burrows as close as possible and in direct contact to the sensor foil. If this does not happen, PO measurement may lead to underestimation of the bioirrigation effect on key properties around the burrow (O_2 penetration depth, oxic volume, O_2 fluxes) (Satoh and Okabe, 2012; Polerecky et al., 2006).

Furthermore, a thin layer of water attached to the sensor foil could separate foil and sediment, leading to a smeared concentration gradient at interfaces (i.e. SWI, burrow linings, interstices of permeable sand). A particular issued was apparent in this study from O_2 profiles after exposure to advection. While obtained in the dark, a typical light profile with a subsurface O_2 peak was obtained instead of a dark profile shape with expected deep penetration owing to advection. It is unlikely that the high O_2 concentrations in the sediment were produced by MPB community through photosynthesis with only 3 s of light exposure from the camera in every 5 min of the pictures acquisition. In most chambers (6 out of 9 chambers), the first (captured) image was taken before stirring started (0 min with dark diffusive regime) already showed high O_2 concentration just below SWI. Other than the long lasting attachment of a thin layer of water with high O_2 concentration, this phenomena could link to persistent O_2 pool as a result of entrapment and low consumption rate (details in "discussion of O_2 distribution"). For this particular case, O_2 fluxes were calculated only from the lower concentration gradient of the derived O_2 profile.

Although care was taken to prevent unnecessary light exposure of the foils during incubation of the benthic chambers, the long-term incubation might still play a role in the decline of the sensor stability. During recalibration after the conclusion of the experiment, under exposure to air and air-bubble water for 100% atmospheric equilibrium, conspicuous and uneven color zonation were observed along the foil: above, below, and at the former position of sediment surface. These observations were further evaluated by comparing the value of the color ratio (R ratio) of these distinctive color zonation (upper, middle, and lower part of the foil) employing the two-point calibrations with the valid range of R ratio provided by tests during fabrication of the sensor foils. This comparison revealed that the stability of the upper and middle part of the sensor foil declined by 44 % and 22 % respectively, while the lower part of the foil remain stable over months. It is speculated that the higher stability of the lower part of the foil was link to the protection by the sediment, while the upper part of the foil was in direct contact with overlying water and light sources, making it more susceptible to photo- bleaching. Phototactic microorganism might also alter the stability of the upper part of the foil. These microorganisms are known to be attracted by blue light and could migrate and colonize the light exposed area of the sensor foil. Furthermore, growth of

a biofilm in dark brown color were observed in the upper part of the foils. Taken into account, that the planar optode system of VisiSense TD is based on color ratiometric, this growth might have impeded the reading of the luminescence signal.
Although O_2 profiles obtained by planar optodes agreed well with the profiles measured with microelectrodes. However, in the anoxic part of the sediment and soil, the pixel values ranged between c.+2 and -2 (%atm). During image processing, this range could lead to misleading color-coding of the substrate, as the high values are colored as being different from zero, although the substrate is completely anoxic (Lenzewski et al., 2018). Moreover, due to higher signal to noise ratio, less precise OCR values has been observed from planar optode measurements (Polerecky et al., 2005). Despite this systematic drawback, the PO technique is proven to be powerful in providing additional insight into the dynamic distribution and metabolism of O_2 in sediment and soil.

4.2 Benthic O_2 distribution in sandy permeable sediment inhabited by a diatom dominated-MPB community

Small scale variability of O_2 distribution was documented in this study from O_2 microelectrode and planar optode data. The influence of light and transport regimes are summarized in Figure 4.1. Under dark diffusive condition, O_2 penetration depth and concentration in the sediment were similar in C and RC chambers. The variation of O_2 penetration depth indicated a characteristic patch size of ~ < 0.5 cm, i.e. profiles separated less than this distance exhibited similar depth distribution. On the other hand, microtopography appeared as irregular position of the sediment surface with 0.5-2 mm difference between individual O_2 profiles at ~ 5 mm horizontal distance. Since the presence of fauna was deliberately excluded in this study, this heterogeneity under diffusive condition was likely determined by the thickness of DBL, microtopography-related patchiness of the MPB, the availability of oxidizable substances (organic and reduced chemical), and the volume-specific OCR (microbial respiration) at the different sites in the sediment. In detailed microsensor studies, it has been shown that the patchiness of the microbial mat resulted from the irregular growth of diatoms (Jørgensen et al.1983) as well as lateral migration of cyanobacterial filaments under exposure to high light intensity (Kühl et al. 1996).

Oxygen pools were observed just below the sediment surface and deeper down to 6 mm depth almost in all chambers. Although it is reported in literatures that formation and release of O_2 bubbles started at light intensity of ~100 µmol photon m^{-2} s^{-1}, this local occurrence was most likely due to formation, buildup, and entrapment of O_2 bubbles throughout the long incubation time coupled with low OCR of the system. Focusing on microzonation of photosynthetic microbial mats, Jørgensen et al. (1983) discovered that gas bubbles found in their mat had short as well as long-lasting lifetime. Short lived bubbles were mainly due to the intensive photosynthesis in the diatom layer (enlarge on diatom tufts) at the surface of the mat, while the latter were produced by cyanobacterial photosynthesis in the deeper layer of the mat. Covered within a thin biofilm, the formed gas developed and trapped deep within the mat. Cook et al. (2007) reported a similar observation of O_2 subsurface maxima from their *in situ* O_2 profiles. They suggested that the interplay between

wave-driven pulses of deep advective O_2 injection into the sediment and varying O_2 consumption rates within the sediment is one possible explanation for these long-lasting O_2 pools. De Beer et al. (2005) and Werner et al. (2006) discussed similar patterns where sediments might remain oxygenated for a period due to imbalances between transport and reaction (low OCR and changing advective flow conditions). In this study, spatial heterogeneity in O_2 consumption rates seems high enough to show such patterns when no light was present and transport conditions varied between diffusion and advection (Figure 3.9).

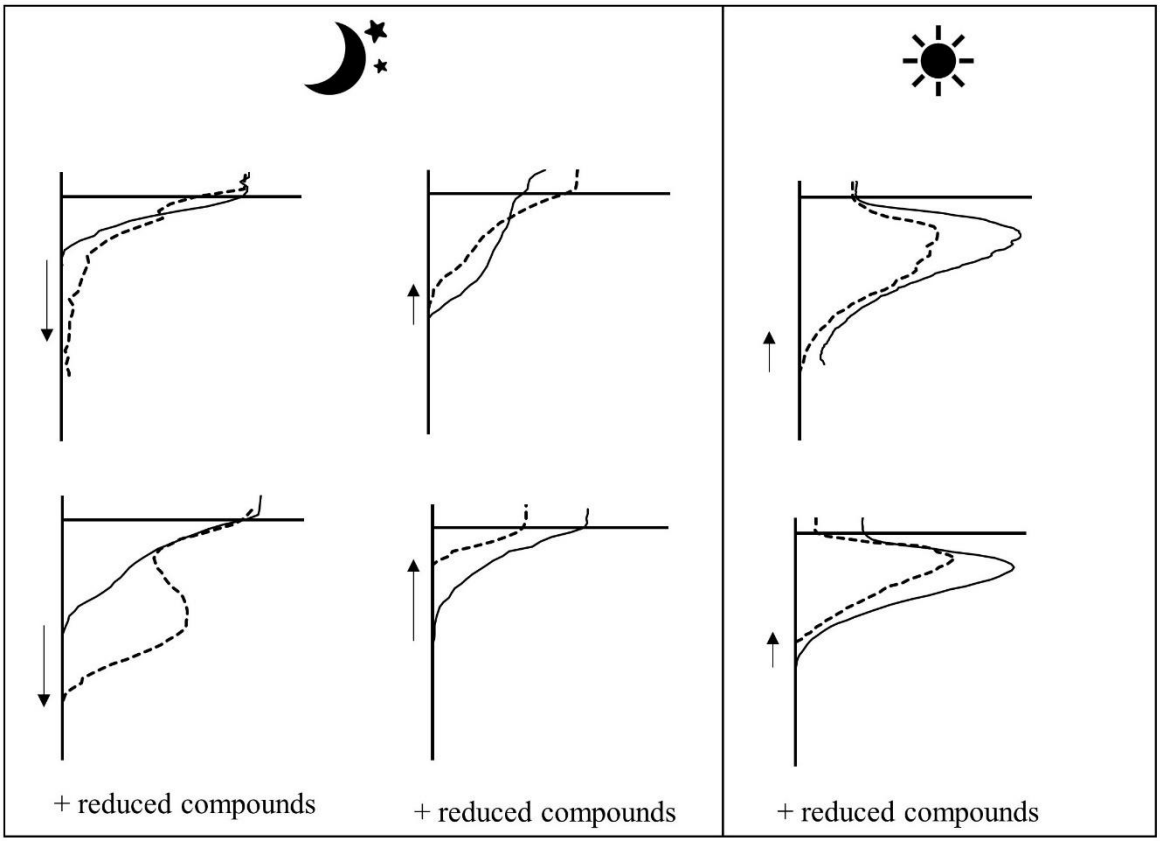

Figure 4. 1 Summary of the effect of light (left vs right panel) and change in transport regime (straight curve line under diffusive condition, dashed curve line after exposure to advection) on the O_2 distribution measured with microelectrode in chamber without (upper panel) and with reduced compounds (lower panel). The variation of O_2 distribution in the dark in association with advection and nutrient regimes is shown by the two profiles curved (in the left, upper and lower panel), while in the light, O_2 distribution showed a uniform pattern (in the right, upper and lower panel). The arrow represents the change in O_2 penetration depth (not to scale), and the horizontal axis represents concentration (dark vs light condition was 1:3 ratio).

As a consequence of photosynthesis (upon illumination and further with increasing light intensity), O_2 concentrations rose and subsequently oxic layer and O_2 penetration depth expanded downward to the initially anoxic layer in both C and RC chambers, with higher values in C chambers. The presence of reduced compounds diffusing from below and their oxidation likely limit the O_2 content and penetration depth in RC chambers. Despite differences in conditions such as temperature, salinity, and nutrient availability, similar observations of light and reduced compounds (from deeper anoxic compartments) influence on O_2 distribution have been reported for microbial mats, intertidal muddy sediment, and

sandy sediment. In addition to processes causing small scale heterogeneity mentioned above, the non-synchronous vertical migration of the MPB community under exposure to light (to more optimal light condition and avoiding photoinhibitory light levels) might contribute to changes in spatial distribution of O_2 in the deeper layer of the sediment (Denis et al. 2012; Cartaxana et al., 2016). Focusing on the diel pattern of MPB primary production, several authors documented that the typical light-driven vertical migration ranged from 0.5 – 1.5 mm (Haro et al., 2019; Cartaxana et al., 2016; Cartaxana et al., 2016).

On average, the O_2 microprofiles measured after exposure to dark advection showed contrasting effect of advection on O_2 penetration depth between chamber types: increased penetration in C chambers, slightly decreased to stable penetration in RC chambers, and similar effects on O_2 concentration (reduced by ~ 14 %) in either chamber types. Considering the flow pattern generated through stirring of the benthic chamber, the similar permeability of the sediment in both chamber types, and the position of the microprofilling close to the chamber wall (downwelling zone), the difference in O_2 penetration could to a large extent be explained by the difference in availability of reduced compounds. Moreover, despite the attempt to level out the sediment surface before stirring of the chamber, irregular microtopography were still present. The topography-advection interaction could modulate the distribution of O_2, pore water nutrient, and reduced substances, thus controlling O_2 distribution and biogeochemical zonation in the sediment (Forster et al., 1996; Huettel et al., 1998; Werner et al., 2006; Cook et al., 2007). The decrease in the maximum O_2 concentration in both chamber types could have been caused by advection mediated reduction of the DBL thickness and the wash-out effect by advection transporting anoxic pore water out of the sediment at the upwelling zone inside the chamber. This speculation is in line with previous studies indicating that a decreased in DBL thickness would increase the effective export of O_2 out of the sediment (Berninger and Huettel, 1997; Glud et al., 1994; Jørgensen and Revsbech, 1985).

In the light, O_2 microprofiles did not show significant dependence on advection of the applied magnitude in either sediment type. O_2 penetration depth and O_2 peak concentration depth remained stable with higher values in C chambers. This observation is different from previous observation of declining O_2 concentration in the light with flow due to more effective export of O_2 (explained above/ previously), downward migration of MPB to avoid resuspension, and impaired activity of MPB community attribute to changes of the chemical environment with flow (Berninger & Huettel, 1997; Kühl et al. 1996; Jørgensen & Glud et al. 1994; Revsbech, 1985). This study therefore indicates that the produced O_2 in the light was high enough (more than enough) to counteract the effect imposed by advection and reductive compounds on O_2 distribution in this system.

4.3 Benthic O_2 metabolism in sandy permeable sediment inhabited by diatom dominated-MPB community

4.3.1 Benthic O_2 consumption

In this study, benthic O_2 consumption is determined in laboratory experiments using three approaches: diffusive O_2 uptake quantified with microelectrode, total O_2 uptake with

chamber enclosure, and volumetric O_2 consumption rates. Generally, the R_{Dark} fluxes in this study are comparable with values reported in other studies (in *situ* and *ex-situ*) from coastal waters (Table 4.1). R_{Dark}'s small-scale spatial variability (heterogeneity) between chamber type and replicates can be observed. R_{Dark} was calculated from the obtained O_2 profile according to Eq. 1 and from the depth-integrated O_2 consumption-production through a modeling approach (Eq. 7). Assuming constant values or slight change in the value of water temperature, salinity, and sediment porosity of individual chambers, the primary variable driving the obtained R_{Dark} fluxes in this study is the difference in O_2 concentration gradient, thus the related mechanisms.

Spatial variation in R_{Dark} has been linked to small-scale processes such as deposition (hot spot) of organic matter (Archer & Devol, 1992), thickness of DBL, microtopography of sediment surface (Røy et al., 2005; Rasmussen & Jørgensen, 1992; Jørgensen & Des Marais, 1990), horizontal diffusion from biological structures (Jørgensen & Revsbech, 1985), fauna activity, hydrodynamic processes, O_2 penetration depth coupled with O_2 consumption rates, and availability of reduced compounds diffusing upward from deeper sediment layers (Canfield et al., 1993). With the absence of fauna-mediated O_2 uptake, the variability of R_{Dark} within a chamber and between chamber types (C vs. RC) is most likely due to one or more of the following: the patchiness of the MPB-generating microtopography, the amount of biomass (OM) produced and oxidized, the availability of the reduced compounds inside the chambers, and the biomass of the heterotrophic community (microorganism) and their respiration rate.

The combination of the small-scale processes in the sediment and the 1D limitation of the microelectrode approach eventually control the spread of the R_{Dark} value and its variability. High R_{Dark} values might have been obtained from profiling in the hotspot of easily degradable organic matter deposit, generated reduced compounds (organic and inorganic) and intense microbial activity. On the other hand, lateral diffusion of O_2 will generate a mid-depth zone of linear O_2 gradient with limited electron donors and low volumetric O_2 consumption rates (Rabouille et al., 2003; Glud et al., 1994). Profiling in such setting will resulted in low R_{Dark} value. The temporal variability of R_{Dark} was not explicitly explored in this study. Nevertheless, the difference in measurement and termination time of individual chambers, which span from 1 to 12 weeks, might contribute to differences in OM production and, thus, the obtained fluxes. Temporal variation in R_{Dark} has been associated with bottom water oxygenation, water temperature, and OM supply (quantity and quality) (Thamdrup et al., 1998; ; Epping & Helder, 1997; Jørgensen, 1996). The long-term incubation in this study, with controlled temperature, salinity, and aeration, rules out these variables as the driving force in different R_{Dark}s and highlights the OM supply from the MPB production and availability of reduced compounds.

On average, TOU was five times and nine times higher than R_{Dark} in C and RC chambers, respectively. Previous studies have reported the ratio of TOU to R_{Dark} ranging from 2:1 to 7:1 in continental slope /shelf sediment and 1:1 in deep-sea sediment (Hicks et al., 2017; Rabouille et al., 2003; Glud et al., 2003; Glud et al., 1994). In most of these global studies, the difference between TOU and R_{Dark} mainly quantifies the fauna-mediated O_2 uptake (FOU). In coastal settings, FOU typically accounts for ~40-50 % of the TOU (Glud

et al., 2003; Forster et al., 1999). With the absence of fauna in this study, FOU cannot explain the discrepancy between TOU and R_{Dark}. By incorporating the effect of microtopography, the 3D R_{Dark} fluxes could account for ~ 10 – 49 % more of 1D R_{Dark} (Glud et al., 2003; Roy et al., 2002; Jorgensen & Des Marais, 1990). Still, this cannot fully explain the difference between TOU and R_{Dark} .

Differences in TOU versus R_{Dark} might also emerge from the measurement technique: the medium where O_2 was measured, the surface area covered, and the processes covered by the respective techniques (Archer & Devol, 1992). In particular, the author underlines the oxidation of reduced compounds in the overlying water, measured by the chamber approach but not by microelectrode. Almost all of the microprofiles in this study were obtained near the chamber wall. During the benthic chamber's stirring, O_2-rich water moved downwards at this position. On the other side, stirring generated an upward movement of reduced compounds-rich pore water at the center of the chamber. While R_{Dark} measurement with microelectrode covered only the well-oxygenated area of the sediment (considering the pore water flow circulation pattern), TOU measurement covered the whole surface area of the chamber. In addition, bacterial mats were observed on the walls of the chambers. This mat could also contribute to the higher rates in TOU measurement, which was then included in TOU measurement but not in R_{Dark} measurement.

The measured TOU in this study is similar to values measured in previous studies. In particular, the rates assessed in this study fell within those reported from the Baltic Sea (Gazeau et al., 2004; Sundbäck et al., 1996). Higher rates of TOU in RC than C chambers are in line with those of R_{Dark}; thus, processes that were involved in controlling the rates availability of OM and reduced compounds, chemical oxidation, and microbial respiration rates. The TOU measurement was mainly done at the end of the sequence of O_2 measurement per individual chamber, meaning individual chambers have been exposed to advection and daily light to higher light intensity. Although recuperation time was always given before commencing the TOU measurement, light and advection might have intensified the production and distribution of O_2, OM, and reduced compounds, leading to higher TOU in RC chambers.

The organic content measured in this study was substantially low and comparable to previous *in-situ* and *ex-situ* measurements from the region of the Southwestern Baltic Sea (Schade, 2019; Kuriyama et al., 2021). This sediment was poor in organic carbon but exhibited a high O_2 uptake rate compared to the average sediment organic content versus median O_2 uptake rates: 0.65 % DW vs 13.7 mmol m^{-2} d^{-1} reported from a compilation of 60 studies by Canfield and Teske (1996). Measuring benthic respiration at three sandy sites of the German Bight, Janssen et al. (2005) reported a similar observation, where their TOU rates range from 17 – 37.3 mmol m^{-2} d^{-1} for organically poor sediments (organic matter content of 0.023 % DW). From this observation, the organic matter content could not be the sole driver for O_2 uptake rates in sandy sediment. High mineralization rates could occur in sandy permeable sediment inhabited by the MPB community through oxidation of labile organic matter produced by the microalgae (Rao et al.,2012; Billerbeck et al., 2007;Rasheed et al., 2004; Fenchel and Glud, 2000).

Measurement of TOU in this study included re-oxidation of reduced substances such as NH_4^+, H_2S, CH_4, Fe^{2+}, and Mn^{2+}, originating from the deeper sediment layer and diffusing upwards. At the measuring points of the microelectrode, the oxic layer was down to several mm thick, suggesting that anoxic porewater did not get advected into the water column and that the reduced compounds were most likely oxidized in or at the lower end of the oxic layer of the sediment. Nevertheless, the relative contribution was calculated from the pore water profile of ammonium. The upward flux of ammonium was ~18 and 5 mmol m^{-2} d^{-1} in C and RC chambers, respectively.

R_{Dark} measured after advection exposure did not show a significant dependence on advection in either chamber type. Even though profiling was deliberately placed at the supposed down welling position inside the chamber, the expected O_2 profile, deeper penetration with a shallower/lower concentration gradient, was not always the case. Steepening and flattening of O_2 concentration gradients, thus increasing and decreasing R_{Dark} after advection, were both obtained. Advection could intensify the reaction of oxidant and reductant as well as diminish the reaction: advection increases the supply of O_2 and OM flushed into the sediment, facilitating aerobic mineralization, advective supply of O_2 might foster reoxidation of reduced compounds, advection could promote redistribution of O_2, OM, and reduced compound, preventing any oxidation. Furthermore, repetitive flushing might increase the oxidation and the flushing out of the reduced compounds, leaving the sediment to be electron donor limited.

There are limited studies employing microelectrode to assess the influence of advection on diffusive O_2 uptake of permeable sediment (Berninger & Huettel, 1997; Kühl et al., 1996). Assessing the influence of boundary flow on O_2 flux in intertidal sediment, Berninger and Huettel (1997) reported a decrease in respiration in relation to gross production of O_2 (~30 % of GP=130 mmol m^{-2} d^{-1}) at a flow velocity of 0-5 cm s^{-1} and a slight increased (~4% of GP =20 mmol m^{-2} d^{-1}) at a flow velocity of 5 to 15 cm s^{-1}. Measuring the O_2 flux of epilithic cyanobacterial biofilm under varying flow conditions, Kühl et al.(1996) observed a decrease in the downward flux of O_2 with flow from (~76 % GP=126 mmol m^{-2} d^{-1}) at the stagnant condition to (45 % GP=76 mmol m^{-2} d^{-1}) at a flow velocity of 5 cm s^{-1}.

Microelectrode was mainly used to describe the distribution of O_2 in the sediment upon advection, while the influence of advection on benthic O_2 fluxes was primarily measured with chamber enclosure and flow-through techniques (de Beer et al., 2005; Polerecky et al., 2005; Werner et al., 2006). Previous studies employing stirred benthic chambers reported a doubling in TOU (Jansen et al., 2005; Forster et al., 1996) with advection. The increase in TOU due to advection depends on the residence time of water advected into the pore spaces and the volumetric consumption rate of the sediment (Cook et al., 2007; Forster et al., 1996).

Further insight into small-scale variations of O_2 consumption in the sediment was obtained by determining the volumetric OCR. This method quantifies the spatial distribution of potential OCR independent of the in situ sediment condition, and hotspots of high mineralization rates can be identified. Higher OCR measured with microelectrode than planar optode is most likely due to the difference in the working principle of the techniques,

1D vs. 2D (see above: evaluation of the methods). The recorded depletion of O_2 concentration over time by microelectrode was not always linear, indicating that the measurement captured the combined effect of sediment O_2 consumption and molecular diffusion (Precht et al., 2004). The spatial resolution of this method was coarse (1 point) due to time constraints and the need to use multiple sensors for simultaneous measurement in the horizontal direction. OCR values after advection exposure fell within the range reported in the literature (Werner et al., 2006; Polerecky et al., 2005; de Beer et al., 2005; Precht et al., 2004). Although the average value of OCR in C and RC chambers fell within the same magnitude, the range values showed higher OCR in RC than in C chambers. This discrepancy was consistent with the difference in Chl *a* concentration, and therefore likely OM content, as well as the availability of reduced compound. However, the extent to which OM and reduced compound affected the measured OCR is beyond the scope of this study. Furthermore, OCR measurement was only performed after 2 h exposure to advection, during which the OM and reduced substance could have been already oxidized to an unknown extent or redistributed to another region in the sediment.

Previous volumetric OCR measurements incorporating advective pore water flow in permeable sediment were conducted only in the dark (Werner et al., 2006; Polerecky et al., 2005; de Beer et al., 2005; Precht et al., 2004). In this study, next to advection, the volumetric OCR of photosynthetically active sediment was investigated after exposure to light. OCR after exposure to advection in light was higher than OCR after exposure to advection in the dark. OCR after exposure to light under diffusive conditions was still higher than OCR after exposure to light under advective conditions. These findings highlight the different roles of advection in combination with the photosynthetic potential of the sediment and, particularly, the role of light, nutrients, and phototrophic community in producing labile organic matter as fuel for mineralization (respiration) in the dark.

4.3.2 Benthic Primary Production

The diffusive NP and GP fluxes obtained in this study were comparable with values from permeable sands and biofilms (Table 4.1). However, measurements for the southwestern Baltic Sea are still limited (Kuriyama et al., 2021 Rieder, 2011; Schade, 2019) and were mainly obtained with the chamber enclosure technique. Parameters for photosynthesis performance are within the lower range of reported value for comparable locations (Table 4.2). The P-I response of the MPB community exhibited saturation at low light. This observation is supported by the measurement of photosynthetic performance of several diatom species from the Southern Baltic Sea (Prelle et al., 2019; Woelfel et al., 2014), which showed low light requirement. The net productions from the microsensor approach and maximum rate calculated with the curve fitting approach (Pmax) were similar for C chambers and within a factor of 1.5 for the RC chamber.

The range of GP estimates for diffusive and advective condition (0.6-0.9 mmol O_2 m^{-2} h^{-1}) fall within the range of the global average estimates for benthic microalgae productivity for 0 to 5 m depth range in temperate regions (~0.8 mmol C m^{-2} h^{-1}; Cahoon, 1999). The calculated GP rates are also comparable to rates reported from the Southwestern Baltic Sea (Kuriyama et al., 2021; Schade,2019). Water column production rates were not measures during this study, thus the contribution of MPB production to the total primary production

is subject to future study. Nevertheless, studies from the nearest site in southern Baltic Sea indicated that 20 – 40 % of the total primary production may originate from benthic production (Urban-Malinga and Wiktor, 2003; Meyercord et al., 1999).

As in the dark, small-scale-spatial heterogeneity was also demonstrated by the O_2 microprofiles in the light, thus the calculated NP fluxes between chamber replicates. The difference between chamber types was more pronounced in the light. The upward fluxes increased significantly right after illumination and with increased light intensity. In addition to variability sources previously mentioned for R_{Dark}, NP variability is tightly linked to photosynthesis activity. Reasons could also be related to the organism, i.e. difference in the composition and relative abundance of phototroph and heterotrophic communities, their horizontal and vertical distribution (heterogeneity), their response to light at different sites in the sediment, and the availability of nutrients and DIC in the pore and water column.

MPB community composition and abundance have shown different photosynthetic capacities (Santema and Huettel, 2018; Woelfel et al., 2010; Hancke and Glud, 2004; Meyercordt et al., 1999; Epping and Jørgensen, 1996). Although the same diatom cultures were added to C and RC chambers, a rapid microscope examination of MPB community composition from both chambers in the end did show distinction, where the diatom species *Hyalodiscus scoticus* was not found in C chambers. Also, photosynthetic activity has been reported to be higher and more efficient in thinner and densely populated surfaces (Cartaxana et al., 2016). Indeed, the surface layer in C chambers was characterized by loose structure and relatively thinner mat compared to dense structure and thicker mat surface in RC chambers. This appearance might have reflected a lower cell density in the C chambers.

The Chl. *a* concentration as a proxy for MPB biomass was lower in C than in RC chambers. This observation aligns with the visual appearance of the sediment surface of the chambers mentioned above, indicating that composition and the abundance of the MPB community might have played a role in regulating the magnitude of NP. However, for every chamber, the Chl. *a* sampling was only performed at the end of the incubation and took place roughly 3-5 days after the NP measurement. Short and long-term variations of Chl *a* vs NP have been documented in other studies, where positive correlation is not always the case (Santema and Huettel, 2018; Cartaxana et al., 2016; Jesus et al., 2009; Cartaxana et al., 2006) (see below). Nevertheless, the Chl. *a* concentration vs. NP in this study is comparable with in situ and *ex-situ* measurements from the Southwestern Baltic Sea.

Light is considered the main factor influencing MPB photosynthetic activity (Gattuso et al., 2006; Cahoon, 1999). NP in C and RC chambers increased with increased light intensity. Although a linear trend is generally observed, several chambers showed a slight decrease in NP at the highest light intensity. Photo-inhibition in the MPB community has been reported due to exposure to high irradiance (Cartaxana et al., 2013; Serôdio et al. 2012; Kromkamp et al., 1998), however the MPB community in this study was exposed to low light. Therefore, the drop in NP might be related to the behavioral response of the MPB community in the form of downward migration, particularly a non-synchronous migration, as well as a physiological phototoprotection response.

Light quantity and spectral quality at the sediment surface might vary and change below the MPB mat and sediment sand grains, thus influencing photosynthetic activity. Light harvesting pigment could scatter and absorb the incident light, thus impeding the total available light for the MPB community (Kühl & Jørgensen, 1992; Kühl et al., 1996). Particularly in sandy sediment, an increase in subsurface scalar irradiance up to 150% of incident light has been reported, as well as a reduction to 85 % in spectral light quality (Cartaxana et al., 2016; Ploug et al., 1993).

Nutrient availability has been related to the growth and productivity of MPB (Underwood & Provot 2000; Underwood et al. 1998; Kromkamp et al., 1995). Pore water measurement demonstrates the higher nutrient availability in RC than in C chambers. Thus, it could partially explain the higher photosynthetic rates. There were no direct pH and DIC measurements during the experiment. Based on estimated fluxes of DIC in the light, Larkum et al. (2003) have proposed that DIC is likely to be a significant limiting factor for photosynthesis. These authors argue that the presence of DBL under light saturation could limit the influx of DIC into the photic zone. Determining an accurate boundary layer thickness from O_2 microprofiles was difficult in this study. The applied vertical resolution of 100 µm was too high to record the DBL.

The presented GP in this study was calculated by adding the R_{Dark} in the dark to the NP, both derived from steady-state O_2 microprofiles. With this approach, R_{Dark} is assumed to be constant. Therefore, GP increased with increasing light intensity in line with NP. The assumption of constant respiration rate in the dark and the light is similar to the bell jar measurement. However, by comparing R_{Dark} in the dark and the downward fluxes in the light, it is clear that the respiration rate was not constant but increased with increased light intensity. Per unit surface area, downward flux in the light is up to 2 times and nine times higher than R_{Dark} in the dark in C chambers and RC chambers, respectively.

The calculated GP_{LDS} rates showed significantly higher production rates than those obtained by adding R_{Dark} and NP. From a five-depth measurement, GP_{LDS} could exhibit rates that are 5 (C chambers) and 6 (RC chambers) times higher than the summation approach. Comparison of GP_{LDS} between C and RC chambers was limited by the lack of measurement in C chambers (only one measurement available), which was also distorted by the presence of gas bubbles. Full GP_{LDS} measurement in RC chambers showed comparable rates with five-depth measurements, but with slightly higher rates, up to 8 times higher than GP by adding NP and R_{Dark}. This result confirmed the possibility and effectiveness of estimating GP_{LDS} using only several depths (Revsbeh and Jørgensen, 1981).

The difference between GP_{LDS} and NP derived from steady-state O_2 microprofiles has been widely used to estimate R_{Light} (Fenchel & Glud, 2000; Kühl et al., 1996; Glud et al., 1992). By this means, respiration in the light exceeds respiration in the dark up to 20 and 27 times in C and RC chambers, respectively. With this approach, however, it should be noted that the consumed O_2 in the light was not exclusively used for the mineralization of organic C but also for oxidation of the end product from anaerobic mineralization pathways. At the lowest light intensity, the NP accounted for 58% of the GP_{LDS} in C chambers, while it was only 12 % in RC chambers. In other words, ~ 42 % (in C chambers) and 88 % (in RC chambers) of the O_2 produced by photosynthesis was consumed in the photic zone.

Light-stimulated O_2 consumption in photosynthetic communities has been previously documented. This phenomenon has been observed in microbial mats and sediments (Epping & Jørgensen, 1996; Kühl et al., 1996; Glud et al., 1999). Several proposed mechanisms include the Mehler reaction, photorespiration, expansion of the oxic zone, and stimulation of heterotrophic respiration due to excessive photosynthate production during photosynthesis.

Mehler reaction is a coping mechanism when electron flow from photosystem II overflows the electron demand for CO_2 assimilation (Beardall, 1989; Raven & Beardall, 1981). High levels of O_2 are reduced to form hydrogen peroxide. This reaction, however, does not result in any net production of O_2. Therefore, this was not likely involved in this study.

Photorespiration is the oxygenation of RuBP by RUBISCO followed by photorespiratory glycolate metabolism. It arises because rubisco can act as either a carboxylase (incorporating CO_2) or an oxygenase (incorporating O_2). At relatively high CO_2 levels, rubisco acts mainly as a carboxylase. However, when O_2 levels are high, rubisco acts as an oxygenase. Although photorespiration may contribute to O_2 consumption in light, it is unlikely to be the primary cause for excessive consumption due to the low light intensity here. Glud et al. (1992) experimented to evaluate the effect of different O_2/CO_2 on the respiration rate of a diatom-biofilm. They found that under elevated O_2 concentration, photorespiration accounted for only 17 % of the GP_{LDS}. Furthermore, some microalgae and non-motile episamic diatoms can control photorespiration via carbon-concentrating mechanisms (CCM) and physiological photoprotection (Raven, 1997; Badger and Price, 1992).

In C chambers, the light-enhanced respiration was accompanied by an increase in O_2 penetration depth. This expansion of the oxic zone indicates that a large volume of sediment respired the O_2. However, the volumetric rate of respiration was relatively constant. Indeed, the biomass involved and the availability of reduced compounds are lower in C chambers compared to RC chambers. Epping and Jørgensen (1996) noted that this expansion of the oxic zone due to change in light intensity is a common effect of change in gross photosynthesis, which facilitates reoxidation of reduced compound deeper in the sediment or biofilm with less labile oxidizable substrate.

Enhanced volumetric O_2 respiration in the light has also been linked to enhanced bacterial mineralization of exuded photosynthate. Particularly for diatom-dominated sediment, this observation has been reported by Cartaxana et al. (2016), Lindeboom et al.(1985), and Fenchel and Glud (2000), where a significant change in O_2 penetration depth did not accompany the change in GP rates. Furthermore, from a planar optode study, Glud et al. (1999) observed a co-occurrence of net O_2 production and consumption sites, suggesting a tight spatial coupling between phototrophs and heterotrophs within the photic zone. This mechanism most likely occurred in RC chambers, where O_2 penetration depth was relatively constant despite the increase in light intensity.

The impact of advection on net and gross production varies. The variability arises from the different responses of the O_2 concentration gradients, upward and downward, upon advection. Advection reduced/diminished both upward and downward fluxes of O_2 out of

the photic/oxic zones of the sediment in C chambers, while advection enhanced upward fluxes and reduced downward fluxes in RC chambers. As a result, advection decreased calculated NP in C chambers while it increased NP in RC chambers. By summing the average value of NP and R_{Dark} after advection (both C and RC showed a decrease in fluxes), the GP value from both the chamber types corresponded to the NP values.

Photosynthesis measurements with the microelectrode LDS approach in combination with the advective transport is still limited. The influence of advection on photosynthesis also varied. Measuring GP_{LDS} before and after exposure to flow, Berninger and Huettel (1997) reported a decrease in photosynthetic activity, while Kühl et al. (1996) reported a constant GP. Furthermore, these studies observed different responses of upward and downward flux with flow, hence their NP: the former observed a decrease in upward and downward flux after flow, while the latter reported an increase in upward flux and a decrease in downward flux with flow. Both authors address the reduction of the thickness of DBL with flow as one explanation for more efficient diffusive exchange between substrate and water column, hence higher upward flux. However, there are methodological differences in their way on estimating their upward flux. Thus, their NP rates differed. Berninger and Huettel (1997) calculated NP as the combined upward and downward flux from the photosynthetically active zone within the sediment. Kühl et al. (1996) also combined the fluxes, however, their upward flux was measured across the DBL. Employing a flow velocity of 10 cm s^{-1}, Kühl et al. (1996) measured an increase of 50% in net production (upward flux) compared to stagnant conditions. Conversely, in the presence of flow (2 – 15 cm s^{-1}), a decrease in net production and upward fluxes by ~50 % was observed by Berninger and Huettel (1996).

NP estimation after advection in this study was in line with Berninger and Huettel (1996), and the effect of advection on reducing NP was similar in C chambers. Berninger and Huettel (1996) attribute the decrease in photosynthesis at higher flow velocity to the combination of behavioural responses of the benthic phototroph to change in flow conditions and the effect of flow on the chemical environment of the sediment. In addition to avoiding intense light and thus photoinhibition, vertical migration is a well-known protection mechanism in benthic diatom and cyanobacterial populations to avoid sediment resuspension from higher hydrodynamic forcing. As for the phototrophic community living directly at the sediment surface, advection could modify their mat structure (towering clusters), promoting a shading effect for the phototroph living in deeper sediment, thus decreasing their photosynthetic activity.

Higher photosynthesis rates with enhanced percolation have been reported from *in-situ* and *ex-situ* incubation of permeable sediment inhabited by MPB (Jahnke et al., 2000; Cook & Roy, 2006; Glud et al., 2008). Several factors have been considered to support this finding: flushing could alleviate the nutrient limitation, inhibiting the effect of pH on photosynthesis, and inorganic C limitation. It has been demonstrated that advection in permeable sediment could facilitate a rapid supply of nutrients from the deeper layer of the sediment (Huettel et al., 2003; Precht and Huettel, 2004; Huettel et al., 1998). The nutrient profiles in this study showed the availability of higher nutrients in RC than in the C chamber, which might support the higher photosynthesis rate in the RC chamber. Higher pH has been

documented to impair the physiological effect on the cell of phototrophic algae. Moreover, higher pH could limit the availability of CO_2, limiting photosynthesis to predominantly HCO_3^- assimilation. However, provided that there is available free CO_2, particularly advected from deeper sediments, photosynthesis could still proceed even at higher pH. In addition, the occurrence of flow could reduce the imposed limit of the CO_2 supply into the photic zone by reducing the thickness of the DBL.

The observed discrepancy in the effect of advection on NP between C and RC chambers reemphasizes the difference in the phototrophic community, nutrient content, and availability of reduced compound. Under advection, at the downwelling position, the nutrient content at the upper layer of the sediment was likely transported deeper into the sediment and replaced by the nutrient-poor water originating from the overlying water. On the other hand, at the upwelling zone, the upward intrusion of nutrient-rich pore water would benefit the phototrophs residing directly in this zone. Assuming both mechanisms occurred in both chamber types, the amount of produced and consumed O_2, which depends on the phototrophic community and processes consuming O_2, is the tipping point of the NP. Considering higher volumetric O_2 consumption and produced biomass in the RC chamber, it is safe to assume that under advection, the produced O_2 was very high (supported by the abundance of phototrophic community and higher nutrient content) and enough to mask the influence of advection on O_2 consumption and distribution.

Field and laboratory studies presenting data on primary production by microphytobenthos from several coastal settings is compiled in Table 4.1. Using the reported fluxes in light and dark, R_{dark}, NP, and GP on an hourly base were calculated and transformed reported value in C equivalent to an O_2 equivalents (photosynthetic quotient = 1). The daily net ecosystem metabolism (NEM) were estimated as the difference between GP and R_{dark}, accounting for the day length of the given time of year and region. The influence of advection on NEM varied: decreased NEM in C-chambers, increased NEM in RC-chambers. The decrease in NEM due to advection is align with field measurements of Schade (2019), where the benthic system changed from autotrophy to heterotrophy due to advection. Overall, the positive NEM values (regardless of chamber type and transport regime) in this study indicate net O_2 release of the benthic system (autotrophy).

Table 4. 1 Benthic primary production, respiration, and net ecosystem metabolism of Southwestern Baltic Sea compared with rates reported from other coastal sediment in the literature.

Reference	Date	Location	Water Depth (m)	Method	Light Intensity (µmol m^{-2} s^{-1})	Hours of day (h)	Flow/ Stirring Rotation	Benthic Metabolism (mmol O_2 m^{-2} h^{-1})			Benthic Metabolism (mmol O_2 m^{-2} d^{-1})	Chl.*a* content (mg m^{-2})	Permeability (x 10^{-11} m^2) or sediment type
								R	NP	GP	NEM		
Cahoon and Cooke (1992)*	Aug 1984-1989	Onslow Bay, North Carolina, USA	14.6-41	IC	115	13		1.67	-0.19	1.48	-20.76	22.9	-
Jahnke et al. (2000)*	Aug 1996 St 27	South Atlantic Bight, Georgia, Florida, USA	14-40	IC	55-83	13		4.64	1.82	6.46	-27.29	12.3 – 37.7	4.7
Jahnke et al. (2008)*	Jul 2003 St 27	South Atlantic Bight, Georgia, Florida, USA	27		55.6	13.5		0.33	2.33	2.67	26.67	43.81	
Berg and Huettel (2008)		Apalachicola Bay-Florida Northeast Gulf of Mexico	0-10	IC & EC	19-278	13		5.77	-4.54	1.23	-138.46		1.3
Santema and Huettel (2018)	Jun 2008-Sep 2010 St A	Big Bend, West Florida Shelf, Florida, USA	5	LC	200			0.28	0.75	1.03	5.70	0.2 µg/ g dry sed	64-230
Rasheed et al. (2004)		Shark Bay, Herond Island, Great Barrier Reef, Australia	0.2-2.5	IC		9	10 rpm	1.04	5.71	6.76	35.80		0.122
							20 rpm	2.33	12.89	15.21	81.10		
							20 rpm	2.80	5.93	8.73	11.40		
Glud et al. (2008)	Nov 2005	Inner reef flat, Heron Island, Australia	0.3-1.8	IC		13						11.1 - 15.2	1.6 - 6
							0 rpm	6.88	5.77	12.64	-0.63		
							40 rpm	9.00	11.08	20.08	45.00		
							80 rpm	10.75	18.92	29.67	127.75		
Rao et al. (2012)	Apr 2010	Shark Bay, Heron Reef, Great Barier Reef, Australia	0.2-2	IC	55-1000	11	11					20 µg/ g dry sed	0.7 - 7.4
							10 rpm	1.51	2.64	4.15	9.41		
							40 rpm	2.24	4.19	6.43	16.97		
							60 rpm	2.58	1.93	4.51	-12.31		

Reference	Date	Location	Water Depth (m)	Method	Light Intensity (µmol m^{-2} s^{-1})	Hours of day (h)	Flow/ Stirring Rotation	Benthic Metabolism (mmol O_2 m^{-2} h^{-1})		(mmol O_2 m^{-2} d^{-1})		Chl.*a* content (mg m^{-2})	Permeability (x 10^{-11} m^2) or sediment type
								R	NP	GP	NEM		
				L-ME						2.79	15.33		
Denis et al. (2012)	Apr 2008	Canche Estuary, English Channel, UK	5	I-ME	664	14							
Hancke and Glud (2004)	May 2000	Adventfjord, Svalbard, Norway	1.3	L-ME	140	12		1.04	0.65	1.69	-4.68	2.7	sandy
Sundbäck and Jönsson (1988)	Feb-Oct 1984	Laholm Bay, Kattegat, Sweden	2-20	L-14C	0-360	15				1.61-2.31		1-87 (1984-1986)	sandy-silty
Cook et al. (2007)	Apr 2003, Jul 2004	Sylt-German Wadden Sea	0.5	LC								13 µg/ g dry sed	2
						17		2.13	0.01	2.13	-14.73		
Billerbeck et al. (2007)	Aug 2002	Hausstrand, Sylt Island, German Wadden Sea	1.5-2	IC		15	20 rpm	1.45	2.79	4.24	28.80	185 (176 - 194)	3.9
Berninger and Huettel (1997)		Cuxhaven, Germany		L-ME	120 - 400	14.5	no flow	11.64	8.36	20.00	10.64		54
							flow (2 cm/s)	5.24	3.76	9.00	4.79		
Cook et al. (2007)	Aug 2003, Apr 2004	Hel Peninsula, Baltic Coast, Poland	1.5	IC		16		1.92	-0.38	1.53	-23.00	3 µg/ g dry sed	2.9
Urban-Malinga and Wiktor (2003)*	May 1998 - May 1999	Sandy beach Sopot, Gulf of Gdanks, Poland	0.5-1	IB & I-ME	57.2	16-17		1.53	1.00	2.53	5.06	14	sandy sediment
Meyercordt and Meyer-Reil (1999)*	May, Jul, Sep 1996; Jan, Apr 1997	Coastal Lagoon, Southern Baltic Sea, Germany		IB & LC	20-800	16-17							
		Kirr-Bucht, Central of DarsstZingst Boden	0.6-0.8		KB: 1800	16.5		1.10	-0.04	1.06	-8.94	106	sandy
		Rassower Storm, North Rhugen Boden, Germany	3.2-4.2		RS: 1900			0.72	0.13	0.85	-3.61	45	sandy-muddy
Kuriyama et al. (2021)*	Apr & Jul 2017	Southwestern Baltic Sea, Germany	3-6.2	LC	0-750	17		0.37	0.53	0.90	6.48	28 - 87.7	

Reference	Date	Location	Water Depth (m)	Method	Light Intensity (µmol m^{-2} s^{-1})	Hours of day (h)	Flow/ Stirring Rotation	Benthic Metabolism (mmol O_2 m^{-2} h^{-1}) R	NP	GP	Benthic Metabolism (mmol O_2 m^{-2} d^{-1}) NEM	Chl.*a* content (mg m^{-2})	Permeability (x 10^{-11} m^2) or sediment type
Schade (2019)		Southwestern Baltic Sea	0.5-6.5	IC	30-90	16						59-80	2.3 -4.6
	Jul 2017 & Aug 2018	St. 41					0	0.42	0.92	1.33	11.33		
							45 rpm	0.88	0.48	1.35	0.67		
		St.23					0	0.61	-0.06	0.55	-5.75		
							45 rpm	0.52	0.25	0.77	-0.26		
This Study	Jun-Jul 2020	Southwestern Baltic Sea		L-ME	0- 100	16						24-91	2.5
		diff-C					0	0.14	0.46	0.60	6.25		
		diff-RC					0	0.20	0.48	0.68	6.08		
		adv-RC		LC			40 rpm	0.20	0.37	0.56	4.32		
		adv-RC					40 rpm	0.31	0.60	0.91	7.10		

*Originally reported as C production, converted to O_2 production assuming PQ of 1. Methods; EC: eddy correlation, IB: *in situ* bottle, IC: *in situ* chamber, I-ME: *in situ* microelectrode, LC: laboratory chamber; L-ME: laboratory microelectrod

Table 4. 2 Derived variable from Photosynthesis-Irradiance (P-I) curve of our study compared with other studies in literature

Location	R (mmol O_2 m^{-2} d^{-1})	Pm (mmol O_2 m^{-2} d^{-1})	α	Ik (µmol m^{-2} s^{-1})	Ic (µmol m^{-2} s^{-1})	References
Skødstrup, Denmark	63.07	259	0.008	92-110	17.5	Kühl et al. (1996)
Laholm Bay, Kattegat, Sweden		34.7		30-320		Sundbäck & Jönsson (1988)
Rassower Strom and Kirr-Bucht, Southern Baltic Sea, Germany	(-1.2) – (-26.4)	9.6-120	0.005 – 0.033	65-310	15-55	Meyercordt & Meyer-Reil (1999)
Daneborg, Young Sound, NE Greenland	(-5)-(-8)	23-63	4.2-6.3	21.6	0.42 – 2.7	Roberts et al. (2002)
Pond of Salin-de- Giraud, Camargue, France	(-60.5)	112 - 138		127-230	17-43	Wielend & Kühl (2006)
Lake La Saladda de Chiprana, NE Spain		950		250		Polerecky et al. (2008)
Odense Fjord, Denmark	-17.28	43.2-86.4	0.1-0.3	75	6-30	Hancke et al. (2014)
Boiensdorfer Werder, Southern Baltic Sea, Germany			0.7-3.4	34-100		Woelfel et al. (2014)
Hütelmoor, NE Rostock, Baltic Sea, Germany			0.88-1.88	31.6-151	7.3-45.5	Prelle et al. (2019)
Rostock, Germany (Laboratory Chambers)	(-0.12) – (-10.37)	8-85	0.3-1.9	9-97	0.6-16	This Study

4.4 Macrofauna behavior in flooded substrates of coastal peatlands

In MCF Exp 1, *H. diversicolor* showed a high survival rate (100 %) and capability to burrow into the two flooded substrates: sediment and soil. Br^- pore water profiles showed higher penetration depth in the control core of marine sediment than in the control core of terrestrial soil. Deeper penetration and higher concentrations of Br^- were obtained in faunated cores of each substrate, suggesting faster porewater transport via the animal's burrows.

The measurement of bioirrigation activity through Br^- inventory, area-specific bioirrigation, and weight-specific bioirrigation of *H.diversicolor* in MCF Exp 1 clearly showed higher values and intensity in sediment cores than in soil cores. Investigating flooded cultivated and uncultivated soil, Valdermarsen et al. (2018) obtained area-specific bioirrigation comparable with the present study but at ~ 4 times higher biomass of *H. diversicolor*. This suggests higher ventilation activity of *H. diversicolor* in the present study. Although *H. diversicolor* seems to prefer the lower organic content and the sandy structure of the sediment, it is evident that the animal was able to mediate solute transport via ventilation in the soil.

The behavioral response of key bioturbators was further investigated in MCF Exp 2 using peat soil as substrate. *M. arenaria* had the highest survival rates but lowest burrowing depths and was incapable of forming burrows in flooded peat soil. The highest recovery rate indicated a high tolerance of *M. arenaria* to changing water chemistry following flooding of the peat soil. The dense network of plant roots possibly acted as a barrier for the clams to burrow deeper into the substrate. *H. diversicolor* and *M. neglecta* showed a lower percentage of recovery than *M. arenaria*, although it is still within the range typically reported in marine-based colonization experiments (Renz and Forster 2013; Kristensen et al., 2011; Michaud et al., 2006). Both polychaetes were capable of constructing burrows, although with shallower burrow depth than usually found in marine sediment. It is speculated that using their jaws, both polychaetes were able to chew and grind the plant roots and move (peristaltically) easily with their mucus-covered bodies. Furthermore, *M. neglecta* and *H. diversicolor* exhibited high avoidance behavior (several individuals escaping) during incubation. This behavior indicates animals' preference for better environmental conditions and their inability to cope and tolerate the unfamiliar physical and chemical conditions of the substrate and the overlying water. In particular, *M. neglecta* did not cope well with the incubation. The added specimen of *M. neglecta* turned pale after addition to the flooded peat soil. At the end of the incubation, a small number individuals (1 – 3 out of 9 added animal) were recovered in the cores and individuals escaped (5 out of 49 total added animal) from the cores into the tank were found. In comparison, the higher survival rate (25 -50 %) and deeper penetration depth (down to 2 cm down) of *H. diversicolor* agreed with the result from MCF Exp 1 (100 % survival rate, penetration depth 4 to 7 cm depth), albeit with lower values. Furthermore, almost 2 years after the flooding of the coastal peatland (Drammendorf), occasional field observations showed the dominant dispersal of *H. diversicolor* with deep burrowing depths (penetration depth down to 15 cm depth). This was particularly evident in the site at locations with permanent water coverage, even with a dense

network of plant roots. *H. diversicolor* is known for its status as a pioneer species and its tolerance to stressful environmental conditions in estuaries and coastal water (Hahlbeck et al., 2000; Fritzche and Oertzen, 1995; Vismann, 1990).

Generally, the measured bioirrigation intensity (Br^- inventory, area-specific bioirrigation, and weight-specific bioirrigation) of the tested animals was lower than those reported from marine sediments and coastal flooded agriculture soil (Kristensen and Kostka, 2005; Valdemarsen et al., 2018). Comparison between Br- inventory in control and faunated cores indicated low activity from the colonizers in general. With similar Br- inventory and area-specific bioirrigation between colonized cores, the high value of weight-specific bioirrigation of cores with *M. neglecta* resulted from the small recovered biomass. Soil texture and soil composition may have influenced the burrowing and bioirrigation performance of the animals. Valdermarsen et al. (2018) proposed that the unconsolidated structure of the root layer, together with high water content and porosity, might generate an additional obstacle for optimal burrow construction, thus decreasing the efficiency of burrow ventilation.

4.5 Macrofauna impact on peat soil biochemistry

The calculated TOU in MCF Exp 1 and TOU in MCF Exp 2 mainly represent the integrated measure of diffusive and fauna-mediated benthic O_2 uptake (FOU). The TOU found in the control cores of sediment, soil, and peat soil are in the same order of magnitude as previously reported from *ex-situ* (colonization experiment) and in situ TOU measurement of shallow coastal sandy sediment (Schade, 2019; Renz and Forster 2013; Quintana et al., 2011), agricultural soil (Valdmarsen et al., 2018; Sjøgaard et al., 2017), and peat soil (Askaer et al., 2010). TOU values from control cores of the two types of substrate in MCR Exp 1 showed small variation among replicates, while in MCR Exp 2, the TOU of the control core of peat soil varied significantly. Furthermore, the TOU of the control core in MCR Exp 2 fluctuated throughout the experiment. Since the O_2 concentration of the water was kept constant through water exchanged before every TOU measurement, the TOU variation among cores and fluctuations in control cores were most likely due to vary and high organic matter degradation and varying re-oxidation of reduced compounds from anaerobic microbial processes as a consequence of soil inundation.

TOU in colonized cores (MCF Exp 1 and Exp 2) was comparable to measured TOU values in literatures for *H. diversicolor* (Kristensen & Hansen 1999; Hansen & Kristensen 1997; Kristensen et al. 1992;), *M. arenaria* (Schade et al., 2019; Camillini et al., 2019; Michaud et al., 2005), and *M. neglecta* (Renz and Forster, 2013; Urban-Malinga et al., 2013; Kristensen et al., 2011). In comparison to the TOU of other treatments, slightly higher TOU rates exhibited by *M. neglecta* cores in MCR Exp 2 might be as a result of decomposing dead individuals indicated by the low recovery per core.

The FOU was calculated as the difference between TOU in control and faunated cores. FOU encompasses fauna respiration, fauna-stimulated microbial respiration, and re-oxidation of reduced compounds from microbial-driven anaerobic respiration (Kristensen, 2000). In MCR Exp 1, the stimulation of TOU by *H. diversicolor* (25 -140 %) was only measurable in terrestrial soil. The measurement from faunated sediment showed a lower

consumption rate than control cores. Since measurements were conducted in the dark, any photosynthetic production of O_2 to compensate for consumption may be excluded. Therefore, the result was considered an error, most likely caused by the O_2 measurement system. In MCF Exp 2, the presence of macrofaunas increased TOU: *H.diversicolor* by 38 %, *M. arenaria* by 36 %, *M. neglecta* by 44 %. These values were within the range reported in literatures cited above for respective species: *H.diversicolor* by 25-140%, *M. arenaria* by 38-190 %, *M. neglecta* by 18-120%. 25 - 35% (Kristensen et al. 1992), 100 - 140% (Hansen & Kristensen 1997), and 38 - 122% (Kristensen & Hansen 1999). Several factors have been proposed to explain trends of O_2 uptake for each species, including, specific respiration rates of organisms, micro- and meiobenthic respiration, substrate characteristics and oxidation of reduced metabolites (Glud, 2008; Aller, 2001; Kristensen, 2000).

In MCF Exp 2, the proportion of animal respiration and microbial O_2 consumption was estimated based on the added and recovered biomass. The respiration rate of *H. diversicolor* and *M. neglecta* was calculated based on their wet weight following Banta et al. (1999) and Urban-Malinga et al. (2013), respectively. The respiration rate of *M. arenaria* was calculated based on shell-free dry weight (SFDW) (Schade et al., 2019), where SFDW was calculated from dry weight-length relation. With comparable biomasses, *H. diversicolor* and *M. neglecta* initially had twice as high calculated respiration rates as *M. arenaria.* However, based on recovered biomass, *H. diversicolor* and *M arenaria* had similar respiration rates (~4 mmol m^{-2} d^{-1}), while the rate of *M. neglecta* dropped significantly (~10 times its initial rate). The respiration rates of *H. diversicolor* in this study is slightly higher than range reported in literatures (Schade,2019; Braeckman et al., 2010), while the range values of *M. arenaria* and *M. neglecta* fall within the range documented in several studies (Schade et al., 2019; Camillini et al., 2019; Renz and Forster, 2013; Quintana et al., 2007). The contrast trend between respiration rate and TOU of each treatment indicate that difference in respiration rate could not solely responsible for difference in TOU.

The O_2 uptake at the burrow wall ($OU_{burrows}$) of the added fauna was calculated as the difference between FOU and fauna respiration rates. All calculated $OU_{burrows}$ showed negative values except for *M. neglecta* (respiration rates based on recovered biomass). An overestimation of the respiration rate based on biomass might explain why exceedingly high respiration rates compared to FOU lead to negative results. Particularly for *M. arenaria*, lower biomass has been reported during spawning, thus leading to erroneously high respiration rates. On the other hand, fauna may have mediated very little to no O_2 consumption. Under hypoxic to anoxic condition *H. diversicolor, M. neglecta,* and *M arenaria* have been reported to reduced their metabolic heat dissipation rate and O_2 consumption (Ouillon et al., 2023; Fritzsche and von Oertzen, 1995; Schöttler et al., 1990). Change in environmental conditions such as O_2 concentration, salinity, temperature, pH, and pollution by different types of substances (e.g., Hg, HS^-, NH_3) have already reported to affect the behavior, physiology, and ecology of benthic macrofauna (Bass et al., 2021; Worm and Lotze, 2021; Poloczanska et al., 2016; IPCC 2007; Pörtner et al., 2005, 2004). In this study the water inside the tanks and soil cores were kept in controlled temperature and salinity, and well oxygenated. The pH of the water (7.3 – 8.8) were above the pH-threshold reported for *H. diversicolor* (pH 6.1-6.5, Freitas et al., 2016; Rodrihuez-Romero et al., 2014), within

the range measured in the field (pH 7.8-8.3, Breznikar et al., 2022), though within the lower limit of acute pH drop to end-of-century level (7.6, Feugere et al.,2021). Thus, independently, these factors might have contributed less to the avoidance behavior and mortality of the tested macrofauna observed in MCF Exp 2.

In contrast, in MCF Exp 2, pore water nutrients profiles clearly show an excessive amount of pore water NH_4^+, NO_3^-, PO_4^{3-}, which have been reported to induce toxic effect on bivalves and polychaetes (Sartori et al., 2024; Constable et al., 2003; Epifanio and Srna, 1975). For comparison, the 2 mmol l^{-1} NH_4^+ fluxing out of the peat soil (0.2 – 5 mmol m^{-2} d^{-1}) was significantly higher than the NH_4^+ threshold values for aquatic invertebrates reported in literatures: 0.001-0.03 mmol l^{-1} (bivalve) (Cong et al., 2021) and 0.6 mmol l^{-1} (polychacetes) (EEDP US army water way, 1995). A recent study (Sartori et al., 2024) on larval development *P. lividus* (sea urchin) indicate the halfway effect concentration (EC_{50}) of NH_4^+ at 0.04 mmol l^{-1} under 72 h exposure at temperature of 18 °C. Though NH_4^+ is relatively neutral in aquatic setting, alkaline condition induced the formation of NH_3, which can permeate biological membranes (Carmago and Alonso, 2006; Eddy, 2005). High levels of NH_3 can interrupt ion regulation and lead to osmoregulatory stress, impairing moulting, growth, reproduction, and survival of crustacean, mollusk, and polychaetes (De Schryver et al., 2008; Kiko et al., 2011; Lang et al., 1987; Cong et al., 2019, 2021). In addition, during experiment MCF Exp 2, animals were not feed. This could lead to a dormancy stage, where the animal stays on top of the substrate and does not burrow. This has been observed particularly for *M. arenaria*, where food scarcity leads to a hibernation state (Heider et al., 2020). This study emphasized the need to research the influence of highly concentrated $NH4^+$ exposure on the metabolic activity of early colonizer benthic macrofauna species in coastal peatlands.

The difference in TOU between substrates is also reflected by the difference in the physical properties of the substrates. Several characteristics, such us grain size, permeability, mud content, bulk density, and organic content have been investigated in correlation to benthic macrofauna species occurrence and behavior (Wieseborn et al., 2021; Kristensen et al., 2013; Grabowski et al., 2011; Volkenborn et al., 2009). With regard to porosity and carbon content, the highest values was obtained in peat soil, followed by mixed soil and sediment, while TOU (control cores) was the highest in sediment (~32 mmol m^{-2} d^{-1}), peat soil (15 – 20 mmol m^{-2} d^{-1}), and lastly terrestrial soil (~13 mmol m^{-2} d^{-1}). Higher porosity and carbon content in peat and terrestrial soils did not foster higher TOU, which underlines the importance of carbon reactivity in microbial respiration.

The bioavailability of carbon is believed to be highly dependent on the origin and degree of decomposition of its source (Hill and Cardaci, 2004; Cook & Allan, 1992). Hill and Cardaci (2004) compared terrestrial sediments containing a lot of peat with a very high carbon content with aquatic sediments that were poorer in organic matter. Despite the highly divergent total carbon contents, the amounts of soluble, mineralizable, and bioavailable carbon were very similar. Align to the previous studies, despite a higher organic content, the terrestrial-origin substrates and peat soil used in this study most likely contained low amounts of labile carbon. A considerable amount of O_2 consumed in mix and peat soil core were likely due to the reoxidation of reduced compounds. Reduced condition was evident

from the occurrence of black layer, particularly in peat soil, and the measured high concentration of pore water nutrients that associated mostly with higher fluxes.

The highest pore water concentration of NH_4^+ was found in peat soil, followed by sediment and soil. The NH_4^+ concentration in the pore water of each substrate was higher than in the overlying water: 3 - 24 times higher in marine sediment, 8 - 9 times higher in soil, and 10 - 100 times higher in peat soil. NH_4^+ release was highest directly after flooding the peat soil cores and declined throughout the weeks of incubations. This observation is in line with previous studies on salinization of coastal wetlands (Brezniker et al., 2023; Steinmuller et al., 2019; Liu and Lennarts, 2019b). Accordingly, salinization induces competition between Na^+ cations and $NH4^+$ for binding sites (cation exchange processes), which resulted in NH_4^+ desorption from soil particles (Baldwin et al., 2006). Ranging from 4 mmol m^{-2} d^{-1} in control cores to 3 mmol m^{-2} d^{-1} in faunated cores, the magnitude of NH_4^+ efflux is comparable to flux estimation from in situ study (4.5 mmol m^{-2} d^{-1}) accounting for the total permanently inundated area of 0.5 km^2 (Brezniker et al., 2023).

The porewater NH_4^+ concentration in the control cores of both experiments (MCF Exp 1 and 2) showed a higher concentration than the in faunated cores. This might indicate animal ventilation flushing $NH4^+$ from pore water into the water column. A higher concentration of NH_4^+ at 8 cm depth of faunated cores of marine sediment (MCF Exp 1) was most likely linked to the buildup of NH_4^+ (product of animals' excretion) at parts of the burrows with little ventilation. Judging by the difference in $NH4^+$ concentration between control and faunated cores at each depth, in MCF Exp 1, *H. diversicolor* appears to pump more in sediment than in soil, while *M. neglecta* outcompete *H. diversicolor* and *M. arenaria* in ventilating in peat soil (MCF Exp 2).

Fauna stimulation on NH_4^+ flux is evident throughout the incubation, where colonized cores released higher $NH4^+$ fluxes, particularly cores with *H. diversicolor*. The measured NH_4^+ fluxes in MCF Exp 2 were comparable with NH_4^+ effluxes reported earlier for sandy sediment inhabited by *H. diversicolor* (4 and 9 mmol m^{-2} d^{-1}) (Kristensen 1985, Kristensen & Hansen 1999), *M. neglecta* (3 – 6 mmol m^{-2} d^{-1}) (Renz and Forster, 2013), and *Mya arenaria* (2-3.6 4 and 9 mmol m^{-2} $d^{-}1$) (Michaud et al., 2006). It is important to note that the worms used in these previous studies established burrows as deep as 35 cm while in MCF Exp 2 burrowing was extremely shallow.

The flux direction of porewater NH_4^+ was in line with NH_4^+ flux directions measured in the overlying water, both indicating a substantial release of $NH4^+$ into the pore and overlying water. However, NH_4^+ concentration was 10^3 higher in pore water than in overlying water, suggesting a rapid and intensive removal of $NH4^+$ between substrate and water interface. In the oxic zone of the substrate and water column, NH_4^+ can be directly nitrified to NO_2^- and NO_3^-.

NO_3^- formation in the water column was evident in the majority of the weekly measurements of control cores. On the other hand, NO_3^- fluxes in colonized cores vary in magnitude and direction. NO_3^- formation in the water column relies on the availability of O_2 and NH_4^+ to bacterial populations, and other reductants competing for O_2. Furthermore, the thickness of the oxic and anoxic zone controls the coupled nitrification-denitrification

process. The balance between all these factors controls the prevailing processes in the water column.

While NO_3^- fluxes in the water column vary throughout the incubation (among treatments and replicates), the pore water profile of NO_3^- of all treatments exhibited a uniform pattern of rapid consumption in the first 2 cm depth. Likewise, NO_3^- concentration in the pore water was 10^3 higher than in overlying water. Under sub-anoxic conditions, NO_3^- can be removed through denitrification, NO_3^- ammonification (DNRA), and annamox pathways. The present study, however, cannot conclude the process.

In MCF Exp 1, PO_4^{3-} concentration in the overlying water and pore water of the sediment were within the range of values reported from the Baltic Sea (Gogina et al., 2018; Lipka et al., 2018). The influence of *H. diversicolor* was evident from higher PO_4^{3-} concentrations in the overlying water in the colonized cores than in control cores filled with sediment, showing that *H. diversicolor* stimulate the release PO_4^{3-}. Previous studies suggest the release of PO_4^{3-} as a consequence of longer resting period of *H. diversicolor* and dominance of PO_4^{3-} mobilization (diffusing) from deeper sediment layers and from phosphate-containing mucus-lining in the burrows of *H. diversicolor*. In contrast, PO_4^{3-} was undetectable in the overlying and pore water of the inundated soil cores. The lack of dissolved PO_4^{3-} might relate to the higher ratio of iron-phosphate in soil. Any available PO_4^{3-} might have been bound by an excessive amount of iron or/and PO_4^{3-} scavenging bacteria (Schulz-Vogt et al., 2019), leading to scarcity of PO_4^{3-}. However, due to the lack of PO_4^{3-} flux measurement in the overlying water, the fate of PO_4^{3-} across the SWI cannot be drawn conclusively.

In MCF Exp 2, PO_4^{3-} concentration in the water column (0.1 – 0.7 µmol L^{-1}) of the inundated peat soil were similar to values reported from in situ measurement (0.3 µmol L^{-1} in the spring, 0.5 µmol L^{-1} in the summer, 0.4 µmol L^{-1} in autumn and winter) (Brezniker et al., 2023). However, in contrast to an estimated 0.04 mmol m^{-2} d^{-1} of net exported PO_4^{3-} from the peatland (Brezniker et al., 2023), control and faunated cores in this study showed no detectable PO_4^{3-}increase in the water column, thus no flux to the water column. With overlying water PO_4^{3-} concentrations 10^3 times lower than that in the pore water, and core incubation demonstrating steady state to PO_4^{3-} uptake, PO_4^{3-} must have been absorbing at the peat soil-water interface. Several substantial mechanisms exist for PO_4^{3-} removal from marine water columns and sediments, including organic phosphorus burial, burial into phosphorite, inorganic precipitates, and adsorption onto clay and iron oxyhydroxide (Canfield et al., 2005). At low pH, as observed during the incubation, PO_4^{3-} absorption into iron oxyhydroxide generally thrives. When reactive Fe (III) is present, an effective phosphorus trap (“iron cap”) can be formed at the sediment surface, leading to uptake of PO_4^{3-} from the water column.

The lower concentration of pore water PO_4^{3-} in control than in faunated cores indicated fauna-mediated microbial PO_4^{3-} production and/or enhanced PO_4^{3-} desorption. Furthermore, the pore water PO_4^{3-} profiles of control, *M. arenaria*, and *M. neglecta* were similar to the typical profiles of increasing PO_4^{3-} concentration with depth beneath the oxidized layer (0-2.5 cm depth). The release and production of PO_4^{3-} is most likely due to anoxic conditions facilitating the dissimilatory reduction of Fe (III). Much of this PO_4^{3-} may

be re–trapped onto Fe oxides (as mentioned above) and did not escape into the water column. Below this layer, the drop in PO_4^{3-} concentration was generally a result of a decrease in metabolic activity with depth.

The PO_4^{3-} pore water profiles of *H. diversicolor* were slightly different from control and other treatment cores, with higher PO_4^{3-} concentration at the surface layer. Ventilation of *H. diversicolor* might have transported PO_4^{3-} from the deeper substrate layer into the water column. In addition, under reduced conditions, PO_4^{3-} might have originated from sulfide-mediated Fe (III) reduction. Through this pathway, precipitation of Fe sulfides potentially releases all iron-bound PO_4^{3-} , which then diffuses into the water column.

Pore water SO_4^{2-} concentration in this study are within the range documented in the literature, particularly from coastal peatland of the southwestern of Baltic Sea (0.01 – 10 mM) (Gutekunst et al., 2022; Gosch et al., 2019). Higher SO_4^{2-} concentration in faunated cores than in control cores indicated an enhancement of SO_4^{2-} transport associated with fauna activity. A similar observation on fauna mediated SO_4^{2-} transport was reported by Valdemarsen et al (2018), though with higher value than this study (Valdermarsen et al (2018): 5-23 mM, present study: 1-6 mM).

Flooding with brackish to saline water has been shown to change the heterotrophic microbial community of the terrestrial origin substrates, thus, the organic matter degradation pathway (Gutekunst et al., 2022; Sjøgaard et al., 2017; Asano et al., 2011) where anaerobic sulfate reduction dominates the pathway. Judging from the pore water SO_4^{2-} distribution, this could be the case in sediment and peat soil, while sulfide oxidation might have occurred in mixed soil. However, the lack of measurement of the sulfate reduction rate could not elucidate this assumption. Moreover, a study of SO_4^{2-} transport in peat soil by Gosch et al. (2019) documented that SO_4^{2-} penetration was dependent on the physical properties of the peat soil and that the composition and decomposability of the organic matter was more critical to enabling decomposing processes than the presence of SO_4^{2-} as the terminal electron acceptors.

4.6 Macrofauna colonization

Due to the lack of sampling, this study could not conclusively confirm a spatiotemporal pattern of benthic macrofauna colonization and succession in the restored area of Drammendorf. Nevertheless, fauna assemblages can be compared qualitatively using the data collected at the seaside (prior to flooding) and inside the restored area. Eighteen identified species at the seaside of the restored area were all found inside the flooded area, with the addition of several species that were not recorded at the seaside prior to the breach of the dike. This discrepancy is likely linked to the seasonal variation in fauna distribution and the low sampling coverage at the seaside. In line with the taxa variation, the density at the seaside (14.690 – 20.587 ind. m^{-2}) was lower than that inside the flooded area (135 319 ind. m^{-2}) after 1 year of inundation. With the dominance of epifauna (primarily crustaceans), the total density and species composition of benthic macrofauna found in this study are supported by other colonization studies in wetlands such as tidal and estuarine marsh and flooded agriculture-restored wetlands (Cheng et al., 2012; Valdermarsen et al., 2018; Mazik et al., 2007; Levin et al., 1996).

The succession of benthic macrofauna colonization in coastal wetlands has been related to proximity to sources of population, hydrodynamic condition, dispersal ability (larval, juveniles, and adults), feeding mode, and species tolerant to environmental conditions (Garbut et al., 2006; Bolam et al., 2004; Moseman et al., 2004 Levin et al.,1996). Of the tested bioturbators in MCF Exp 2, *H.diversicolor* and *M.arenaria* were among the early colonizers found in Drammendorf, while *M. neglecta* was not found. *H. diversicolor and M. arenaria* most likely arrived in the restored area as juveniles and adults via bedload transport from the adjacent sea. Conversely, the species dispersal limit, avoidance behavior, and low tolerance of *M. neglecta* (larva, juvenile, and adult) to the flooded peat soil (as observed for the adult one in MCF Exp 2) could be the reason why this species was not found in the flooded area.

The occasional field sampling in Drammendorf revealed that the colonization only occurred in the permanently flooded area where the substrate contained a mud-sand portion, but not in the area where dense roots and peaty soil covered the substrate. While *H. diversicolor* were able to construct burrows, *M.arenaria* was found lingering on top of the peat soil. This observation underlines the substrate type as a limiting factor for macrofauna succession, which was also evident from MCF Exp 2. Similar observations were reported from several previous studies in restored, managed realignment, and created marine habitats (Chiu Cheng et al., 2021; Mazik et al., 2007; Garbutt et al., 2006), where benthic infauna only colonized areas with accreted sediment. Furthermore, substrate compaction, bulk density, and grain size were also found to limit the succession of burrowing benthic macrofauna in created intertidal areas (Evans et al., 1999).

Burrowing macrofauna plays an essential role in the ecosystem functions of coastal and wetlands environments. Through bioturbation, they aid decomposition and nutrient cycling, and their occurrence provides trophic support for higher-order consumers, e.g., fish, large crustaceans, and shorebirds (Kristensen et al., 2018; Levin et al., 2001). In a created and restored area, the ecosystem service delivery will rely on the benthic macrofauna community development rate. The rate of benthic macrofauna development could occur within days to decades (Masik et al., 2007; Moseman et al., 2004; Craft and Sacco, 2003; Levin et al., 1996), depending on the intensity of interaction between the benthic community and local environmental condition. Despite the limitation in faunal sampling and physical data, the substrate type, distribution, and development are thought to be the main factors influencing the development of the benthic macrofauna community in the restored coastal peatland of Drammendorf. The succession of the benthic community colonization will have to wait for the dense grass to decompose and sediment to accrete.

4.7 O_2 dynamic associated with bioirrigation of *H. diversicolor*

O_2 concentration at the surface was higher in sediment than in soil. This could indicate a lower O_2 consumption in the sediment than in the soil. In the case of aquaria with artificial burrows, the latter was contradicted by the vertical O_2 profile, showing steeper O_2 concentration gradients and shallower O_2 penetration depth in the sediment than in the soil. Therefore, a more efficient diffusive transport was most likely driven by the higher O_2 concentration in the sediment than in the soil.

With the addition of *H. diversicolor*, shallower O_2 concentration gradients at SWI and deeper O_2 penetration depth were observed in sediment, while the gradient was steepened in soil. This could be linked to the fact that *H. diversicolor* ventilated more frequently in the sediment than the soil and to the lower content of reduced compound in sediment than in soil. Ventilation not only transported O_2-rich water into the burrow but also stimulated the upward transport of reduced compounds and, eventually, the re-oxidation of these compounds. The ventilation rate in the soil was lower than in the sediment. Thus, the content of reduced compounds in the soil must have been higher than in the sediment.

O_2 concentrations and penetration depths at the burrow were lower than at the surface, regardless of burrow and substrate type. The maximum O_2 concentration in the burrow was only 31 % and 87 % of the mean O_2 concentrations in the overlying water in sediment and soil, respectively. One plausible explanation for this phenomenon is the amount of ventilated O_2-rich water that was smaller than the volume of the burrow cavity (Pischedda et al., 2012; Kristensen et al., 1991; Aller et al., 1983). The supplied water was sufficient to support the physiological needs of the animal, however, the velocity of water flushing into the burrow could limits the extent of burrow oxygenation (Kristensen et al., 1999; Aller et al., 1983). O_2 concentrations and penetration depths at the burrow could further be limit by a higher microbial consumption rates.

The average O_2 fluxes at the SWI and the burrow of *H. diversicolor* estimated in this study are in the lower range of values measured in the burrow of the same species and of another polychaetes in coastal sediment (Murphy & Reidenbach, 2016 Wenzhöfer & Glud, 2004; Pischedda et al. 2008, 2012;). On average, O_2 fluxes within the burrow wall were similar to those at SWI in sediment but 3 times lower in soil. Similar observations were documented in another study of 2D-O_2 dynamics in the burrow of *H. diversicolor* (Pischedda et al., 2012; Pischedda et al., 2008). Similar to these previous studies, the low O_2 concentration in the burrow could explain the calculated low fluxes, particularly in the sediment. In soil, an additional factor influencing the obtained O_2 fluxes was the higher porosity of the substrate. In the same fashion as at the SWI, the availability of organic matter and reduced compounds in the burrow wall and the microbial consumption rate further drive the O_2 flux in the burrow wall.

Bioturbating macrofauna is known to increase benthic metabolism by increasing the solute exchange area of the sediment through ventilation. *H. diversicolor* has been reported to increase the area of the oxic-anoxic interface by a factor of 1.3 - 5 (Kristensen & Hansen, 1999; Hansen & Kristensen, 1997; Fenchel, 1996; Kristensen et al., 1992). In this study, with a burrow diameter of 2 mm and a burrow length of approximately 20 cm, one ideal U-shape burrow of *H. diversicolor* covered a total area of 12.6 cm^2. With a density of 380 individuals per m^2, *H. diversicolor* expands the oxic-anoxic interface area by up to 48 % compared to the SWI (by a factor of 0.5). Considering the average O_2 flux from the burrow wall of *H. diversicolor* into the substrate (sediment: 1 mmol m^{-2} d^{-1} O_2, soil: 2 mmol m^{-2} d^{-1} O_2), 380 individuals per m^2 would result in an additional O_2 flux of 0.5 and 1 mmol m^{-2} d^{-1} O_2 in sediment and soil, respectively. These values are significantly lower than the measured TOU in the respective substrate, i.e., average TOU was 22 mmol m^{-2} d^{-1} in sediment and 13

mmol m^{-2} d^{-1} in soil. Burrow-mediated O_2 uptake could account for 2 % (in sediment) and 8 % (in soil) of the TOU in the respective substrate.

By combining the O_2 penetration depth at the sediment surface and around the burrow with the corresponding surface exchange area, the volume of the oxic substrate at the surface and within the ventilated burrow of *H. diversicolor* was calculated. In this study, the volume of oxygenated substrate around the burrow was approximately 32 % (sediment) and 36 % (soil) of the oxic sediment volume below the surface. This estimation is lower than previously reported in other studies (Wenzhöfer & Glud, 2004 ; Kristensen, 2000; Fenchel, 1996). The volume of the oxygenated substrate is dependent on the burrow size and density of the burrow. For instance, for almost twice the density of *H. diversicolor*, Wenzhöfer and Glud (2004) found that the oxygenated sediment volume around the burrow exceeds the oxic volume at the sediment surface by 54 – 70 %.

Following the approach described by Wenzhöfer and Glud (2004), the volume-specific O_2 consumption rate in the oxygenated substrate around the burrow of *H. diversicolor* was 0.01 and 0.02 µmol cm^{-3} h^{-1} in sediment and soil, respectively. The rate around the burrow was ~2 times higher than the corresponding rate obtained at the sediment surface (5.7 x 10^{-3} µmol cm^{-3} h^{-1}), while it was slightly lower than the value at the soil surface (0.03 µmol cm^{-3} h^{-1} in soil). Burrow walls are hot spots of intensive mineralization (Aller & Aller, 1986). With narrow redox zonation, steep chemical gradients, and the presence of mucus lining enriched in labile organic carbon, burrow walls possess a dynamic microbial community and activity. In particular, for *H. diversicolor,* Aller & Aller (1986) and Kristensen (2000) found that the worm produced a labile degradable substrate (mucopolysaccharide) for microbial growth. Furthermore, enhanced porewater transport due to burrow ventilation might facilitate the decomposition of old organic matter and the removal of porewater CO_2 and other reduced compounds, which subsequently consume O_2 through reoxidation along the oxic wall of the burrow (Kristensen, 2000). In this study, the primary site for O_2 consumption was around burrow structures, presumably due to intensified mineralization in the mucus layer and reoxidation of reduced compounds from the anaerobic degradation.

The volume-specific O_2 consumption rate around the burrow in this study was lower than the estimated rate (0.7 – 1 µmol cm^{-3} h^{-1}) from similar-sized *H. diversicolor* used in a previous study (Wenzhöfer & Glud, 2004). However, the calculated OCRs (0.4 µmol cm^{-3} h^{-1} in sediment, 0.2 µmol cm^{-3} h^{-1} in soil) from the average concentration change over time in designated ROI in the middle of the burrow were comparable to the range reported by Wenzhöfer and Glud (2004). This mismatch can be explained by the uncertainty originating from the respective approaches. The estimation of the volume-specific O_2 consumption rate involved O_2 fluxes along the burrow walls and O_2 penetration depth extracted from the O_2 concentration profile; both were subject to overestimation due to uncertainty on Ds and inherent to the planar optode technique. On the other hand, OCRs were extracted from an area over time.

5 CONCLUSION AND OUTLOOK

The first part of this study demonstrated the importance of light and pore water advection governing O_2 distribution and metabolism in sandy permeable sediment. In the dark, under diffusive conditions, O_2 distribution is governed by the O_2 concentration in the overlying water, small-scale heterogeneity of microtopography, microbial respiration rates, and the availability of reduced compounds. Light facilitates benthic metabolism (both photosynthesis and respiration by MPB and the microbial community) and further affects O_2 distribution. In the dark, advection enhanced O_2 transport to deeper sediment layers with varied impacts on dark respiration, which was tightly coupled with the availability of reduced compound. Although advection facilitated the distribution of solutes and benthic exchange with the range of the applied stirring rate in this study, the influence of light on O_2 distribution and metabolism overruled those of advection.

MPB photosynthetic activity in permeable sandy sediment may contribute substantially to total primary production in shallow coastal water of the Southwestern Baltic Sea. The role of nutrients in the form of reduced compounds, diffusing upward, appears to shape the MPB community composition and promote different photosynthetic capacities of the low-light adapted MPB. This study also documented the occurrence of light-stimulated O_2 respiration in OM-poor sandy sediment for the first time. The ecological consequence of this phenomenon still needs to be well addressed and is subject to future study. These findings challenge the accuracy of the bell jar incubation approach in reporting gross photosynthesis value by simply summing the dark respiration and net photosynthesis.

The pressure gradient at the advective stirrer setting is considered to be representative of normal calm weather conditions (Schade, 2019) and similar to those of the few existing measurements in permeable sediments (Glud et al., 2008; Cook et al.,2007; Janssen et al., 2005). Nonetheless, frequent and occasional extreme weather events are predicted under the climate change scenario in the southwestern Baltic Sea region. Therefore, more detailed studies incorporating pore water advection are needed. Varying the advection, i.e., increasing the stirring speed of a benthic chamber and incorporating different sediment permeabilities and topography, are the main topics to be addressed in future studies concerning benthic O_2 distribution and metabolism.

Implementing a multi-approach in measuring benthic O_2 distribution and metabolism in permeable sediment covered by the photosynthetically active community is essential to gaining relevant insight into benthic O_2 dynamics (mechanisms and exchange rates). The sediment heterogeneity and patchiness of the MPB were well documented with microelectrode ID point measurement. At the same time, the occurrence of a "hotspot" with high metabolic activity can be identified spatiotemporally with 2D planar optode measurement. The total organic matter mineralization was obtained from the benthic chamber enclosure equipped with an O_2 sensor spot; however, due to the shading of the stirring disk inside the benthic chamber, the total benthic production is still unresolved with this approach. Moreover, this study is conducted under limited *ex-situ* conditions compared to strongly fluctuating *in-situ* environmental conditions. For future studies, it is recommended that in situ and *ex-situ* seasonal measurements be performed using combined techniques in measuring benthic O_2 flux. For instance, a recent promising approach is the in

situ eddy correlation technique that measures aquatic O_2 flux non-invasively by capturing the vertical turbulent fluxes within aquatic boundary layers (Berg et al., 2015; 2003).

The second part of this study indicates that the extent of macrofauna stimulation in O_2 and nutrient dynamics relies on the intensity of faunal-environmental interaction. Substrate characteristics and chemical environment of the water and pore water emerged as significant factors in limiting bioturbation activity. These findings notably echoed in flooded, degraded coastal peatland with potential high nutrient leaching. Further assessment of the role of the benthic infauna community at the sediment-water interface will need to consider not only the individual role of each species but also the interactions among species. Biological interaction is yet to be explored, e.g., multi-species in one core, as shown in a study by Kristensen et al. (2011).

Substrate preference and suitability are essential in restoration projects focusing on benthic community development and colonization. Laboratory experiments confirm the ability of *H. diversicolor* to colonize, survive, and perform bioirrigation in terrestrial soil flooded with seawater, albeit with lower intensity than in marine sediment. *H. diversicolor, M. neglecta*, and *M. arenaria* generally could survive in colonization experiments. However, the physical characteristics of the substrate and the chemical consequence of the inundation imposed challenging conditions for the key bioturbators to survive, burrow, and irrigate their burrow. This laboratory result was partly confirmed in the occasional field observation, where colonization occur only in areas with less grass and mud-sandy layer.

Studies on macrofauna colonization have mostly reported from intertidal salt marsh where the newly created areas will provide a familiar substrate for early colonizers. However, studies on colonization of benthic macrofauna in degraded coastal peatlands are still scarce. Combining the results from our experimental and field observation, it is evident that the ability to cope with the chemical and physical stressors that emerge from rewetting the peatland will be the critical point for the succession of the early colonizing benthic macrofauna in peatland restoration. Topography reconstruction, which will allow constant inundation and water exchange, might reduce the effect of nutrients leaching through water buffering capacity. Permanent inundation will increase the peat soil's water content, allowing easier penetration from burrowing fauna. A permanent inundation also facilitates sediment entrapment and deposition in between and on top of the root structure of the degraded soil, which provides a preferable and familiar burrowing ground for the macrofauna.

6 REFERENCES

Aller, J. Y., & Aller, R. C. (1986). Evidence for localized enhancement of biological associated with tube and burrow structures in deep-sea sediments at the HEEBLE site, western North Atlantic. *Deep Sea Research Part A. Oceanographic Research Papers*, *33*(6), 755-790.

Aller, R. C. (1980). Relationships of tube-dwelling benthos with sediment and overlying water chemistry. *Marine benthic dynamics*, 285-308.

Aller, R. C. (1983). The importance of the diffusive permeability of animal burrow linings in determining marine sediment chemistry. *Journal of marine Research*, *41*(2), 299-322.

Aller, R. C. (2001). 11 TRANSPORT AND REACTIONS IN THE BIOIRRIGATED ZONE. *The benthic boundary layer: transport processes and biogeochemistry*, 269.

Aller, R. C. (2001). 11 TRANSPORT AND REACTIONS IN THE BIOIRRIGATED ZONE. *The benthic boundary layer: transport processes and biogeochemistry*, 269.

Aller, R. C., & Aller, J. Y. (1998). The effect of biogenic irrigation intensity and solute exchange on diagenetic reaction rates in marine sediments. *Journal of Marine Research*, *56*(4), 905-936.

Archer, D., & Devol, A. (1992). Benthic oxygen fluxes on the Washington shelf and slope: A comparison of in situ microelectrode and chamber flux measurements. *Limnology and Oceanography*, *37*(3), 614-629. doi: 10.4319/lo.1992.37.3.0614

ARMY ENGINEER WATERWAYS EXPERIMENT STATION VICKSBURG MS. (1995). Environmental Effects of Dredging: Naturally Occurring Levels of Ammonia and Sulfide in Pore Water: An Assessment of the Literature.

Asano, R., Nakai, Y., Kawada, W., Shimura, Y., Inamoto, T., & Fukushima, J. (2013). Seawater inundation from the 2011 Tohoku tsunami continues to strongly affect soil bacterial communities 1 year later. *Microbial ecology*, *66*, 639-646.

Askaer, L., Elberling, B., Glud, R. N., Kühl, M., Lauritsen, F. R., & Joensen, H. P. (2010). Soil heterogeneity effects on O2 distribution and CH4 emissions from wetlands: In situ and mesocosm studies with planar O2 optodes and membrane inlet mass spectrometry. *Soil Biology and Biochemistry*, *42*(12), 2254-2265.

Attard, K. M., Rodil, I. F., Glud, R. N., Berg, P., Norkko, J., & Norkko, A. (2019). Seasonal ecosystem metabolism across shallow benthic habitats measured by aquatic eddy covariance. *Limnology and oceanography letters*, *4*(3), 79-86.

Badger, M. R., & Price, G. D. (2003). CO2 concentrating mechanisms in cyanobacteria: molecular components, their diversity and evolution. *Journal of experimental botany*, *54*(383), 609-622.

Baird, A. J., & Gaffney, S. W. (2000). Solute movement in drained fen peat: a field tracer study in a Somerset (UK) wetland. *Hydrological Processes*, *14*(14), 2489-2503.

Baldwin, D. S., Rees, G. N., Mitchell, A. M., Watson, G., & Williams, J. (2006). The short-term effects of salinization on anaerobic nutrient cycling and microbial community structure in sediment from a freshwater wetland. *Wetlands*, *26*(2), 455-464.

Banta, G. T., Holmer, M., Jensen, M. H., & Kristensen, E. (1999). Effects of two polychaete worms, Nereis diversicolor and Arenicola marina, on aerobic and anaerobic decomposition in a sandy marine sediment. *Aquatic microbial ecology*, *19*(2), 189-204.

Bass, A., Wernberg, T., Thomsen, M., & Smale, D. (2021). Another decade of marine climate change experiments: Trends, progress and knowledge gaps. *Frontiers in Marine Science*, *8*, 714462.

Beardall, J. (1989). Photosynthesis and photorespiration in marine phytoplankton. *Aquatic Botany*, *34*(1-3), 105-130.

Berg, P., & Huettel, M. (2008). Monitoring the seafloor using the noninvasive eddy correlation technique. *Oceanography*, *21*(4), 164-167.

Berg, P., Long, M. H., Huettel, M., Rheuban, J. E., McGlathery, K. J., Howarth, R. W., ... & Marino, R. (2013). Eddy correlation measurements of oxygen fluxes in permeable sediments exposed to varying current flow and light. *Limnology and Oceanography*, *58*(4), 1329-1343.

Berg, P., Risgaard-Petersen, N., & Rysgaard, S. (1998). Interpretation of measured concentration profiles in sediment pore water. *Limnology and Oceanography*, *43*(7), doi: 1500-1510. 10.4319/lo.1998.43.7.1500

Berner, R. A. (1980). *Early diagenesis: a theoretical approach* (No. 1). Princeton University Press.

Berninger, U. G., & Huettel, M. (1997). Impact of flow on oxygen dynamics in photosynthetically active sediments. *Aquatic Microbial Ecology*, *12*(3), 291-300. doi:10.3354/ame012291

Billerbeck, M., Røy, H., Bosselmann, K., & Huettel, M. (2007). Benthic photosynthesis in submerged Wadden Sea intertidal flats. *Estuarine, Coastal and Shelf Science*, *71*(3-4), 704-716. doi: 10.1016/j.ecss.2006.09.019

Bolam, S. G., Whomersley, P., & Schratzberger, M. (2004). Macrofaunal recolonization on intertidal mudflats: effect of sediment organic and sand content. *Journal of Experimental Marine Biology and Ecology*, *306*(2), 157-180.

Boudreau, B. P. (1997). Diagenetic models and their implementation (Vol. 505). Berlin: Springer

Braeckman, U., Provoost, P., Gribsholt, B., Van Gansbeke, D., Middelburg, J. J., Soetaert, K., ... & Vanaverbeke, J. (2010). Role of macrofauna functional traits and density in biogeochemical fluxes and bioturbation. *Marine Ecology Progress Series*, *399*, 173-186.

Breznikar, A., Pönisch, D. L., Lorenz, M., Jurasinski, G., Rehder, G., & Voss, M. (2024). Rewetting effects on nitrogen cycling and nutrient export from coastal peatlands to the Baltic Sea. *Biogeochemistry*, 1-21.

Brisch, A. (2015). Erkundung von Torfmächtigkeit und Vegetation in zwei potenziellen Wiedervernässungsgebieten

bei Rambin und Grosow (Rügen), Unpublished expert opinion by Naturschutzstiftung Deutsche Ostsee.

Cahoon, L. B. (1999). The role of benthic microalgae in neritic ecosystems. In *Oceanography and Marine Biology, An Annual Review, Volume 37* (pp. 47-86). CRC Press.

Cahoon, L. B., & Cooke, J. E. (1992). Benthic microalgal production in Onslow bay, North Carolina, USA. *Marine Ecology Progress Series*, 185-196.

Cahoon, L. B., & Cooke, J. E. (1992). Benthic microalgal production in Onslow bay, North Carolina, USA. *Marine Ecology Progress Series*, 185-196.

Camargo, J. A., & Alonso, Á. (2006). Ecological and toxicological effects of inorganic nitrogen pollution in aquatic ecosystems: a global assessment. *Environment international*, *32*(6), 831-849.

Camillini, N., Larsen, M., & Glud, R. N. (2019). Behavioural patterns of the soft-shell clam Mya arenaria: implications for benthic oxygen and nitrogen dynamics. *Marine Ecology Progress Series*, *622*, 103-119.

Canfield, D. E. (1993). Organic matter oxidation in marine sediments. In *Interactions of C, N, P and S biogeochemical cycles and global change* (pp. 333-363). Springer Berlin Heidelberg.doi: 10.1007/978-3-642-76064-8_14

Canfield, D. E., & Teske, A. (1996). Late Proterozoic rise in atmospheric oxygen concentration inferred from phylogenetic and sulphur-isotope studies. *Nature*, *382*(6587), 127-132.

Canfield, D. E., Kristensen, E., & Thamdrup, B. (2005). Aquatic geomicrobiology.

Carman, R., & Cederwall, H. (2001). Sediments and macrofauna in the Baltic Sea—characteristics, nutrient contents and distribution. In *A systems analysis of the Baltic Sea* (pp. 289-327). Berlin, Heidelberg: Springer Berlin Heidelberg.

Cartaxana, P., Cruz, S., Gameiro, C., & Kühl, M. (2016). Regulation of intertidal microphytobenthos photosynthesis over a diel emersion period is strongly affected by diatom migration patterns. *Frontiers in microbiology*, *7*, 872. doi: 10.3389/fmicb.2016.00872

Cartaxana, P., Domingues, N., Cruz, S., Jesus, B., Laviale, M., Serôdio, J., & da Silva, J. M. (2013). Photoinhibition in benthic diatom assemblages under light stress. *Aquatic Microbial Ecology*, *70*(1), 87-92.

Cartaxana, P., Mendes, C. R., Van Leeuwe, M. A., & Brotas, V. (2006). Comparative study on microphytobenthic pigments of muddy and sandy intertidal sediments of the Tagus estuary. *Estuarine, Coastal and Shelf Science*, *66*(1-2), 225-230.

Cartaxana, P., Ribeiro, L., Goessling, J. W., Cruz, S., & Kühl, M. (2016). Light and O2 microenvironments in two contrasting diatom-dominated coastal sediments. *Marine Ecology Progress Series*, *545*, 35-47.

Cheng, C., van Donk, S., Walles, B., Ysebaert, T., van Belzen, J., Wiesebron, L., ... & de Vet, L. (2021). *Perkpolder-Phase 2 (2019-2024): the transition from a freshwater agricultural area to a saltwater nature reserve* (No. C097/21). Wageningen Marine Research.

Cong, M., Li, Y., Xu, H., Lv, J., Wu, H., & Zhao, Y. (2021). Ammonia nitrogen exposure caused structural damages to gill mitochondria of clam Ruditapes philippinarum. *Ecotoxicology and Environmental Safety*, *222*, 112528.

Cong, M., Li, Y., Xu, H., Lv, J., Wu, H., & Zhao, Y. (2021). Ammonia nitrogen exposure caused structural damages to gill mitochondria of clam Ruditapes philippinarum. *Ecotoxicology and Environmental Safety*, *222*, 112528.

Cong, M., Wu, H., Cao, T., Ji, C., & Lv, J. (2019). Effects of ammonia nitrogen on gill mitochondria in clam Ruditapes philippinarum. *Environmental Toxicology and Pharmacology*, *65*, 46-52.

Constable, M., Charlton, M., Jensen, F., McDonald, K., Craig, G., & Taylor, K. W. (2003). An ecological risk assessment of ammonia in the aquatic environment. *Human and Ecological Risk Assessment*, *9*(2), 527-548.

Cook, B. D., & Allan, D. L. (1992). Dissolved organic carbon in old field soils: compositional changes during the biodegradation of soil organic matter. *Soil Biology and Biochemistry*, *24*(6), 595-600.

Cook, P. L., Wenzhöfer, F., Glud, R. N., Janssen, F., & Huettel, M. (2007). Benthic solute exchange and carbon mineralization in two shallow subtidal sandy sediments: Effect of advective pore-water exchange. Limnology and Oceanography, 52(5), 1943-1963. doi: 10.4319/lo.2006.51.4.1594

Cook, Perran LM, and Hans Røy. "Advective relief of CO2 limitation in microphytobenthos in highly productive sandy sediments." *Limnology and Oceanography* 51.4 (2006): 1594-1601.

Craft, C., & Sacco, J. (2003). Long-term succession of benthic infauna communities on constructed Spartina alterniflora marshes. *Marine Ecology Progress Series*, *257*, 45-58.

Crossland, C. J., Baird, D., Ducrotoy, J.-P., Lindeboom, H., Buddemeier, R. W., Dennison, W. C., … Swaney, D. P. (2005). The Coastal Zone — a Domain of Global Interactions (pp. 1–37).

de Beer, D., Wenzhöfer, F., Ferdelman, T. G., Boehme, S. E., Huettel, M., van Beusekom, J. E., ... & Dubilier, N. (2005). Transport and mineralization rates in North Sea sandy intertidal sediments, Sylt-Rømø basin, Wadden Sea. Limnology and Oceanography, 50(1), 113-127. doi: 10.4319/lo.2005.50.1.0113

De Schryver, P., Crab, R., Defoirdt, T., Boon, N., & Verstraete, W. (2008). The basics of bio-flocs technology: the added value for aquaculture. *Aquaculture*, *277*(3-4), 125-137.

Denis, L., Gevaert, F., & Spilmont, N. (2012). Microphytobenthic production estimated by in situ oxygen microprofiling: short-term dynamics and carbon budget implications. *Journal of Soils and Sediments*, *12*, 1517-1529. doi: 10.1007/s11368-012-0588-8

Deppe, M., Knorr, K. H., McKnight, D. M., & Blodau, C. (2010). Effects of short-term drying and irrigation on CO 2 and CH 4 production and emission from mesocosms of a northern bog and an alpine fen. *Biogeochemistry*, *100*, 89-103.

Diaz, R. J. (2001). Overview of hypoxia around the world. *Journal of environmental quality*, *30*(2), 275-281.

Diaz, R. J., & Rosenberg, R. (2011). Introduction to environmental and economic consequences of hypoxia. *International Journal of Water Resources Development*, *27*(1), 71-82.

Eddy, F. B. (2005). Ammonia in estuaries and effects on fish. *Journal of Fish Biology*, *67*(6), 1495-1513.

Epifanio, C. E., & Srna, R. F. (1975). Toxicity of ammonia, nitrite ion, nitrate ion, and orthophosphate to Mercenaria mercenaria and Crassostrea virginica. *Marine Biology*, *33*, 241-246.

Epping, E. H., & Helder, W. (1997). Oxygen budgets calculated fromin situ oxygen microprofiles for Northern Adriatic sediments. *Continental Shelf Research*, *17*(14), 1737-1764.

Epping, E. H., & Jørgensen, B. B. (1996). Light-enhanced oxygen respiration in benthic phototrophic communities. *Marine Ecology Progress Series*, *139*, 193-203. doi:10.3354/meps139193

Evans, P. R., Ward, R. M., Bone, M., & Leakey, M. (1999). Creation of temperate-climate intertidal mudflats: factors affecting colonization and use by benthic invertebrates and their bird predators. *Marine Pollution Bulletin*, *37*(8-12), 535-545.

Fenchel, T. (1996). Worm burrows and oxic microniches in marine sediments. 1. Spatial and temporal scales. *Marine Biology*, *127*, 289-295.

Fenchel, T., & Glud, R. N. (2000). Benthic primary production and O_2-CO_2 dynamics in a shallow-water sediment: spatial and temporal heterogeneity. *Ophelia*, *53*(2), 159-171. doi: 10.1080/00785236.2000.10409446

Feugere, L., Angell, L., Fagents, J., Nightingale, R., Rowland, K., Skinner, S., ... & Wollenberg Valero, K. C. (2021). Behavioural stress propagation in benthic invertebrates caused by acute pH drop-induced metabolites. *Frontiers in Marine Science*, *8*, 773870.

Forster, S., & Graf, G. (1995). Impact of irrigation on oxygen flux into the sediment: intermittent pumping by Callianassa subterranea and “piston-pumping” by Lanice conchilega. *Marine Biology*, *123*(2), 335–346. https://doi.org/10.1007/BF00353625

Forster, S., Huettel, M., & Ziebis, W. (1996). Impact of boundary layer flow velocity on oxygen utilisation in coastal sediments. *Marine Ecology Progress Series*, *143*, 173-185. doi:10.3354/meps143173

Freitas, R., Pires, A., Moreira, A., Wrona, F. J., Figueira, E., & Soares, A. M. (2016). Biochemical alterations induced in Hediste diversicolor under seawater acidification conditions. *Marine environmental research*, *117*, 75-84.

Fritzsche, D., & Von Oertzen, J. A. (1995). Metabolic responses to changing environmental conditions in the brackish water polychaetes Marenzelleria viridis and Hediste diversicolor. *Marine Biology*, *121*, 693-699.

Garbutt, R. A., Reading, C. J., Wolters, M., Gray, A. J., & Rothery, P. (2006). Monitoring the development of intertidal habitats on former agricultural land after the managed realignment of coastal defences at Tollesbury, Essex, UK. *Marine pollution bulletin*, *53*(1-4), 155-164.

Gattuso, J. P., Gentili, B., Duarte, C. M., Kleypas, J. A., Middelburg, J. J., & Antoine, D. (2006). Light availability in the coastal ocean: impact on the distribution of benthic photosynthetic organisms and their contribution to primary production. *Biogeosciences*, *3*(4), 489-513.

Gazeau, F., Smith, S. V., Gentili, B., Frankignoulle, M., & Gattuso, J. P. (2004). The European coastal zone: characterization and first assessment of ecosystem metabolism. *Estuarine, Coastal and Shelf Science*, *60*(4), 673-694. doi: 10.1016/j.ecss.2004.03.007

Glud RN, Ramsing NB, Gundersen JK, Klimant I. 1996b. Planar optodes, a new tool for fine scale measurements of two dimensional O2 distribution in benthic communities. Marine Ecology Progress Series 140:21726.

Glud, R. N. (2006). Microscale techniques to measure photosynthesis: a mini-review. Functioning of Microphytobenthos. Amsterdam: Royal Netherlands Academy of Arts and Sciences. p 31Á42.

Glud, R. N. (2008). Oxygen dynamics of marine sediments. *Marine Biology Research*, *4*(4), 243-289. doi: 10.1080/17451000801888726

Glud, R. N., Eyre, B. D., & Patten, N. (2008). Biogeochemical responses to mass coral spawning at the Great Barrier Reef: Effects on respiration and primary production. *Limnology and Oceanography*, *53*(3), 1014-1024. doi: 10.4319/lo.2008.53.3.1014

Glud, R. N., Forster, S., & Huettel, M. (1996). Influence of radial pressure gradients on solute exchange in stirred benthic chambers. *Marine Ecology Progress Series*, *141*, 303-311.

Glud, R. N., Gundersen, J. K., Jørgensen, B. B., Revsbech, N. P., & Schulz, H. D. (1994). Diffusive and total oxygen uptake of deep-sea sediments in the eastern South Atlantic Ocean: in situ and laboratory measurements. *Deep Sea Research Part I: Oceanographic Research Papers*, *41*(11-12), 1767-1788. doi: /10.1016/0967-0637(94)90072-8

Glud, R. N., Gundersen, J. K., Røy, H., & Jørgensen, B. B. (2003). Seasonal dynamics of benthic O2 uptake in a semienclosed bay: Importance of diffusion and faunal activity. *Limnology and Oceanography*, *48*(3), 1265-1276. doi: 10.4319/lo.2003.48.3.1265

Glud, R. N., Gundersen, J. K., Røy, H., & Jørgensen, B. B. (2003). Seasonal dynamics of benthic O2 uptake in a semienclosed bay: Importance of diffusion and faunal activity. *Limnology and Oceanography*, *48*(3), 1265-1276.

Glud, R. N., Kühl, M., Kohls, O., & Ramsing, N. B. (1999). Heterogeneity of oxygen production and consumption in a photosynthetic microbial mat as studied by planar optodes. *Journal of Phycology*, *35*(2), 270-279. doi: 10.1046/j.1529-8817.1999.3520270.x

Glud, R.N., Ramsing, N.B. and Revsbech, N.P., 1992. Photosynthesis and Photosynthesis-Coupled Respiration in Natural Biofilms Quantified with Oxygen Microsensors 1. *Journal of Phycology*, 28(1), pp.51-60. doi: 10.1111/j.0022-3646.1992.00051.x

Gogina, M., Lipka, M., Woelfel, J., Liu, B., Morys, C., Böttcher, M. E., & Zettler, M. L. (2018). In search of a field-based relationship between benthic macrofauna and biogeochemistry in a modern brackish coastal sea. *Frontiers in Marine Science*, *5*, 489.

Gosch, L., Townsend, H., Kreuzburg, M., Janssen, M., Rezanezhad, F., & Lennartz, B. (2019). Sulfate mobility in fen peat and its impact on the release of solutes. *Frontiers in Environmental Science*, *7*, 189.

Grabowski, R. C., Droppo, I. G., & Wharton, G. (2011). Erodibility of cohesive sediment: The importance of sediment properties. *Earth-Science Reviews*, *105*(3-4), 101-120.

Graf, G., Bengtsson, W., Diesner, U., Schulz, R., & Theede, H. (1982). Benthic response to sedimentation of a spring phytoplankton bloom: process and budget. *Marine Biology*, *67*, 201-208.

Graf, G., Schulz, R., Peinert, R., & Meyer-Reil, L. A. (1983). Benthic response to sedimentation events during autumn to spring at a shallow-water station in the Western Kiel Bight: I. Analysis of processes on a community level. *Marine Biology*, *77*, 235-246.

Grasshoff, K., Kremling, K., & Ehrhardt, M. (Eds.). (2009). Methods of seawater analysis. John Wiley & Sons.

Gray, J. S., Wu, R. S. S., & Or, Y. Y. (2002). Effects of hypoxia and organic enrichment on the coastal marine environment. *Marine ecology progress series*, *238*, 249-279.

Gundersen, J. K., & Jorgensen, B. B. (1990). Microstructure of diffusive boundary layers and the oxygen uptake of the sea floor. *Nature*, *345*(6276), 604-607.

Gutekunst, C. N., Liebner, S., Jenner, A. K., Knorr, K. H., Unger, V., Koebsch, F., ... & Jurasinski, G. (2022). Effects of brackish water inflow on methane-cycling microbial communities in a freshwater rewetted coastal fen. *Biogeosciences*, *19*(15), 3625-3648.

Hahlbeck, E., Arndt, C., & Schiedek, D. (2000). Sulphide detoxification in Hediste diversicolor and Marenzelleria viridis, two dominant polychaete worms within the shallow coastal waters of the southern Baltic Sea. *Comparative Biochemistry and Physiology Part B: Biochemistry and Molecular Biology*, *125*(4), 457-471.

Haider, F., Timm, S., Bruhns, T., Noor, M. N., & Sokolova, I. M. (2020). Effects of prolonged food limitation on energy metabolism and burrowing activity of an infaunal marine bivalve, Mya arenaria. *Comparative Biochemistry and Physiology Part A: Molecular & Integrative Physiology*, *250*, 110780.

Hancke, K., & Glud, R. N. (2004). Temperature effects on respiration and photosynthesis in three diatom-dominated benthic communities. *Aquatic Microbial Ecology*, *37*(3), 265-281. doi:10.3354/ame037265

Hancke, K., Sorell, B. K., Lund-Hansen, L. C., Larsen, M., Hancke, T., & Glud, R. N. (2014). Effects of temperature and irradiance on a benthic microalgal community: A combined two-dimensional oxygen and fluorescence imaging approach. *Limnology and Oceanography*, *59*(5), 1599-1611. doi: 10.4319/lo.2014.59.5.1599

Hansen, H. P., & Koroleff, F. (1999). Determination of nutrients. *Methods of seawater analysis*, 159-228.

Hansen, K., & Kristensen, E. (1997). Impact of macrofaunal recolonization on benthic metabolism and nutrient fluxes in a shallow marine sediment previously overgrown with macroalgal mats. *Estuarine, Coastal and Shelf Science*, *45*(5), 613-628.

Harley, C. D. G., Hughes, A. R., Hultgren, K. M., Miner, B. G., Sorte, C. J. B., Thornber, C. S., … Williams, S. L. (2006, February). The impacts of climate change in coastal marine systems. *Ecology Letters*. https://doi.org/10.1111/j.1461-0248.2005.00871.x

Haro, S., Bohórquez, J., Lara, M., Garcia-Robledo, E., González, C. J., Crespo, J. M., ... & Corzo, A. (2019). Diel patterns of microphytobenthic primary production in intertidal sediments: the role of photoperiod on the vertical migration circadian rhythm. *Scientific Reports*, *9*(1), 13376.

Herman, P. M. J., Middelburg, J. J., Van de Koppel, J., & Heip, C. H. R. (1999). Ecology of estuarine macrobenthos. *Advances in ecological research*, *29*(780), 195-240.

Hicks, N., Ubbara, G. R., Silburn, B., Smith, H. E., Kröger, S., Parker, E. R., ... & Stahl, H. (2017). Oxygen dynamics in shelf seas sediments incorporating seasonal variability. *Biogeochemistry*, *135*, 35-47. doi: 10.1007/s10533-017-0326-9

Hill, A. R., & Cardaci, M. (2004). Denitrification and organic carbon availability in riparian wetland soils and subsurface sediments. *Soil Science Society of America Journal*, *68*(1), 320-325.

Holst, G., Kohls, O., Klimant, I., König, B., Kühl, M., & Richter, T. (1998). A modular luminescence lifetime imaging system for mapping oxygen distribution in biological samples. *Sensors and Actuators B: Chemical, 51(1-3), 163-170.*

Huettel, M., & Gust, G. (1992). Impact of bioroughness on interfacial solute exchange in permeable sediments. *Marine ecology progress series*, 253-267.

Huettel, M., & Gust, G. (1992). Solute release mechanisms from confined sediment cores in stirred benthic chambers and flume flows. *Marine ecology progress series. Oldendorf*, *82*(2), 187-197.

Huettel, M., & Webster, I. T. (2000). Porewater flow in permeable sediments. *The benthic boundary layer: transport processes and biogeochemistry*, *144*, 177.

Huettel, M., & Webster, I. T. (2001). Porewater flow in permeable sediments. *The benthic boundary layer: Transport processes and biogeochemistry*, *144*, 177.

Huettel, M., Røy, H., Precht, E., & Ehrenhauss, S. (2003). Hydrodynamical impact on biogeochemical processes in aquatic sediments. In *The Interactions between Sediments and Water: Proceedings of the 9th International Symposium on the Interactions between Sediments and Water, held 5–10 May 2002 in Banff, Alberta, Canada* (pp. 231-236). Springer Netherlands.

Huettel, M., Ziebis, W., & Forster, S. (1996). Flow-induced uptake of particulate matter in permeable sediments. *Limnology and Oceanography*, *41*(2), 309-322.

Huettel, M., Ziebis, W., Forster, S., & Luther Iii, G. W. (1998). Advective transport affecting metal and nutrient distributions and interfacial fluxes in permeable sediments. *Geochimica et Cosmochimica Acta*, *62*(4), 613-631.

Huettel, M., Ziebis, W., Forster, S., & Luther Iii, G. W. (1998). Advective transport affecting metal and nutrient distributions and interfacial fluxes in permeable sediments. *Geochimica et Cosmochimica Acta*, *62*(4), 613-631.

IPCC.Intergovernmental Panel on Climate Change. 2007

Jahnke, R. A., Nelson, J. R., Marinelli, R. L., & Eckman, J. E. (2000). Benthic flux of biogenic elements on the Southeastern US continental shelf: influence of pore water advective transport and benthic microalgae. *Continental Shelf Research*, *20*(1), 109-127.

Jahnke, R. A., Nelson, J. R., Richards, M. E., Robertson, C. Y., Rao, A. M. F., & Jahnke, D. B. (2008). Benthic primary productivity on the Georgia midcontinental shelf: Benthic flux measurements and high-resolution, continuous in situ PAR records. *Journal of Geophysical Research: Oceans*, *113*(C8). doi: 10.1029/2008JC004745

Janssen, F., Huettel, M., & Witte, U. (2005). Pore-water advection and solute fluxes in permeable marine sediments (II): Benthic respiration at three sandy sites with different permeabilities (German Bight, North Sea). *Limnology and Oceanography*, *50*(3), 779-792.

Jesus, B., Brotas, V., Ribeiro, L., Mendes, C. R., Cartaxana, P., & Paterson, D. M. (2009). Adaptations of microphytobenthos assemblages to sediment type and tidal position. *Continental Shelf Research*, *29*(13), 1624-1634.

Jørgensen, B. B. (1982). Mineralization of organic matter in the sea bed—the role of sulphate reduction. *Nature*, *296*(5858), 643-645.

Jørgensen, B. B. (1996). Material flux in the sediment. *Eutrophication in coastal marine ecosystems*, *52*, 115-135.

Jørgensen, B. B., & Des Marais, D. J. (1990). The diffusive boundary layer of sediments: oxygen microgradients over a microbial mat. *Limnology and Oceanography*, *35*(6), 1343-1355. doi: 10.4319/lo.1990.35.6.1343

Jørgensen, B. B., & Revsbech, N. P. (1985). Diffusive boundary layers and the oxygen uptake of sediments and detritus 1. *Limnology and oceanography*, *30*(1), 111-122. doi: 10.4319/lo.1985.30.1.0111

Jørgensen, B. B., Cohen, Y., & Revsbech, N. P. (1988). Photosynthetic potential and light-dependent oxygen consumption in a benthic cyanobacterial mat. *Applied and Environmental Microbiology*, *54*(1), 176-182.

Jorgensen, B. B., Revsbech, N. P., & Cohen, Y. (1983). Photosynthesis and structure of benthic microbial mats: Microelectrode and SEM studies of four cyanobacterial communities 1. *Limnology and Oceanography*, *28*(6), 1075-1093.

Jurasinski, G., Janssen, M., Voss, M., Boettcher, M. E., Brede, M., Burchard, H., ... & Lennartz, B. (2018). Understanding the coastal ecocline: Assessing sea–land interactions at non-tidal, low-lying coasts through interdisciplinary research. *Frontiers in Marine Science*, *5*, 342.

Karsten, U., Kuriyama, K., Hübener, T., & Woelfel, J. (2021). Benthic diatoms on sheltered coastal soft bottoms (Baltic Sea)—seasonal community production and respiration. *Journal of Marine Science and Engineering*, *9*(9), 949.

Kiko, R., Hauss, H., Buchholz, F., & Melzner, F. (2016). Ammonium excretion and oxygen respiration of tropical copepods and euphausiids exposed to oxygen minimum zone conditions. *Biogeosciences*, *13*(8), 2241-2255.

Kimpel, N. (2020) Sauerstoffeintrag durch *Hediste diversicolor* (Müller, 1776) in Küstensedimente mit unterschiedlichem organischem Gehalt. [thesis]. [Rostock]: University of Rostock

Klimant, I., Kühl, M., Glud, R. N., & Holst, G. (1997). Optical measurement of oxygen and temperature in microscale: strategies and biological applications. Sensors and Actuators B: Chemical, 38(1-3), 29-37.

Knorr, K. H., & Blodau, C. (2009). Impact of experimental drought and rewetting on redox transformations and methanogenesis in mesocosms of a northern fen soil. *Soil Biology and Biochemistry*, *41*(6), 1187-1198.

Kristensen, E. (1985). Oxygen and inorganic nitrogen exchange in a" Nereis virens"(Polychaeta) bioturbated sediment-water system. *Journal of Coastal Research*, 109-116.

Kristensen, E. (2000). Organic matter diagenesis at the oxic/anoxic interface in coastal marine sediments, with emphasis on the role of burrowing animals. Hydrobiologia, 426(1–3), 1–24.

Kristensen, E. (2000). Organic matter diagenesis at the oxic/anoxic interface in coastal marine sediments, with emphasis on the role of burrowing animals. In *Life at Interfaces and Under Extreme Conditions: Proceedings of the 33rd European Marine Biology Symposium, held at Wilhelmshaven, Germany, 7–11 September 1998* (pp. 1-24). Springer Netherlands.

Kristensen, E. (2000). Organic matter diagenesis at the oxic/anoxic interface in coastal marine sediments, with emphasis on the role of burrowing animals. In *Life at Interfaces and Under Extreme Conditions: Proceedings of the 33rd European Marine Biology Symposium, held at Wilhelmshaven, Germany, 7–11 September 1998* (pp. 1-24). Springer Netherlands.

Kristensen, E., & Hansen, K. (1999). Transport of carbon dioxide and ammonium in bioturbated (Nereis diversicolor) coastal, marine sediments. *Biogeochemistry*, *45*, 147-168.

Kristensen, E., & Hansen, K. (1999). Transport of carbon dioxide and ammonium in bioturbated (Nereis diversicolor) coastal, marine sediments. *Biogeochemistry*, *45*, 147-168.

Kristensen, E., & Kostka, J. E. (2005). Macrofaunal burrows and irrigation in marine sediment: microbiological and biogeochemical interactions. *Interactions between macro-and microorganisms in marine sediments*, *60*, 125-157.

Kristensen, E., Andersen, F. Ø., & Blackburn, T. H. (1992). Effects of benthic macrofauna and temperature on degradation of macroalgal detritus: the fate of organic carbon. *Limnology and Oceanography*, *37*(7), 1404-1419.

Kristensen, E., Hansen, T., Delefosse, M., Banta, G. T., & Quintana, C. O. (2011). Contrasting effects of the polychaetes Marenzelleria viridis and Nereis diversicolor on benthic metabolism and solute transport in sandy coastal sediment. *Marine Ecology Progress Series*, *425*, 125-139.

Kristensen, E., Hansen, T., Delefosse, M., Banta, G. T., & Quintana, C. O. (2011). Contrasting effects of the polychaetes Marenzelleria viridis and Nereis diversicolor on benthic metabolism and solute transport in sandy coastal sediment. *Marine Ecology Progress Series*, *425*, 125-139.

Kristensen, E., Hjorth Jensen, M., & Aller, R. C. (1991). Direct measurement of dissolved inorganic nitrogen exchange and denitrification in individual polychaete (Nereis virens) burrows. *Journal of Marine Research*, *49*(2), 355-377.

Kristensen, E., Neto, J. M., Lundkvist, M., Frederiksen, L., Pardal, M. Â., Valdemarsen, T., & Flindt, M. R. (2013). Influence of benthic macroinvertebrates on the erodability of estuarine cohesive sediments: Density-and biomass-specific responses. *Estuarine, Coastal and Shelf Science*, *134*, 80-87.

Kristensen, E., Penha-Lopes, G., Delefosse, M., Valdemarsen, T., Quintana, C. O., & Banta, G. T. (2012). What is bioturbation? The need for a precise definition for fauna in aquatic sciences. *Marine ecology progress series*, *446*, 285-302.

Kristensen, E., Røy, H., Debrabant, K., & Valdemarsen, T. (2018). Carbon oxidation and bioirrigation in sediments along a Skagerrak-Kattegat-Belt Sea depth transect. *Marine Ecology Progress Series*, *604*, 33-50.

Kromkamp, J., Barranguet, C., & Peene, J. (1998). Determination of microphytobenthos PSII quantum efficiency and photosynthetic activity by means of variable chlorophyll fluorescence. *Marine Ecology Progress Series*, *162*, 45-55.

Kromkamp, J., Peene, J., van Rijswijk, P., Sandee, A., & Goosen, N. (1995). Nutrients, light and primary production by phytoplankton and microphytobenthos in the eutrophic, turbid Westerschelde estuary (The Netherlands). *Hydrobiologia*, *311*, 9-19. doi: 10.1007/BF00008567

Kromkamp, J., Peene, J., van Rijswijk, P., Sandee, A., & Goosen, N. (1995). Nutrients, light and primary production by phytoplankton and microphytobenthos in the eutrophic, turbid Westerschelde estuary (The Netherlands). *Hydrobiologia*, *311*, 9-19.

Kühl, M., & JØrgensen, B. B. (1992). Spectral light measurements in microbenthic phototrophic communities with a fiber-optic microprobe coupled to a sensitive diode array detector. *Limnology and Oceanography*, *37*(8), 1813-1823.

Kühl, M., Glud, R. N., Ploug, H., & Ramsing, N. B. (1996). Microenvironmental Control Of Photosynthesis And Photosynthesis-Coupled Respiration In An Epilithic Cyanobacterial Biofilm 1. *Journal of Phycology*, *32*(5), 799-812.

Kuriyama, K., Gründling-Pfaff, S., Diehl, N., Woelfel, J., & Karsten, U. (2021). Microphytobenthic primary production on exposed coastal sandy sediments of the Southern Baltic Sea using ex situ sediment cores and oxygen optodes. *Oceanologia*, *63*(2), 247-260. doi: 10.1016/j.oceano.2021.02.002

Laine, A. O. (2003). Distribution of soft-bottom macrofauna in the deep open Baltic Sea in relation to environmental variability. *Estuarine, Coastal and Shelf Science*, *57*(1-2), 87-97.

Lalli, C. M. & Parson, T. R. 2004. *Biological Oceanography: An Introduction (*2nd edition). Butterworth-Heinemann

Lampe R(1996) Küstentypen. In: Rheinheimer G (ed) Meereskunde der Ostsee, 2nd edn. Springer, Berlin Heidelberg, pp 17–25

Lang, T., Peters, G., Hoffmann, R., & Meyer, E. (1987). Experimental investigations on the toxicity of ammonia: effects on ventilation frequency, growth, epidermal mucous cells, and gill structure of rainbow trout Salmo gairdneri. *Diseases of aquatic organisms*, *3*(3), 159-165.

Larkum, A. W. D., Koch, E. M. W., & Kühl, M. (2003). Diffusive boundary layers and photosynthesis of the epilithic algal community of coral reefs. *Marine Biology*, *142*, 1073-1082.

Lennartz, B., & Liu, H. (2019). Hydraulic functions of peat soils and ecosystem service. *Frontiers in Environmental Science*, *7*, 92.

Lenzewski, N., Mueller, P., Meier, R. J., Liebsch, G., Jensen, K., & Koop-Jakobsen, K. (2018). Dynamics of oxygen and carbon dioxide in rhizospheres of Lobelia dortmanna–a planar optode study of belowground gas exchange between plants and sediment. *New Phytologist, 218(1), 131-141.*

Levin, L. A., Boesch, D. F., Covich, A., Dahm, C., Erséus, C., Ewel, K. C., ... & Weslawski, J. M. (2001). The function of marine critical transition zones and the importance of sediment biodiversity. *Ecosystems*, *4*, 430-451.

Levin, L. A., Talley, D., & Thayer, G. (1996). Succession of macrobenthos in a created salt marsh. *Marine Ecology Progress Series*, *141*, 67-82.

Lindeboom, H. J., Sandee, A. J., & Driessche, H. A. D. K. V. (1985). A new bell jar/microelectrode method to measure changing oxygen fluxes in illuminated sediments with a microalgal cover 1. *Limnology and Oceanography*, *30*(3), 693-698.

Lipka, M., Woelfel, J., Gogina, M., Kallmeyer, J., Liu, B., Morys, C., ... & Böttcher, M. E. (2018). Solute reservoirs reflect variability of early diagenetic processes in temperate brackish surface sediments. *Frontiers in Marine Science*, *5*, 413.

Liu, H., & Lennartz, B. (2019). Hydraulic properties of peat soils along a bulk density gradient—A meta study. *Hydrological Processes*, *33*(1), 101-114.
Liu, H., & Lennartz, B. (2019). Short term effects of salinization on compound release from drained and restored coastal wetlands. *Water*, *11*(8), 1549.
Liu, H., Forsmann, D. M., Kjaergaard, C., Saki, H., & Lennartz, B. (2017). Solute transport properties of fen peat differing in organic matter content. *Journal of environmental quality*, *46*(5), 1106-1113.
Macintyre, H. L., Geider, R. J., & Miller, D. C. (1996). Microphytobenthos: The ecological role of the "secret garden" of unvegetated, shallow-water marine habitats. I. Role in sediment stability and shallow-water food webs. *Estuaries*, *19*, 202-212.
Mazik, K., Smith, J. E., Leighton, A., & Elliott, M. (2007). Physical and biological development of a newly breached managed realignment site, Humber estuary, UK. *Marine Pollution Bulletin*, *55*(10-12), 564-578.
Meier, H. M. (2006). Baltic Sea climate in the late twenty-first century: a dynamical downscaling approach using two global models and two emission scenarios. *Climate dynamics*, *27*, 39-68.
Meier, R. J., Schreml, S., Wang, X. D., Landthaler, M., Babilas, P., & Wolfbeis, O. S. (2011). Simultaneous photographing of oxygen and pH in vivo using sensor films. *Angewandte Chemie International Edition*, *50*(46), 10893-10896.
Meyercordt, J., Gerbersdorf, S., & Meyer-Reil, L. A. (1999). Significance of pelagic and benthic primary production in two shallow coastal lagoons of different degrees of eutrophication in the southern Baltic Sea. *Aquatic Microbial Ecology*, *20*(3), 273-284. doi:10.3354/ame020273
Meysman, F. J., Middelburg, J. J., & Heip, C. H. (2006). Bioturbation: a fresh look at Darwin's last idea. *Trends in Ecology & Evolution*, *21*(12), 688-695.
Michaud, E., Desrosiers, G., Mermillod-Blondin, F., Sundby, B., & Stora, G. (2006). The functional group approach to bioturbation: II. The effects of the Macoma balthica community on fluxes of nutrients and dissolved organic carbon across the sediment–water interface. *Journal of Experimental Marine Biology and Ecology*, *337*(2), 178-189.
Michaud, E., Desrosiers, G., Mermillod-Blondin, F., Sundby, B., Stora, G., 2005. The functional group approach to bioturbation: The effects of biodiffusers and gallery-diffusers of the Macoma balthica community on sediment oxygenuptake. J. Exp. Mar. Biol. Ecol. 326, 77–88.
Middelburg, J. J., Barranguet, C., Boschker, H. T., Herman, P. M., Moens, T., & Heip, C. H. (2000). The fate of intertidal microphytobenthos carbon: An in situ 13C-labeling study. *Limnology and oceanography*, *45*(6), 1224-1234.
Moseman, S. M., Levin, L. A., Currin, C., & Forder, C. (2004). Colonization, succession, and nutrition of macrobenthic assemblages in a restored wetland at Tijuana Estuary, California. *Estuarine, Coastal and Shelf Science*, *60*(4), 755-770.
Nilsson, H. C., & Rosenberg, R. (2000). Succession in marine benthic habitats and fauna in response to oxygen deficiency: analysed by sediment profile-imaging and by grab samples. *Marine ecology progress series*, *197*, 139-149.
Ouillon, N., Forster, S., Timm, S., Jarrett, A., Otto, S., Rehder, G., & Sokolova, I. M. (2023). Effects of different oxygen regimes on ecological performance and bioenergetics of a coastal marine bioturbator, the soft shell clam Mya arenaria. *Science of The Total Environment*, *860*, 160459.
Pischedda, L., Cuny, P., Esteves, J. L., Poggiale, J. C., & Gilbert, F. (2012). Spatial oxygen heterogeneity in a Hediste diversicolor irrigated burrow. *Hydrobiologia*, *680*, 109-124.
Platt, T., Gallegos CL, Harrison, WG (1980). Photoinhibition of photosynthesis in natural assemblages of marine phytoplankton. Journal of Marine Research, 38, 687-701.
Ploug H, Lassen C, Jørgensen BB (1993) Action spectra of microalgal photosynthesis and depth distribution of spectral scalar irradiance in a coastal marine sediment of Limfjorden, Denmark. FEMS Microbiol Ecol 102: 261–270
Polerecky, L., Franke, U., Werner, U., Grunwald, B., & de Beer, D. (2005). High spatial resolution measurement of oxygen consumption rates in permeable sediments. *Limnology and Oceanography: Methods*, *3*(2), 75-85. doi: 10.4319/lom.2005.3.75
Polerecky, L., Lott, C., & Weber, M. (2008). In situ measurement of gross photosynthesis using a microsensor-based light-shade shift method. *Limnology and Oceanography: Methods*, *6*(8), 373-383. doi: 10.4319/lom.2008.6.373
Polerecky, L., Volkenborn, N., & Stief, P. (2006). High temporal resolution oxygen imaging in bioirrigated sediments. *Environmental Science & Technology*, *40*(18), 5763-5769.
Poloczanska, E. S., Burrows, M. T., Brown, C. J., García Molinos, J., Halpern, B. S., Hoegh-Guldberg, O., ... & Sydeman, W. J. (2016). Responses of marine organisms to climate change across oceans. *Frontiers in Marine Science*, *3*, 180581.

Pönisch, D. L., Breznikar, A., Gutekunst, C. N., Jurasinski, G., Voss, M., & Rehder, G. (2023). Nutrient release and flux dynamics of CO 2, CH 4, and N 2 O in a coastal peatland driven by actively induced rewetting with brackish water from the Baltic Sea. *Biogeosciences*, *20*(2), 295-323.

Pörtner, H. O., Langenbuch, M., & Michaelidis, B. (2005). Synergistic effects of temperature extremes, hypoxia, and increases in CO2 on marine animals: From Earth history to global change. *Journal of Geophysical Research: Oceans*, *110*(C9).

Pörtner, H. O., Langenbuch, M., & Reipschläger, A. (2004). Biological impact of elevated ocean CO 2 concentrations: lessons from animal physiology and earth history. *Journal of oceanography*, *60*, 705-718.

Precht, E., & Huettel, M. (2003). Advective pore-water exchange driven by surface gravity waves and its ecological implications. *Limnology and Oceanography*, *48*(4), 1674-1684.

Precht, E., & Huettel, M. (2004). Rapid wave-driven advective pore water exchange in a permeable coastal sediment. Journal of Sea Research, 51(2), 93-107. doi: 10.1016/j.seares.2003.07.003

Precht, E., & Huettel, M. (2004). Rapid wave-driven advective pore water exchange in a permeable coastal sediment. *Journal of Sea Research*, *51*(2), 93-107.

Precht, E., Franke, U., Polerecky, L., & Huettel, M. (2004). Oxygen dynamics in permeable sediments with wave-driven pore water exchange. *Limnology and Oceanography*, *49*(3), 693-705.Doi: 10.4319/lo.2004.49.3.0693

Prelle, L. R., Graiff, A., Gründling-Pfaff, S., Sommer, V., Kuriyama, K., & Karsten, U. (2019). Photosynthesis and respiration of Baltic Sea benthic diatoms to changing environmental conditions and growth responses of selected species as affected by an adjacent peatland (Hütelmoor). *Frontiers in microbiology*, *10*, 1500. doi: 10.3389/fmicb.2019.01500

Quintana, C. O., Hansen, T., Delefosse, M., Banta, G., & Kristensen, E. (2011). Burrow ventilation and associated porewater irrigation by the polychaete Marenzelleria viridis. *Journal of Experimental Marine Biology and Ecology*, *397*(2), 179-187.

Quintana, C. O., Tang, M., & Kristensen, E. (2007). Simultaneous study of particle reworking, irrigation transport and reaction rates in sediment bioturbated by the polychaetes Heteromastus and Marenzelleria. *Journal of Experimental Marine Biology and Ecology*, *352*(2), 392-406.

Rabouille, C., Denis, L., Dedieu, K., Stora, G., Lansard, B., & Grenz, C. (2003). Oxygen demand in coastal marine sediments: comparing in situ microelectrodes and laboratory core incubations. *Journal of Experimental Marine Biology and Ecology*, *285*, 49-69. doi: /10.1016/S0022-0981(02)00519-1

Rao, A. M., Polerecky, L., Ionescu, D., Meysman, F. J., & De Beer, D. (2012). The influence of pore-water advection, benthic photosynthesis, and respiration on calcium carbonate dynamics in reef sands. *Limnology and Oceanography*, *57*(3), 809-825. doi: 10.4319/lo.2012.57.3.0809

Rasheed, M., Wild, C., Franke, U., & Huettel, M. (2004). Benthic photosynthesis and oxygen consumption in permeable carbonate sediments at Heron Island, Great Barrier Reef, Australia. *Estuarine, Coastal and Shelf Science*, *59*(1), 139-150. doi: 10.1016/j.ecss.2003.08.013

Rasmussen, H., & Jørgensen, B. B. (1992). Microelectrode studies of seasonal oxygen uptake in a coastal sediment: role of molecular diffusion. *Marine ecology progress series. Oldendorf*, *81*(3), 289-303.

Raven, J. A. (1981). Respiration and photorespiration. *Fish. Aquat. Sci.*, *210*, 55-82.

Raven, J. A. (1997). CO2-concentrating mechanisms: a direct role for thylakoid lumen acidification?. *Plant, Cell & Environment*, *20*(2), 147-154.

Renz, J. R., & Forster, S. (2013). Are similar worms different? a comparative tracer study on bioturbation in the three sibling species Marenzelleria arctia, M. viridis, and M. neglecta from the baltic sea. Limnology and Oceanography, 58(6), 2046–2058.

Revsbech, N. P. (1989). An oxygen microsensor with a guard cathode. *Limnology and Oceanography*, *34*(2), 474-478.

Revsbech, N. P. (1989). Diffusion characteristics of microbial communities determined by use of oxygen microsensors. *Journal of Microbiological Methods*, *9*(2), 111-122.

Revsbech, N. P., & Jørgensen, B. B. (1983). Photosynthesis of benthic microflora measured with high spatial resolution by the oxygen microprofile method: capabilities and limitations of the method 1. Limnology and Oceanography, 28(4), 749-756. doi: 10.4319/lo.1983.28.4.0749

Revsbech, N. P., JØrgensen, B. B., & Brix, O. (1981). Primary production of microalgae in sediments measured by oxygen microprofile, H14CO3-fixation, and oxygen exchange methods 1. *Limnology and Oceanography*, *26*(4), 717-730. Doi: 10.4319/lo.1981.26.4.0717

Revsbech, N. P., Jorgensen, B. B., Blackburn, T. H., & Cohen, Y. (1983). Microelectrode studies of the photosynthesis and O2, H2S, and pH profiles of a microbial mat 1. *Limnology and Oceanography*, *28*(6), 1062-1074. doi: 10.4319/lo.1983.28.6.1062

Revsbech, N. P., Madsen, B., & Jørgensen, B. B. (1986). Oxygen production and consumption in sediments determined at high spatial resolution by computer simulation of oxygen microelectrode data. *Limnol. Oceanogr*, *31*(2), 293-304. doi: 10.4319/LO.1986.31.2.0293

Rhoads, D. C., & Boyer, L. F. (1982). The effects of marine benthos on physical properties of sediments: a successional perspective. In *Animal-sediment relations: The biogenic alteration of sediments* (pp. 3-52). Boston, MA: Springer US.

Rieder, K. (2011) Wechselbeziehungen zwischen der benthischen primärproduktion und den nematodengemeinschaften eulitoraler sandsedimente der südlichen deutschen ostseeküste dissertation]. [Rostock]: University of Rostock

Roberts, R. D., Kühl, M., Glud, R. N., & Rysgaard, S. (2002). Primary production of crustose coralline red algae in a high arctic fjord1. *Journal of Phycology*, *38*(2), 273-283.

Roberts, R. D., Kühl, M., Glud, R. N., & Rysgaard, S. (2002). Primary Production Of Crustose Coralline Red Algae In A High Arctic Fjord1. *Journal of Phycology*, *38*(2), 273-283.

Rodil, I. F., Attard, K. M., Norkko, J., Glud, R. N., & Norkko, A. (2019). Towards a sampling design for characterizing habitat-specific benthic biodiversity related to oxygen flux dynamics using Aquatic Eddy Covariance. *PLoS One*, *14*(2), e0211673.

Rodriguez-Romero, A., Basallote, M. D., Manoela, R., DelValls, T. Á., Riba, I., & Blasco, J. (2014). Simulation of CO2 leakages during injection and storage in sub-seabed geological formations: metal mobilization and biota effects. *Environment international*, *68*, 105-117.

Røy, H., Huettel, M., & Jørgensen, B. B. (2005). The influence of topography on the functional exchange surface of marine soft sediments, assessed from sediment topography measured in situ. *Limnology and oceanography*, *50*(1), 106-112.

Røy, H., Hüttel, M., & Jørgensen, B. B. (2002). The role of small-scale sediment topography for oxygen flux across the diffusive boundary layer. *Limnology and Oceanography*, *47*(3), 837-847.

Santema, M., & Huettel, M. (2018). Dynamics of microphytobenthos photosynthetic activity along a depth transect in the sandy northeastern Gulf of Mexico shelf. *Estuarine, Coastal and Shelf Science*, *212*, 273-285. doi: /10.1016/j.ecss.2018.07.016

Sartori, D., Macchia, S., & Gaion, A. (2024). Did you consider ammonium? A possible confounding factor in evaluating the toxicity of marine sediments. *Marine Pollution Bulletin*, *199*, 116021.

Satoh, H., & Okabe, S. (2013). Spatial and temporal oxygen dynamics in macrofaunal burrows in sediments: a review of analytical tools and observational evidence. *Microbes and environments*, *28*(2), 166-179.

Schade H. (2019) Respiration of sandy Baltic Sea sediment. [dissertation]. [Rostock]: University of Rostock

Schade H. (2019) Respiration of sandy Baltic Sea sediment. [dissertation]. [Rostock]: University of Rostock

Schade, H., Arneth, N., Powilleit, M., & Forster, S. (2019). Sand gapers' breath: respiration of Mya arenaria (L. 1758) and its contribution to total oxygen utilization in sediments. *Marine environmental research*, *143*, 101-110.

Schiewer, U. (2008). *Ecology of Baltic coastal waters* (p. 428). Berlin: springer.

Schöttler, U., Daniels, D., & Zapf, K. (1990). Influence of anoxia on adaptation of euryhaline polychaetes to hyposmotic conditions. *Marine Biology*, *104*, 443-451.

Schulz-Vogt, H. N., Pollehne, F., Jürgens, K., Arz, H. W., Beier, S., Bahlo, R., ... & Schott, T. (2019). Effect of large magnetotactic bacteria with polyphosphate inclusions on the phosphate profile of the suboxic zone in the Black Sea. *The ISME journal*, *13*(5), 1198-1208.

Serôdio, J., & Campbell, D. A. (2021). Photoinhibition in optically thick samples: effects of light attenuation on chlorophyll fluorescence-based parameters. *Journal of Theoretical Biology*, *513*, 110580.

Shum, K. T. (1992). Wave-induced advective transport below a rippled water-sediment interface. *Journal of Geophysical Research: Oceans*, *97*(C1), 789-808.

Sjøgaard, K. S., Treusch, A. H., & Valdemarsen, T. B. (2017). Carbon degradation in agricultural soils flooded with seawater after managed coastal realignment. *Biogeosciences*, *14*(18), 4375-4389.

Soetaert, K., Herman, P. M., & Middelburg, J. J. (1996). A model of early diagenetic processes from the shelf to abyssal depths. *Geochimica et Cosmochimica Acta*, *60*(6), 1019-1040.

Steinmuller, H. E., Dittmer, K. M., White, J. R., & Chambers, L. G. (2019). Understanding the fate of soil organic matter in submerging coastal wetland soils: A microcosm approach. *Geoderma*, *337*, 1267-1277.

Sundbäck, K., & Jönsson, B. (1988). Microphytobenthic productivity and biomass in sublittoral sediments of a stratified bay, southeastern Kattegat. *Journal of Experimental Marine Biology and Ecology*, *122*(1), 63-81.

Sundbäck, K., Nilsson, P., Nilsson, C., & Jönsson, B. (1996). Balance between autotrophic and heterotrophic components and processes in microbenthic communities of sandy sediments: a field study. *Estuarine, Coastal and Shelf Science*, *43*(6), 689-706.

Testa, J. M., Kemp, W. M., Hopkinson Jr, C. S., & Smith, S. V. (2012). Ecosystem metabolism. *Estuarine ecology*, 381-416.

Thamdrup, B., Hansen, J. W., & Jørgensen, B. B. (1998). Temperature dependence of aerobic respiration in a coastal sediment. *FEMS Microbiology Ecology*, *25*(2), 189-200.

Tschiersch, H., Liebsch, G., Borisjuk, L., Stangelmayer, A., & Rolletschek, H. (2012). An imaging method for oxygen distribution, respiration and photosynthesis at a microscopic level of resolution. *New Phytologist*, *196*(3), 926-936.

Tschiersch, H., Liebsch, G., Stangelmayer, A., Borisjuk, L., & Rolletschek, H. (2011). Planar oxygen sensors for non invasive imaging in experimental biology. In *Microsensors*. IntechOpen. doi: 10.5772/17893

Underwood, g. J., phillips, j., & Saunders, K. (1998). Distribution of estuarine benthic diatom species along salinity and nutrient gradients. *European Journal of Phycology*, *33*(2), 173-183.

Underwood, G., & Provot, L. (2000). Determining the environmental preferences of four estuarine epipelic diatom taxa: growth across a range of salinity, nitrate and ammonium conditions. *European Journal of Phycology*, *35*(2), 173-182.

Underwood, G.J.C. & Kromkamp, J. (1999) Primary production by phytoplankton and microphytobenthos in estuaries. *Adv. Ecol. Res., 29*:93-153

Urban-Malinga, B., & Wiktor, J. (2003). Microphytobenthic primary production along a non-tidal sandy beach gradient: an annual study from the Baltic Sea. *Oceanologia*, *45*(4).

Urban-Malinga, B., Warzocha, J., & Zalewski, M. (2013). Effects of the invasive polychaete Marenzelleria spp. on benthic processes and meiobenthos of a species-poor brackish system. *Journal of Sea Research*, *80*, 25-34.

Valdemarsen, T., Quintana, C. O., Thorsen, S. W., & Kristensen, E. (2018). Benthic macrofauna bioturbation and early colonization in newly flooded coastal habitats. PLoS ONE, 13(4), 1–21.

Vismann, B. (1990). Sulfide detoxification and tolerance in Nereis(Hediste) diversicolor and Nereis(Neanthes) virens(Annelida: Polychaeta). *Marine ecology progress series. Oldendorf*, *59*(3), 229-238.

Volkenborn, N., Robertson, D. M., & Reise, K. (2009). Sediment destabilizing and stabilizing bio-engineers on tidal flats: cascading effects of experimental exclusion. *Helgoland Marine Research*, *63*, 27-35.

Von Storch, H., Omstedt, A., Pawlak, J., Reckermann, M., Borzenkova, I., Zorita, E., ... & Koff, T. (2015). *Second assessment of climate change for the Baltic Sea Basin*. Springer.

Wang, X. D., Meier, R. J., Link, M., & Wolfbeis, O. S. (2010). Photographing oxygen distribution. *Angewandte Chemie International Edition*, *29*(49), 4907-4909.

Wang, M., Liu, H., & Lennartz, B. (2021). Small-scale spatial variability of hydro-physical properties of natural and degraded peat soils. Geoderma, 399, 115123.

Wenzhöfer, F., & Glud, R. N. (2004). Small-scale spatial and temporal variability in coastal benthic O2dynamics: Effects of fauna activity. Limnology and Oceanography, 49(5), 1471–1481.

Werner, U., Billerbeck, M., Polerecky, L., Franke, U., Huettel, M., Van Beusekom, J. E., & De Beer, D. (2006). Spatial and temporal patterns of mineralization rates and oxygen distribution in a permeable intertidal sand flat (Sylt, Germany). *Limnology and Oceanography*, *51*(6), 2549-2563. doi: 10.4319/lo.2006.51.6.2549

Wieland, A., & Kühl, M. (2006). Regulation of photosynthesis and oxygen consumption in a hypersaline cyanobacterial mat (Camargue, France) by irradiance, temperature and salinity. *FEMS microbiology ecology*, *55*(2), 195-210. doi: 10.1111/j.1574-6941.2005.00031.x

Wiesebron, L. E., Steiner, N., Morys, C., Ysebaert, T., & Bouma, T. J. (2021). Sediment bulk density effects on benthic macrofauna burrowing and bioturbation behavior. *Frontiers in marine science*, *8*, 707785.

Winterthaler B, Flodén T, Ignatius H, Axberg A, Niemistö L (1981) Geology of the Baltic Sea, Elsevier oceanography series. Elsevier, Amsterdam

Woelfel, J., Schoknecht, A., Schaub, I., Enke, N., Schumann, R., & Karsten, U. (2014). Growth and photosynthesis characteristics of three benthic diatoms from the brackish southern Baltic Sea in relation to varying environmental conditions. *Phycologia*, *53*(6), 639-651. doi: 10.2216/14-019.1

Woelfel, J., Schumann, R., Peine, F., Flohr, A., Kruss, A., Tegowski, J., Blondel, P., Wiencke, C. and Karsten, U., (2010). Microphytobenthos of Arctic Kongsfjorden (Svalbard, Norway): biomass and potential primary production along the shore line. *Polar Biology*, *33*, pp.1239-1253. doi: 10.1007/s00300-010-0813-0

Worm, B., & Lotze, H. K. (2021). Marine biodiversity and climate change. In *Climate change* (pp. 445-464). Elsevier.

Ziebis, W., Huettel, M., & Forster, S. (1996). Impact of biogenic sediment topography on oxygen fluxes in permeable seabeds. *Marine Ecology Progress Series*, *140*, 227-237. doi:10.3354/meps140227

Ziebis, W., Huettel, M., & Forster, S. (1996). Impact of biogenic sediment topography on oxygen fluxes in permeable seabeds. *Marine Ecology Progress Series*, *140*, 227-237.

7 Appendix

Table A. 1 Summary of laboratory O_2 microprofiles measurements in different light and transport regimes.

	C chambers			
Light and transport regime	dark diffusive	dark advective	light diffusive	light advective
O_2 penetration depth (mm)	4.31 ± 0.68	6.40 ± 1.39	8.81 ± 2.37	8.70 ± 2.97
Peak [O_2] (µmol l^{-1})	260 ± 35.26	224.34 ± 2.53	830.32 ± 477.53	889.13 ± 499.92
$R_{Dark–NP}$ (mmol m^{-2} d^{-1})$_{Man}$	-2.98 ± 1.34	-2.10 ± 0.03	17.91 ± 11.59	29.05 ± 28.35
$R_{Dark–NP}$ (mmol m^{-2} d^{-1})$_{Mod}$	-3.42 ± 1.83	-4.71 ± 0.65	11.09 ± 6.60	8.83 ± 1.14
GP (mmol m^{-2} d^{-1})$_{Man}$	-	-	20.90 ± 12.88	14.99 ± 4.43
GP (mmol m^{-2} d^{-1})$_{Mod}$	-	-	14.51 ± 8.35	11.20 ± 1.24
	RC chambers			
Light and transport regime	dark diffusive	dark advective	light diffusive	light advective
O_2 penetration depth (mm)	4.74 ± 2.61	3.58 ± 2.44	6.29 ± 2.18	6.13 ± 3.72
Peak [O_2] (µmol l^{-1})	257.6 ± 24.54	228 ± 33.70	658.46 ± 197.74	648.86 ± 238.05
$R_{Dark–NP}$ (mmol m^{-2} d^{-1})$_{Man}$	-4.41 ± 2.32	-5.02 ± 3.03	14.54 ± 3.37	14.32 ± 5.62
$R_{Dark–NP}$ (mmol m^{-2} d^{-1})$_{Mod}$	-4.86 ± 2.71	-7.50 ± 4.69	11.55 ± 3.38	14.41 ± 6.17
GP (mmol m^{-2} d^{-1})$_{Man}$	-	-	18.95 ± 4.19	19.06 ± 5.09
GP (mmol m^{-2} d^{-1})$_{Mod}$	-	-	14.77 ± 3.83	18.80 ± 3.71

Light intensity: 100 µmol m^{-2} s^{-1}. Man: Manual calculation based on the change in O_2 concentration gradients. Mod: the calculation was based on Sensor Trace modeling software.

Table A. 2 Summary of laboratory O_2 microprofiles measurements in different light intensities.

Chamber type	C chamber			
Light Intensity (µmol m^{-2} s^{-1})	0	40	70	100
O_2 penetration depth (mm)	6.00 ± 2.37	9.27 ± 3.04	10.86 ± 0.6	11.6 ± 0.6
Peak [O_2] (µmol l^{-1})	237.13 ± 25.94	569.98 ± 179.6	863.72 ± 133.43	892.77 ± 96.3
DOU-NP (mmol m^{-2} d^{-1})$_{Man}$	-2.0 ± 0.4	10.3 ± 5.1	12.2 ± 3.2	11.3 ± 2.5
DOU-NP (mmol m^{-2} d^{-1})$_{Mod}$	-2.3 ± 0.2	7.2 ± 2	10.6 ± 6.9	8.7 ± 1.2
GP (mmol m^{-2} d^{-1}) $_{Man}$		14.5 ± 4.7	16.3 ± 0.9	13.3 ± 2.9
GP (mmol m^{-2} d^{-1}) $_{Mod}$		9.43 ± 1.93	12.9 ± 6.8	11 ± 1.2
GP $_{LDS}$ (mmol m^{-2} d^{-1})		11.89 ± 9.03	25.54 ± 31.79	50.18
R_{Light} (mmol m^{-2} d^{-1})		4.7	14.9	41.5

Chamber type	RC chamber			
Light Intensity (µmol m^{-2} s^{-1})	0	40	70	100
O_2 penetration depth (mm)	3.97 ± 2.53	5.7 ± 2.5	6.49 ± 2.75	6.99 ± 2.84
Peak [O_2] (µmol l^{-1})	260.9 ± 30.3	553.2 ± 190.8	781.4 ± 242.7	1014 ± 196.8
DOU-NP (mmol m^{-2} d^{-1})$_{Man}$	-6.1 ± 1.8	12.4 ± 3.9	18.1 ± 7.1	22.5 ± 5.9
DOU-NP (mmol m^{-2} d^{-1})$_{Mod}$	-5.5 ± 3	10.3 ± 3.1	13.2 ± 4.2	18.9 ± 4.6
GP (mmol m^{-2} d^{-1})$_{Man}$		18.5 ± 5.5	24.1 ± 8.7	28.6 ± 7.3
GP (mmol m^{-2} d^{-1})$_{Mod}$		15.68 ± 3.4	18.7 ± 5.6	24.4 ± 7.4
GP LDS (mmol m-2 d-1)		84.68 ± 75.12	66.68 ± 19.3	65.8 ± 43.03
RLight (mmol m-2 d-1)		74.1	53.1	47

Table A. 3 Parameter of respective PI-curves (Figure 3.4): three C chambers and six RC chambers.

Chambers ID	R	Pm-Pn	Pg	α	I_k	Ic
C	-2.94	10	12.94	0.6	16	4
C	-2.59	12	14.59	1.04	12	2
C	-1.87	8	9.87	0.3	28	5
RC	-8.36	31	39.36	0.5	62	15
RC	-10.37	51	61.37	0.6	81	15
RC	-1.59	85	86.59	0.3	37	16
RC	-0.12	16	16.12	1.9	9	0.6
RC	-8.19	35	43.19	0.7	49	10
RC	-2.2	30	32.2	0.3	97	7

Table A. 4 Sampling date of (pilot study.soil collection. and sediment collection)

Date	Work package	Type of sample/ measurement	Measured water variable				Measured solid variable						
			T	Salinity	Ph	DO	Bulk density	Particle density	Water content	Porosity	LOI	Grain size analysis	C and N
June 2019	Oxy Macrofauna: Pilot study & Exp 1	Soil core					x		x	x	x		x
July 2019	Oxy Macrofauna: Pilot study	Water Variable	x	x	x	x							
September 2019	Oxy Macrofauna: Pilot study	Soil core					x	x	x	x	x	x	x
November 2019	Oxy Macrofauna: Exp 2	Soil core					x	x	x	x	x	x	x
August 2020	Oxy Macrofauna: Exp 2	Water Variable and Soil core	x	x	x	x	x	x	x	x	x	x	x
September 2021	Oxy Macrofauna: Exp 2	Water Variable and Soil core	x	x	x	x	x	x	x	x	x	x	x

Table A. 5 Soil physical characteristics Pilot study per. June 2019 (transect from board walk)

Station	Latitude	Longitude	Bulk density wet	Water Content β (%)	Bulk density dry	LOI (%)	Particle density	Porosity Marine (ϕ)	Porosity Terrestrial (ϕ)	C : N
D7.1	54.370634	13.244825	0.84 ± 0.1	16.2 ± 0.4	0.7 ± 0.1	16.8 ± 0.4	2.4 ± 0.01	0.13 ± 0.01	0.7 ± 0.02	12.6 ± 1.5
D7.2	54.370634	13.244825	0.77 ± 0.03	19.6 ± 1.6	0.6 ± 0.02	20.6 ± 1.7	2.4 ± 0.02	0.15 ± 0.01	0.7 ± 0.1	13.3 ± 0.1
D7.3	54.370634	13.244825	0.94 ± 0.01	32 ± 0.3	0.6 ± 0.01	26.7 ± 0.2	2.3 ± 0.01	0.3 ± 0.01	0.7 ± 0.01	13.2 ± 0.1
D7.4	54.370634	13.244825	1.05 ± 0.01	70.3 ± 1.9	0.3 ± 0.02	58.5 ± 5.2	1.9 ± 0.1	0.7 ± 0.02	0.8 ± 0.01	13.4 ± 0.4

Table A. 6 Sampling date of initial macrofauna colonization in Drammendorf

Date	Station	Type of sample
July 2019	D1-Sea Side	Soil Core
September 2019	D1- D4 Sea Side	Soil Core
March 2020	D1-Sea Side	Soil Core
September 2020	D1-Sea Side	Soil Core
September 2021	D1-Sea Side and Board Walk	Soil Core and benthic shovel net

Table A. 7 Water variable Per July 2019 (Ditches Station)

Station	Latitude	Longitude	Water Variable			
			T	Sal	pH	DO (mg/L)
D1	54.372383	13.237459	23.8	9.46	8.165	10.33
D2	54.371767	13.239	22.8	9.6	7.663	6.96
D3	54.370817	13.2387	23.3	9.57	7.362	4.38
D4	54.371883	13.240917	23.3	4.03	7.242	3.25
D5	54.372017	13.24263	21.8	3.42	7.183	0.31
D6	54.372883	13.243417	24.9	5.32	6.978	N.A
D7	54.370634	13.244825	20.2	0.97	7.539	4.84
D8	54.37314	13.241526	29.8	3.03	7.262	3.3
D10	54.371783	13.239367	N.A	N.A	N.A	N.A
D7.2	54.370307	13.244719	20.4	0.97	7.183	9.37

Table A. 8 Soil physical characteristics Pilot study per. September 2019

Station	Latitude	Longitude	Bulk density wet	Water Content β (%)	Bulk density dry	LOI (%)	Particle density	Porosity Marine (ϕ)	Porosity Terrestrial (ϕ)	C : N
1	54.37197	13.24040	0.95 ± 0.1	76.84 ± 6.5	0.22 ± 0.1	70.55 ± 19.6	1.77 ± 0.3	0.73 ± 0.1	0.88 ± 0.02	15.42 ± 0.5
2	54.37205	13.24132	1.34 ± 0.1	52.86 ± 6.1	0.64 ± 0.1	25.72 ± 5.9	2.33 ± 0.1	0.70 ± 0.02	0.73 ± 0.1	15.65 ± 0.3
3	54.37213	13.24263	1.05 ± 0.1	76.33 ± 11.5	0.25 ± 0.2	62.49 ± 23.9	1.87 ± 0.3	0.79 ± 0.1	0.87 ± 0.1	14.37 ± 0.2
4	54.37258	13.24312	1.28 ± 0.3	48.27 ± 0.5	0.66 ± 0.1	43.50 ± 1.5	2.11 ± 0.02	0.63 ± 0.1	0.69 ± 0.1	15.00 ± 0.3
5	54.37337	13.24223	1.10 ± 0.2	70.74 ± 9.8	0.33 ± 0.2	64.67 ± 19.4	1.84 ± 0.2	0.76 ± 0.01	0.83 ± 0.1	12.99 ± 0.2
6	54.37340	13.24112	0.69 ± 0.2	31.67± 14.5	0.49 ± 0.3	56.53 ± 18.8	1.94 ± 0.2	0.20 ± 0.01	0.75 ± 0.1	13.41 ± 0.5
7	54.37345	13.24010	0.64 ± 0.2	20.76 ± 2.8	0.51 ± 0.1	43.76 ± 8.8	2.10 ± 0.1	0.13 ± 0.02	0.76 ± 0.1	13.26 ± 0.3
8	54.37292	13.24220	0.77 ± 0.2	48.25 ± 10	0.41 ± 0.2	53.67 ± 14.2	1.98 ± 0.2	0.36 ± 0.01	0.80 ± 0.1	14.73 ± 0.1
9	54.37288	13.24037	0.74 ± 0.1	27.27 ± 6	0.54 ± 0.1	43.68 ± 4.6	2.10 ± 0.1	0.20 ± 0.1	0.74 ± 0.04	14.35 ± 0.1
10	54.37218	13.23980	1.39 ± 0.3	11.22 ± 1.8	1.23 ± 0.3	9.59 ± 2.8	2.53 ± 0.03	0.15 ± 0.03	0.51 ± 0.1	13.23 ± 0.02
11	54.37080	13.24430	NA	NA	NA	NA	NA	NA	NA	13.08 ± 0.2
12	54.37075	13.24422	1.11 ± 0.2	44.31 ± 6.7	0.63 ± 0.2	41.54 ± 10.2	2.13 ± 0.1	0.48 ± 0.02	0.71 ± 0.1	14.45 ± 0.3
13	54.37095	13.24352	NA	NA	NA	NA	NA	NA	NA	14.10 ± 0.3
14	54.37090	13.24320	0.62 ± 0.03	20.53 ± 1.7	0.49 ± 0.02	34.45 ± 2.9	2.22 ± 0.04	0.13 ± 0.01	0.78 ± 0.01	14.09 ± 0.1
15	54.37078	13.24248	0.77 ± 0.02	18.70 ± 1	0.62 ± 0.02	35.70 ± 3.6	2.20 ± 0.1	0.14 ± 0.01	0.72 ± 0.01	15.62 ± 0.3
16	54.37085	13.24133	NA	NA	NA	NA	NA	NA	NA	52.37 ± 66.1
17	54.37090	13.24067	0.65 ± 0.01	28.70 ± 11.6	0.46 ± 0.03	39.57 ± 3.3	2.16 ± 0.04	0.19 ± 0.1	0.79 ± 0.01	14.80 ± 0.6
18	54.37165	13.24400	0.64 ± 0.03	25.30 ± 0.9	0.48 ± 0.03	45.22 ± 4.9	2.08 ± 0.1	0.16 ± 0.01	0.77 ± 0.001	13.26 ± 0.6
19	54.37078	13.24425	0.74 ± 0.2	29.48 ± 8.7	0.52 ± 0.1	38.71 ± 1.3	2.17 ± 0.02	0.22 ± 0.1	0.76 ± 0.1	13.87 ± 0.3

Acknowledgments

This thesis is the product of solid teamwork. Thank you to everyone who has helped me along the sandy and Bodden coast of the Southwestern Baltic Sea and beyond.

First of all, to my supervisor, Stefan Forster. Thank you for accepting me as a PhD student and allowing me to work on this topic. You introduced me to oxygen and its dynamics in coastal zones, taught me how to handle different kinds of oxygen sensors, guided me throughout all my experiments, and shared your expertise throughout the modeling, calculation, and data interpretation. Thank you for all your patience and effort in pushing me towards the end and improving my manuscripts. It was a very long and challenging journey for me to be able to reach this endpoint; it would not have been possible without you. You always had an open door, open ears, a big heart, and super positive enthusiasm towards all the ups and downs of my work-life situations. You truly inspired me scientifically and personally. Thank you for your constant support, understanding, and, more than anything, your trust in me when I almost could not find a way to.

I am very thankful to GRK Baltic TRANSCOAST for their financial support over this Ph.D project. Thank you to Martin Sperling and the Steering committee for their support and encouragement.

I am grateful to all past and present members of our working group, the Marine Biology team, for the scientific and non-scientific support they provide me. I want to thank Martin Powilleit for his guidance during my lab and fieldwork, chlorophyll, and grain size analysis. I also thank him for introducing me to the macrofauna of the southwestern Baltic Sea. Thanks to Inna, Heike, and Eugine for all their support and encouragement. Thanks to Holger Pielenz for all the technical support during my experiments. I want to thank Elke Meier for all the C and N analysis and general help around the labs. Dear Fouzia, Hanna, Christopher, Natascha, Jenny, Friederike, and Abby, thank you for all your help with my German life, inside and outside the academic world. I have no idea how I will survive it without you guys around. Dear Fang li, Torben, Hui, Leo, Ngiah, Lynda, and Eugenie, thank you for picking up the baton when the others left and always being willing to help. Thank you to Niklas for his work with *Hediste diversicolor* and Fabian for sorting the collected macrofauna. I am very grateful to Amanda for improving our manuscript, though publication is still pending.

I am grateful to Prof. Karsten, Lara, and Petra of Applied Ecology and Phycology Uni-Rostock for their help with benthic diatom cultures, microscopic work, and my P-I curve.

I am grateful to Cintia, Erik, and Ronnie of the Department of Biology at Uni-Southern Denmark for all their insight, tips, and tricks in working with colonization experiments and benthic oxygen measurements. Thank you for sharing your experience.

I thank Dr. Robert Meier of PreSens Precision Sensing GmbH for all the technical details and guidance concerning the planar optode and for all the spontaneous meetings, discussions, and answers to all my unsophisticated questions.

I want to thank Claudia Lott of Aquatic Ecology Uni-Rostock for all the F (1/2) and Silica solutions she prepared during my microphytobenthos experiment.

I want to thank Christian Burmeister of IOW, Evelyn Boltzmann, and Stefan Köhler of AUF Uni-Rostock for all the measurements of the nutrients and solutes.

Thanks to Stephan Scholz for the microcomputer tomography analysis of our peat soil.

Outside the scientific world, I was able to push through with the support of local people and the community in Rostock. Thank you to my psychologist and my mentor, my GP, all the nurses in the Gyno department of the Uni-Hospital, and my physiotherapists. I know you were only doing your job. But with all the mental and physical challenges I faced, particularly over the last 2.5 years, I am so lucky and grateful for your care. Thank you to Maria, Silvi, Isi, Sinah, and the morning club in Ronja Espresso. Thank you for making me feel welcome with all the warm and pleasant conversation over coffee. Thank you to my bouldering-climbing, tennis, and swimming instructors and partners. Beyond health and fitness goals, the training had kept me going. When things seemed so stuck, endless, and blurry, I knew in my mind that I could still have some fun, learn, focus, and improve by climbing the wall, taking a dip, and hitting the green balls.

Dear Harry, Hermione, Ron, and Tailor Swift, Thank you for all the comfort and sanctuary you have given me over the years.

Dear Fellow Ph.D of the Baltic Transcoast. I have been lucky to share the journey with you all. Dear Anne and Daniel, thank you for sharing your insight into the water column measurement in Drammendorf and all the fun we shared in the field and at the conference. Thanks to Cheryl, Hao Jie, Marvin, Anna, Leonie, Catia, Simeon, and Miao for all their practical help and for being such a compassionate listener. Thank you for all the light to heavy and deep talks, laughs, cries, and pep talks throughout coffee, walks, dinners, and barbeque. I am grateful to Tina for her care and compassion; she shared her apartment while I was down so badly. Thanks to Erwin, Sate, and Cordula, who opened their hearts to me and swiftly became the most supportive, fun, and understanding partners in crime.

A special thanks go to Irini, Mbak Diana, Samira, and Pauline. I am so lucky to have you as a friend and sister I never had. Thank you for always caring and understanding. You guys never fail to provide me with mental support, humor, and encouragement. To Tamara, Annerieke, Lyn, Nomikos, and Reinier, thank you for your open shelter from Holland and beyond; I get the luxury of your warm company all over Europe. Dear Karin, Vita, Vindi, Mbak Desi, Mbak Datik, and Mbak Yoko, thank you for always cheering me up and lifting my spirit with all the Indonesian vibe, mainly plesiran and food.

Thank you to my family. On the Dutch side, Dear Mam and Séna, thank you for always being there for me. Your open arms to take me in is such a blessing that it still feels surreal to this very day. I am so lucky to have you both. I know I can always count on you and that Prof. Poelstraat 29's door will

always open for me (I have the keys though). On the Indonesian side, Dear Mama and Papa, Thank you for your understanding and sacrifice through and throughout, giving me all the freedom to follow my unconventional interests and lifestyle. I will not make it this far without your everlasting love, support, and faith. To my brothers, thank you for all the support and understanding (with minimum complaints) in all my unorthodox endeavors.

To God-Jesus-Buddha-Universe, thank you for my life. Words cannot describe how grateful I am.

And finally, last but not least, to Werna, Thank you for not giving up on me.

Declaration of Authorship

I hereby certify that the submitted thesis is entirely my original work except and otherwise stated in the dissertation. I am aware of the University's regulations regarding plagiarism, including the regulations concerning disciplinary actions that may result from plagiarism. Any use of works of other authors is properly acknowledged. I did not seek advice from any commercial organization for writing or experimenting during my work. This thesis is prepared by me without any outside help. The thesis has not been previously submitted to any other institution.

Werna Werna, MSc.

Rostock, June 2024

Curriculum Vitae

Werna Werna
Department of Marine Biology
University of Rostock, Germany
Albert-Einstein-Str. 3 & 21, 18059 Rostock
werna.werna@uni-rostock.de

EDUCATION

Jan 2019 – Oct 2024	**Ph.D. (Dr. rer. nat) in Marine Biology, University of Rostock** DFG Research Training Group of Baltic Transcoast – University of Rostock, Germany Topic: Oxygen dynamics and material cycling at the sediment-water interface
Sep 2016-Aug 2018	**MSc Marine Sciences, University of Utrecht, The Netherlands** Funded by Stuned Master Scholarship Program Thesis: "Holocene benthic foraminifera in two marine lakes in Misool, Raja Ampat (Indonesia)" at Marine Palynology and Paleoceanography, University of Utrecht, in cooperation with Naturalis Biodiversity Center, Leiden
Aug 2009-Mar 2015	**Bachelor of Geological Engineering**, University of Hasanuddin, Indonesia Major in Marine Geology Thesis: "Coastal characteristic based on sediment grain size distribution in the coast of Kalukubodo, South Galesong District, Takalar Regency, South Sulawesi Province, Indonesia" at the Laboratory of Sedimentology and Coastal Morphodynamics, University of Hasanuddin

MANUSCRIPT IN PREPARATION

Werna Werna, Hanna Schade, and Stefan Forster. *Benthic oxygen fluxes in sandy sediment of the shallow coastal water of the Baltic Sea: influence of light intensity and pore water advection*

Werna Werna and Stefan Forster. *Bioturbation is not the first process to affect transition from soil to sediment in a recently inundated terrestrial peatland*

Stefan Forster, Werna Werna, and Hanna Schade. *The role of surface sediment permeability for benthic oxygen exchange in a shallow coastal environment in the Southern Baltic Sea*

CONFERENCES / PRESENTATION

Oral

Werna W., Kimpel, N., and Forster, S. (2022, August 22-26). *Winner or Loser: which bioturbator will thrive in peatland restoration?* [conference presentation]. 6th Nereis Park International conference and bioturbation thematic school 2022, Logonna Daoulas, France.

Werna W., & Forster, S. (2022, May 30-June 03). *Microphytobenthos in sandy permeable sediment of the Southern Baltic Sea: laboratory study of potential primary production and respiration quantified with oxygen microelectrodes*

[conference presentation]. 4th Baltic Earth Conference 2022, Jastarnia, Hel Peninsula, Poland.

Werna W., & Forster, S. (2021, April 19-30). *Benthic Oxygen dynamics: Influence of pore water advection and microphytobenthos in a permeable sediment* [conference presentation]. General Assembly of the European Geosciences Union (EGU) 2021. online, EGU21-1239, https://doi.org/10.5194/egusphere-egu21-1239, 2021.

Poster

Forster, S., Schade, H., and Werna, W. (2024, April 14-19). *Surface sediment permeability and reactivity in a shallow coastal environment.* General Assembly of the European Geosciences Union (EGU) 2024, on-site, Vienna, Austria.

RESEARCH EXPERIENCE

Jul 2021	**Ph.D Summer course**, **DFG -Baltic Transcoast, University of Rostock.** Topic: Eutrophication in coastal environments
Sep 2020	**Intensive workshop**, Unisense. Topic: Microsensor in the field of biogeochemistry
Aug 2019	**Intensive 2-week PhD course, The University of Southern Denmark.** Topic: Aquatic Microbial and Molecular Ecology (AMME)
May 2018-Agu 2018	**Internship at NIOZ**, **the Royal Netherlands Institute for Sea Research-Yerseke.** Project: **"**A mesocosm study of sediment bulk density and its influence in shaping macrobenthos communities in the intertidal zone**"** Report: "Specific study on the burrowing depth of *Macoma balthica, Cerastoderma edule* and *Scrobicularia plana* in different sediment water content"
Jul 2018 (15 days)	**Oceanographers in training-Research Cruise** Netherlands Initiative Changing Oceans (NICO) Expedition leg 11-Texel-Horta.
May 2017–Aug 2017	**Guided Research at Department of Marine Palynology and Paleoceanography**, **Utrecht University.** Project: Dinoflagellates cyst assemblages in surface sediment sample for upper water column environmental condition in Indonesia and distribution of potentially toxic species
Jul 2017 (14 days)	**NIOZ Marine Master Summer School.** Project: Reconstructing past Wadden Sea water temperature using Ca/Mg in shells of Pacific Oyster
Sep 2013–Feb 2014	**Geological Mapping** Project: Salo Bulu - Bulu, Tonra-Bone Regency, South Sulawesi Province, Indonesia